INFORMATION TO USERS

This manuscript has been reproduced from the microfilm master. UMI films the text directly from the original or copy submitted. Thus, some thesis and dissertation copies are in typewriter face, while others may be from any type of computer printer.

The quality of this reproduction is dependent upon the quality of the copy submitted. Broken or indistinct print, colored or poor quality illustrations and photographs, print bleedthrough, substandard margins, and improper alignment can adversely affect reproduction.

In the unlikely event that the author did not send UMI a complete manuscript and there are missing pages, these will be noted. Also, if unauthorized copyright material had to be removed, a note will indicate the deletion.

Oversize materials (e.g., maps, drawings, charts) are reproduced by sectioning the original, beginning at the upper left-hand corner and continuing from left to right in equal sections with small overlaps. Each original is also photographed in one exposure and is included in reduced form at the back of the book.

Photographs included in the original manuscript have been reproduced xerographically in this copy. Higher quality 6" x 9" black and white photographic prints are available for any photographs or illustrations appearing in this copy for an additional charge. Contact UMI directly to order.

UMI

A Bell & Howell Information Company
300 North Zeeb Road, Ann Arbor MI 48106-1346 USA
313/761-4700 800/521-0600

GEOPHYSICAL AND GEOCHEMICAL STUDIES OF MAFIC DIKE SWARMS OF WESTERN INDIA AND THEIR APPLICATIONS TO DECCAN FLOOD VOLCANISM

by

RAJESH SHARMA

A dissertation submitted to the Graduate Faculty in Earth and Environmental Sciences in partial fulfillment of the requirement for the degree of Doctor of Philosophy, The City University of New York

1997

This manuscript has been read and accepted for the Graduate Faculty in Earth and Environmental Sciences in satisfaction of the dissertation requirement for the degree of Doctor of Philosophy.

August 11, 1997
Date

Somdev Bhattacharji
Professor Somdev Bhattacharji
Chair of Examining Committee

August 13, 1997
Date

Professor Frederick C. Shaw
Executive Officer

Professor Hannes Brueckner

Professor Kathleen Crane

Professor Evan Williams

Supervisory Committee

THE CITY UNIVERSITY OF NEW YORK

ABSTRACT:

GEOPHYSICAL AND GEOCHEMICAL STUDIES OF MAFIC DIKE SWARMS OF WESTERN INDIA AND THEIR APPLICATIONS TO DECCAN FLOOD VOLCANISM

by

RAJESH SHARMA

Advisor: Professor Somdev Bhattacharji

The size, shape, density and chemistry of mafic bodies from the Saurashtra peninsula, western margin, and Narmada-Tapti rifts of India was investigated using a variety of geophysical and geochemical modelling techniques. The three dimensional shape of the magma chamber from which NE-SW trending dike swarm in the Deccan volcanic province of western India was emplaced deciphered by using the aspect ratios (thickness:length) of the dikes and the inferred viscosities of the magmas. The aspect ratios vary from $22x10^{-2}$ to $6.7x10^{-2}$. The average estimated viscosities of rhyolite, trachyte and dolerite are $1.7x10^{7}$ Pas, $1.13x10^{6}$ Pas and $1.9x10^{3}$ Pas, respectively. The estimated magma driving pressures for the dikes is lowest (20.1 MPa) at the center and show a gradual increase from 30MPa to 51MPa and from 62MPa to 66MPa at the outer margin. The probable depth of origin for the dikes is ≈ 3.2 km at the center and ≈ 15.8 km at the peripheral region. Thus the probable shape of the magma chamber from which these dikes originated was convex upward. The projections of the dikes on to the surface of a magma chamber reveal that the magma chamber was zoned at the time of their emplacement. The convex shape and the estimated compositional Rayleigh number ($\approx 5.1x10^{14}\ \Delta S$, where ΔS is the difference in solute concentration) for the magma suggest that the convective fractionation was responsible for the zoning in the magma chamber

from which various differentiated dikes originated.

Three dimensional gravity modelling of +70 mGal Bouguer and +25 mGal free air gravity highs extending in N-S and NNW-SSE directions along the western continental margin of India indicate the presence of two subsurface high density mafic bodies. The body at the north western continental margin is ellipsoidal to dumbbell shaped occurring at a depth between 6±0.6 km to 18±1.8 km, and has an average density of 2940 kg/m^3. This body is approximately 300±30 km long and 50±5.0 km wide. The southern mafic body is also ellipsoidal in shape with an average density of 2930 kg/m^3 and occur at a depth from 6±0.6 km to 13±1.3 km. It has the lateral dimensions of 150±15 km, 30±3.0 km and shows +25 mGal free air gravity anomaly. Three dimensional gravity modelling of +10 mGal to -30 mGal Bouguer gravity highs along the intraplate Narmada-Tapti rift indicates the presence of eight small isolated high density mafic bodies. These mafic bodies are convexly upward, emplaced at a depth of 6.7±0.6 km and have an average density of 2910 kg/m^3. These isolated mafic bodies have estimated average width of 16±1.6 km and length 25±2.5 km. Average thickness of these mafic bodies is estimated to be 10±1.0 km.

Saurashtra peninsula is characterized by the presence of three SW-NE trending Bouguer gravity highs of +40 mGal, +30 mGal and +60 mGal respectively. Three dimensional gravity modeling of these gravity highs indicates the presence of high density gabbroic type mafic bodies. Estimated top and bottom width of the mafic body beneath +40 mGal gravity high are 3±0.3 km and 8±0.8 km and the length and thickness are 18±1.8 km and 14±1.4 km respectively. The mafic body responsible for +30 mGal gravity high is 6.5±0.6 km and 15±1.5 km wide at the top and the bottom, length of 20±2 km and

thickness of 10±1.0 km. The largest mafic body of +60 mGal gravity high has width of 11±1 km and 16±1.6 km at the top and bottom, length of 20±2 km and thickness of 15±1.5 km. These dimensions suggest that all three mafic bodies have higher ellipticity at the top than the bottom. Different ellipticity of these mafic bodies is caused by the drag exerted by upward increase in viscosity of the upper lithosphere and may also be related to asymmetrical thermal aureole. Emplacement of mafic plutons as diapirs in the upper crust is a result of differential drag due to strain softening of upper lithosphere.

The difference in shape, length and width of high density mafic bodies along the western continental margin of India and the intraplate Narmada-Tapti rifts (covered mostly by Deccan Traps) suggest that the migration and the concentration of a more continuous body of gabbroic type high density magma in the upper lithosphere was dominant along the western margin rift. Based on two and three dimensional gravity modelling it is conjectured that the emplacement of ellipsoidal high density mafic bodies along the western continental margin of India were related to western margin rifting and formation of isolated magma bodies during intraplate Narmada-Tapti rift reactivation. These mafic magma bodies in the upper lithosphere appear to be a major source for rapid and copious Deccan flood basalts eruptions and associated dike swarms emplaced during and post-Deccan basalts eruptions.

A model for the combined effects of venting, replenishment, assimilation and fractional crystallization (VRAFC) on the geochemical evolution of trace elements in a magma chamber is developed. This VRAFC model was applied to the differentiated dikes like rhyolite, trachyte, dolerite and pitchstone and lava flows of basalt and rhyolite from Deccan volcanic province of western India. Variation diagrams of total alkalis (wt% from 3.4 to 8.84) against

SiO_2, (wt% from 51.78 to 75.93), K_2O (wt% from 1.45 to 8.46) versus SiO_2 and Na_2O (wt% from 0.28 to 3.37) versus K_2O suggest that the rocks are transitional type and show a systematic evolution from basic to acidic types by combined effects of fractional crystallization and assimilation. The ratios of highly incompatible HFSE, LILE and LREE (i.e. Ba/La ≈11.45, Ba/Nb ≈33.88, Rb/Nb ≈9.25, Rb/La ≈2.85, Zr/Nb ≈16.27, Th/Nb ≈1.37, Th/La ≈0.46 and La/Nb ≈2.96) indicate that low pressure, fractionation controlled origin of more silicic magma from more basic magma. Chondritic, N-MORB and OIT normalized-trace-elements spider diagrams indicate contamination of the rocks by the crustal rocks of granitic composition. Fractional crystallization, crustal contamination and venting are important factors in the geochemical evolution of rhyolite, trachyte, dolerite, basalt and pitchstone of the Deccan Volcanics. The ratio between the assimilation rate of upper crustal rocks of granitic composition and the crystallization rate of fractionating phases which ranges from 0.1 to 0.15 could generate the geochemical characteristics of the differentiated rocks of Rajula and associated Deccan basalts if the parent magma is of N-MORB type. The venting fractional crystallization modelling (VFC) of the rocks of Rajula and the rocks from different parts of Deccan Traps and Reunion islands indicates that the ratio v (ratio between the mass of magma vented and the mass of magma fractionated) ranges from 0.4 to 0.6, suggesting that only 40% to 60% of the magma vented out from the magma chambers. The residual magma (60% to 40%) is explained by Bouguer gravity highs analyzed by three dimensional gravity modelling along the western margin of continental India and Saurashtra which in turn suggests the presence of high density gabbroic bodies in the upper crust along the continental western margin, the intraplate Narmada-Tapti rifts and in eastern Saurashtra.

ACKNOWLEDGEMENTS

I would like to express sincere thanks to my research advisor Professor Somdev Bhattacharji for his proper guidance and help throughout this work. Thanks are due to my supervisory committee members Professor Hannes Brueckner of Queens college, Professor Kathleen Crane of Naval Research Laboratory and Professor Evan Williams of Lewis and Clarke College for their cooperation in this study.

Field work in Deccan Volcanic Provinces, India and the chemical analyses of rocks at the National Laboratory in Nancy, France were financially supported by NSF International and PSC-CUNY grants to Professor Somdev Bhattacharji. I thank them for the financial support of this work.

Special thanks to Professor Frederick Shaw and Professor John Chute of Lehman College for allowing me to use their GIS lab at Lehman College. I would like to thank Mr. Peter Carlo of Graduate Center for helping me during GIS work at Lehman College.

I also like to thank Professor C. E. Nehru, Dr. Ali Kaya, Dr. Golam Sarwar and Professor John Chamberlain of Brooklyn College for their cooperation and help during this study. I also acknowledge financial support from Brooklyn College, Lehman College and Graduate Center.

CONTENTS

LIST OF TABLES

LIST OF FIGURES

CHAPTER 1

INTRODUCTION

1.1 BACKGROUND:

Cooling and fractional crystallizing magma chamber will develop temperature and composition gradients. These gradients form density differences that lead to differential motions between magma and crystals and finally chemical differentiation of magma. The complete description of chemical differentiation processes is a challenging problem because a large number of processes are involved and the shape of a magma chamber can vary widely. The geometrical shape of a magma chamber controls the angular relationship between the thermal and/or compositional boundary layers and gravity. The nature of this boundary layer in turn controls distribution of different sizes and shapes of minerals in a magma chamber. Therefore, the shape of a magma chamber becomes an important parameter for understanding the processes of chemical differentiation in magma.

Rayleigh Fractional crystallization plays an important role in the geochemical evolution of trace elements concentrations and isotopic ratios in a magma chamber undergoing fractional crystallization. DePaolo (1981) extended this fractional model to include assimilation (AFC model for assimilation fractional crystallization) and presented equations describing evolution of trace elements concentrations and isotopic ratios in a magma chamber. Recently,

Aitcheson and Forrest (1994) elaborated the AFC model to an open AFC magmatic system. DePaolo (1985) further extended the AFC model to include the process of replenishment (the RAFC model. Another important process that controls the geochemical evolution of magma is venting or eruption (O'Hara and Mathews, 1981). This is the only process that can be observed directly in volcanic provinces. However, up to this date the way venting controls the evolution of trace elements concentrations, and isotopic ratios in the magma chamber is largely unknown and conjectural. This study will attempt to quantify the role of venting by developing the VRAFC (Venting, Replenishment, Assimilation and Fractional Crystallization) model of a magma chamber.

1.2 REGIONAL GEOLOGY AND TECTONICS OF PENINSULAR INDIA

The Indian peninsula consists mostly of Archean continental nuclei and Proterozoic mobile belts. Peninsular India was once a part of Gondwanaland, between Africa on the west, Australia on the east and Antarctica on the southeast. Initial rifting of India from Gondwanaland started in Jurassic and final collision with Asian plate took place in the mid-Tertiary. Almost uniform crustal thickness of 35 km for the Indian shield has been shown by tele-seismic studies (Narain, 1973; McCarthy *et al.*, 1983), deep seismic sounding (Kaila *et al.*, 1979), and gravity modeling (Verma and Subrahmanyam, 1984). The uniform crustal thickness of peninsular India indicates that the crust was much thicker initially and later thinned by erosion.

Figure 1.1 shows that the peninsula can be divided into seven different domains (blocks) based on gravity, deep seismic sounding, seismicity and heat flow data (Narain and Subrahmanyam, 1986; Rogers, 1986). These domains are (i) Dharwar craton, further subdivided into eastern and western blocks, (ii) southern Granulites, (iii) eastern Ghats granulite belt, (iv) Aravalli range, (v) Bhandara craton, (vi) Singhbhum craton and (vii) Deccan Traps covered gneissic basement. Each of the blocks has characteristic rock types and structures.

The western Dharwar craton (Figure 1.1) contains three suites of N-S oriented schists belts. One suite consists of enclaves of 3000-m.y. old gneisses and proto-granulites. The other two schists' belts contain komatites, metapelites and amphibolites. The eastern Dharwar craton is made up of silicic gneisses and schist belts. The western and eastern Dharwar craton are demarcated by 2500-m.y. old closepet granite. Most of the rocks of eastern block are of amphibolite facies (metamorphosed mafic volcanic rocks) including types very rich in MgO wt%.

The southern Granulite terrain (Figure 1.1) is bordered by transition zone from gneisses to charnockites on the northern side and by the Indian ocean on all other sides. In addition to charnockites and gneisses the Granulite terrain contains metasediments, mafic/anorthositic intrusive bodies and irregularly shaped granites. Prograde charnockite formation occurred about 2500-m.y. ago.

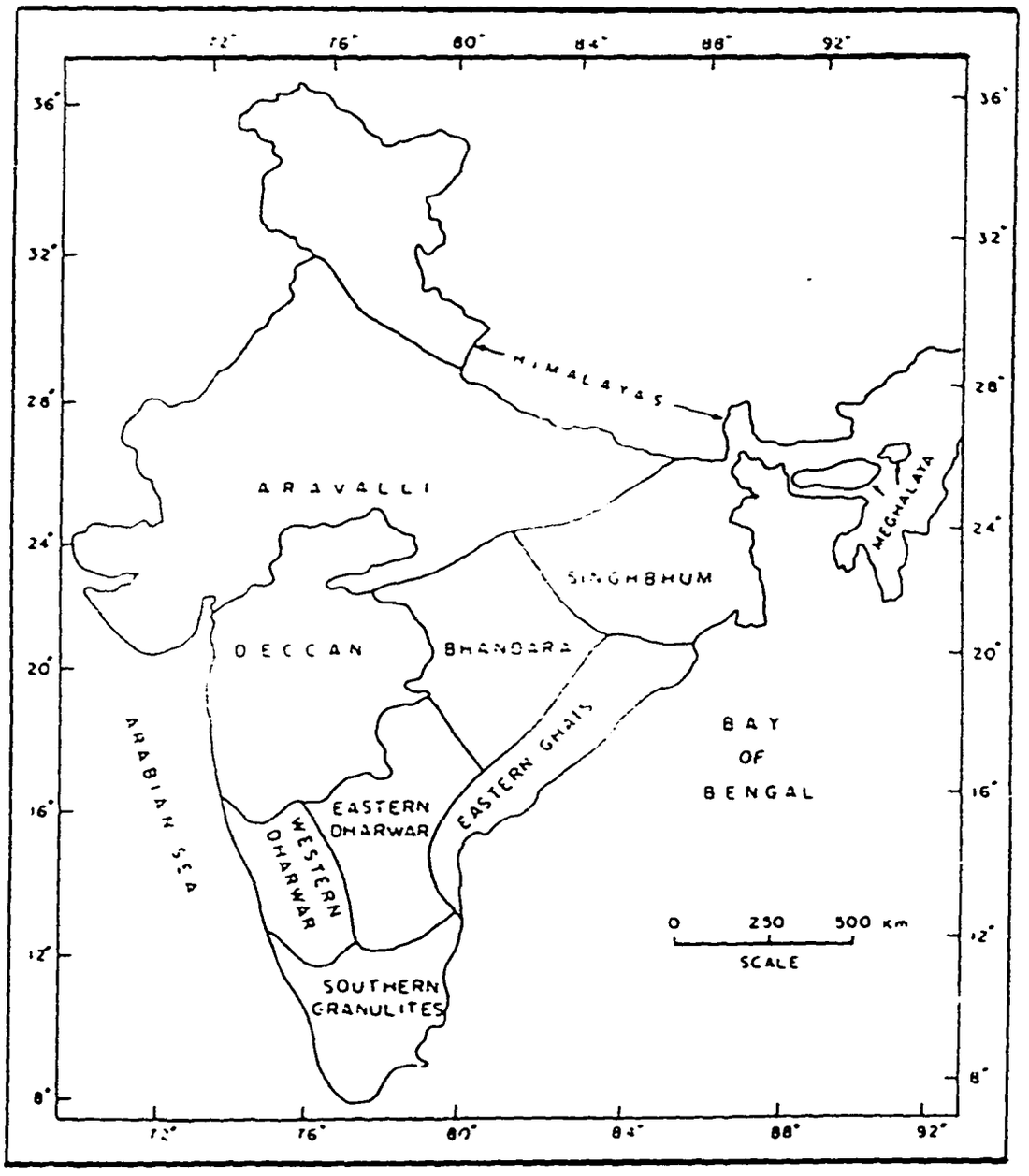

FIGURE 1.1: Tectonic subdivisions of the south Indian craton (after Rogers, 1986).

The eastern Ghat belt extends along the eastern margin of India (Figure 1.1), contains structures (folds, faults, fractures etc.) extending in north-south direction. Rock types are mostly chrnockites and khondalites. Deformed granites and mafic/anorthositic syntectonic bodies are also present in the eastern Ghats belt. These granites are around 1600-m.y. old.

Bhandara craton (Figure 1.1) is made up of folded gneisses and schist belts. These granulitic facies metamorphic rocks are overlain by mid-Proterozoic unmetamorphosed platform sediments contain manganese ores. Some of the metamorphosed suites in Bhandara craton include thick volcanic sequences.

Two separate blocks are present in the Singhbhum craton (Figure 1.1). The Singhbhum nucleus in the south contains the granitic batholith, which is surrounded by various metamorphic suites. One of the metamorphic suites has been proposed to be as old as 3800-m.y. The northern part of the craton is composed of gneisses and granitic rocks and is separated from the Singhbhum nucleus by a suture zone rich in copper.

The Aravalli range (Figure 1.1) contains an extensive section of metasedimentary rocks deposited from late Archean to Proterozoic. Major characteristics of the Aravalli range are the abundance of phosphorite, complete absence of metavolcanic rocks and continuous deformation of supracrustal assemblages from Archean to middle Proterozoic. Aravalli range also contains young sediments of intracratonic basin and scattered rhyolitic to alkaline igneous rocks.

The western and central parts of India are covered by one of the world's largest continental flood basalt provinces, known as the Deccan Volcanics (Traps) (Figure 1.2). Presently, Deccan volcanics occupy an area of 500,000 km^2, but they were of much greater extent originally, exceeding $1.5x10^6$ km^2 (eg. Mahoney, 1988). The dominant tholeiitic lava flows encountered in offshore wells in southern Pakistan and Bombay have also been identified as Deccan Volcanics (Ramanathan, 1981). Most of the flows are nearly horizontal with dip less than 1^0, except for the flows exposed along the west coast and the intraplate Narmada-Tapti rift, where the dip varies from 10^0 to 45^0. The deep seismic sounding surveys carried out by Kaila (1988) along eight profiles over the Deccan Traps indicate that the lava flows are thickest (≈2000m) along the west coast of India and show gradual thinning towards the northeastern part where they are about 100m thick.

The focus of this study will be the Deccan Traps in the Saurashtra peninsula (Figure 1.2). These basalts lie on top of Mesozoic sediments that were deposited in fluvio-deltaic and shallow sea environment. These sediments in turn lie unconformably on an Archean crystalline craton. The Deccan basalts are overlain by shallow- sea carbonates of Mio-Pliocene age. The DSS (Deep Seismic Sounding) surveys carried out by Kaila (1988) in the Saurashtra peninsula reveal that the Deccan volcanics are thickest (≈1500 m) in the central part of the peninsula and the thickness gradually decreases to 100m at the outer margins. However, there are no exposed and continuous Deccan lava flow sequences of such thickness in Saurashtra, because of flat topography, hence, it is extremely difficult to provide exact Deccan Traps stratigraphy in this region.

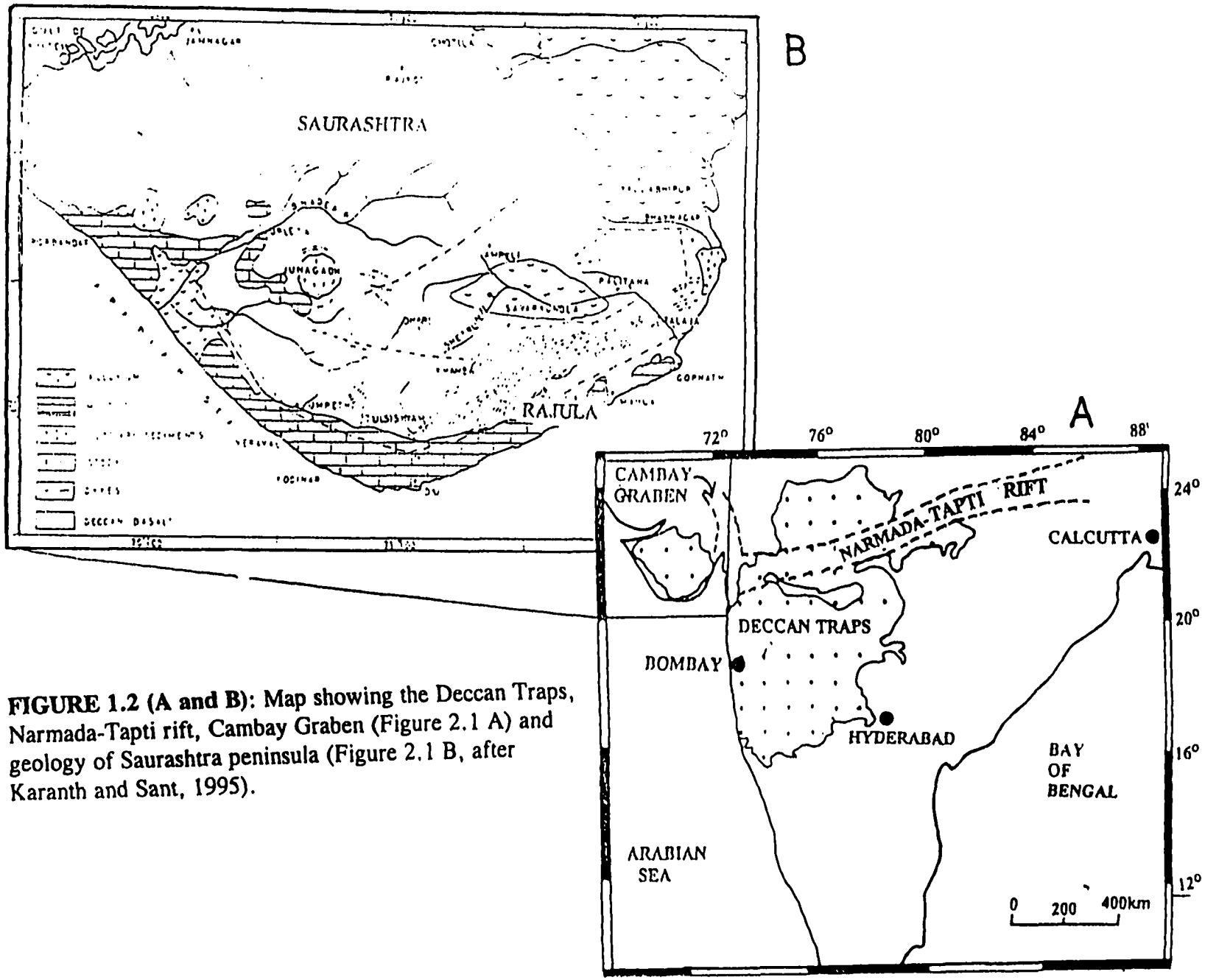

FIGURE 1.2 (A and B): Map showing the Deccan Traps, Narmada-Tapti rift, Cambay Graben (Figure 2.1 A) and geology of Saurashtra peninsula (Figure 2.1 B, after Karanth and Sant, 1995).

Three major tectonic features are present in the western and central parts of peninsular India (Figure 1.3 A), western Margin rift, Narmada-Tapti rift and Cambay graben respectively. The western margin rift extends in N-S direction and is bounded by west coast faults on the eastern side. However, the western boundary is not well ascertained because the faults are buried in Arabian sea. The Narmada-Tapti rift extends in E-W to ENE-WSW direction and is delineated by 65-70^0 northward dipping fault on the southern side. However, southward dipping step listric normal faults (Bhattacharji *et al.*, 1996) act as the northern border. The Narmada-Tapti rift is from 30-40 km wide on the western side to about 120 km on the eastern end and is offsetted by transverse tear faults along its entire length. Numerous hot springs are present along major and transverse faults. The faults of Narmada-Tapti rift have been known to be seismically active from historic times to as recent as 1985. The Cambay graben extends from latitude 21^0 to 24^0 N and longitude 71^0 30' to 73^0 45' E in NNW-SSE direction. The western and eastern margins of Cambay graben are bounded by step faults. Throughout its entire length the Cambay graben is dissected in several major crustal blocks by mantle reaching steeply dipping faults. In the southern most part of Cambay graben the Moho is at a shallow depth of 18 km (Kaila, 1988).

Mafic dikes and dike swarms occur along the western margin and Narmada-Tapti rifts (Figure 1.3B). The dikes and dike swarms along western margin rift are oriented in N-S to NNE and NNW directions. N-S trending dikes are the youngest (Deshmukh and Sehgal, 1988). Most of the dikes along western margin rift are doleritic in composition. However, near Bombay various differentiated dikes and dike swarms such as rhyolite,

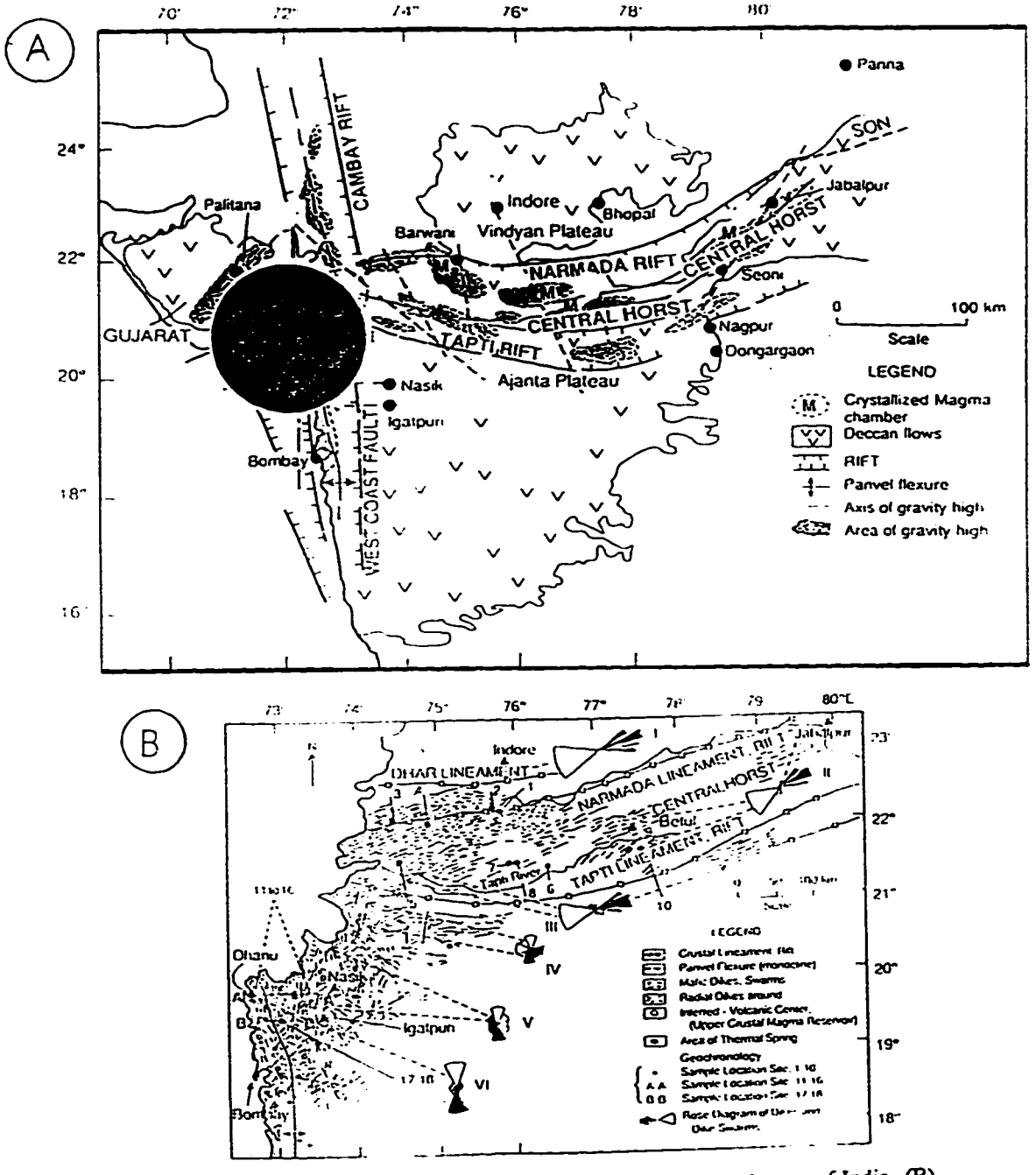

FIGURE 1.3: (A) Major tectonic features along western and central parts of India. (B) Distribution of dikes and dike swarms along western and central parts of peninsular India (After Bhattacharji et al., 1996).

trachyte, dacite and syenite are also present (Lightfoot *et al.*, 1986). In the Narmada-Tapti rift the dikes and dike swarms are oriented in E-W to ENE and ESE directions. Here E-W trending dikes are the oldest. The distribution of dikes also suggest that the frequency of dikes increases from east to west along the Narmada-Tapti rift. However, no marked changes in the frequency of dikes and dike swarms have been observed from north to south along the western margin rift (Deshmukh and Sehgal, 1988). Southeastern part of the Saurashtra peninsula is characterized by the presence of NNW-SSE trending dikes and NE-SW trending dike swarm (Figure 1.2). Rhyolite, trachyte and dolerite are the major rock types for the NE-SW trending dikes. The dikes outcrop in the form of low hill over a plain (host rock) of Deccan tholeiitic basalts.

1.3 OBJECTIVES:

The main objective of this study is to decipher the three dimensional shape(s) of the magma chamber(s) beneath the crust which may have been the source of Deccan basalts and associated dikes and dike swarms in the Saurashtra peninsula on the basis of estimated magma driving pressures and viscosities. The physical processes in a magma chamber not only depend on the perturbations caused by reinjection of magma, eruption and assimilation of host rocks but also on the geometrical shape of the magma chamber. Rubin (1993a; b) has shown that the growth of a dike is controlled by both elastic and viscous responses of the host rock. Recent examinations by Wada (1994) on the relationship between magma viscosity and dike width indicated that viscosity, magma driving pressure, and host rock stiffness control dike width.

In order to estimate the variation in aspect ratios of dikes in a dike swarm emplaced from a magma chamber, a model is developed by combining the visco-elastic model of Rubin (1993a; b) for the behavior of host rock and aspect ratio-viscosity relationship model of Wada (1994) and the estimation of depth of origin of individual dike using Lister's (1990) calculations. This combined model thus developed is applied to the NE-SW trending dike swarm along the Rajula area of Saurashtra in order to decipher the shape of a magma chamber from which these dikes were possibly emplaced.

The three dimensional shape of a magma chamber can also be deciphered by three dimensional gravity modelling. Richardson and Macinnes (1989) have developed a nonlinear inversion scheme for the gravity data into a three dimensional polyhedral model. Recently, Garcia-Abdeslem (1995) solved the forward problem in wave-number domain, where the power spectrum of a gravity anomaly is given by the product of independent functions that describe depth, thickness, horizontal dimensions, and density of source body. To further constrain the three dimensional shape of magma chambers underlying Deccan Volcanics I carried out three dimensional gravity modelling along the western continental margin, intraplate Narmada-Tapti rifts and Saurashtra region gravity highs using Garcia-Abdeslem (1995) scheme.

Another important purpose of the proposed study is to include the process(es) of venting into the RAFC model and to develop a complete VRAFC (for venting, replenishment, assimilation and fractional crystallization) model for a magma chamber. The

inclusion of venting and its effect on the evolution of trace elements concentrations and isotopic ratios in a magma chamber provides insight into the relationship between erupted and residual magma masses. This VRAFC model is applied to the basalts of Deccan volcanics from different geographical areas in order to estimate the ratios between the rate of change of masses of vented (v), assimilated rocks (a) and crystallizing phases. This VRAFC model can also be applied to estimate the above ratios for the magmatic systems, where the time scale for the magma chamber evolution are of the order of decades or centuries and may be used in volcanic hazard evaluation.

1.4 SIGNIFICANCE OF THE PRESENT STUDY:

Combining VRAFC modelling and the shape of a magma chamber will give an insight into the mechanism of development of a boundary layer with density gradients at different angles to the wall of a magma chamber. This boundary layer spans the whole crystallization interval in which the mineral assemblages differ in bulk composition from the melt which results in the development of compositional gradients in the melt of a magma chamber. These gradients result in differential motion between magma and crystals leading to diverse convective flows which are responsible for the chemical differentiation of magma in a magma chamber. The present study also provides information on various models applicable for the estimation of erupted and residual magmas from magma chambers which are the main sources for Deccan flood basalts and associated dikes and dike swarms.

CHAPTER 2

MAGMA DRIVING PRESSURES AND VISCOSITIES OF DIFFERENTIATED DIKES IN DECCAN VOLCANICS OF WESTERN INDIA: INDICATORS OF MAGMA CHAMBER SHAPE, COMPOSITIONAL CONVECTION AND ZONING

2.1 INTRODUCTION:

The orientations of dikes within a dike swarm are controlled by the state of stress at the time of their emplacement, i.e., when the magma propagates its own hydraulic fracture, the dike propagates in a plane normal to the least compressive stress direction (Shaw, 1980; Tsunakawa, 1983). However, according to Currie and Ferguson (1970) and Wilson (1970) the emplacements of dikes take place along older fractures. Delaney *et al.*, (1986) proposed that the distribution of adjacent, local and regional joints that parallel dikes can be used to decipher the emplacement mechanism. Most dikes propagate laterally along the rift zones from the magma chamber as observed in Hawaii (Fiske and Jackson, 1972) and Iceland (Sigurdsson and Sparks, 1978). Recent studies by Rubin (1993,a,b) indicate that the dike growth is controlled by both elastic and viscous response of the host rock. He meant that the same host rock might deform by flow (i.e. viscously) around a high viscosity granitic plutons

but by fracture (i.e. elastically) in response to low viscosity basaltic dikes. Recent examinations by Wada (1994) on the relationship between magma viscosity and dike width indicated that along with viscosity, magma driving pressure and host rock stiffness also control the variation of a dike's width.

2.2 ANALYSES OF PRESSURE SCALES FOR A DIKE: THEORETICAL BACKGROUND

Consider a dike embedded in an elastic host rock, which has a shear modulus μ, Poisson's ratio ν, density ρ_r and the stress intensity factor K (Figure 2.1). The magma in the dike is considered incompressible with the dynamic viscosity η_m, density ρ_m and volume V(t). The dike has a length ℓ, width w and height h. $\Delta\rho$ represents the density difference between the host rock and the magma and is given by:

$$\Delta\rho = \rho_r - \rho_m \qquad (2.1)$$

The elastic response of the host rock depends on the shear modulus μ, and Poisson's ratio ν and is given by:

$$G = \mu / (1- \nu) \qquad (2.2)$$

where G is known as the host rock stiffness.

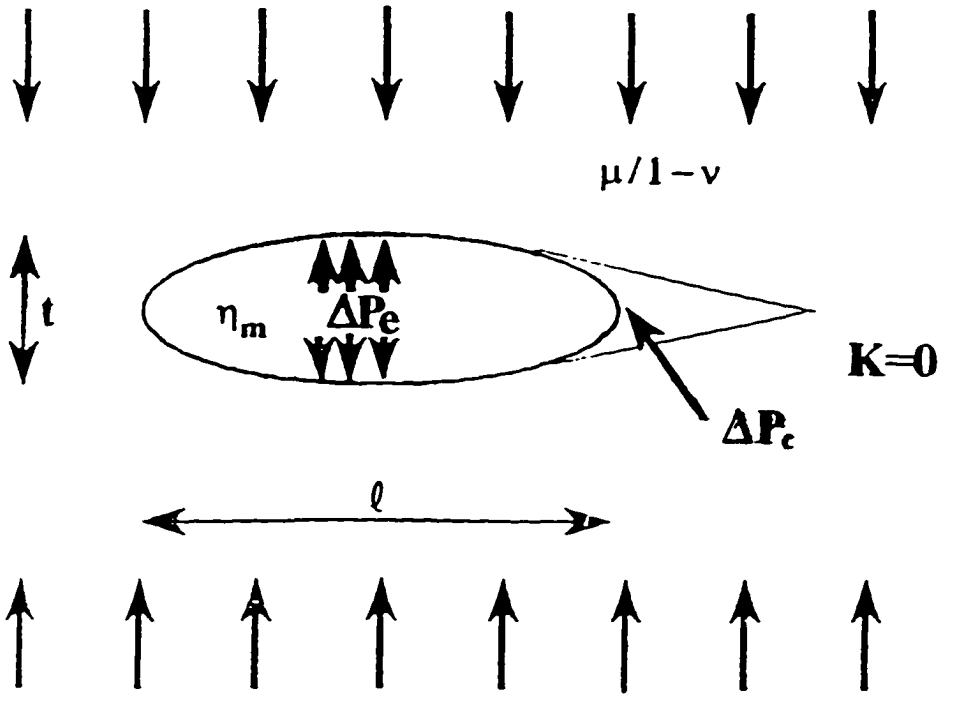

FIGURE 2.1: Schematic diagram of a propagating dike illustrating the partial magma pressure (ΔP_e) and extension pressure (ΔP_c). The magma in the dike is considered incompressible and of viscosity η_m. The other variables are: μ- shear modulus, ν-Poisson's ratio, $G=\mu/(1-\nu)$ host rock stiffness, K-stress intensity factor, t-thickness and ℓ length of the dike. The arrows indicate the direction of least compressive stress.

The propagation of a dike in an elastic medium is controlled by the following four pressures.

(i) **Partial Magma pressure ΔP_e** : The dilation of a magma filled dike requires an increase in the pressure of magma in order to balance the stresses of host rock. This relationship is given by:

$$\Delta P_e \approx G\, a \qquad (2.3)$$

where ΔP_e is the partial magma pressure, G is host rock stiffness and a is the aspect ratio (thickness/length) of the dike. Figure 2.1 shows a two-dimensional dike held open by a constant pressure ΔP_e has an elliptical cross section.

(ii) **Hydrostatic pressure ΔP_h**: When the density of the magma in a dike has the same density as that of the host rock then they are in gravitational equilibrium. In this case magma has neutral buoyancy. However, if the magma is less dense it will tend to rise and if it is more dense then it will tend to descend (Figure 2.2). The propagation of dike due to the difference in the density depends on the hydrostatic pressure gradient and is given by:

$$\Delta P_h \approx (\rho_r - \rho_m)\, g\, h \qquad (2.4)$$

here g is acceleration due to gravity, h is the height of rise and ΔP_h is the hydrostatic

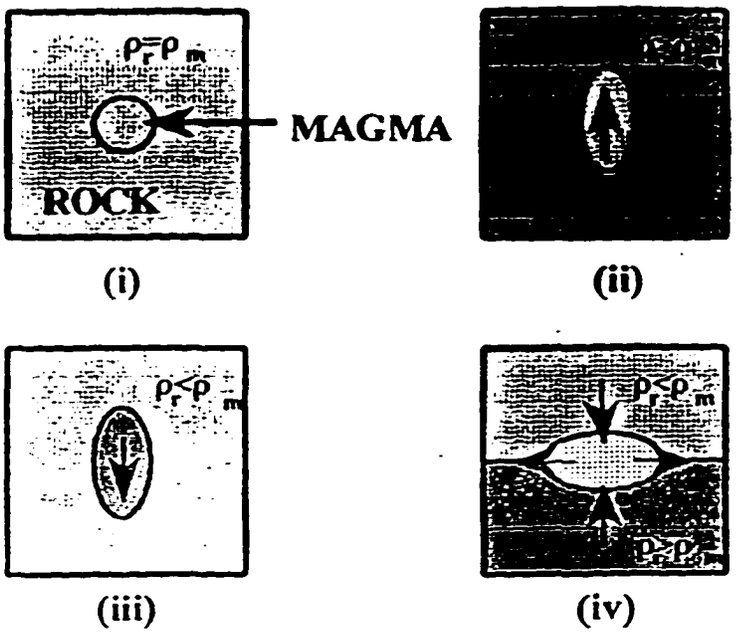

FIGURE 2.2: The propagation of a dike is also governed by the density difference between the magma (ρ_m) and the host rock (ρ_r). (i) When the magma in dike has the same density as the host rock the dike is stationary, it is in neutral buoyancy. (ii) If the ρ_m is less than the ρ_r then it will tend to rise. (iii) In the situation where $\rho_m > \rho_r$ the dike propagates downward. (iv) When the magma in the dike is denser than the overlying host rock but less than the underlying rocks then it will tend to spread laterally.

pressure.

(iii) **Viscous Pressure Drop ΔP_v** : The flow of magma in a dike is driven by the pressure gradient in the magma pressure (Hirs, 1973). The viscous pressure drop ΔP_v in laminar flow along the dike depends on the viscosity of magma, the velocity of the magma, the length and the thickness of the dike. The governing equation is:

$$\Delta P_v = \frac{\eta \ell V}{t^2} \qquad (2.5)$$

where ΔP_v is viscous pressure drop, V and η are the velocity and viscosity of magma and rest of the symbols are same as described earlier.

(iv) **Extension Pressure ΔP_c**: The dike extension pressure depends on the processes at the tip of a propagating dike and is given by:

$$\Delta P_c \approx K/\ell^{1/2} \qquad (2.6)$$

where K is the stress intensity factor of the host rock and ΔP_c is the dike's extension pressure (Figure 2.1). According to Lister (1990) a stable dike can attain a maximum thickness and height depending on the parameters of the following equations:

$$t \approx \left\{ \frac{K^4}{g \Delta \rho G^3} \right\}^{1/3} \qquad (2.7)$$

and the height of rise

$$h \approx \{ K/g \Delta \rho \}^{2/3} \qquad (2.8).$$

Recently. Rubin (1993) has studied the propagation of dikes at a high confining pressure and has given the equation for the propagation velocity of dike:

$$V \approx \frac{\Delta P_e t^2}{3\eta_m \ell} \approx \frac{\Delta P_e \ell}{3\eta_m G} \qquad (2.9)$$

where V is the velocity of propagation. Equation 2.9 states that the velocity of dike propagation is inversely proportional to the viscosity of magma. Hence, viscous rhyolite dike would take longer time to reach the earth's surface than a less viscous basaltic dike.

2.3 CALCULATIONS OF ΔP_c, V, K AND ΔP_c FOR THE DIKES OF NE-SW TRENDING DIKE SWARM IN RAJULA:

The distribution of dikes and dike swarm around Rajula town and adjacent area is shown in Figure 2.3 (for the location of Rajula, Figure 1.1). For the first time I have carried out detailed mapping of the Rajula area. Rhyolite, trachyte and dolerite dikes generally outcrop in the form of low hills. The host rock for these dikes is Deccan volcanics. Two major trends of dikes have been observed in this area. The dominant trend of the dikes is NE-SW. The dikes are sparsely distributed near Rajula but closely spaced near Dedan (Figure 2.3). The dikes exposed near Rajula are larger in size. For example trachyte dike #1 is 2100m long and 210m wide and rhyolite dike #2 is 1900m in length and 315m in width. The dikes exposed near Dedan have smaller dimensions e.g. dolerite dike #14 is 575m long and 115m wide and the rhyolite dike #10 is 825m long and 55m wide. Large dolerite dikes near Vijapardi (Figure 2.3) are few and oriented in approximately NNW-SSE direction. We have not considered these dikes in this study as they cross cut the partially exposed NE-SW trending dikes and hence are younger.

Delaney *et al.*, (1986) showed that the mechanism of emplacement of dikes within a dike swarm can be deciphered by using regional, local and adjacent joints patterns present in the same area. Careful observations in the field area and the aerial photographs of the dike swarm near Rajula indicate that the joints which parallel the dikes are absent. Hence, it can be inferred that each dike created its own fracture passage (Delaney *et al.*, 1986). When magma

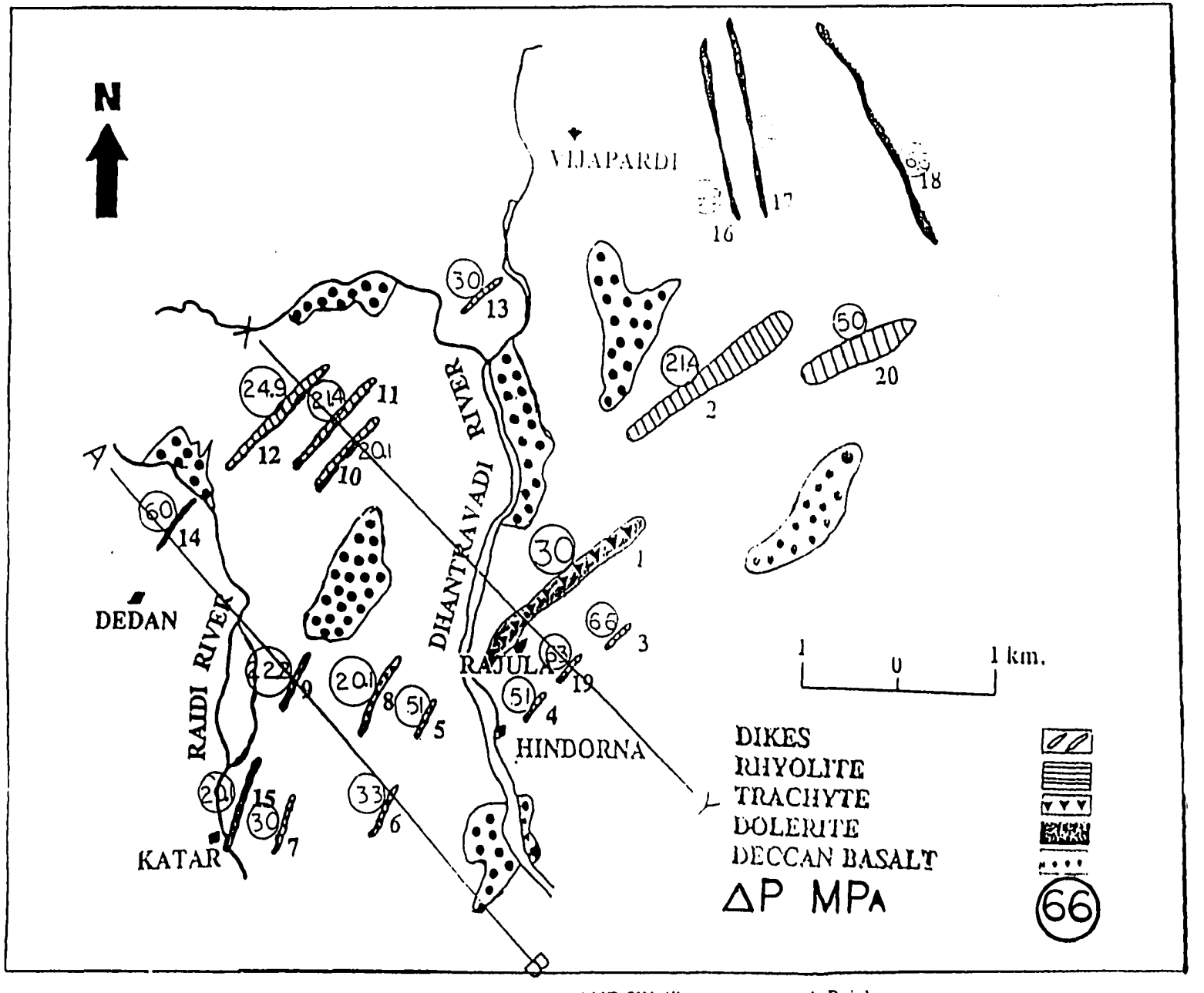

FIGURE 2.3: The distribution of dikes and NE-SW dike swarm around Rajula.

propagates its own hydraulic fracture, the dike propagates along the fracture plane perpendicular to the direction of least compressive stress (Tsunakawa, 1983; and Delaney *et al.*, 1986). Hence the extension direction (σ_3) of the dikes in Rajula area was NW-SE at the time of their emplacement.

Table 2.1 lists the estimated values of ΔP_e, V, ΔP_c and K for the dikes of NE-SW dike swarm. The magma driving pressure (ΔP_e) for each dike was calculated using equation 2.3, in which the value of the host rock stiffness G is taken as 3GPa (Griggs *et al.*, 1960; Rubin and Pollard, 1990). The estimated values of ΔP_e are then used in equation 2.9 to calculate velocity of propagation for each dike. The stress intensity factor K for the host rock is determined by equation 2.7.

Bottinga and Weill (1972), Shaw (1972), Marsh (1981) and McBirney and Murase (1984) have developed empirical equations to estimate magma viscosity. The viscosity of magma for each dike of Rajula area was calculated using the chemical composition, density, temperature, and H_2O and other volatiles concentration following McBirney and Murase (1984).

(i) CHEMICAL COMPOSITION OF DIKES:

Chemical composition of dikes from Rajula is given in Table 2.2. All the values are in wt.%. The whole rock samples were prepared by fusion with $LiBiO_2$ and HNO_3

TABLE 2.1

Dike #	ROCK TYPE	WIDTH (meters) (w)	LENGTH (meters) (l)	ASPECT RATIO (θ)	MAGMA DENSITY (ρ) gcm^{-3}	MAGMA VISCOSITY (η_m) (PaS)	EXTENSION PRESSURE $\Delta P_e x10^3$ (MPa $m^{1/2}$)	PROPAGATION VELOCITY V(m/s)	STRESS INTENSITY FACTOR K(MPa)x10^3	MAGMA DRIVING PRESSURE(ΔP) MPa	DEPTH OF ORIGIN (z) (km)
1	Trachyte	210	2100	$1x10^{-1}$	2.41	$2.34x10^6$	3.9	1	1.8	30	6.1
2	Rhyolite	315	1900	$7.1x10^{-2}$	2.28	$1.1x10^7$	5.9	0.4	2.6	21	3.5
3	Rhyolite	50	225	$2.2x10^{-1}$	2.32	$5.8x10^6$	4.3	0.4	0.64	66	11.4
4	Rhyolite	51	300	$1.7x10^{-1}$	2.33	$2.24x10^7$	3.7	0.07	0.64	51	8.9
5	Rhyolite	60	350	$1.7x10^{-1}$	2.33	$2.7x10^7$	3.9	0.07	0.72	51	8.9
6	Trachyte	55	500	$1.1x10^{-1}$	2.41	$1.9x10^6$	2.9	0.4	0.65	33	6.7
7	Rhyolite	55	550	$1x10^{-1}$	2.3	$5.6x10^7$	2.9	0.01	0.69	30	5
8	Trachyte	52	775	$6.7x10^{-2}$	2.32	$4.3x10^5$	2.3	0.6	0.65	20	3.5
9	Trachyte	39	550	$7.4x10^{-2}$	2.34	$3.4x10^5$	2.2	0.6	0.52	22	4
10	Rhyolite	55	825	$6.7x10^{-2}$	2.28	$6.6x10^6$	2.4	0.04	0.7	20	3.2
11	Rhyolite	78	1100	$7.1x10^{-2}$	2.3	$5.1x10^6$	2.7	0.08	0.89	21	3.6
12	Rhyolite	116	1400	$8.3x10^{-2}$	2.3	$1.3x10^7$	3.2	0.08	1.2	25	4.2
13	Rhyolite	30	300	$1x10^{-1}$	2.24	$4.4x10^6$	2.6	0.01	0.45	30	4.5
14	Dolerite	115	575	$2x10^{-1}$	2.52	$1x10^3$	4.3	460	1.04	60	15.8
15	Trachyte	59	875	$6.7x10^{-2}$	2.3	$6.6x10^5$	2.5	0.4	0.73	20	3.4
16	Dolerite	56	1700	$3.3x10^{-2}$	2.7	$7.2x10^2$	1.1	85	0.47	10	5
17	Dolerite	76	1900	$4x10^{-2}$	2.69	$5x10^3$	1.4	24.3	0.6	12	5.7
18	Dolerite	53	2400	$2.2x10^{-2}$	2.52	$7.2x10^2$	1.2	107.3	0.6	7	1.8
19	Rhyolite	68	325	$2.1x10^{-1}$	2.28	$2.2x10^7$	4.5	0.14	0.82	63	10.2
20	Rhyolite	187	1100	$1.7x10^{-1}$	2.28	$1x10^7$	5.1	0.6	1.7	50	8.2

dissolution. The analyses were performed at National Laboratory, Nancy, France by Inductively Coupled Plasma (ICP) - Emission Technique. The SiO_2 wt% varies from 51.78 to 75.93 and $FeO+Fe_2O_3$ from 1.41% to 10.48% and TiO_2 from 0.16% to 4.82%. Mainly, $FeO+Fe_2O_3$ and TiO_2 wt% control the density of magma.

(ii) DENSITY OF MAGMA AT THE TIME OF EMPLACEMENT:

Approximate density of magma at the time of emplacement has been calculated for each dike. The density of magma is generally controlled by Fe_2O_3 wt% (F3), FeO wt% (F2) and TiO_2 wt% (TI), respectively. The governing equation is : 2.2+0.027x(F3+F2+TI) (McBirney and Murase, 1984). Fe_2O_3 wt% in Table 2.2 for each dike is total Fe_2O_3+FeO wt%. Calculated densities for rhyolite vary from 2.24 to 2.33 gm/cm^3, for trachyte they are 2.3 to 2.41 gm/cm^3 and for dolerite densities are 2.52 to 2.70 gm/cm^3 (Table 2.1).

(iii) H_2O AND OTHER VOLATILES IN MAGMA:

The concentration of H_2O and other volatiles in magma affects its viscosity. The amount of these volatiles are extremely difficult to estimate directly. H_2O content in magma can be calculated indirectly on the basis of H_2O bearing minerals like the phlogopite and pargasite. As these minerals are absent in rhyolite, trachyte and dolerite dikes, we have considered H_2O is absent in magma for calculations of viscosities of these dikes.

TABLE 2.2

DIKE#	2 Rhyolite	4 Rhyolite	7 Rhyolite	11 Rhyolite	5 Rhyolite	13 Rhyolite
SiO_2	75.31	71.92	73.15	74.31	71.9	75.31
Al_2O_3	11.73	11.66	11.44	11.17	11.94	10.8
Fe_2O_3	2.77	4.45	3.84	3.22	4.25	1.41
MnO	0.02	0.03	0	0	0.01	0
MgO	0.07	0.51	0.25	0.41	0.5	0.2
CaO	0.25	0.68	0.83	1.11	0.7	0.43
Na_2O	2.91	1.67	1.5	2.08	1.67	0.28
K_2O	5.25	6.37	7.34	5.72	6.37	8.46
TiO_2	4.82	0.46	0.44	0.45	0.5	0.16
P_2O_5	0.08	0.16	0.15	0.15	0.14	0.07
Loss on Ignition	1.11	1.83	0.78	1.05	1.75	2.02
Total	99.67	99.74	99.72	99.67	99.73	99.76
Q	36.79	34.48	33.38	36.79	34.49	38.45
OR	31	37.62	43.35	33.78	37.62	47.49
AB	24.61	14.13	12.69	17.59	14.13	2.25
AN	0.72	2.33	2.8	4.25	2.56	1.59
DI	0	0	0.29	0.24	0	0
HY	2.62	4.8	3.39	3.2	4.51	1.49
OL	0	0	0	0	0	0
NE	0	0	0	0	0	0
AC	0	0	0	0	0	0
C	1	1.17	0	0	1.36	0.54
AP	0.19	0.37	0.35	0.35	0.33	0.16
JL	0.32	0.88	0.84	0.86	0.95	0.29
MT	1.31	2.15	1.86	1.55	2.03	0.65

TABLE 2.2 cont.

DIKE#	10 Rhyolite	3 Rhyolite	12 Rhyolite	20 Rhyolite	19 Rhyolite
SiO_2	75.31	73.15	74.31	75.31	75.31
Al_2O_3	11.73	11.44	11.17	11.73	10.8
Fe_2O_3	2.77	3.84	3.22	2.77	1.41
MnO	0.02	0	0	0.02	0
MgO	0.07	0.25	0.41	0.07	0.2
CaO	0.25	0.83	1.11	0.25	0.43
Na_2O	2.91	1.5	2.08	2.91	0.28
K_2O	5.25	7.34	5.72	5.25	8.46
TiO_2	4.82	0.44	0.45	4.82	0.16
P_2O_5	0.08	0.15	0.15	0.08	0.07
Loss on Ignition	1.11	0.78	1.05	1.11	2.02
Total	99.67	99.72	99.67	99.67	99.76
Q	36.79	33.38	36.79	36.79	38.45
OR	31	43.35	33.78	31	47.49
AB	24.61	12.69	17.59	24.61	2.25
AN	0.72	2.8	4.25	0.72	1.59
DI	0	0.29	0.24	0	0
HY	2.62	3.39	3.2	2.62	1.49
OL	0	0	0	0	0
NE	0	0	0	0	0
AC	0	0	0	0	0
C	1	0	0	1	0.54
AP	0.19	0.35	0.35	0.19	0.16
IL	0.32	0.84	0.86	0.32	0.29
MT	1.31	1.86	1.55	1.31	0.65

TABLE 2.2 cont.

DIKE #	6 Trachyte	1 Trachyte	15 Trachyte	8 Trachyte	9 Trachyte	14 Dolerite
SiO_2	63.37	65.3	69.18	68.65	69.18	51.78
Al_2O_3	13.28	13.39	13.01	12.91	13.01	14.63
Fe_2O_3	7.08	6.86	4.44	4.33	4.44	10.48
MnO	.07	.07	.03	.02	.03	.13
MgO	.6	.68	.85	1.04	.85	4.73
CaO	3.95	2.66	1.93	2.04	1.93	8.78
Na_2O	3.37	3.29	2.37	2.22	2.37	2.22
K_2O	1.7	4.48	4.77	4.85	4.77	1.45
TiO_2	.79	.75	.63	.59	.63	1.18
P_2O_5	.22	.2	.19	.17	.19	.16
Loss on Ignition	5.26	2.03	2.33	2.9	2.33	3.96
Total	99.69	99.71	99.73	99.72	99.73	99.8
Q	26.37	21.13	30.87	30.14	30.87	7.49
OR	10.04	26.46	28.17	28.64	28.17	8.23
AB	28.5	27.83	20.05	18.78	20.05	18.04
AN	16.08	8.3	8.33	9.01	8.33	24.66
DI	1.79	2.88	0	0	0	13.25
HY	6.33	5.65	5.25	6.13	5.25	12.73
OL	0	0	0	0	0	0
NE	0	0	0	0	0	0
AC	0	0	0	0	0	0
C	0	0	.89	.71	.89	0
AP	.51	.47	.44	.4	.44	.36
IL	1.5	1.5	1.2	1.12	1.2	2.16

(iv) VISCOSITIES OF DIKES AND HOST ROCK:

The calculated magma viscosities based on major oxides for the dikes at 1000° C and 0 kbar of H_2O pressure are listed in Table 2.1 (following McBirney and Murase, 1984). The η_m for the rhyolite vary from $4.4x10^6$ Pas to $5.6x10^7$ Pas and for trachyte they vary from $2.3x10^6$ Pas to $3.4x10^5$ Pas. For dolerite the value is $1x10^3$ Pas.

The magma driving pressures (ΔP_e) vary from 20.1 to 66 MPa for rhyolite dikes, 20.1 to 30 MPa for trachyte dikes and 6.6 MPa to 60 MPa for dolerite dikes. The estimated values of ΔP_e for the rhyolite dikes are more than the trachyte dikes, and the dolerite dikes show lowest ΔP_e, except dike 14, which has a higher aspect ratio ($20x10^{-2}$). Estimated propagation velocities for the rhyolite dikes vary from 0.1 m/s to 0.6 m/s and for the trachyte dikes they vary from 0.4 m/s to 1 m/s. The dolerite dikes, however, show the highest propagation velocities, from 25 m/s to 460 m/s. The injection rates dV/dt vary from 1 m^3/s to 10^6 m^3/s (Swanson *et al.*, 1975; Rubin and Pollard, 1987), and the estimated propagation velocities for the dikes of NE-SW dike swarm are in good agreement with known injection rates. The propagation velocities indicate that the rhyolite dikes reached the upper surface at a much slower rate than the dolerite dikes.

The estimated values of stress intensity factor K (strength of the host rock at the tip of a dike) vary from $0.6x10^5$ MPa to $2.6x10^5$ MPa (Table 2.1). Atkinson (1984) has given

experimental measurements of K for sandstones, granites and basalts at one atmosphere pressure. The values of K for sandstone vary from 0.15 to 0.8 MPa $m^{1/2}$; for granites K varies from 0.5 to 1.6 MPa $m^{1/2}$, and for basalts the values are from 1.4-1.9 MPa $m^{1/2}$. Higher estimated values of K for the host rock near Rajula are due to higher confining pressure of the dikes when they were emplaced. Schmidt and Huddle (1977) observed that the values of K for Indiana limestone increased by a factor of four when the confining pressure increased to 62 MPa. The difference in the values of K for the same host rock indicate that the host rock behaved differently for individual dike depending on the aspect ratio of a dike. Figure 2.4 shows that K is higher for these dikes which have higher aspect ratios and irrespective of rock types. The plot between K and the velocity of propagation (Figure 2.5) shows neither positive nor negative correlation. This suggests that the K depends primarily on the aspect ratio of a dike rather than the velocity of propagation.

The extension pressure ΔP_c for the dikes of NE-SW dike swarm vary from 1.1×10^5 MPa $m^{1/2}$ to 5.9×10^5 MPa $m^{1/2}$. The plot between the ΔP_c and the aspect ratios of the dikes (Figure 2.6) shows a positive correlation. The extension pressure increases when there is an increase in the aspect ratio. As a result the ΔP_c for most of the rhyolite dikes is higher than that for the dolerite dikes. However, for some of the trachyte and the rhyolite dikes ΔP_c is similar because it depends on K and ℓ, not on the composition of the magma. The ΔP_c shows a negative corelationship with the velocity of propagation (Figure 2.7). Hence, the rhyolite dikes propagated slowly than the dolerite dikes but shows higher ΔP_c.

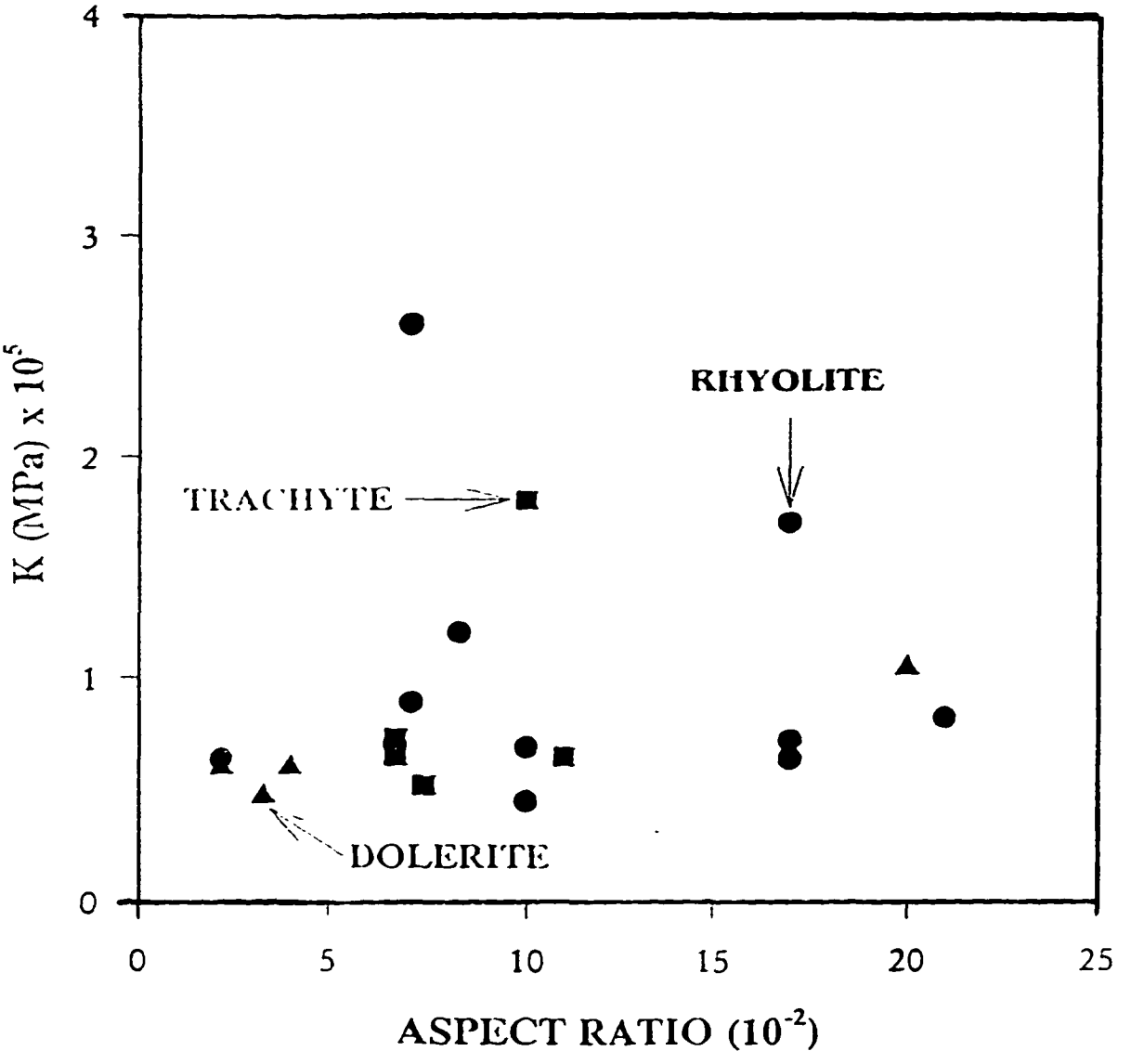

FIGURE 2.4: Variation of stress intensity factor (K) for the host rock with respect to the aspect ratio (a) of the dike. K shows no major variation when there is an increase in the aspect ratio of the dike.

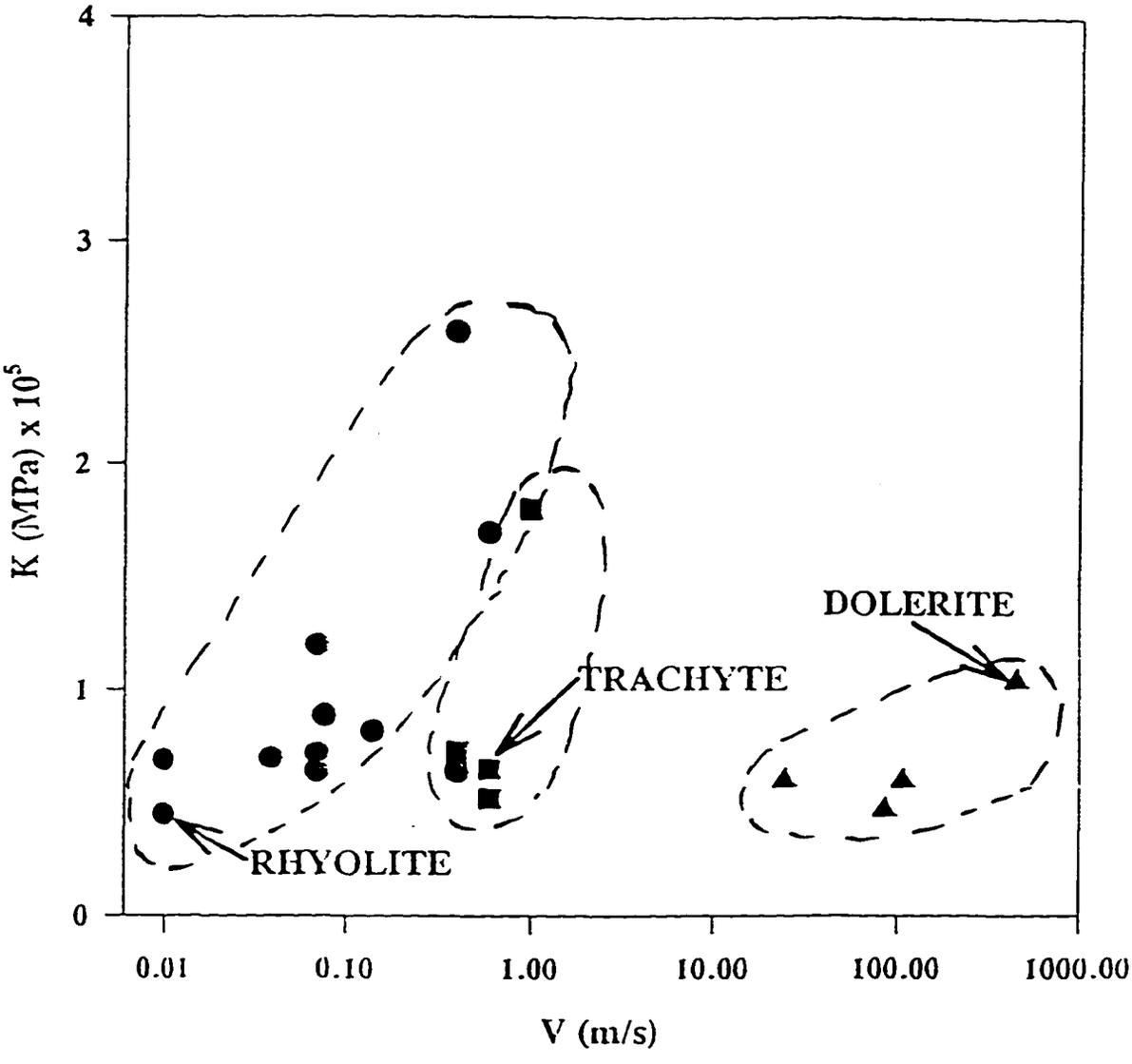

FIGURE 2.5: Plot of stress intensity factor (K) as a function of velocity of propagation (V). K shows no major variation when there is an increase in the velocity of propagation.

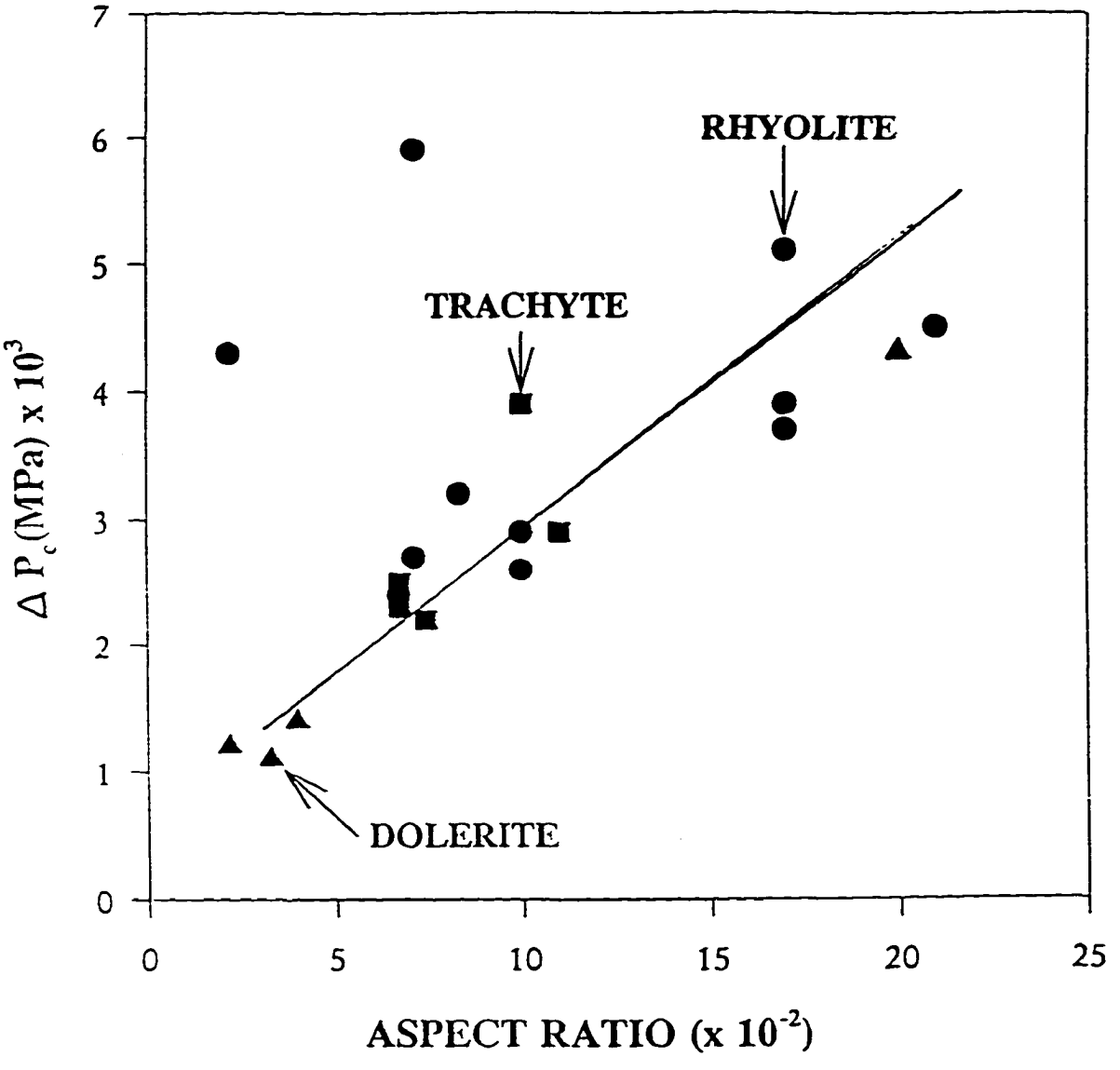

FIGURE 2.6: Extension pressure (ΔP_c) shows a positive correlation with respect to the aspect ratios of the dikes. The minimum value of ΔP_c for dolerite dike with aspect ratio of 3.3×10^{-2} is 1.1×10^3 MPa $m^{1/2}$ and shows a continuous increase to 5.9×10^3 MPa $m^{1/2}$ when the aspect ratio of the dike increases to 7.1×10^{-2}.

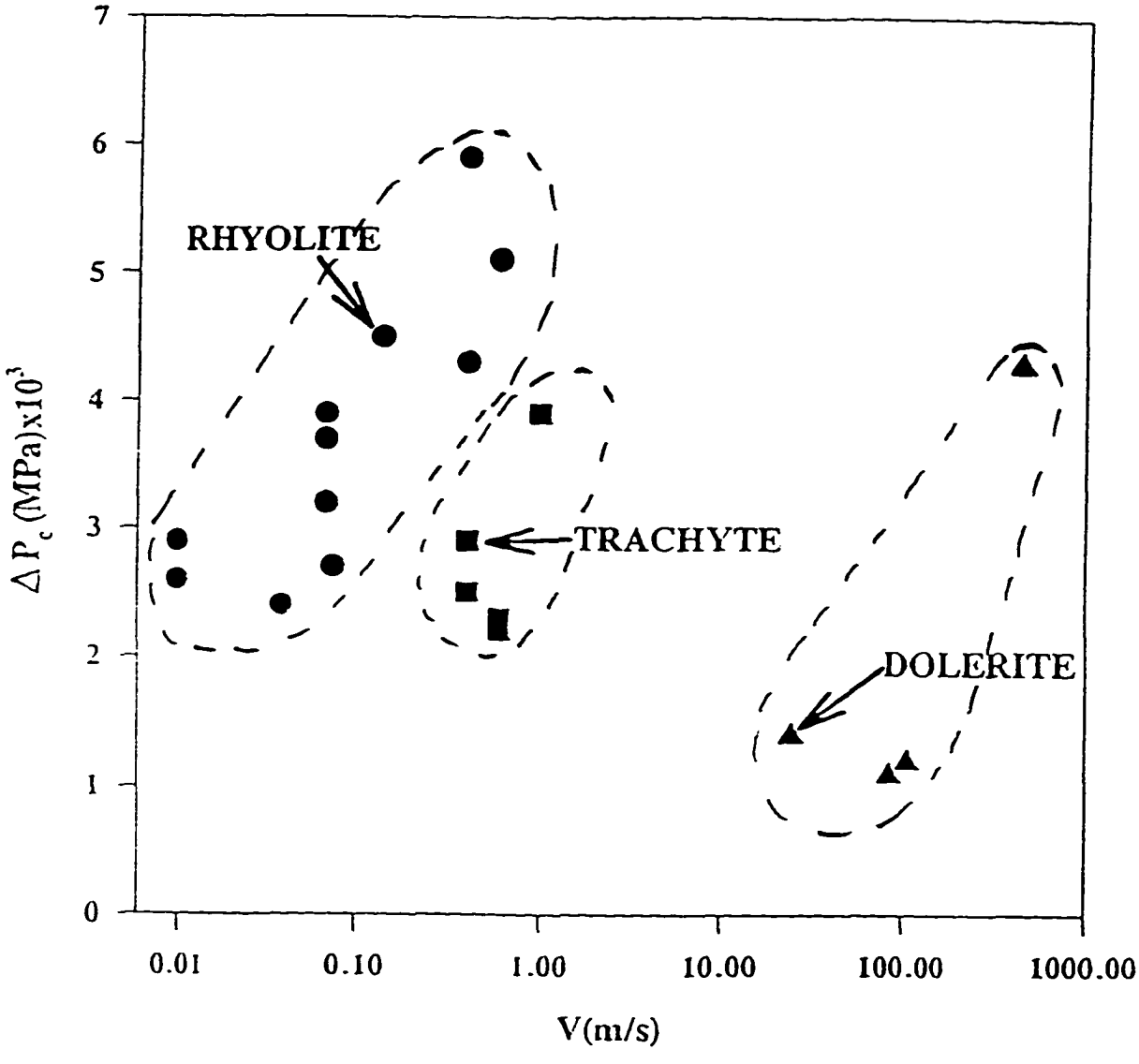

FIGURE 2.7: ΔP_c shows a positive correlation with respect to the velocity of propagation (V).

2.4 ESTIMATED VISCOSITIES OF THE DIKES OF NE-SW DIKE SWARM AND THE BEHAVIOR OF UPPER LITHOSPHERE AT RAJULA:

Recently Rubin (1993a, b) has explored the growth of dikes in visco-elastic medium and calculated the influence of viscosity contrast on the magma transport. According to Rubin (1993a), the dike growth in a visco-elastic medium is governed by the equation:

$$t \approx \Theta \ell \qquad (2.10)$$

where Θ (aspect ratio) is given by the roots of

$$\Theta^3 - (\Delta P_e/G)\Theta^2 - (3\eta_m / 2\eta_r) = 0$$

Here t is thickness and ℓ is length of the dike, ΔP_e is magma driving pressure, G is host rock stiffness ($\mu/(1-\nu)$), where μ is shear modulus, ν is Poisson's ratio, η_m is magma viscosity and η_r is host rock shear viscosity. Two dimensionless parameters, $\Delta P_e/G$ and $3\eta_m / 2\eta_r$ appear in equation 2.10. These two dimensionless ratios govern the mechanism of emplacement of the dikes and the behavior of host rock at the time of their emplacement.

When $\Theta = \Delta P_e/G$, the host rock behaves as a purely elastic medium and the equation is the same as that given by Pollard (1987) and Weertman (1971) who have stated

that the ratio of the average magma driving pressure (i.e. pressure difference between the internal hydrostatic pressure in the dike and the external hydrostatic pressure in the host rock) to the host rock stiffness is approximately equal to the thickness to length ratio (i.e. the "aspect ratio") of the dike when the deformation of the host rock is purely elastic in nature. The results indicate that the dikes with the aspect ratios(Θ values) between 10^{-3} to 10^{-4} require the host rock to be 11 to 14 orders of magnitude higher in viscosity than the magma, therefore leading to the elastic behavior of host rock. The dikes with Θ values less than 10^{-1} require that the host rock deformed predominantly as viscous material.

The aspect ratios (Θ) of the dikes of NE-SW dike swarm are presented in Table 2.1. The aspect ratios for NE-SW trending dikes vary from $2.2x10^{-1}$ to $6.7x10^{-2}$. Dolerite dikes 16, 17 and 18 which trend in NNW-SSE are excluded in the present study as these dikes cut across NE-SW trending dike swarm and are younger in age. When the aspect ratios of the dikes are greater than or equal to 10^{-1} , the host rock is found to behave as a viscous medium. When they are less than 10^{-3}, the host rock behaves as an elastic medium during dikes emplacement. The aspect ratios of the dikes of NE-SW dike swarm are greater than 10^{-3} but less than 10^{-1} . This indicates that the host rock behaved neither as a purely elastic or purely viscous medium but as a visco-elastic medium during their intrusion.

Here I consider purely viscous deformation of the host rock during the intrusion of NE-SW trending dikes in order to estimate the η_r. The governing equation is (Rubin, 1993 a):

$$\Theta \approx (3\eta_m / 2\eta_r)^{1/3} \qquad (2.11).$$

The viscosity of the magma depends on many factors such as temperature, composition, pressure, volatile content, abundance and size of phenocrysts. The viscosities of rhyolite generally vary from 10^4 Pa.s to 10^8 Pa.s, but for some rhyolite the viscosity can be as high as 10^{11} Pa.s (Wickham, 1987). Recently, Wada (1994) has shown that width of a dike is directly proportional to the magma viscosity. His results show that the mafic magmas with viscosities of 10^1 to 10^2 Pa.s form dikes, which are approximately 1 m wide. The mafic (dolerite) dikes in the Rajula area are from 53 to 115 m wide suggesting that its not the width but the aspect ratio is dependent on the magma driving pressure, host rock stiffness and magma viscosity. Equation 2.11 is used to calculate η_r (host rock viscosity i.e. Deccan tholeiitic basalts) for different values of η_m (Table 2.1). Estimated values of η_r for rhyolite vary from 5.4×10^8 to 5.6×10^{10} Pas, for trachyte the values range from 8.4×10^8 to 2.4×10^9 Pas, and for dolerite dikes the value is 1.25×10^5 Pas which are extremely low values. Different values of host rock viscosity for different types of magma suggest that Equation 2.11 is not well constrained for the calculation of η_r. Rubin (1993 a) has shown that the $(\eta_m/\eta_r)^{1/3}$ is not a good approach for the estimation of aspect ratios in a viscous host rock.

Next I considered whether the host rock behaved as purely elastic medium during the intrusion of NE-SW trending dikes and calculated magma driving pressure for individual dike. Kaila *et al.*, (1980) and Kaila (1988) have carried out Deep Seismic Sounding

(DSS) just NW of this area. This DSS profile revealed a 0.9 km to 1.5 km thick crust of the Deccan basalts underlain by Mesozoic sediments with an inferred thickness of ≈0.85 km which are then underlain by crystalline basement with an inferred thickness of ≈3.8 km. The total thickness of the upper crust (the crystalline basement, Mesozoic sediments and the Deccan basalts) NW of Rajula is ≈6.15 km. In order to calculate the magma driving pressures for these dikes (if the host rock behaved as a perfectly elastic medium) we have used equation 2.3. The value of host rock stiffness (G) for the host rock at Rajula is taken as 3 GPa following Rubin and Pollard (1987) and Pollard (1987). Calculated values of ΔP_e for the dikes with the highest aspect ratio (2.2×10^{-1}) is 660 MPa and for the dikes with lowest aspect ratio (6.7×10^{-2}) is 201 MPa. These values are one order of magnitude higher for the magma driving pressures of rhyolite and trachyte dikes. Hence the host rock(s) did not behave as a purely elastic medium at the time of emplacement of NE-SW dike swarm. The estimated η_r for the host rock show very low values, from 1.25×10^5 Pas to 5.6×10^{10} Pas. However, the calculated ΔP_e values for rhyolite, trachyte and dolerite are very high (from 660 MPa to 66 MPa). This indicates that the host rock deformed neither as purely viscous nor as purely elastic material. Hence the host rock(s) behaved as a visco-elastic medium during the intrusion of these differentiated dikes. In order to obtain a better estimate of ΔP_e for these dikes intruding the visco-elastic host rock, the values of estimated ΔP_e are divided by 10 (when we have taken into account purely elastic deformation of the host rock) those are the values presented in Table 2.1.

2.5 DEPTH OF ORIGIN FOR THE DIKES OF NE-SW DIKE SWARM:

An important result of the present study is that the estimated values of ΔP_e for the dikes at the central part of dike swarm are lower (20.1MPa) and show a gradual increase from 30MPa to 51MPa and 62MPa to 66MPa at the outer margin (Figure 2.3). The depth of origin of dikes of a dike swarm can be estimated on the basis of magma driving pressure and the difference between the density of the host rock and the density of magma. This is given by:

$$\Delta P_e = (\rho_r - \rho_m)gz \qquad (2.12)$$

where ρ_r is the density of the host rock, ρ_m is the density of the magma, g is acceleration due to gravity and z is the height above the magma source. Thus the depth of origin using equations 2.3 and 2.12 for the dikes of NE-SW trending dike swarm in Rajula and adjacent areas is given by:

$$z = A(t/\ell) \qquad (2.13)$$

where,

$$A = G/\{(\rho_r - \rho_m)g\}$$

The density of the host rock (Deccan Basalts) is taken as 2.90 gms/cm^3 and the densities of the dike's magma at the time of emplacement is calculated using the method given by McBirney and Murase (1984) and are given in Table 2.1. The depth of origin of each dike is calculated using equation 2.14 and the values are given in Table 2.1. The estimated depth of

origin for the rhyolite dikes with 20.1 MPa magma driving pressure is about 3.2 km, however, the depth of origin for the dolerite dike with 60.0 MPa magma driving pressure is 15.8 km. According to Rubin (1993a) the aspect ratio of a dike is more important than its actual length and width for the estimation of magma driving pressure. Hence, I have assigned only one point at the center of individual dike representing its magma driving pressure at the time of emplacement. In order to draw contours of equal magma driving pressures Minimum Curvature gridding method is used (Briggs, 1974). In this method original data points of ΔP_e are used to generate calculated data points on a regularly spaced grid of 49 lines in N-S and E-W directions where no original data exists (Figure 2.8). Other interpolation schemes used on ΔP_e of the study area for comparison of generated contour diagrams are Inverse distance to a power and Triangulation methods (Davis, 1986; Jones, 1986). Figure 2.9 (A, B) shows the contour diagrams generated by these schemes. Both Figures 2.8 and 2.9 show low magma driving pressure contours at the center and high at the peripheral regions of the map. However, I have applied Minimum curvature method in this entire study because it generates smoothest possible contours while honoring the original data as closely as possible. The depth of origin for the dikes of NE-SW trending dike swarm indicates that the dikes at the central part of the dike swarm originated from a shallower depth than the dikes at the outer margin of the area (Figure 2.8). This observation implies that the shape of the magma chamber from which these dikes have originated is convex upward (i.e. apex of the magma chamber is at a depth of 3.2 km at the central part of the Rajula area and the flanks are at a depth of 15.8 km at the periphery. In order to determine the possible shape of the magma chamber based on the depth of origin of the dikes of NE-SW dike swarm, the points are gridded in the grid size of

FIGURE 2.8: Contour map of upper surface (depth in km) of the magma chamber deduced from the magma driving pressures of the dikes of NE-SW dike swarm in Rajula. Crosses represent center point of each dike. Minimum curvature method on mesh of 49 lines in N-S and E-W directions in used for contouring.

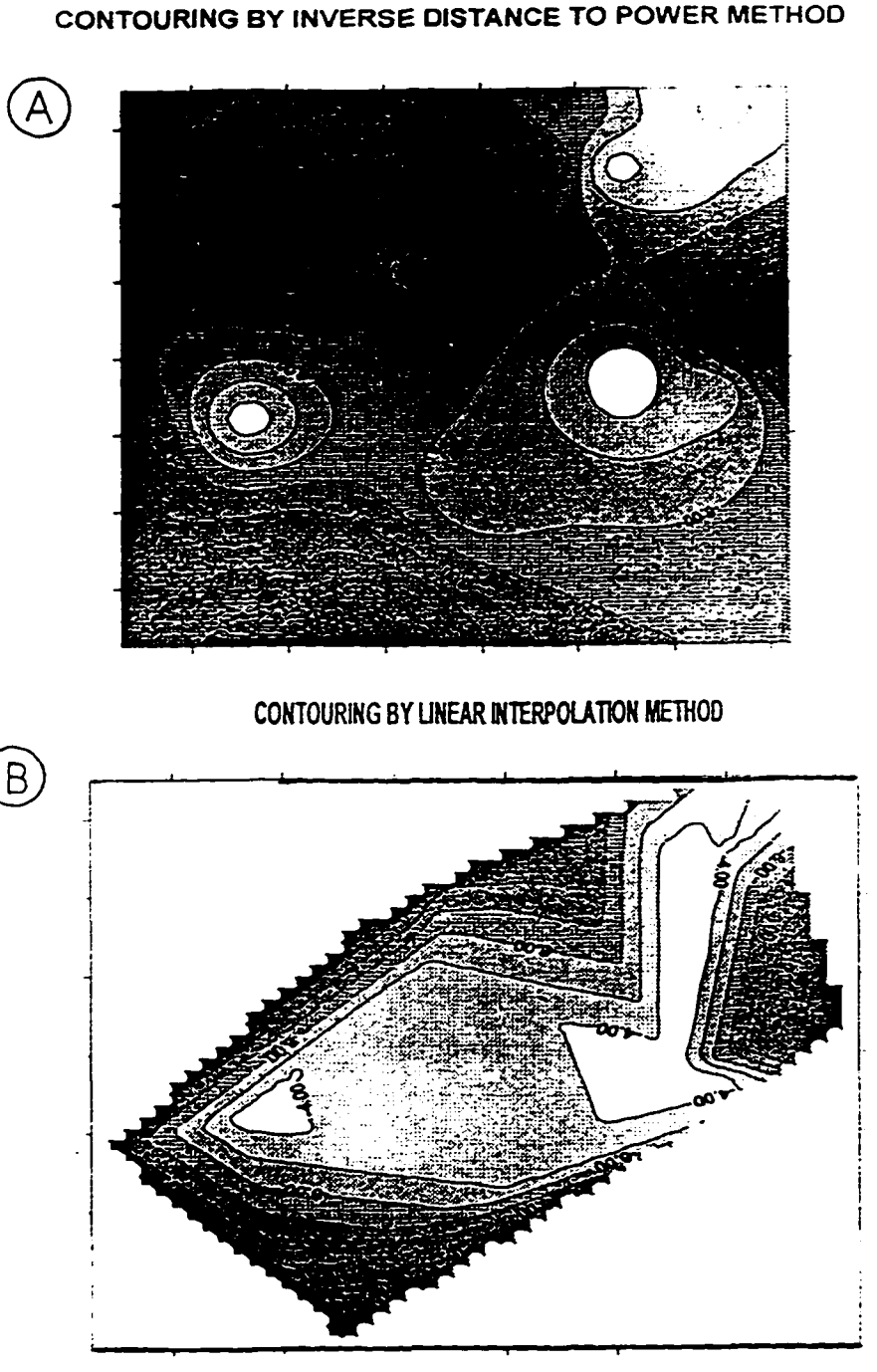

FIGURE 2.9: The contour diagrams of the depth of upper surface of the magma chamber generated by (A) Inverse distance to Power and (B) Triangulation methods. All the schemes of interpolation show lower depth contours at the center and higher depth contours at the peripheral regions.

49x49 in north-south and east-west directions. The search method used to locate the data points of dikes was octant and gridding interpolation method was Minimum Curvature. Figure 2.10 shows the possible shape of the magma chamber as viewed from the SE side at a tilt angle of 30^{0}.

The depth of origin of rhyolite, trachyte and dolerite dikes may be ascertained by plotting them on normative quartz, albite and orthoclase triangular diagram. This is semi-quantitative estimation of most recent pressure of equilibration for rhyolite, trachyte and dolerite dikes. Table 2.2 shows the calculated CIPW norms for the dikes of Rajula area. Figure 2.11 shows that the estimated depth of equilibration for rhyolite and trachyte (black squares, < 5 kbar) is upper crust and for dolerite dikes (black circles, 4 to 10 kbar) varies from middle to lower crust. This also suggest that the rhyolite and trachyte dikes originated from shallower depth and dolerite from slightly deeper parts of crust (magma chamber).

2.6 TWO AND THREE DIMENSIONAL GRAVITY MODELLING ALONG RAJULA:

The presence of high density rocks below the Deccan basalts has been inferred on the basis of Bouguer gravity anomalies in Rajula area. The Bouguer gravity anomaly data for Rajula area was compiled by Kaila (1988). This area lies on top of a NE-SW extended +40 mGal Bouguer gravity anomaly. In order to estimate the possible shape of the high density mafic body beneath the Rajula area, I have used Kaila's (1988) data. To determine the crustal structure in this area I used the results of Deep Seismic Sounding (DSS) profile of

FIGURE 2.10: Possible shape of a magma chamber on the basis of ΔP as viewed from southeast direction.

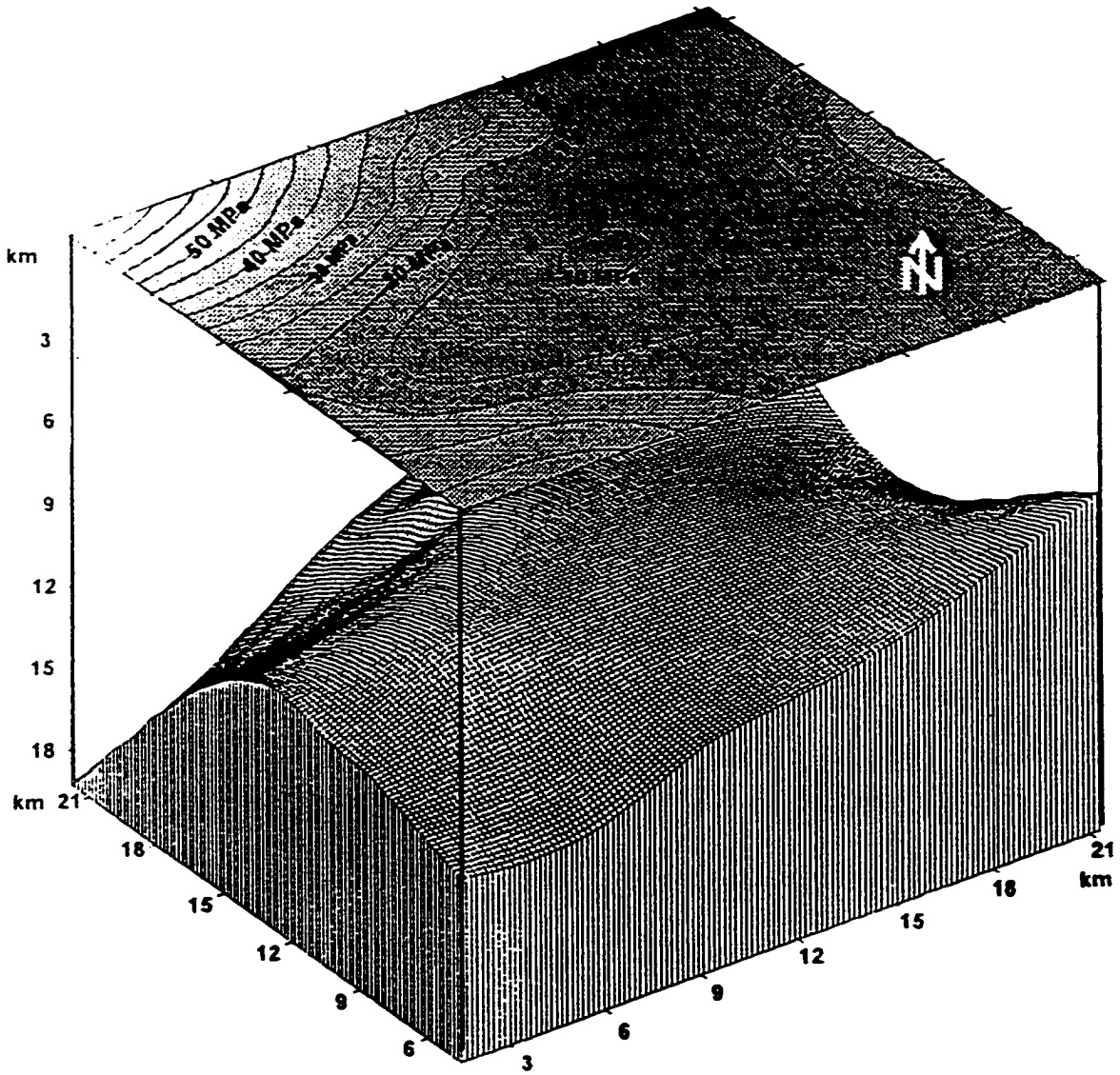

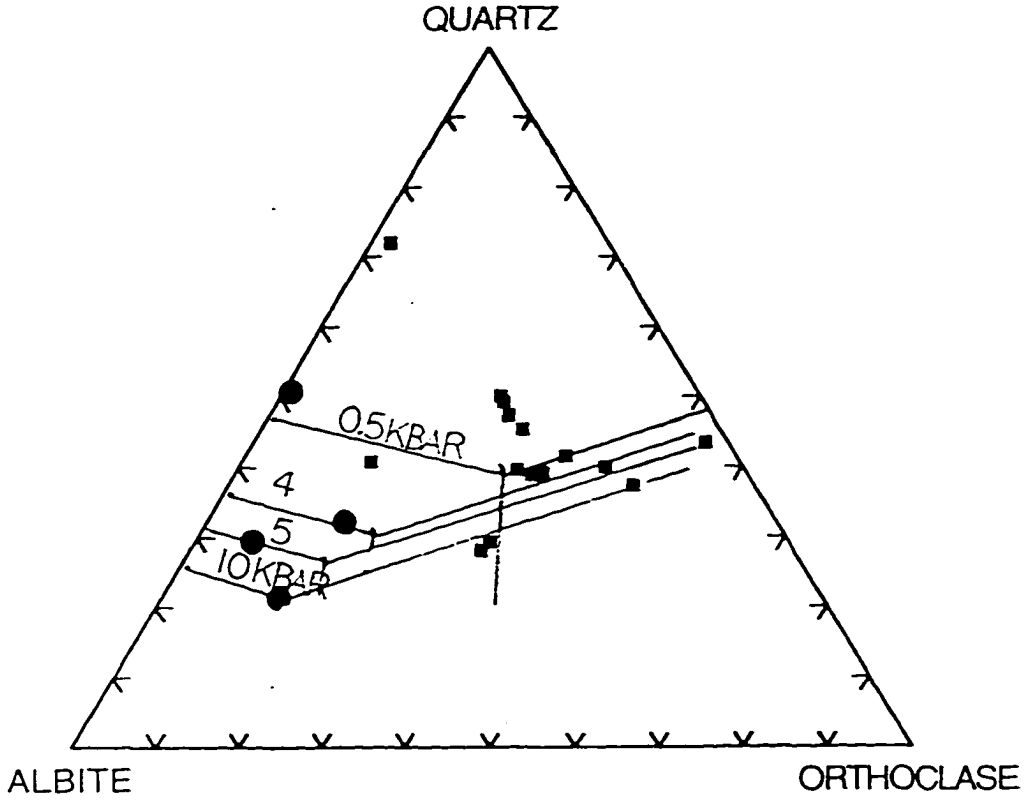

FIGURE 2.11: Normative quartz, albite and orthoclase triangular diagram with pressure contours (after Winkler, 1979). The rhyolite and trachyte (solid squares) plot at significantly lower pressure than dolerite and basalts (solid circles).

Kaila *et al.*, (1980) for NW part of Rajula. The E-W extended profile shows the 5.5 km/s P_v for the Deccan Traps and its thickness vary from 1.5 km on the western part to around 400 m on the eastern part of the profile. The Mesozoic sediments (P_v, 4.4 km/s) below the Deccan Traps are around 850 m thick on the western part, decreasing to 200 m on the eastern side of the profile. The western part of the profile is marked by +40 mGal Bouguer gravity anomaly, which decreases to -20 mGal on the eastern side. Figure 2.12 shows the observed (solid circles) and theoretically calculated (continuous curve) gravity anomaly along the profile. The calculated gravity anomaly due to the combined effect of Deccan Traps and Mesozoic sediments does not provide the observed +40 mGal anomaly. However, the observed and calculated anomalies match well if a high density mafic body with 2960 kg/m^3 density is assumed to be present at a depth of 6km. The estimated width of this mafic body is 16 ± 1.6 km and 30 ± 3 km at the top and bottom with a thickness of 12 ± 1.2 km.

Figure 2.13 shows the two dimensional observed and theoretically calculated gravity anomaly along A-B over Rajula. The best fit of the observed and calculated anomalies is obtained when a convex shaped mafic body with an excess mass is considered to have emplaced at a depth of 6 ± 0.6 km. The average density of this mafic body is 2950 kg/m^3 suggesting a gabbroic type lithology. By considering the depth of the mafic body at 6 ± 0.6 km and the thickness of 14 ± 1.4 km, we have carried out the three dimensional gravity modelling of the mafic body. Initial top and bottom depths of the mafic body responsible for the gravity high of +40 mGal are taken as 3 ± 0.3 km and 8 ± 0.8 km, respectively. Figure 2.14 shows the probable three dimensional shape of the magma body determined by three dimensional gravity

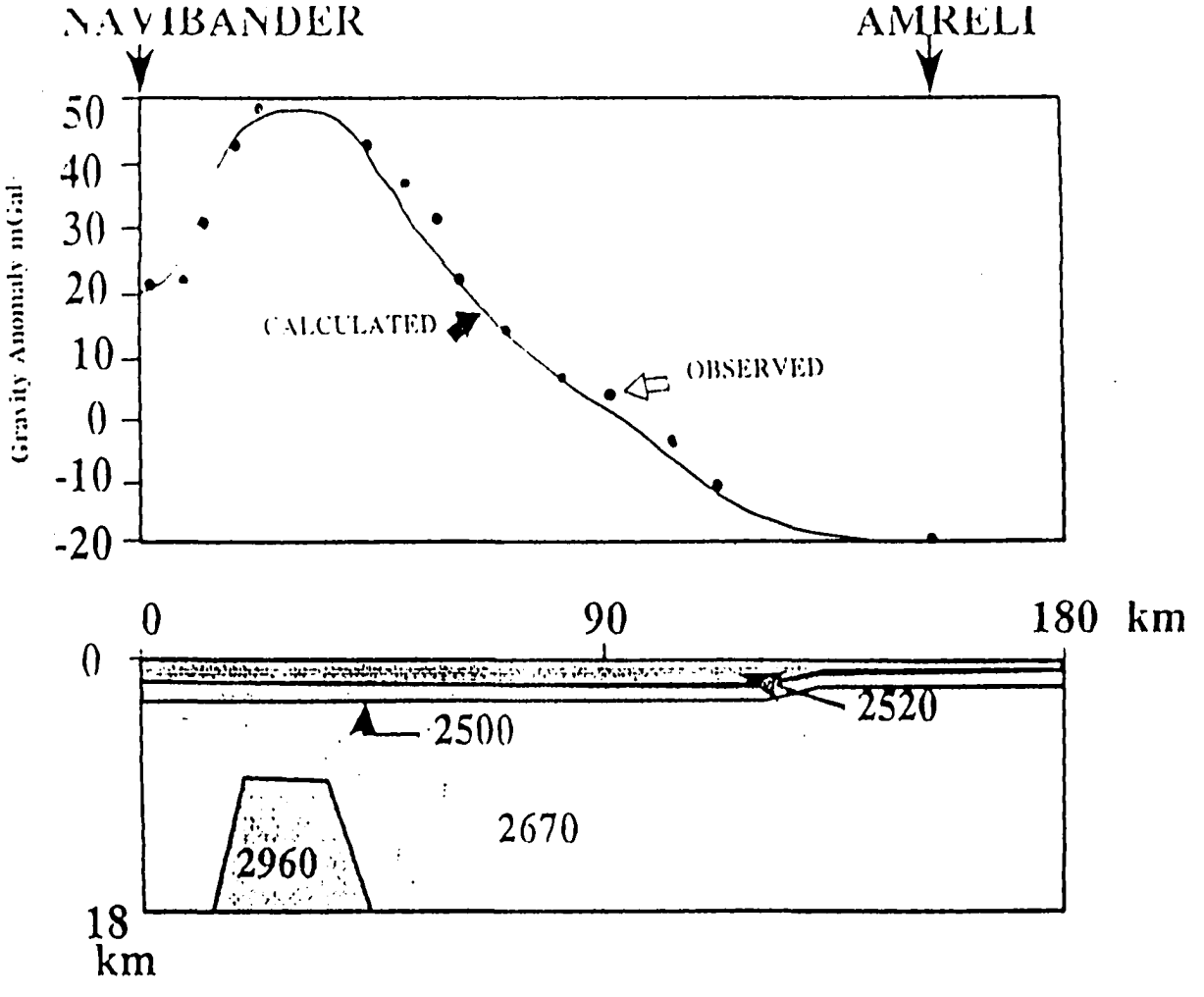

FIGURE 2.12: Observed and theoretically calculated gravity anomalies along the Navibander-Amreli profile (Figure 1.2). Calculated and observed anomalies match well when a mafic body is assumed at a depth of $6 \pm .6$ km with the density of 2.96 gm/cm^3. Estimated widths of the mafic body are 16 ± 1.6 km and 30 ± 3 km at the top and bottom and thickness is 12 ± 1.2 km.

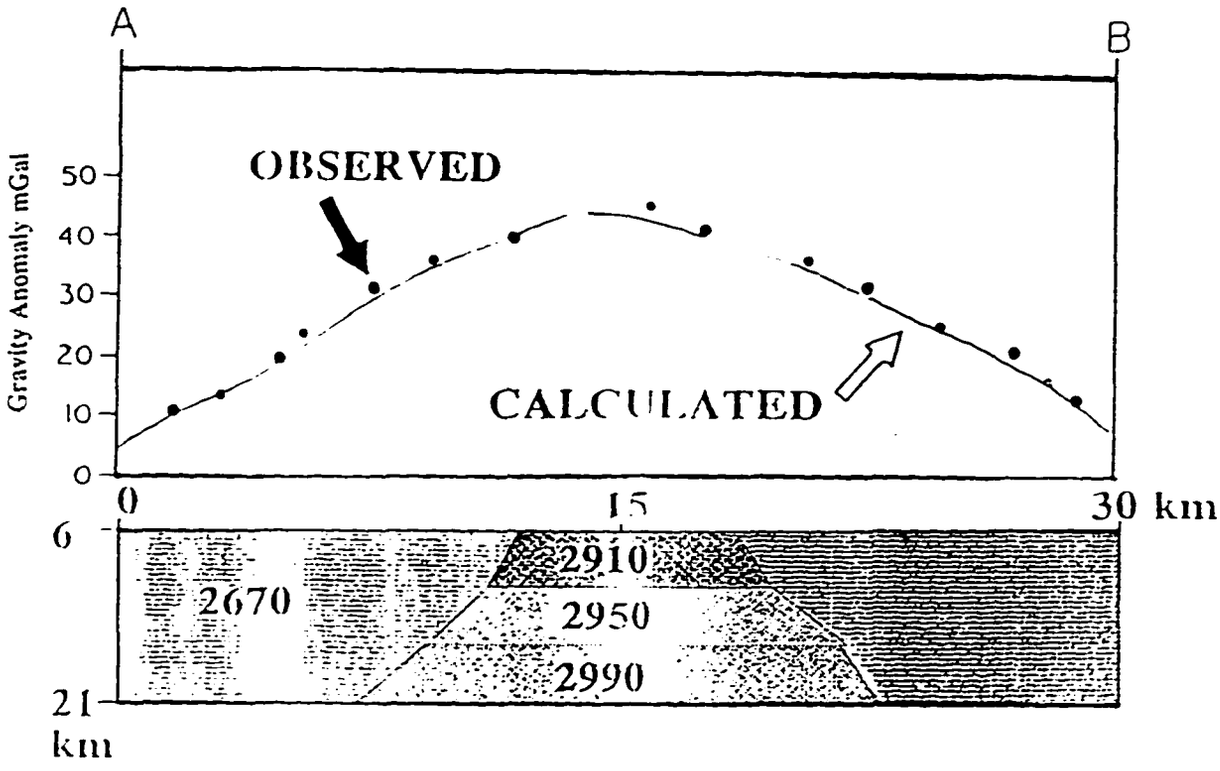

FIGURE 2.13: Observed and calculated gravity anomalies at Rajula. The crustal structure beneath Rajula is considered similar to that encountered along the Navibander-Amreli profile. Calculated and observed anomalies match well with a high density mafic body at a depth of 6 ± 0.6 km.

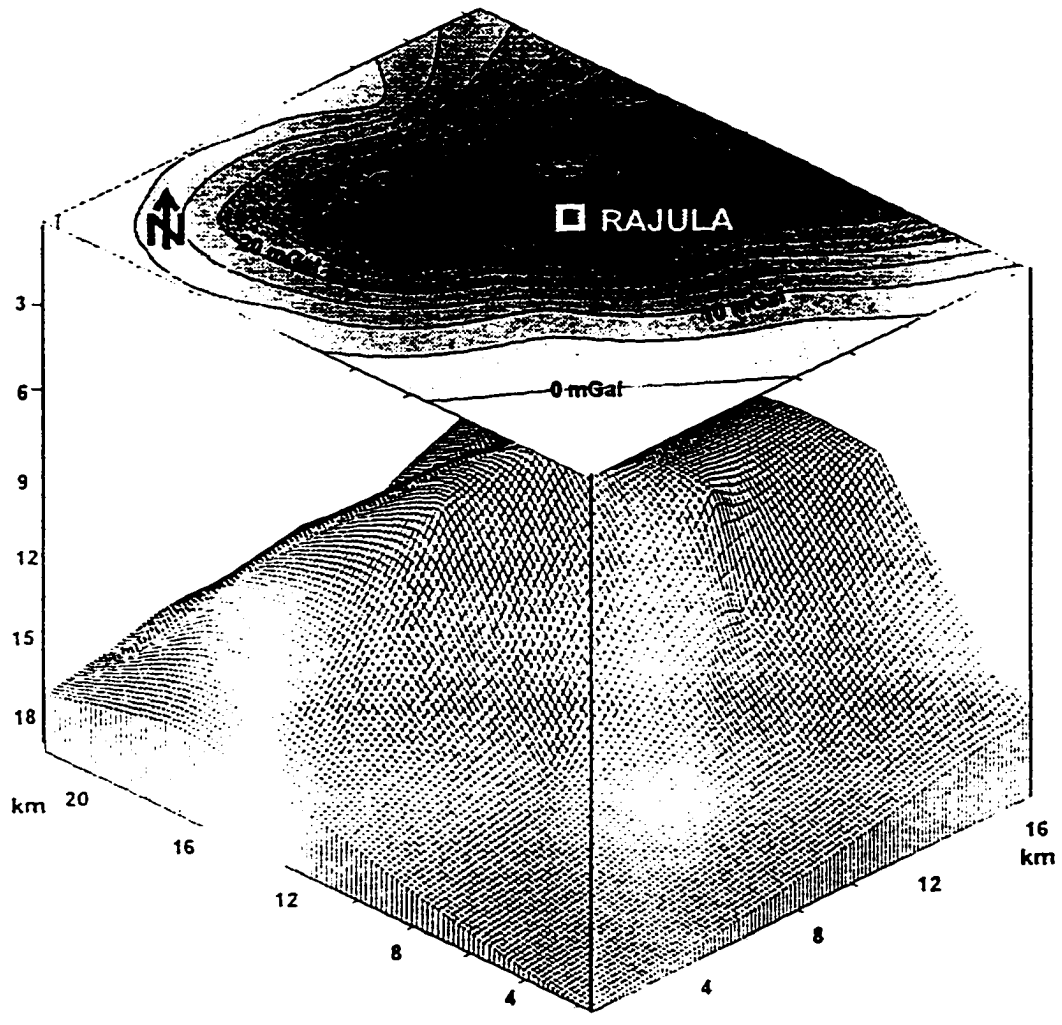

FIGURE 2.14: The shape of the magma chamber as deduced from the positive Bouguer gravity anomaly. Positive gravity anomaly data points are gridded in grid size of 49x49 in north-south and east-west directions, Minimum Curvature is the gridding interpolation algorithm which is used in this study.

modelling. The positive anomaly data points are gridded in the grid of 49x49 in N-S and E-W directions and an average density of the mafic body is considered as 2950 kg/m^3. The octant search method is used to locate the data points and for gridding interpolation we have used the minimum curvature algorithm (Briggs, 1974). The most probable shape of a magma chamber as deduced from ΔP and Bouguer gravity anomaly data is convexly upward beneath Rajula area. This is the possible source of NE-SW dike swarm.

2.7 CONVECTIVE FRACTIONATION AND ZONING IN MAGMA CHAMBER:

According to Hamilton (1988), Clemens and Mawer (1992), and Petford *et al.*, (1993) the zone of lateral extension of the crust is an ideal location for the emplacement of magmatic bodies. However, the main objection to this model is that the extension rates are too slow and slip magnitudes are too small to form a magma chamber at most of the places in the upper crust. Recently, Hanson and Glazmer (1995) have estimated the time and thermal requirements for a steady state magma chamber formation in the upper crust. Their results indicate that the chambers at a depth of 8km can form within 9,000 years at an extension rate of 4 cm/yr. High temperature required to form magma chambers can be maintained even at a rate of 1 cm/yr.

The estimated thickness of the magma(fluid) in convexly upward magma chamber in Rajula is around 12.6 km (thickness here is the difference between the apex and the bottom of the walls of the magma chamber). We have calculated the range of the heat flux

from the magma chamber after its emplacement at its present position as it controls the rate of crystallization. compositional and thermal convection. Knapp and Norton (1981) have suggested that the steep horizontal thermal gradients along the margins of a magma chamber could develop thermal stresses of significant magnitude to fracture the country rock. We have shown earlier that magma can propagate laterally along the hydraulic fractures and form dikes. The cooling time of a magma chamber from liquidus to solidus depends on the depth of emplacement of magma chamber, size of the magma chamber and the local geothermal gradient of the region (Spera, 1980 and Spera *et al.*, 1982). Other factors which may influence the cooling time are volatile content, initial crystal content, composition of the magma and the hydrothermal system surrounding the magma chamber.

The type of convection (compositional versus thermal) in a magma chamber is controlled by the viscosity of the magma, processes at the boundary which produce lighter or denser fluid than that in the interior of the chamber and the shape and size of the chamber (Turner and Campbell, 1986). The density contrast ($\Delta\rho$) between the fluid in the interior of a magma chamber and the fluid along the roof and side walls determines the initial motion (Turner and Campbell, 1986). $\Delta\rho$ may develop due to temperature differences or due to compositional changes resulting from crystallization or melting of the wall rock. Turner and Campbell (1986) have shown that compositional convection generally dominates over thermal convection.

Turner and Campbell (1986) and Huppert *et al.*, (1986) have studied the influence

of magma chamber geometry on compositional convection. Experiments of Huppert *et al.*, (1986) reveal that when a flux of light fluid is released in a convexly upward magma chamber due to crystallization or melting, it flows upward along the sides of the magma chamber and the dense residual fluid moves downward parallel to the slope and some of the dense fluid separates from the boundary layer and mix with the fluid of underlying region. As a result, stable stratification at the apex of the magma chamber is produced. In their experiments the buoyant low density stratified layer at the top was separated by a sharp horizontal interface from the lower well mixed layer of denser fluid. The shape of magma chamber from which the dikes of NE-SW trending dike swarm originated is also proposed to be convexly upward. Figure 2.15 shows the shape of the magma chamber along sections X-Y and A-B of Figure 2.8. Here the dikes along sections X-Y and A-B are projected downward to the magma chamber. Figure 2.15 shows that the upper part of the magma chamber was filled by the rhyolitic magma underlain by the trachytic magma. The thicknesses of the inferred rhyolitic magma at the top of magma chamber along sections X-Y and A-B are 1.1 km and 1.7 km respectively. The difference in the thickness of rhyolitic magma along the sections X-Y and A-B can be explained on the basis of different shapes of the magma chamber. Along the section A-B, walls of the magma chamber are steeper than along section X-Y. Less denser fluids (rhyolite and trachyte) were released due to crystallization of more denser components (olivine and/or pyroxene) which convected upward and formed layers at the apex of the magma chamber. This resulted as the walls of the magma chamber along section A-B are steeper and close to each other relative to the walls of the chamber along section X-Y. This gave rise to the formation of thick rhyolite layer along A-B. Normally, continuous and

FIGURE 2.15

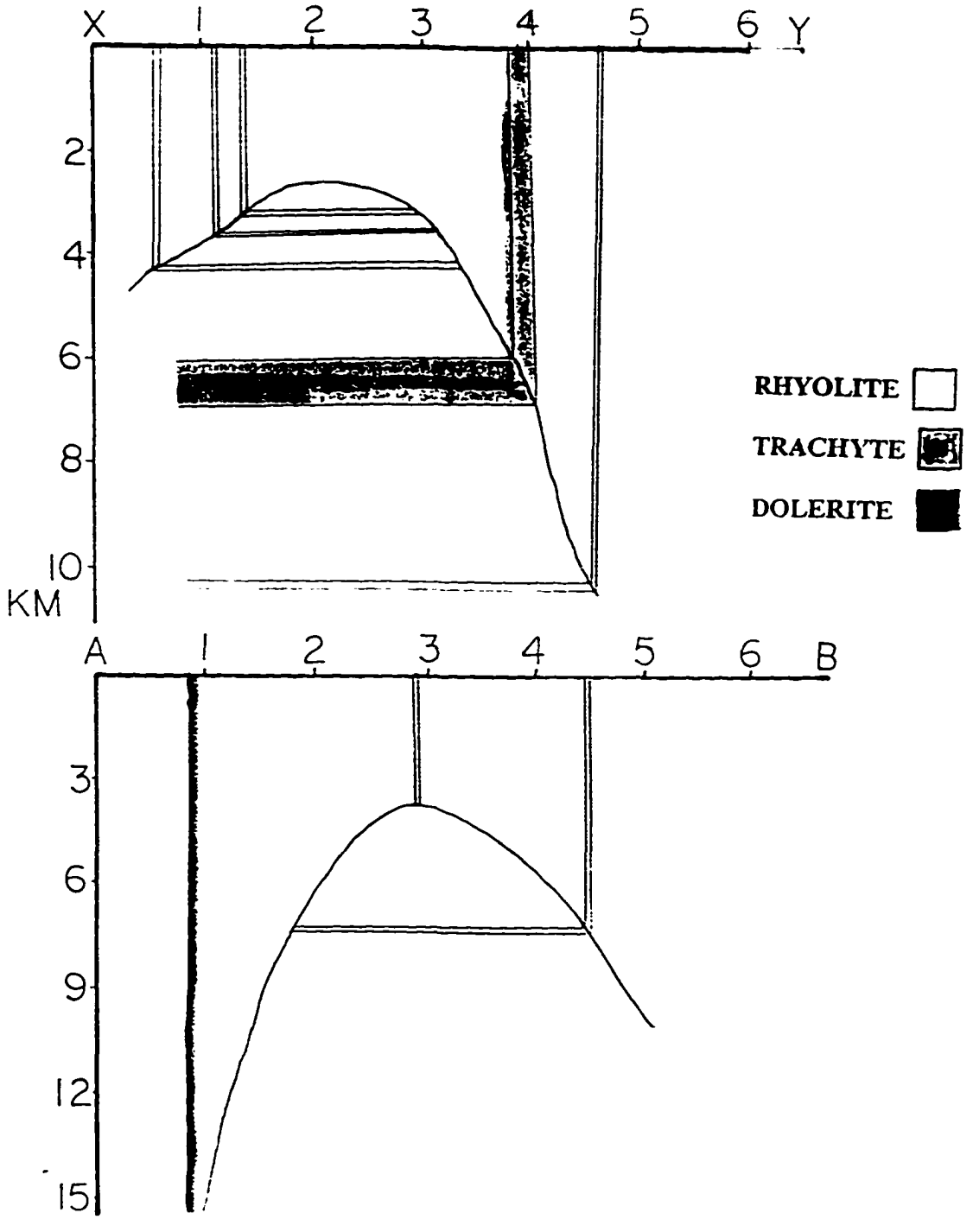

stepwise zonings can be formed due to compositional convection in a magma chamber. In a continuously zoned magma chamber no drastic compositional and/or phenocrysts size gradients occur between the adjacent layers (i.e. the layers in the magma chamber show a continuous compositional and/or phenocrysts size gradients in a magma chamber). However, in a stepwise zoned magma chamber drastic compositional gap and/or change in phenocrysts size occurs between each layer in a magma chamber. This study, (Sharma and Bhattcharji, 1993,1994), suggests that the magma chamber beneath Rajula was continuously zoned. Zoned magma chambers have been reported from other areas by Bailey *et al.*, (1976), Hildreth (1981) , and Ritchey (1980).

I have examined whether the zoning in Rajula magma chamber was largely due to compositional convection or by thermal convection. The compositional convection often dominates over the thermal convection (Turner and Campbell, 1986). The compositional Rayleigh number (Rs) is calculated using equation 2.14 of Martin *et al.*, (1987):

$$R_s = \frac{g \beta \Delta S h^3}{\epsilon \kappa_s} \qquad (2.14)$$

where g is acceleration due to gravity, β is compositional expansion coefficient, κ_s is diffusivity of solute in magma, h is the thickness of the fluid (the difference in height between

the apex and the bottom of the walls of the magma chamber), k_s is the diffusivity of solute in magma, ϵ is the kinematic viscosity and ΔS is the change in melt composition. The value of κ_S is taken as 10^{-10} m^2s^{-1} and using method described by Lange and Carmichael (1990) β is calculated as 2.92×10^{-2}. The value of ϵ is taken as $10^{-5}m^2s^{-1}$ (Martin *et al.*, 1987) and h is 12.6×10^3m depth of the magma from the apex to the bottom of the walls of the magma chamber beneath Rajula area. Using these assumed values the estimated compositional Rayleigh number for the magma chamber is $\approx 5.7 \times 10^{26}$ ΔS. The mass flux Rayleigh number (Rs_f) due to crystallization of the heavier components (olivine and/or pyroxene) was calculated using the equation:

$$Rs_f = \frac{g \beta f h^4}{\epsilon \kappa_s^2} \qquad (2.15)$$

where f is the mass flux of the magma due to crystallization of heavier components. Calculated Rs_f number for the magma chamber beneath Rajula is $\approx 2.5 \times 10^{40} f$. Very high values of Rs and Rs_f suggest that the convection due to compositionally induced buoyancy was dominant and responsible primarily for the zoning of magma chamber.

The thermal Rayleigh Number is calculated based on the equation (Martin *et al.*,1987):

$$Ra = \frac{g \alpha \Delta T h^3}{\epsilon \kappa_T} \qquad (2.16)$$

where g is acceleration due to gravity, α is thermal expansion coefficient, ΔT is drop in temperature across the chamber, h is the height of the chamber or the depth of fluid, ϵ is kinematic viscosity of the magma and κ_T is diffusivity of heat in magma. Martin *et al.*, (1987) calculated the value of α for the Bushveld magma based on the data of Irvine *et al.*, (1983) as $5.46 \times 10^{-5}\ ^0C^{-1}$ and according to Turcotte and Schubert (1982) for the silicic magma the value of α is generally 1.5 times higher than the basaltic magma. Calculated value of α for the magma chamber beneath Rajula is $8.24 \times 10^{-5}\ ^0C^{-1}$. The value of g is taken as 9.8 ms^{-2}, κ_T as $8 \times 10^{-7}\ m^2s^{-1}$ and h is 12.6×10^3 m. The value of ϵ for the silicic magma chamber is around $10^5\ m^2s^{-1}$ (Martin *et al.*, 1987). Estimated thermal Rayleigh number for the magma is $1.1 \times 10^9\ \Delta T$. Figure 2.16 shows the plot between the thermal Rayleigh number and the magma chamber thickness for rapidly cooled chambers (broken lines) and slowly cooled chambers (solid lines) following Martin *et al.*, (1987). The values of kinematic viscosity are taken as 10^{-3}, 10^{-1}, 10^2 and 10^5 respectively. The area in the vertically shaded region in Figure 2.16 is for mafic intrusions and horizontally shaded region is for granitic intrusions. The solid hexagon represents the position of estimated thermal Rayleigh number when ΔT is taken as 200^0C

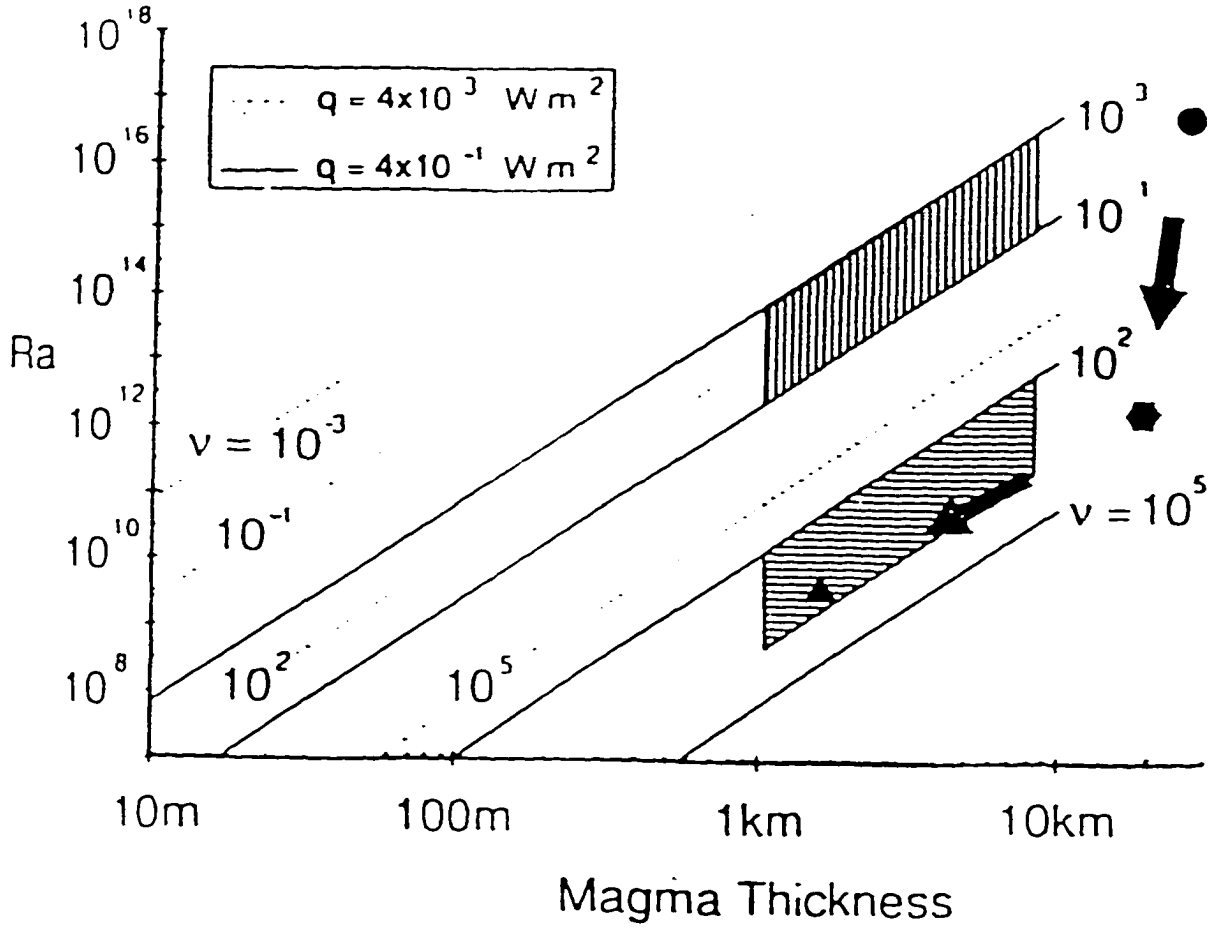

FIGURE 2.16: A plot between thermal Rayleigh numbers (Ra) and thickness of magma (h). Here, ν is kinematic viscosity, solid and broken lines are for slowly and rapidly cooled magma chambers. The position of Ra of Rajula magma chamber (hexagon), rhyolite layer at the apex of the magma chamber (triangle) and the mafic type magma from which the rhyolite and trachyte magmas were produced (circle) beneath Rajula . Vertically shaded box is for slowly cooled mafic magma chambers and horizontally shaded box for slowly cooled granitic magma chambers . Arrows show how Ra decreased as the magma chamber cooled.

(Spera *et al.*, 1986) for slowly cooled magma chamber beneath Rajula. According to Chen and Turner (1980), Turner (1980) and Turner and Campbell (1986), the transition from laminar to turbulent flow takes place when the $Ra \geq 10^6$. This suggests that the convection was highly turbulent even if the drop in temperature across the chamber was low. As mentioned earlier, the magma chamber beneath Rajula area was zoned. The apex of the magma chamber was occupied by the rhyolite magma (Figure 2.15) with an average thickness around 1.4 km. The estimated thermal Rayleigh number for the rhyolite layer is $10^8 \Delta T$ (here ΔT is considered as 200 ^oC) and this is plotted as triangle in Figure 2.16. According to Williams and McBirney (1979), Wikham (1987), and Martin *et al.*, (1987) the first appearance of the rhyolitic and trachytic magmas occur when the total mass of the magma remain constitute around 30% of the initial magma and the first appearance of the mafic magma occurs when the remaining magma is ≈90% of the initial magma (i.e. the mafic magma produced from the source magma is ≈60%). Hence, if total volume of rhyolite and trachyte magmas is known then the initial volume (and/or mass) of the mafic magma can be estimated. As total thickness of magma in the magma chamber beneath Rajula was around 12.6 km, the minimum depth of mafic magma from which rhyolitic and trachytic magmas were fractionated should be at least around 25.2 km. Substituting $h = 25.2 \times 10^3$ m in equation 2.16 and values of rest of the parameters as used before on obtain the thermal Rayleigh number as around 10^{16} for the mafic magma. This is represented by a solid circle in Figure 2.16. When magma cools, the intensity of thermal and compositional convection decreases continuously until the magma chamber is solidified. Arrows in Figure 2.16 indicate how the thermal Rayleigh number decreased as the magma cooled in the magma chamber.

The thermal convection depends on the heat flux through the boundaries of the magma in a magma chamber. The thermal Rayleigh number based on the heat flux is calculated using Martin *et al.*, 1987 equation:

$$Ra_f = \frac{g \alpha q h}{\epsilon \kappa^2 \rho C_p} \qquad (2.17)$$

where q is the heat flux out of magma chamber, C_p is specific heat capacity and ρ is the density of the magma at its liquidus. The thermal flux Rayleigh number is calculated for the kinematic viscosity of 10^5 m^2s^{-1} for the heat flux $4x10^3$ Wm^{-2} (Carlsaw and Jaeger, 1959; Huppert and Sparks, 1980).Best estimated value of Ra_f for the magma chamber beneath Rajula is $9x10^{16}$ (for $\epsilon=10^5$ m^2s^{-1} and $q=4x10^3$ Wm^{-2}). In the present case the rate of cooling can be defined by two factors. They are: (i) the rate of heat loss out of the magma chamber through time and (ii) the rate of release(increase) of latent heat due to crystallization of heavier component like olivine and/or pyroxene.

The ratio between the total heat flux from the magma chamber to the heat flux only due to conduction provides efficiency with which a magma transports heat by convection. This ratio of actual heat flux from the magma chamber in the absence of convection is given by the Nusselt number (Nu). The Nusselt number is calculated using the

equation:

$$Nu = \frac{q\,h}{\kappa_f \rho\, C_p \Delta T} = \frac{Ra_f}{Ra} \qquad (2.18)$$

The Nusselt number for the magma chamber beneath Rajula is $8.1 \times 10^7/\Delta T$ when we consider the value of heat flux as $4 \times 10^5/\Delta T$ Wm^{-2}. This high value of Nu for Rajula magma chamber indicates that the heat loss from the magma chamber was extremely high as a result of conduction through host rock as well as turbulent convection of magma.

2.8 DISCUSSION

Although the analyses presented above are based on the measurements of NE-SW trending dike swarm in the Rajula area, they can be applied to other dike swarm(s) elsewhere. An important conclusion of the present analysis is that in an area where each dike of a dike swarm has created its own fracture into a single host rock by hydraulic fracturing it is possible to infer the shape of the magma chamber from which these dikes originated. This study also indicates that the magma driving pressure for the dikes of a dike swarm will show a systematic variation depending upon the shape of the magma chamber. For example, when the magma driving pressure for the dikes at the peripheral part of a dike swarm have lower

values than the dikes at the central part, then the magma chamber should be concave upward. However, when the values of magma driving pressure for the dikes at the central part are lower than the dikes at the outer margin of a dike swarm then the magma chamber should be convexly upward shape as shown in the present study. Irregularities in the shape of the magma chamber will be reflected in the form of irregular distribution of ΔP of dikes originated from the magma chamber.

We conclude that (i) the rhyolite, trachyte and dolerite dikes of NE-SW dike swarm in Deccan volcanic province, western India made their own hydraulic fractures; (ii) the host rock behaved visco-elastically at the time of emplacement of dikes; (iii) the projections of dikes on the surface of magma chamber indicate that the upper part was filled by the rhyolitic magma which was underlained by the trachytic magma, and thus showing zoning of the Rajula magma chamber; (iv) the crystallization of olivine and/or pyroxene (the dense medium) along the sides of convex shape magma chamber was responsible for the upward migration and accumulation of rhyolite and trachyte at the apex; (v) compositional Rayleigh number and compositional flux Rayleigh numbers suggest that the convection was driven by the crystallization of heavier components hence compositional convection was dominant over the thermal convection; and (vi) zoning of magma chamber is the result of compositional convection.

CHAPTER 3

TWO AND THREE DIMENSIONAL GRAVITY MODELLING ALONG WESTERN CONTINENTAL MARGIN AND NARMADA-TAPTI RIFTS, DECCAN VOLCANICS, INDIA

3.1 INTRODUCTION:

The western and central parts of peninsular India are demarcated by a complex pattern of gravity anomalies exhibiting lateral variations in density at different depths (Thakur *et al.*, 1993). Qureshi (1981) analyzed the regional tectonics of western and central India from the Bouguer gravity anomaly map of the Indian sub-continent. Mishra (1977) on the basis of regional Bouguer gravity and air-borne magnetic anomalies suggested possible extension of the intraplate Narmada-Tapti rift on the peninsular Indian lithosphere crossing the western continental margin rift beyond the Cambay bay towards the Arabian sea and to the eastern syntaxial bend of the Himalayas.

More recently, Kaila (1988) has compiled Bouguer gravity data and presented a detailed gravity anomaly map of the western and central parts of India covered mainly by Deccan flood basalts (Figure 3.1 A,B,C). A prominent positive gravity anomaly of 70 mGal extending in N-S direction, from Surat to Bombay along the west coast of India (Figure 3.1A).

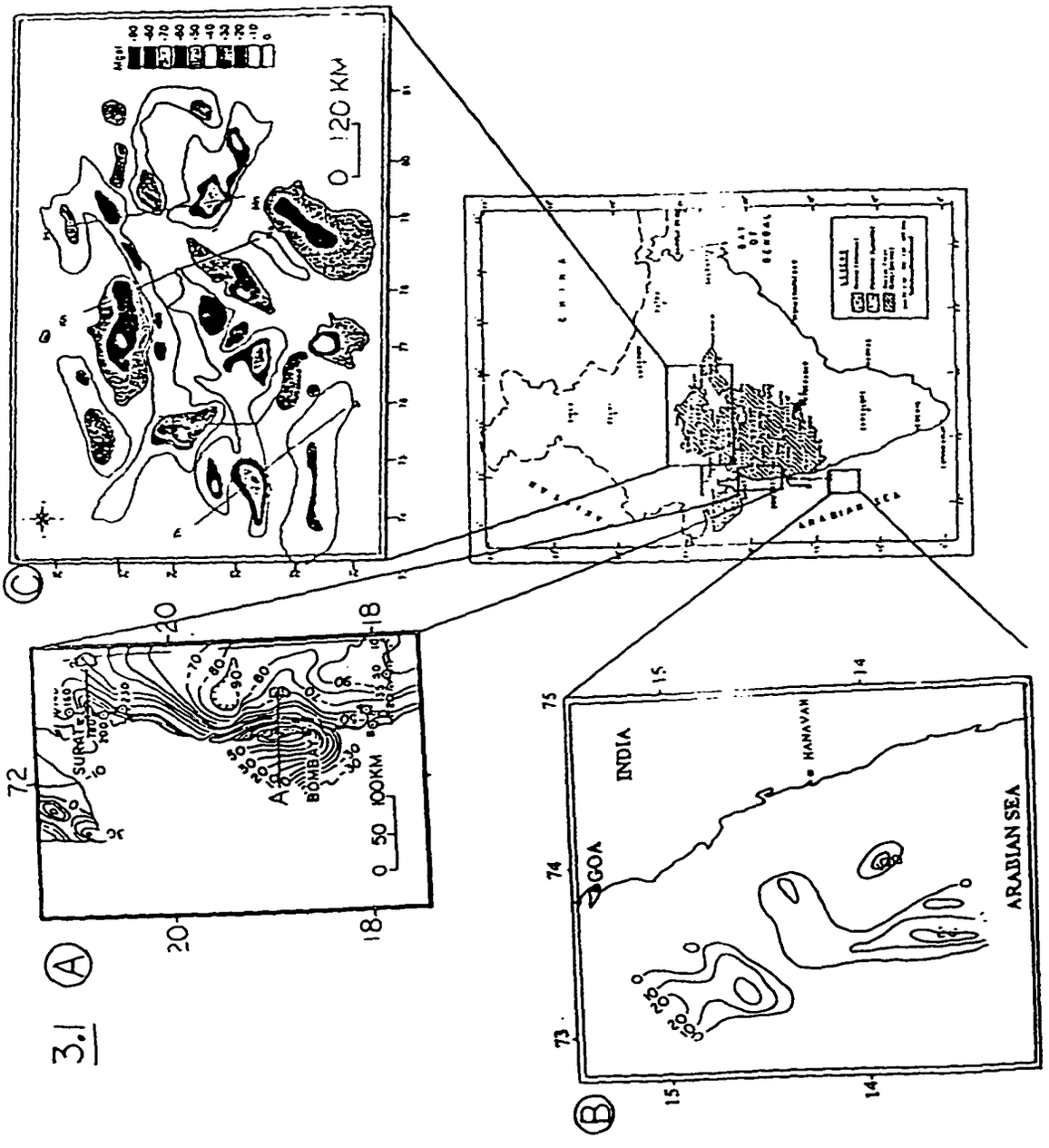

3.1

Rest of the peninsular India covered by the Deccan Traps is characterized by negative gravity anomalies (from -10 mGal to -110 mGal). The lowest gravity anomaly of -110 mGal is encountered around 19°N and 74°E. An important feature of the Bouguer gravity anomaly pattern for the west coast of India is the presence of a number of gravity "highs" and "lows" in sequence. Detailed analysis of regional gravity data of peninsular India by Kailasam *et al.*, (1972) indicates that the anomalies are not related to various thickness of high density Deccan basalts. He interpreted that the "lows" are the manifestation of the sedimentary basins underneath the Deccan Traps and the N-S extending gravity highs represent a prominent deep seated structural feature under the Deccan Traps largely submerged in the Arabian sea.

The main objective of this study is to use two dimensional gravity models for the four deep seismic sounding (DSS) profiles across the intraplate Narmada-Tapti rift and two profiles across the western continental margin rift of India Kaila (1988). We also provide three dimensional gravity models for the western continental margin and the Narmada-Tapti rifts in order to determine the three dimensional shape of high density mafic bodies, their depths of occurrence and their probable roles in voluminous and copious eruptions of Deccan basalts along the rifts when India was stationed over the Reunion hotspot.

3.2 METHODOLOGY: TWO AND THREE DIMENSIONAL GRAVITY MODELLING

The depth and mass of the mafic bodies responsible for the gravity highs along the western continental margin and Narmada-Tapti rifts are estimated. According to Sharma

(1986) the amplitude of a gravity anomaly is an index of the depth of the mafic body. The depth of a body can be estimated from a given gravity anomaly by considering a regular sphere, horizontal cylinder and slab shape for a geological body. Smith (1959, 1960) has provided the depth-estimation formulae for local gravity and magnetic anomalies which are independent of the shape of the anomalous mass. These are based on Δg_{max} and $\Delta g'$, the maximum gravity anomaly values and their gradients and the depth Z_g to the top of the body which can be expressed as:

$$Z_g \leq 0.86 \mid \Delta g_{max} / \Delta g' \mid \qquad (3.1)$$

When the magnitude of an anomaly is partly known, the gravity value at a point $\Delta g(x)$ and its horizontal gradient $\Delta g'(x)$, can be used to calculate the depth by using the equation:

$$Z_x \leq 1.5 \mid \Delta g(x) / \Delta g'(x) \mid \qquad (3.2)$$

The gravity anomaly of +70 mGal on the western margin of India is primarily elongated in N-S direction. For such type of elongated anomalies Sharma (1986) has considered a buried horizontal cylindrical body. The gravity anomaly due to such bodies is given by the relationship

$$\Delta g = \{(2\pi G R^3 \Delta\rho/Z_c)[1/(1 + (x/z)^2)]\} \qquad (3.3)$$

The symbols are the same as those used in equations 3.1 and 3.2, respectively (Sharma, 1986). For a horizontally elongated body the approximate depth to the center is equal to the "half width($x_{1/2}$)." When the density contrast $\Delta\rho$ is reasonably known, then the size of the convex and elongated bodies can be estimated using equations 3.2 and 3.3.

Talwani *et al.*, (1959) provided an analytical expression for both the vertical and horizontal components of gravitational attraction due to a n sided polygon (body) at a given point. The accuracy of theoretically calculated Bouguer anomaly depends on how closely a polygon fits to a given geological body and this fit can be improved by either increasing the sides of the polygon or by increasing the number of polygons.

Braille *et al.*, (1974) and Fisher and Howard (1980) used an approach of inversion of gravity data to decipher the three dimensional shape of the prism (body) by taking into consideration only the variation in density of the body. Recently, Richardson and Macinnes (1989) developed a nonlinear inversion scheme for the gravity data incorporated into a three dimensional polyhedral model. Their procedure considers both the density and shape variations of the subsurface body. In this study we have used the methods of Garcia-Abdeslem (1995) for the inversion of gravity data in order to construct three dimensional shape of subsurface bodies along the western continental margin and the Narmada-Tapti rifts. Garcia-Abdeslem (1995) has solved the forward problem in wave-number domain, in which the gravity anomaly power spectrum is given by the product of functions, such as the density, depth, thickness and the horizontal dimensions (width and length) of the

subsurface body. The representation of this power spectrum is given by the function:

$$g(k) = \text{Ln}\left(\frac{1}{2\pi}\int_0^{2\pi} d\theta \left|\Delta g\,(k,\theta)\right|^2\right) = C + H(k,h) + T(k,t) + S(k, a,b) \qquad (3.4)$$

where,

$$C = 2\,\text{Ln}\,(2\pi G\rho) \qquad (3.4\,a)$$

$$H(k,h) = -2hk \qquad (3.4\,b)$$

$$T(k,t) = 2\text{Ln}\,\{k^{-1}[\,1 - e^{-kt}\,]\,\} \qquad (3.4\,c)$$

and,

$$S(k, a,b) = \text{Ln}\left(\frac{1}{2\pi}\int_0^{2\pi} d\theta \left|s(k,\theta)\right|^2\right) \qquad (3.4\,d).$$

Here a and b are the length and width of the body, t is thickness= h_1 -h_2 (the difference in the top and bottom of the body), u and v are the wave-numbers in x and y directions and k $=(u^2+v^2)^{1/2}$ is the magnitude of the wave-number vector, G is the gravitational constant and ρ is the density of the body. H(k,h) , T(k,t) and S(k, a,b) are the depth, thickness and horizontal dimension (length and width) functions, respectively.

3.3 TWO AND THREE DIMENSIONAL GRAVITY MODELLING ALONG THE WESTERN CONTINENTAL MARGIN RIFT OF INDIA:

The positive Bouguer gravity anomaly along the western continental margin of India (from 72°20' to 73°25' E and 18°14' to 20°60') with a high of +70mGal near Bombay (Figure 3.1A) extends in a north-south direction. Takin (1966) interpreted this gravity high as a subsurface structure of a high density body but no relationship was found to exist between the Deccan basalts thickness and the gravity high. Kaila (1988) tried to explain this gravity high in terms of presence of a transitional crust of very thin granitic layer underlain by a thick basaltic layer. However, the specific depth and density contrast between granitic and basaltic layers and their theoretical gravitational effects were not considered in his study. Recently, Negi *et al.*, (1992) used the technique of spectral analyses for the gravity data and came to the conclusion that this gravity high indicates presence of two subsurface structures at depths of 4.5 ± 0.5 km and 18 ± 2.0 km, respectively. These subsurface features represent the basement and the upwarped Moho. By taking an initial depth of 17.7 km and a density contrast of 0.43 gm/cm^3 between this high density structure and surrounding lower crust, Negi *et al.*, (1992) concluded that the gravity high represents a conduit, a pipe-like, funnel-shaped structure. They also suggested that this magma conduit was loci for the main Deccan basalts eruption. They attributed this structure to be a site of large bolide impact at the Cretaceous/Tertiary boundary. Recently, Bhattacharji *et al.*, (1996) suggested that many tholeiitic dikes along the western continental margin and the Narmada-Tapti rifts gravity highs served as primary feeders to the

main Deccan lavas originating from upper crustal magma chambers during rifting and rift activation.

The eastern side of the Bouguer gravity high of +70mGal near Bombay has a steeper gradient of 3 mGal/km and the western side show a gradient of 1.25 mGal/km. Figure 3.2 shows two dimensional gravity modelling along A-B near Bombay (Figure 3.1A). The observed anomaly (solid circles) matches well with theoretically calculated gravity anomaly (continuous curve) when a zoned mafic body of 2900 kg/m^3 to 2970 kg/m^3 densities was assumed to have emplaced at a depth of 6$\pm$0.5 km. Estimated dimensions of this mafic body is approximately 25 km wide at the top and 40 km at the bottom. Interestingly, total thickness of the Deccan basalts here does not conform with the observed high of +30 mGal near Surat (Figure 3.1A). However, the observed anomaly near Surat (solid circles, Figure 3.3) matches with the theoretically calculated gravity anomaly (continuous curve, for 300 gravity stations) if one assumes a zoned mafic body emplaced at a depth of 6$\pm$0.5 km. The horizontal dimensions of this mafic body can not be estimated as the gravity anomaly contours are open in offshore area.

Three dimensional shapes of the mafic bodies responsible for the gravity highs of +70 mGal and +30 mGal along the west margin of India are deciphered on the basis of physical parameters calculated from two dimensional modelling (Table 3.1). For three dimensional gravity modelling, the thickness of the mafic body is taken as 12 km at a depth of 6$\pm$0.5 km with the densities of 2900 and 2970 kg/m^3 for initial calculations for the +70 mGal

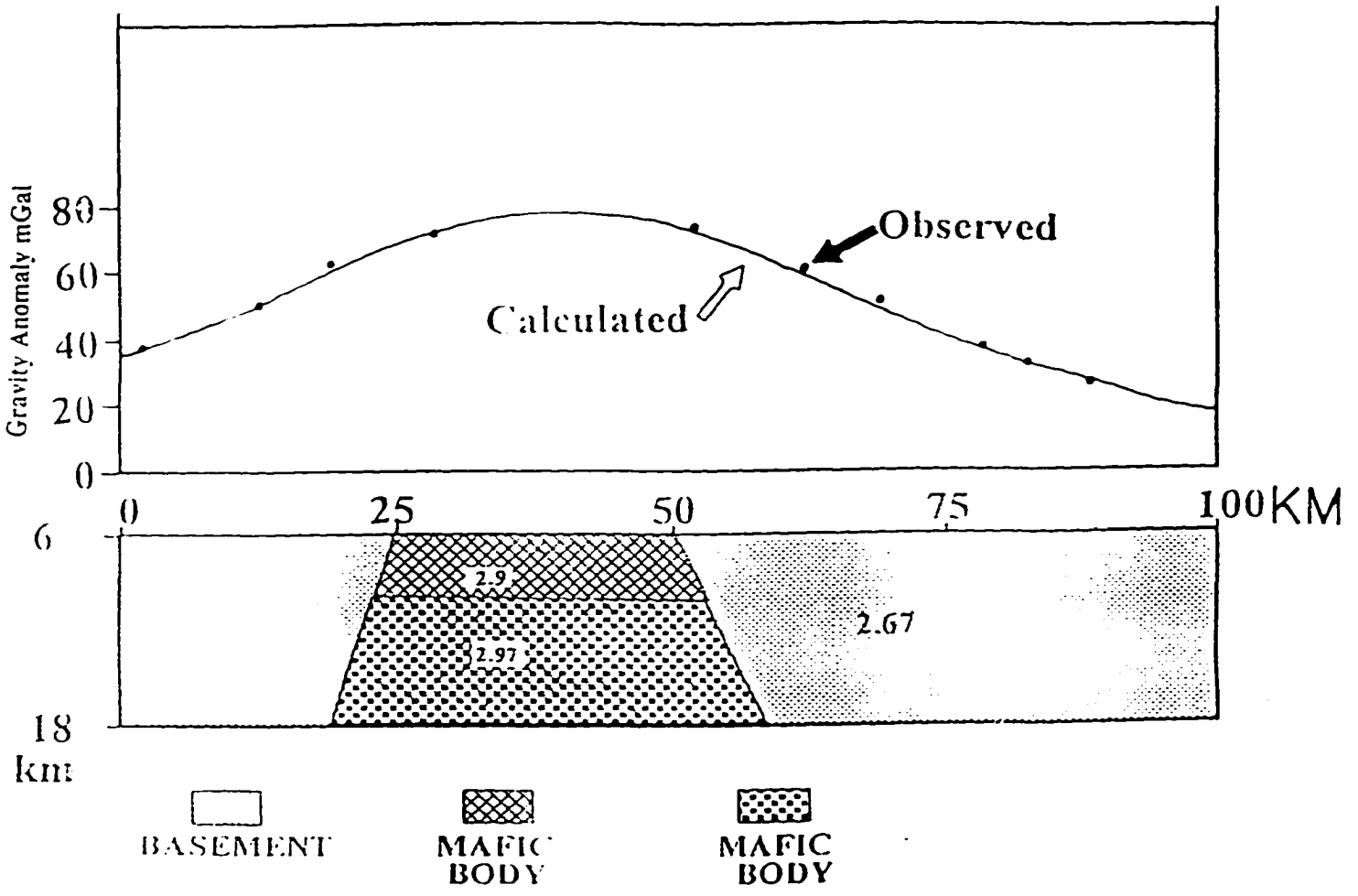

FIGURE 3.2 : Two dimensional gravity modelling along A-B near Bombay (Figure 3.1A). The observed and theoretically calculated anomalies match well when a zoned mafic body with 2900 kg/m^3 and 2970 kg/m^3 densities is assumed at a depth of 6±0.6 km. The mafic body is 25±2.5 km wide at the top and 40±4 km wide at the bottom.

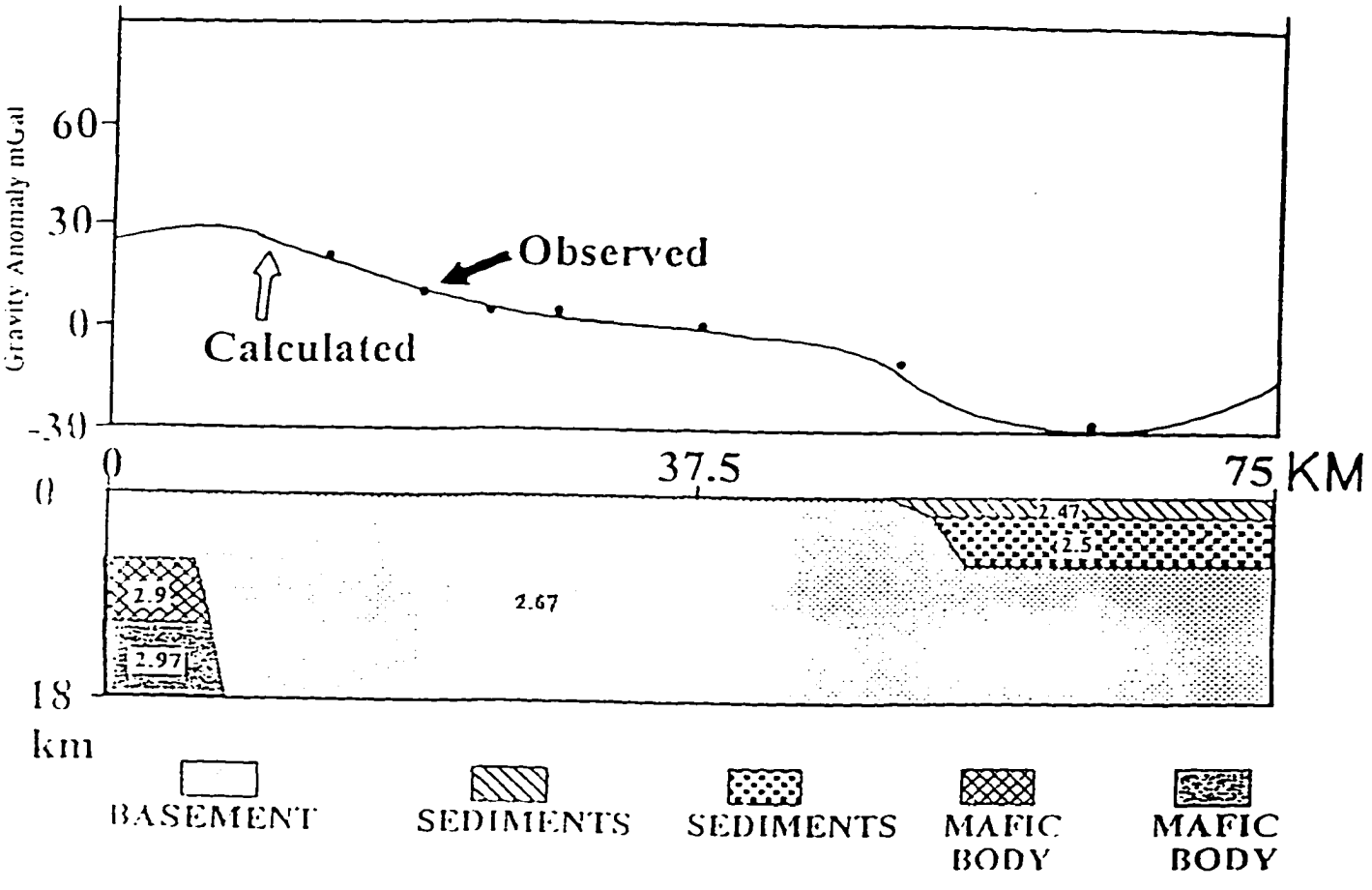

FIGURE 3.3 : Two dimensional gravity modelling near Surat (Figure 3.1A) indicates the presence of density stratified mafic body emplaced at a depth of 6±.6 km. The horizontal dimensions of the mafic body are unknown because the gravity anomaly contours are open offshore of western coast of India.

TABLE 3.1: Width (top and bottom), length (top), thickness, depth and density of mafic bodies along the western margin. The dimensions of the mafic body near Bombay are larger.

LOCATION	WIDTH TOP (km)	WIDTH BOTTOM (km)	LENGTH TOP (km)	THICKNESS (km)	DEPTH (km)	DENSITY (kg/m^3)
NORTHERN GRAVITY HIGH (NEAR BOMBAY)	25±2.5	40±4	300±30	12±1.2	6±0.6	2900±290 2970±297 Density Stratified
SOUTHERN GRAVITY HIGH	10±1	25±2.5	120±12	7±0.7	6±0.6	2900±290 Unstratified

anomaly. Figure 3.4 shows the three dimensional shape of such a mafic body from the SW direction. The shape of mafic body deduced on the basis of three dimensional gravity models clearly indicate that there is only one continuous mafic body responsible for two gravity highs of +70 mGal and +30 mGal along the western continental margin of India instead of two separate and isolated mafic bodies proposed earlier by Negi *et al.*, (1992). The shape of the mafic body can be described as two halves of an ellipsoid connected to each other at an apex. The longer axis of both the ellipsoids extends in the N-S direction. Both halves of the ellipsoids are open at each end (Figure 3.4) near offshore of the western coast of India.

Along the western margin of India, south of Bombay (Figure 3.1B) a free-air gravity high of +25 mGal extending in NNW-SSE is present (Naini and Talwani, 1982). The crustal structure along this gravity high was studied by Subramanyam *et al.*, (1991) and Krishna *et al.*, (1994). Subramanyam *et al.*, (1991) deciphered the two dimensional crustal structure by applying the constraints from the bathymetric and magnetic data of Naini and Talwani (1982), seismic reflection and well-log studies (Ramaswami and Rao, 1980) and from seismic refraction studies (Rao, 1970). The gravity high was attributed to a mafic layer of 26 km thickness overlain by a granitic layer of 0.5 to 3 km thickness. However, Krishna *et al.*, (1994) modeled the +25 mGal high as a subsurface ridge at a depth of 6.0 km with a density of 2880-2900 kg/m^3, width 30 km and 45 km at the top and bottom, respectively. We have digitized the gravity data of Subramanyam *et al.*, (1991) and Krishna *et al.*, (1994) for the three dimensional modelling of the +25 mGal gravity anomaly along the western continental margin. The mafic body responsible for this gravity high is considered at a depth of 6$\pm$0.6

FIGURE 3.4: Three dimensional gravity modelling of +70 mGal gravity high along the western margin, India. The orthographic view is from north west.

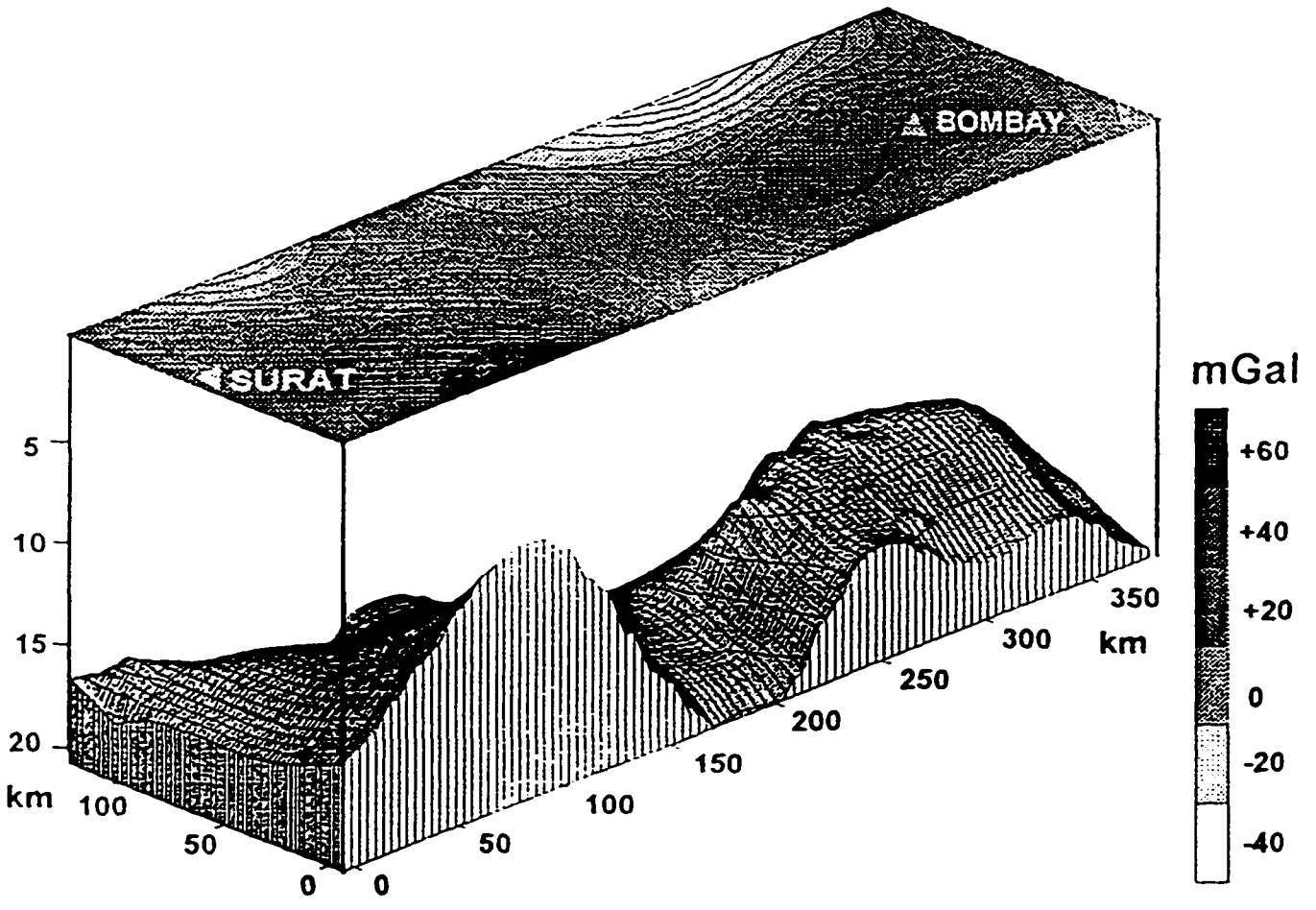

km (Krishna *et al.*, 1994) with average density of 2900 kg/m^3. Figure 3.5 shows that the shape of the mafic body is made up of two ellipsoid connected to each other at an apex. The shape of this mafic body is similar to that of the mafic body near Bombay (Figure 3.4).

3.4 TWO AND THREE DIMENSIONAL GRAVITY MODELLING ALONG NARMADA-TAPTI RIFT:

Kaila (1988) has carried out eight Deep Seismic Sounding (DSS) profiles, ranging from 200 km. to 300 km. in length over different parts of the Deccan Traps. Five of these profiles were across the Narmada-Tapti rift, one E-W profile in Saurashtra peninsula (Gujarat) and two profiles along the western continental margin over Deccan volcanics. Recently, Verma and Banerjee (1992) have studied the nature of continental crust along the Narmada-Tapti rift using these DSS profiles and gravity anomalies. To study the relationship between the Deccan Traps thickness and Moho depth we have used the DSS profiles across the Narmada-Tapti rift and have digitized the residual gravity maps of Verma and Banerjee (1992), Kaila (1988) and Kailasam (1982), prepared computer generated gravity contour maps (Figure 3.1). These gravity anomaly maps and the DSS profiles (Kaila, 1988) are used for the three dimensional gravity modelling (Figure 3.1C).

(i) Gravity Modelling along Thuadara-Sindad Profile:

The crustal depth section along the Thuadara-Sindad DSS profile (Figure 3.1 C)

FIGURE 3.5: Three dimensional gravity modelling of +25 mGal gravity high along the west coast of India, south of Bombay. The mafic bodies are convexly upward at a depth of 6 ± 0.6 km.

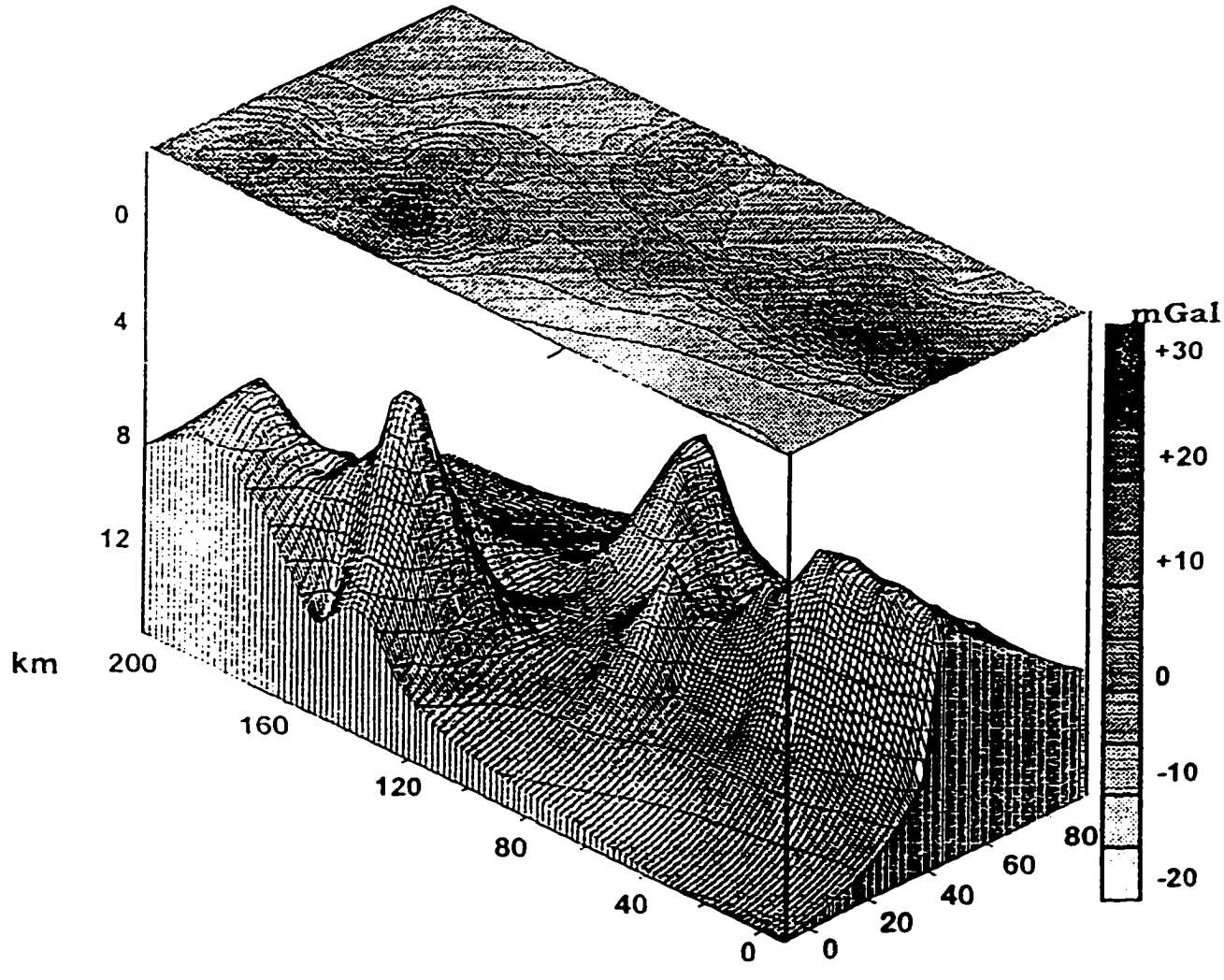

was mapped by Kaila (1988). The thickness of the Deccan lavas along this profile vary from 0 m to 900 m overlying 1.9 km thick Mesozoic sediments. The crustal section reveals five crustal blocks demarcated by deep-seated faults. In this part the depth of Moho was found to vary from 40 km. to 43 km.

Figure 3.6 shows the observed gravity anomaly (solid circles) along this profile. The modeled gravity anomaly curve matches well with the observed anomaly if two mafic bodies are assumed to occur at a depth of 6 ± 0.6 km in the crustal section and the densities of these bodies are taken as 2900 kg/m^3 and 2970 kg/m^3, respectively. The calculated width of the mafic body on the left is 26 ± 2.5 km, whereas width of the intrusive body on the right is 15 ± 1.5 km.

(ii) Gravity Modelling along Ujjain-Mahan Profile:

A DSS profile on the central part of the Narmada-Tapti rift from Ujjain to Mahan was carried out by Kaila (1988). In the northern part of this profile, the Deccan Traps are 100 m thick, however, based on P_v= 4.7 to 5.1 km/sec in the southern side they are 400 m thick . Here the Moho discontinuity is between 35 km. and 40 km. In this section two faults demarcating the Narmada-Tapti rift are also encountered.

Figure 3.7 shows observed and calculated Bouguer gravity anomalies along the Ujjain-Mahan section. Here the gravity anomalies shows a high of 50 mGal. The gravity

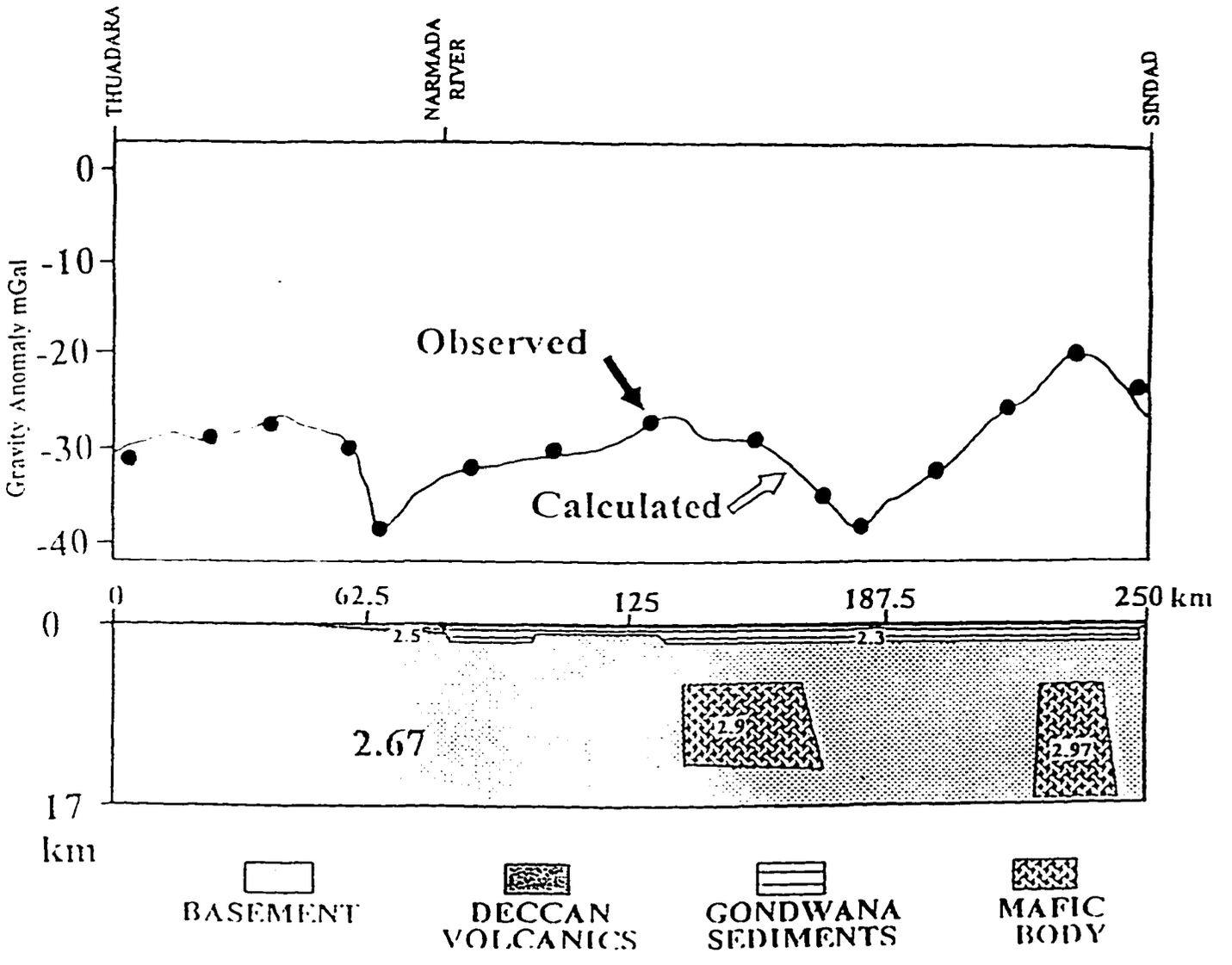

FIGURE 3.6 : Two dimensional gravity modelling along Thuadara-Sindad profile . The observed and theoretically calculated anomalies fit well when two mafic bodies are assumed at a depth of 6±0.5 km.

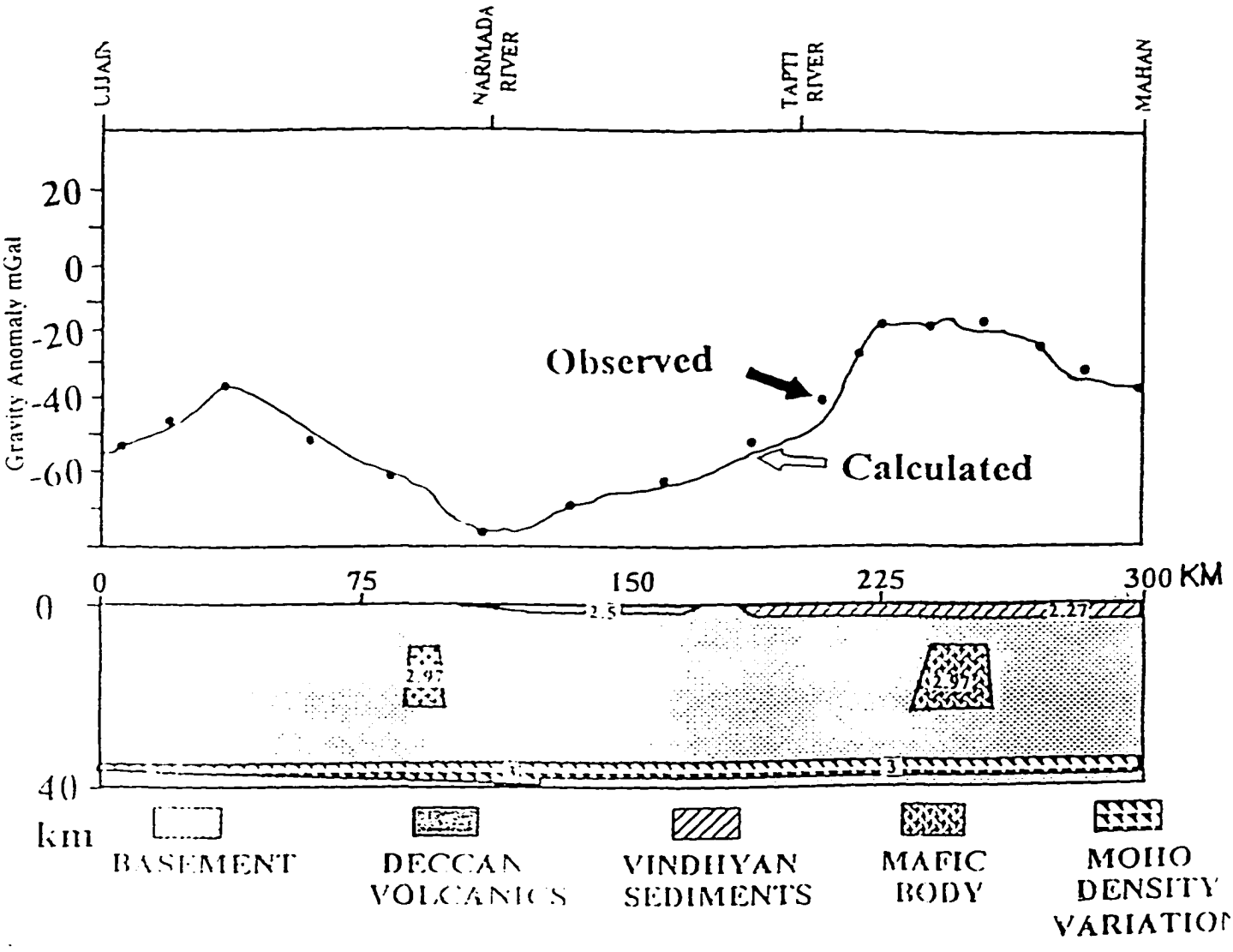

FIGURE 3.7 : Two dimensional gravity modelling along Ujjain-Mahan profile. Calculated and observed anomalies match well if two convexly upward mafic bodies are assumed to occur at a depth of 8±.75 km.

anomaly effects produced by the Deccan volcanics and the Vindhyan sediments can not explain the magnitude of observed anomaly. In order to match observed and theoretical gravity anomalies, we have assumed two mafic bodies of density 2970 kg/m^3 at a depth of 8±0.8 km. The calculated dimensions of width and thickness for the mafic body near Ujjain are 10±1 km and 13±1.3 km respectively. However the mafic body near Mahan is estimated to have width and thickness of 20±2 km and 15±1.5 km, respectively.

(iii) Gravity Modelling along Kajuria Kalan-Pulgaon Profile:

This DSS profile of Kaila *et al.*, (1985) reveals 100 m to 200 m thick Deccan lavas along the Khajuria Kalan - Pulgaon profile. Here Moho is at a depth between 34 km to 37 km. Figure 3.8 shows the observed gravity anomaly (solid circles) along Khajuria Kalan - Pulgaon profile (Kaila and Rao, 1985; Kaila, 1986). The gravity anomaly shows a high of -20 mGal near Tapti river and a low of -50 mGal near Narmada river (Figure 3.8), giving a high of 30 mGal. Presence of two mafic bodies of densities 2970 kg/m^3 in the crustal section are necessary to match calculated and observed gravity anomalies. Approximate depth of these assumed mafic bodies is 6±0.5 km. However, the dimensions (width and thickness) are different. The body in the left side is estimated to be 6±0.5 km wide and 13 km thick and the body at the right side near Pulgaon is estimated to be from 10±1 km to 38±3.5 km wide from top to bottom and 14±1.1 km thick. The intrusive body on the right side also seems to be connected below to a larger mafic body (Figure 3.8).

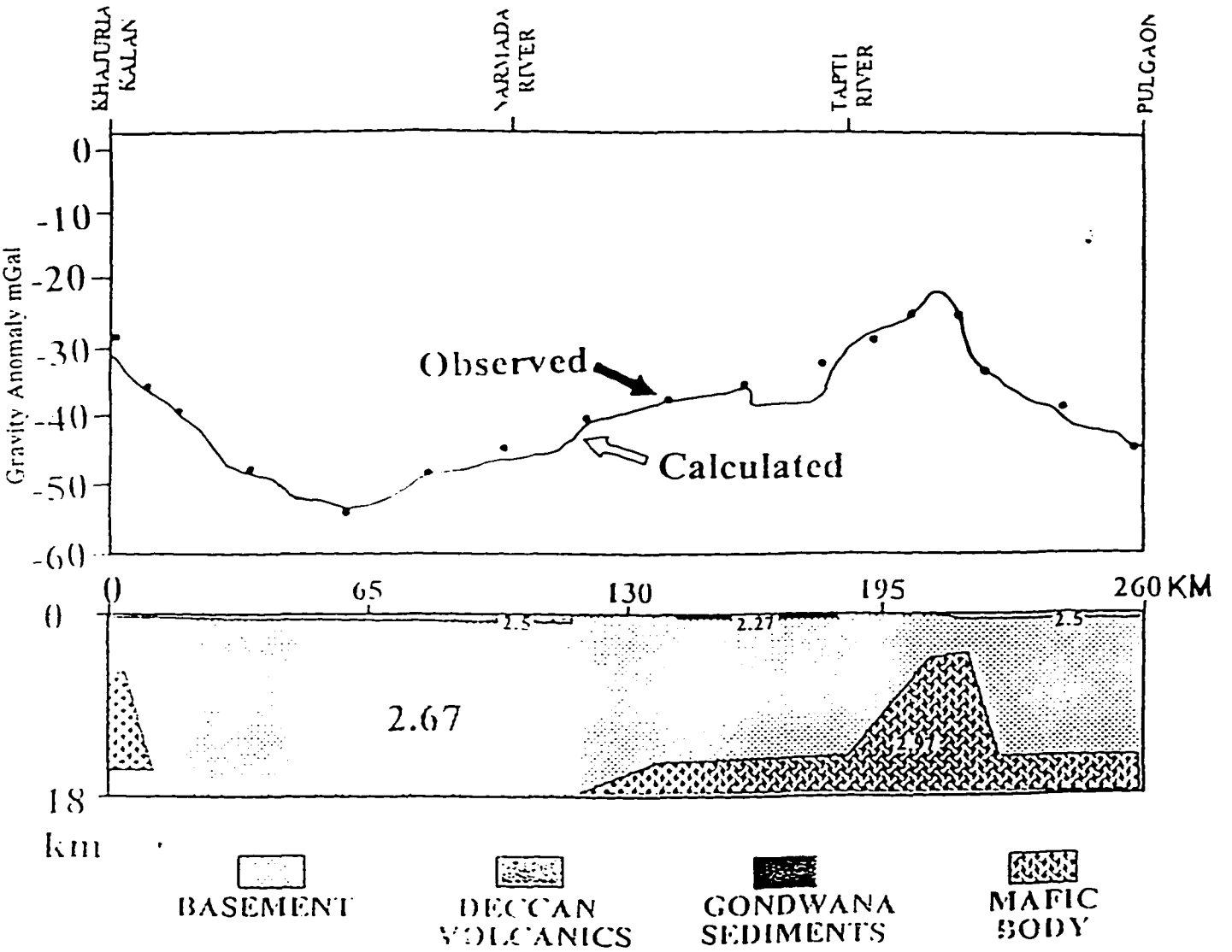

FIGURE 3.8 : Two dimensional gravity modelling along Khajuria Kalan-Pulgaon profile. Emplacement of two mafic bodies are assumed at a depth of 6±0.5 km in order to match the observed and calculated anomalies. Both the mafic bodies have density of 2970 kg/m^3.

(iv) Gravity modelling along Hirapur-Mandla Profile:

The eastern-most DSS profile over Deccan volcanics from Hirapur, Jabalpur to Mandla was carried out by Kaila *et al.*, (1987). Figure 3.9 shows the observed Bouguer gravity anomaly (solid circles) along this profile. The continuous curve shows calculated gravity anomaly for 690 gravity stations along Hirapur and Mandla. The observed anomaly matches well with the modeled gravity anomaly if two hypothetical mafic bodies of density of 2770 kg/m^3 are assumed to be present in the upper crust. The modeled mafic bodies are estimated to be at a depth of 6 ± 0.5 km. The mafic body near Hirapur is estimated to be 6.5 ± 0.5 km wide at the top, and 13 ± 1.3 km wide at the bottom and is 9 ± 1 km thick. However, the body near Mandla is of prism shape with a 23 ± 2 km base and 15 ± 1.5 km thickness. The size and shape of these mafic bodies differ significantly from the modeled dimensions given by Verma and Banerjee (1992). Their estimated sizes are much bigger; (for example, the intrusive body near Mandla is ≈100 km wide).

(v) THREE DIMENSIONAL SHAPE OF MAFIC BODIES FROM GRAVITY DATA:

Three dimensional shapes of the mafic bodies responsible for the gravity highs in and across the Narmada-Tapti rift were computed using the methods given by Garcia-Abdeslem (1995), and equation 3.4. The depth, thickness, horizontal dimensions and the density are taken from two dimensional gravity model along four DSS profiles given by Kaila (1988). Table 3.2 lists the width (top, bottom), length, thickness, depth and densities of mafic

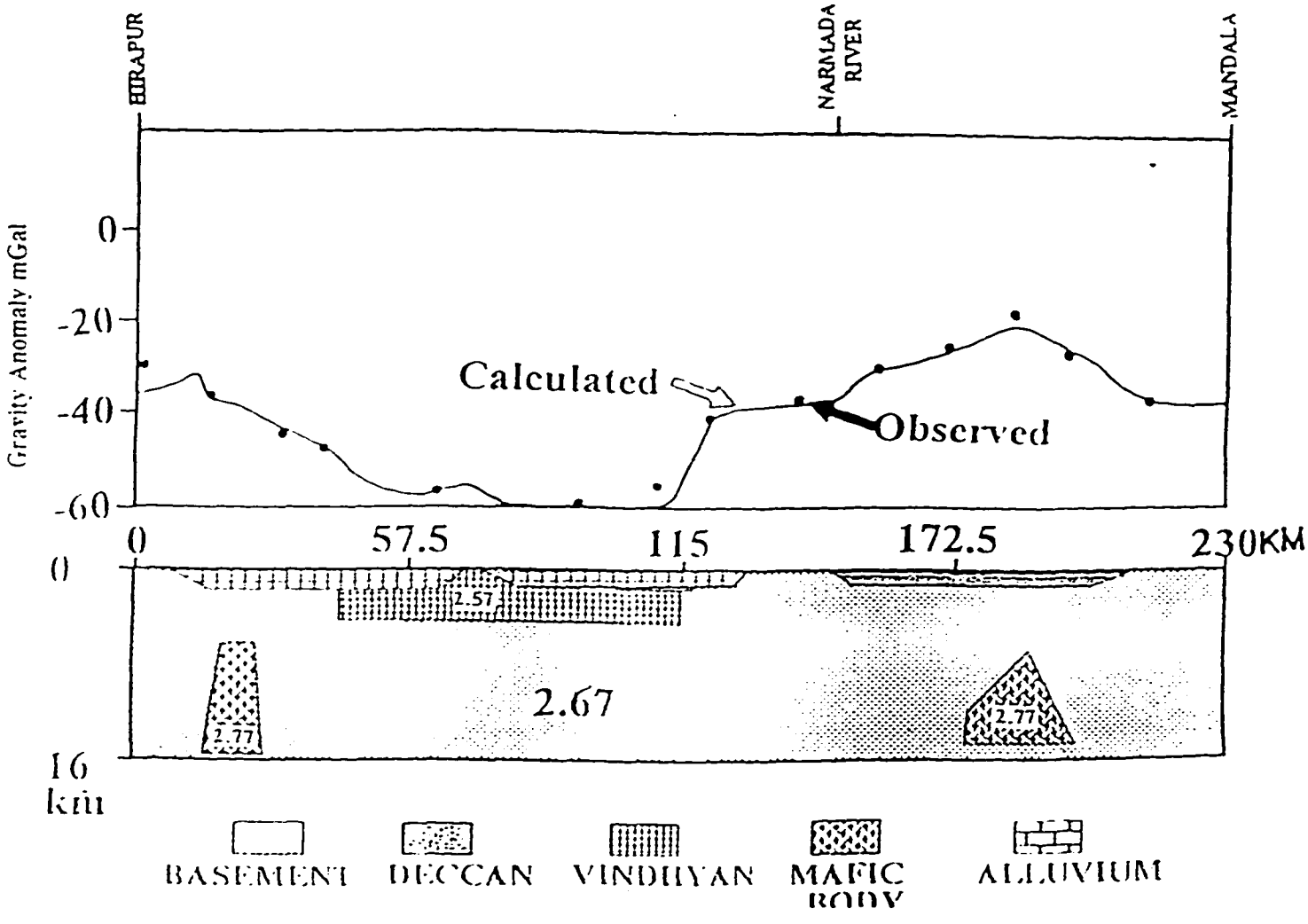

FIGURE 3.9 : Two dimensional gravity modelling along Hirapur-Mandla profile. The observed and the calculated anomalies fit well when two mafic bodies with 2770 kg/m^3 density are assumed at depth of 6±0.5 km.

TABLE 3.2 Three dimensions of left and right mafic bodies, their depth and density along four DSS profiles (Kaila, 1988).

NARMADA-TAPTI RIFT (LEFT MAFIC BODY)

LOCATION	WIDTH TOP (km)	WIDTH BOTTOM (km)	LENGTH TOP (km)	THICKNESS (km)	DEPTH (km)	DENSITY (kg/m³)
HIRAPUR-MANDLA	6.5±0.5	13±1.3	20±2.0	9±1.0	6±0.5	2770±277
KHAJURIA PULGAON	6±0.5	9±0.9	26±2.6	13±1.3	6±0.5	2970±297
UJJAIN-MAHAN	10±1.0	10±1.0	18±1.8	13±1.3	8±0.75	2970±297
THUADARA SINDAD	26±2.5	26±2.5	23±2.3	8±0.75	6±0.5	2900±290

NARMADA-TAPTI RIFT (RIGHT MAFIC BODY)

LOCATION	WIDTH TOP (km)	WIDTH BOTTOM (km)	LENGTH TOP (km)	THICKNESS (km)	DEPTH (km)	DENSITY (kg/m³)
HIRAPUR-MANDLA	0.5	23±2.0	26±2.6	15±1.5	6±0.5	2770±277
KHAJURIA PULGAON	10±1.0	38±3.5	25±2.5	14±1.4	6±0.5	2970±297
UJJAIN-MAHAN	20±2.0	20±2.0	28±2.8	15±1.5	8±0.75	2970±297
THUADARA SINDAD	15±1.5	15±1.5	24±2.4	12±1.2	6±.5	2970±297

bodies (on the left and right hand sides) along four DSS profiles. The dimensions of the bodies are estimated on the basis of two dimensional gravity models along the Narmada-Tapti rift. The average depth of the mafic body responsible for a high of 40 mGal is estimated to be 6 ± 0.6 km. Hence, for three dimensional gravity modelling we have assumed a depth of 6 ± 0.6 km for each high of 40 mGal along the Narmada-Tapti rift. The two dimensional gravity modelling along the Narmada-Tapti rift also shows that the densities of mafic bodies responsible for the gravity highs vary from 2770 kg/m^3 to 2970 kg/m^3. On the basis of this we have assumed an average density of 2940 ± 300 kg/m^3 for all the mafic bodies for three dimensional gravity modelling.

Figure 3.10 shows the modeled three dimensional shape of the mafic body between 73°E and 84°E longitudes and 20°N and 26°N latitudes. The search method to locate the data points was octant and the gridding interpolation algorithm was Minimum Curvature (Briggs, 1974). Here the orthographic view of the mafic body is from south west side with a tilt of 30°. These mafic bodies are responsible for the gravity highs along the Narmada-Tapti rift. Note that all mafic bodies are connected to a larger mafic body at a depth of 25 ± 2.5 km. However, at this depth the larger body is no longer a high density body, because the velocity data given by Kaila (1988) at this depth varies from 6.8 km/s to 7.0 km/s for which calculated densities should vary from 2900 kg/m^3 to 3000 kg/m^3. We have considered an average density of 2940 ± 300 kg/m^3 for mafic bodies beneath the Narmada-Tapti rift, hence, this average density at a depth of 25 ± 2.5 km does not represent a very high density body.

FIGURE 3.10: Three dimensional gravity modelling along Narmada-Tapti rift provide three dimensional shapes of mafic bodies: Note that all the mafic bodies are connected to a larger mafic body.

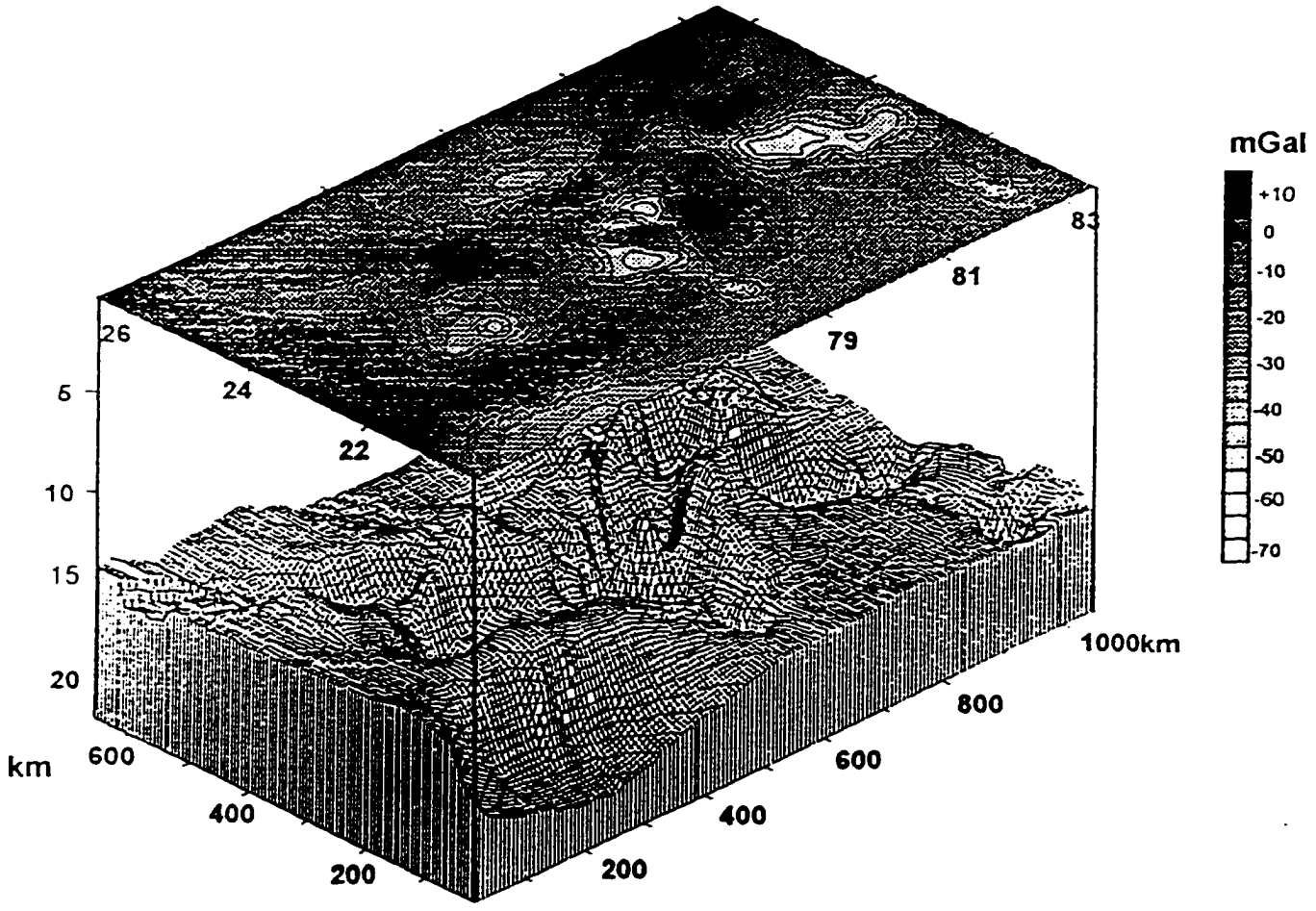

3.5 DISCUSSION:

The Tables 3.1 and 3.2 list the major differences in the gravity highs, and characteristics of modeled mafic bodies along the western continental margin and the Narmada-Tapti rifts of India. The maximum gravity high along the western coast is +70 mGal but along the Narmada-Tapti rift the average gravity high is of 40 mGal. The three dimensional mafic bodies responsible for the gravity highs have different dimensions for both the western continental margin and the Narmada-Tapti rifts. For example, the mafic body along the west coast (Table 3.1) is 300±30 km in length, 35±3.5 km in width, and 12±1.2 km in thickness. In contrast, the width, length and the thickness of an average mafic body along the Narmada-Tapti rift (Table 3.2) are 16±1.6 km, 25±2.5 km and 11±1 km, respectively. Approximate depths and the densities of the gabbroic mafic bodies are however of similar magnitude at both the places.

Morgan (1971) first postulated that the eruption of the Deccan volcanics occurred when the Indian plate was stationed on top of the Reunion hot spot. Recent studies by Richards *et al.*, (1990) and Duncan (1990) also indicate a close relationship between the Reunion hotspot and the Deccan volcanics. Geophysical studies in the eastern Arabian sea and the Indian ocean indicated the existence of submarine ridges (known as Chagos-Laccadive and Prathap ridges, Naini and Talwani, 1982). These volcanic ridges show a trend of decreasing age from north to south and link the Deccan flood basalts to the Reunion hot spot. The geochemical signatures (like trace, rare earth elements and isotopic ratios) of the Deccan

volcanics and the Reunion hotspot also show many similarities (Dupuy and Dostal, 1986).

The interaction of hot mantle plumes with the lithosphere have been held responsible for the extrusion of flood basalts by many workers following Morgan's original proposal in (1972). Campbell and Griffith (1990), Richards *et al.*, (1990) and more recently, Davis (1994) have proposed models for the process of lithosphere thinning through thermo-chemical erosion by a hot mantle plume. According to Davis (1994) the rate of lateral thinning depends on the viscosity and the lateral dimensions of the upwelling. As a result, rapid local thinning is caused by the plume tail rather than the plume head. Hence, the occurrence of narrow volcanic hotspot chains connect the flood basalt to the hot spot. Sleep (1994) however has explained lithospheric thinning by means of secondary convection in the hot plume material ponded at the base of the lithosphere. Recently, the oceanic volcanism and the bathymetric swell over a hot spot have been explained on the basis of density reduction created by melting beneath the hot spot by Morgan *et al.*, (1995). An alternate model has been proposed by Ihinger (1995) to explain the en-echelon seamount segments along the Hawaiian-Emperor hot spot chain . According to this model, each seamount chain represents the surficial expression of the individual mantle diapirs (plumelets). All the models discussed above suggest that the direct melting of mantle plume head and its extrusion are major factors in the development of major flood basalts provinces. In these type of models, rifting is frequent but not universal effect of plume heads. An alternative model involving mantle plumes has been developed by White and McKenzie (1989; 1995). In their model material from a plume accumulates beneath the lithosphere. Continental breakup allows this material to flow into

rifted lithosphere and causes pressure release melting. In this type of model rifting is the necessary cause of flood basalts. Unfortunately, up to this date very little is known about the size and shape of the magma bodies and rate of magma intrusion from the lower to upper lithosphere over a hot spot. How and why the size, shape and the rate of migration of mafic bodies differ from oceanic to continental lithosphere are still conjectural.

The kinematics of flow from a narrow plume through the asthenosphere has been numerically and geometrically investigated by Sleep (1987; 1990) and Richards *et al.*, (1988) and many others. The flow from the plume has been modeled in the form of radial motion interacting with the flow in the asthenosphere. Their study indicates that due to interaction the radial flow from the plume no longer stays radial but takes the shape of a parabola like curve in downflow direction. This model is used to explain the topography, geoid and heat flow anomalies associated with the Hawaiian hotspot (Sleep, 1987; 1990 etc.). This study shows that the shape of the mafic bodies emplaced into the upper lithosphere by the Reunion hotspot are of an ellipsoidal shape in N-S direction along the western continental margin of India (Figures 3.4 and 3.5) and Narmada-Tapti rift (Figure 3.10). Figures 3.4 and 3.5 show the ellipsoidal and convex mafic bodies along western and central India emplaced possibly during Indian plate migration rapidly towards the north from the Reunion hotspot. Further evidence of other ellipsoidal mafic bodies emplaced by the Reunion hotspot come from the positive and negative gravity anomalies of ellipsoidal shape observed in the south of the gravity high of Bombay (Naini and Talwani, 1992; Subramanyam *et al.*, 1991).

The plate reconstructions and the true polar wander studies (Duncan, 1990) indicate that shortly after the Deccan volcanics eruption, the Seychelles Bank and a small western portion of the Deccan volcanic province (they were part of the western India) rifted away from India and were joined to the African plate. The breakup of Seychelles islands from the western continental margin of India can be explained on the basis of size and shape of the emplaced mafic bodies. The Narmada-Tapti rift is marked by the presence of pre-Cambrian ENE-WSW lineaments and is a tectonic boundary between the southern peninsula and northern foreland. The western continental margin is characterized by the presence of N-S oriented lineaments along which the rifting and breakup of India most likely occurred as lineaments act as planes of weakness in the lithosphere (Bhattacharji *et al.*, 1996). The presence or absence of pre-Cambrian lineaments and the alignment of mafic bodies along these lineaments therefore played a role in rifting along Narmada-Tapti as shown by Bhattacharji *et al.*, (1996) such rifting may have also followed by breakup along western continental margin N-S to NNW-SSE oriented lineaments. It is shown that along the Narmada-Tapti rift small discontinuous mafic bodies were emplaced at a depth of 6.7 ± 0.6 km (Table 3.2). These smaller convexly upward mafic bodies appear to be aligned along the rift zone following the pre-Cambrian ENE-WSW Narmada-Tapti lineaments. Figure 3.11 shows the cartoon for possible emplacement of mafic bodies from the Reunion hotspot when India was stationed over it. This figure also shows the direction of asthenospheric flow at the time of emplacement of high density mafic bodies which are aligned along the western continental margin of India. The large dimensions (Table 3.1) of N-S elongated ellipsoidal mafic bodies aligned parallel to the western continental margin may therefore be connected with the continued marginal rifting and

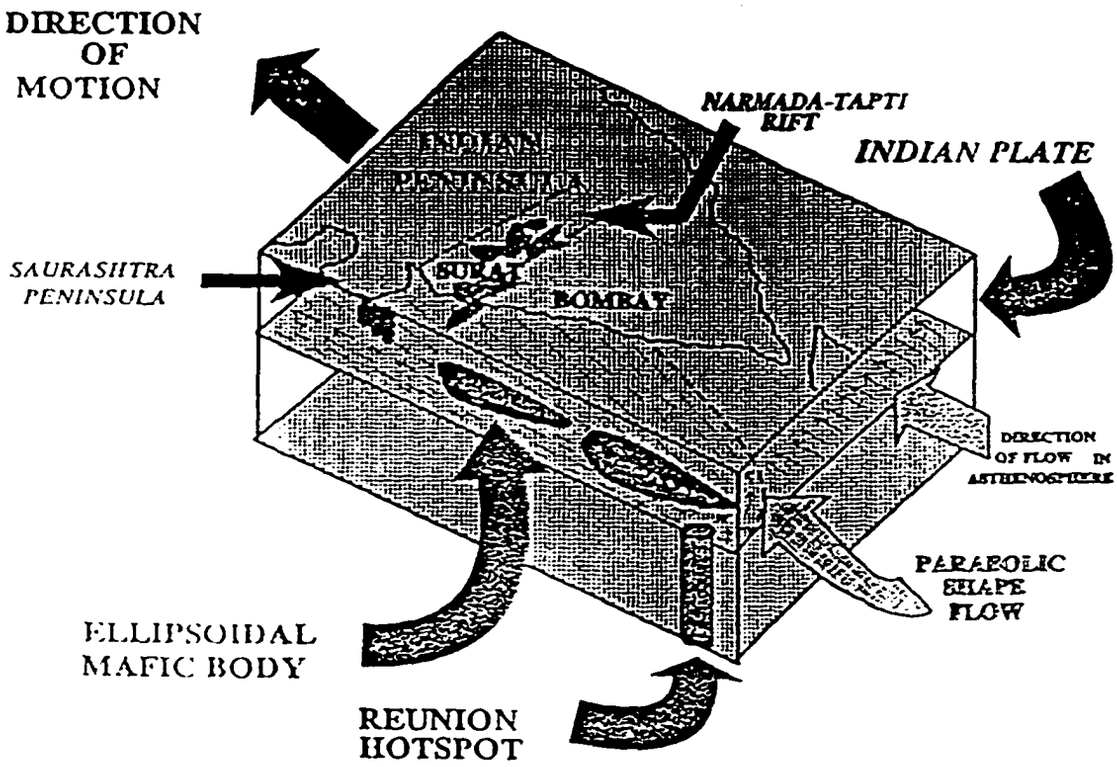

FIGURE 3.11: A model to show the emplacement of mafic bodies from the Reunion hotspot along Saurashtra peninsula, western margin and Narmada-Tapti rifts. The model stipulates that the migration and concentration of the high density mafic magma should be dominant along the western margin than the Saurashtra peninsula and the Narmada-Tapti rift. The alignment and emplacement of ellipsoidal mafic bodies with the N-S elongated pre-Cambrian lineament along the western India are likely related to rifting and eventual breakup of western India and northward rapid movement of the Indian plate.

final breakup of western continental margin of India which resulted their emplacement. This study suggests that the emplacement and alignment of mafic bodies and their orientation with respect to pre-Cambrian lineaments are controlled and related to lineament activated rifting along the Narmada-Tapti rift and continued rifting and eventual breakup of India over the Reunion hotspot along the western margin rift. These larger mafic bodies along the western continental margin rift and smaller mafic bodies along the Narmada-Tapti rift were the immediate source for copious and widely distributed Deccan Volcanics on the peninsular India.

CHAPTER 4

EMPLACEMENT OF MAFIC PLUTONS AS DIAPIRS IN THE UPPER CRUST BELOW DECCAN VOLCANICS, SAURASHTRA PENINSULA, WESTERN INDIA

4.1 INTRODUCTION:

The granitoid plutons in the middle and upper crust generally have a spherical shape (eg. Pitcher, 1979). The mechanism of emplacement of very large granitic plutons in the absence of extensional stresses is uncertain and conjectural. Grout (1932) proposed that the magma may ascend due to rock flowage along the roof and walls and called it the diapiric ascent of magma. Other mechanisms of emplacement suggested for large granitoid plutons are (i) stoping (Daly, 1933), (ii) ring dike intrusion (Anderson, 1936), (iii) granitization (Read, 1948) , (iv) zone melting (Harris, 1957) and (v) as a dike (Petford *et al.*,1993). In comparison with granitic plutons the basaltic magma generally occurs in the middle and upper crust in the form of elongated bodies like dikes and sills. Such basaltic magma rarely occurs in the form of a large pluton. Here we explore the possibility of the existence of large high density basaltic type mafic bodies in the middle and upper crust in the Saurashtra peninsula due to Bouguer gravity high and examines the possible mechanism of formation, ascent and development of such bodies in this region (Figure 4.1).

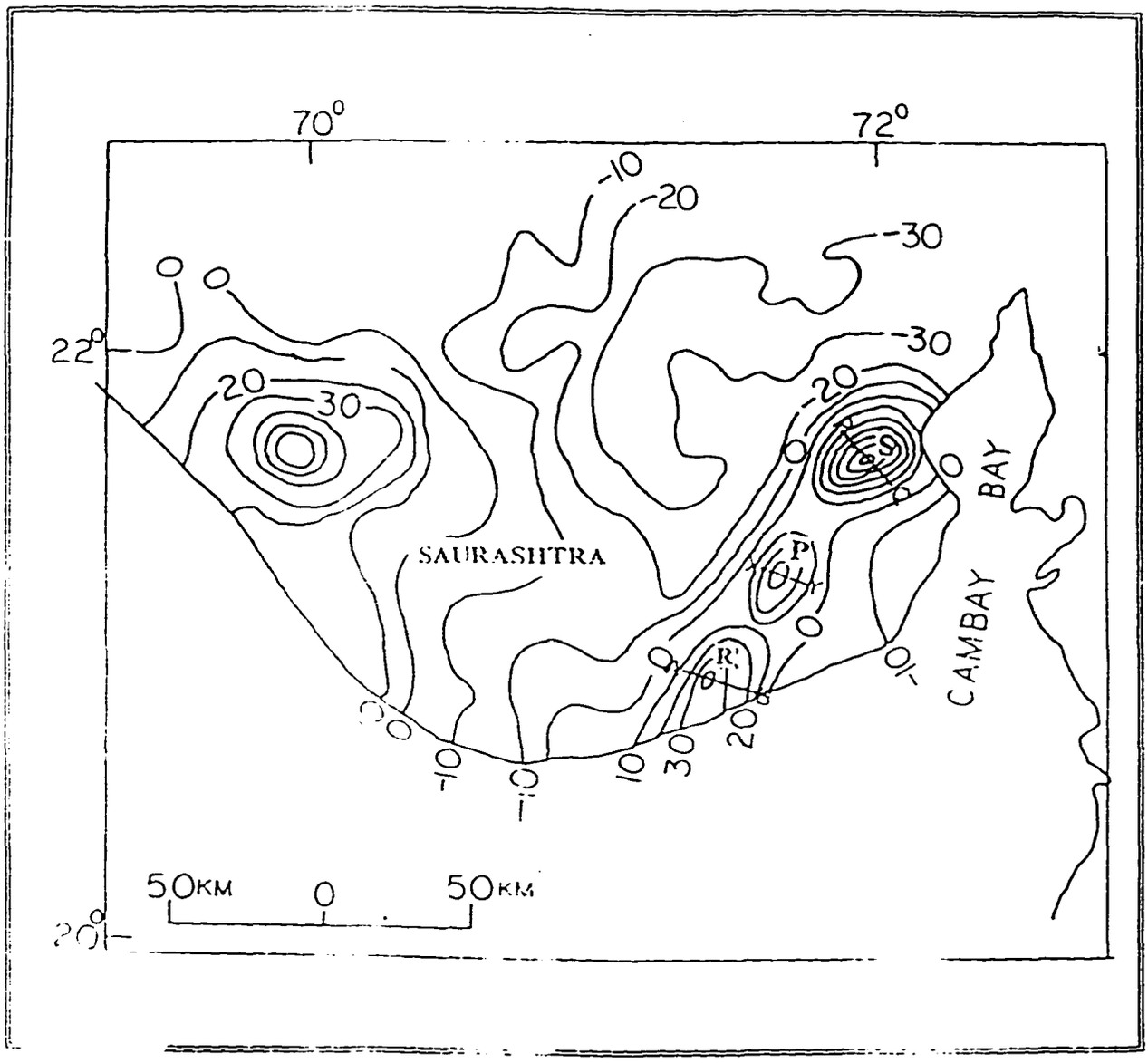

FIGURE 4.1: The Bouguer gravity anomaly map of Saurashtra peninsula. The study areas Rajula (R), Palitana (P), and Shihor (S) are marked by gravity highs of +40 mGal, +30 mGal and +60 mGal respectively. Along A-B, X-Y and P-Q lines two dimensional gravity modelling have been carried out.

I have carried out three dimensional gravity modelling of these three Bouguer gravity anomaly highs in Saurashtra peninsula (Figure 4.1). These gravity highs aligned primarily in NE-SW direction are dominant features in Rajula, Palitana and Shihor. The area around Rajula is marked by a gravity high of +40 mGal, and areas around Palitana and Shihor are marked by +30 mGal and +60 mGal, respectively. The NW part of the Saurashtra is also marked by another +60 mGal high. The central part of Saurashtra shows a low of -30 mGal. Three dimensional shapes of the mafic bodies are determined by three dimensional gravity modelling and a model is presented for the formation and ascent of such large mafic plutons.

4.2 ESTIMATIONS OF DEPTH OF MAFIC BODIES FROM THE POSITIVE BOUGUER GRAVITY ANOMALIES ALONG RAJULA, PALITANA AND SHIHOR, IN SAURASHTRA:

The depth and mass of the mafic bodies responsible for +40 mGal, +30 mGal and +60 mGal gravity highs at Rajula, Palitana and Shihor, respectively, are estimated. According to Sharma (1986) the amplitude of a gravity anomaly is an index of the depth of mafic body. By taking into consideration the shape of a geological body as a sphere, horizontal cylinder, slab which may be responsible for a given gravity anomaly, the depth of body can be estimated. Smith (1959, 1960) has given the depth-estimation formulae for local gravity and magnetic anomalies, which are independent of the shape of the anomalous mass. These are based on Δg_{max} and $\Delta g'$, the maximum gravity anomaly values and its gradient and the depth

Z_g to the top of the body and is expressed as:

$$Z_g \leq 0.86 \mid \Delta g_{max} / \Delta g' \mid \qquad (4.1).$$

When the magnitude of the anomaly is partly known, the gravity value at a point $\Delta g(x)$ and its horizontal gradient $\Delta g'(x)$ can be used to calculate the depth by using the equation:

$$Z_x \leq 1.5 \mid \Delta g(x) / \Delta g'(x) \mid \qquad (4.2).$$

When the gravity anomalies are elongated in one direction (i.e. two dimensional geological body), then the numerical factors in equations 4.1 and 4.2 should be changed to 0.65 and 1 respectively (Sharma, 1986).

Since the three gravity "highs" of Rajula, Palitana and Shihor are more or less circular in form, we can use the equations describing the gravity anomalies produced by a convex and/or spherical bodies (Sharma, 1986). The gravity anomaly caused by such structures is given by:

$$\Delta g = \frac{4 \pi R^3 G \Delta \rho}{3 Z_c^2} \cdot \frac{1}{(1 + (x^2/z^2))^{3/2}} \qquad (4.3)$$

where G is the gravitational constant, $\Delta\rho$ is the density contrast between the geologic body and the surrounding rocks, R is the average radius of body, Δg is the horizontal gradient of the anomaly over a distance x and the Z_c is the depth from the surface to the center of the body (Sharma, 1986). The "half width", $x_{1/2}$ of gravity anomaly is generally used to calculate the Z_c by using:

$$Z_c = 1.305\, x_{1/2} \qquad (4.4)$$

For elongated anomalies Sharma (1986) has considered a buried horizontal cylindrical body. The gravity anomaly due to such bodies is given by the relationship

$$\Delta g = \frac{2\pi G R^3 \Delta\rho}{Z_c} \cdot \frac{1}{(1 + (x/z)^2)} \qquad (4.5)$$

The symbols are same as used in equation 4.3 (Sharma, 1986). For a horizontally elongated body the approximate depth to the center is equal to "half width", $x_{1/2}$. When the density contrast, $\Delta\rho$, is reasonably known, then the size of the convex and elongated bodies can be estimated using equations 4.3 and 4.5 respectively.

Talwani *et al.*, (1959) provided an analytical expression for both vertical and horizontal components of gravitational attraction due to a many sided polygon(body) at a given

point. The accuracy of theoretically calculated Bouguer anomaly depends on how closely a polygon fits a given geological body, which can be improved by either increasing the sides of the polygon or by increasing the number of polygons.

The gravity anomalies along Rajula, Palitana and Shihor extend in the NE-SW direction, hence, the depth to the center of anomalous bodies responsible for the "highs" at each place was estimated by equations 4.3 and 4.4 in NW-SE direction. Here the Z_c in NE-SW direction was calculated using equation 4.5.

Braille *et al.*, (1974) and Fisher and Howard (1980) used an approach of inversion of gravity data to decipher the three dimensional shape of the prism (body) by taking into consideration the variation in density of body. Recently, Richardson and Macinnes (1989) developed a nonlinear inversion scheme for the gravity data into a three dimensional polyhedral model. Their scheme considers the variations in density and shape of subsurface three dimensional body. In this study we have used the methods of Abdeslem (1995) for the inversion of gravity data in order to construct three dimensional shape of subsurface bodies along the Rajula, Palitana and Shihor. Abdeslem (1995) has solved the forward problem in wave-number domain, in which the gravity anomaly power spectrum is given by the product of functions, such as density, depth, thickness and the horizontal dimensions of the subsurface body. The representation of the power spectrum is given by the function:

$$g(k) = \text{Ln}\left(\frac{1}{2\pi}\int_0^{2\pi} d\theta \left|\Delta g(k,\theta)\right|^2\right) = C + H(k,h) + T(k,t) + S(k,a,b) \qquad (4.6)$$

where

$$C = 2\,\text{Ln}(2\pi G\rho) \qquad (4.7)$$

$$H(k,h) = -2hk \qquad (4.8)$$

$$T(k,t) = 2\text{Ln}\{k^{-1}[\,1 - e^{-kt}\,]\} \qquad (4.9)$$

and

$$S(k,a,b) = \text{Ln}\left(\frac{1}{2\pi}\int_0^{2\pi} d\theta \left|s(k,\theta)\right|^2\right) \qquad (4.10)$$

here a and b are the length and width of the body, t is thickness= $h_1 - h_2$ (the difference in the top and bottom of the body), u and v are the wave-numbers in x and y directions and k $=(u^2+v^2)^{1/2}$ which is the magnitude of the wave-number vector, G is the gravitational constant and ρ is the density of the body. H(k,h) , T(k,t) and S(k, a,b) are the depth, thickness and horizontal dimension (length and width) functions, respectively.

4.3 TWO AND THREE DIMENSIONAL GRAVITY MODELLING ALONG RAJULA, PALITANA AND SHIHOR, SAURASHTRA:

The presence of a high density mafic body may be deciphered on the basis of Bouguer gravity anomalies in the Saurashtra peninsula. In order to constrain the crustal structure beneath Rajula, Palitana, and Shihor we have used the Deep Seismic Sounding (DSS) profile carried out by Kaila *et al.*, (1980) in western Saurashtra peninsula. The western most point of the profile is in Navibander town and the eastern most near Amreli (Figure 4.1). From the center of the profile towards the western direction, the thickness of the Deccan traps (5.5 km/sec., P_v) varies from 900 m to 1500 m, whereas towards the eastern side the thickness decreases continuously to 350 m. The Mesozoic sediments below the Deccan Traps are around 850 m thick, when the P_v velocity for them was taken as 4 km/sec. Mesozoic sediments are underlain by 3.8 km pre-Cambrian crystalline basement rocks. The total thickness of the upper crust (Deccan Traps+Mesozoic sediments+Crystalline basement) on the NW of the study area is around 6.15 km. The crustal section along the profile have been demarcated into six blocks by five deep seated Moho cutting faults. The depth of the Moho reflectors along the profile varies from 35 km to 42 km. Figure 4.2 shows the observed (circles) and theoretically calculated (continuous curve) gravity anomaly along the profile. Calculated effect of magnitude of gravity due to Deccan Traps and Mesozoic sediments is not compatible with the observed gravity high of +40 mGal. However, both observed and calculated gravity anomalies match well when a high density mafic body with 2960 kg/m^3 density is considered emplaced at a depth of 6 km. The estimated dimensions of this mafic

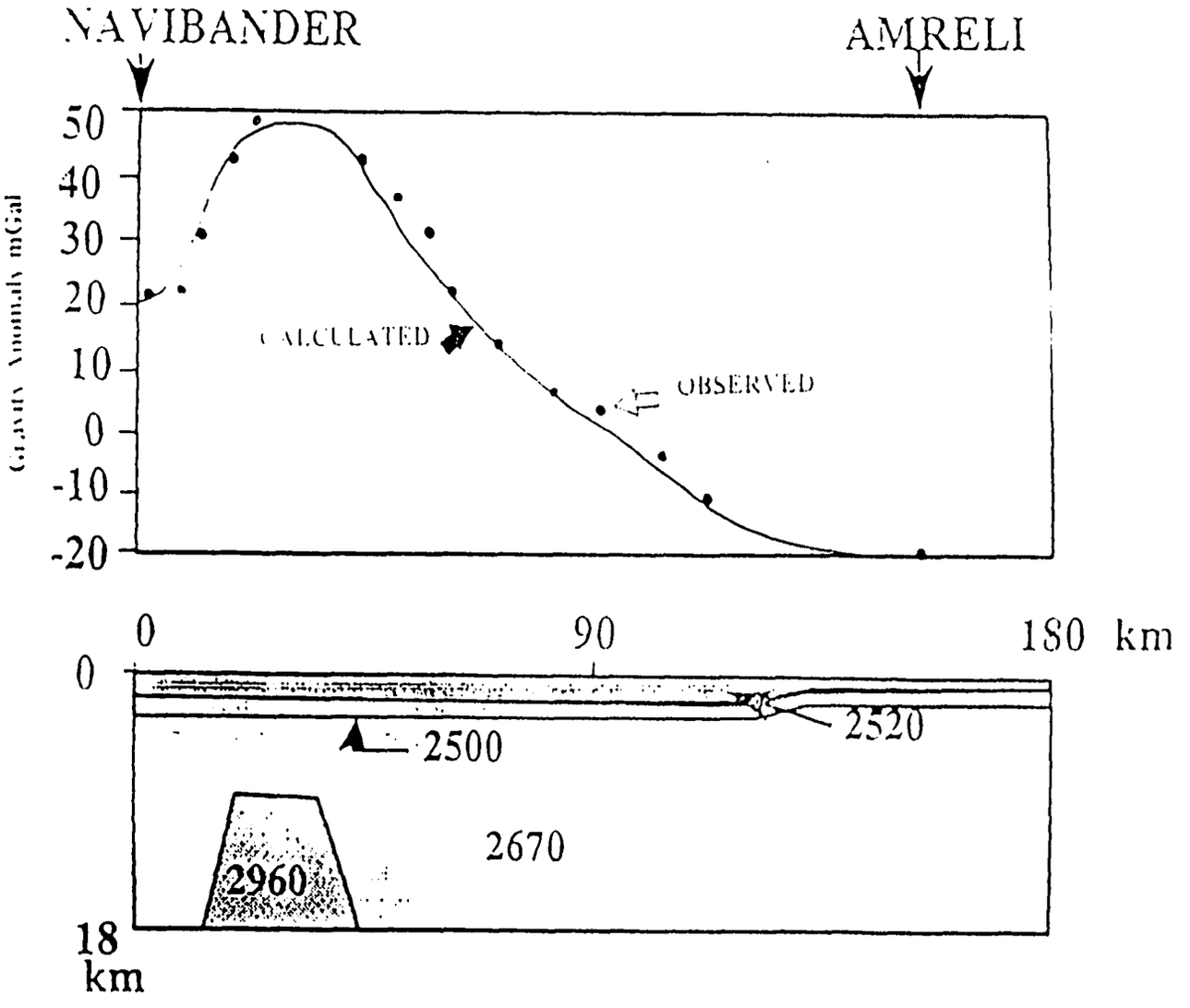

FIGURE 4.2: Observed and theoretically calculated gravity anomalies along Navibander-Amreli profile. The calculated and observed anomalies match well when a mafic body is assumed at a depth of 6±0.6 km with the density of 2960 kg/m^3. The mafic body has a width of 16±1.6 km and 30±3 km at the top and bottom and is 12±1.2 km thick.

body are 16±1.6 km and 30±3 km wide at the top and bottom and the thickness is 12±1.2. Similar crustal structure is considered for gravity modelling of the eastern Saurashtra peninsula.

As mentioned earlier, the region around Rajula is marked by a gravity high of +40 mGal and the $x_{1/2}$ (half width) of +20 mGal in SE direction is at a distance of 9.5±1 km and in NW direction it is 7.2±0.75 km. These $x_{1/2}$ values give Z_c (depth to the center of mafic body, equations 4.1 and 4.2) values of 12.5±1.25 km and 9.4±1 km. The $x_{1/2}$ of +20 mGal in NE direction is at a distance of 12.5±1.25 km, hence Z_c for the anomalous body is at a depth of 12.5±1.25 km. The average depth of the center of excess mass beneath Rajula is estimated to be 11.5±1.2 km (Table 4.1). Figure 4.3 shows two dimensional observed and theoretically calculated Bouguer anomaly along A-B over Rajula. The best fit of observed and calculated gravity anomalies is when a convexly shaped mafic body with an excess mass(300 kg/m^3) is considered to have emplaced at a depth of 6±.6 km. The mafic body has an average density of 2950 kg/m^3. By considering the depth of the mafic body at 6±.6 km and the thickness of 14±1.4 km, we have determined three dimensional shape of this body. Widths of the mafic body at the top and the bottom are taken as 3±0.3 km and 8±0.8 km, respectively. Like previous cases the +ve Bouguer anomaly data points were gridded in the grid of 49x49 in N-S and E-W directions and an average density of the mafic body is taken as 2950 kg/m^3. The Octant search method is used to locate gravity data points in which the area around a grid is divided into eight equal octants and all the gravity data points in these octants are used to estimate the value for the grid. Minimum curvature algorithm (Briggs, 1974) is used for

TABLE 4.1 : ESTIMATED Z_c OF THE MAFIC BODIES BENEATH RAJULA, PALITANA AND SHIHOR, IN SE, NE, NW AND SW DIRECTIONS.

	RAJULA km.	PALITANA km.	SHIHOR km.
SE	12.5	12.7	9.4
NE	12.5	12.5	12.5
NW	9.4	9.4	9.4
SW	Open Contours on SW side	12.5	12.5

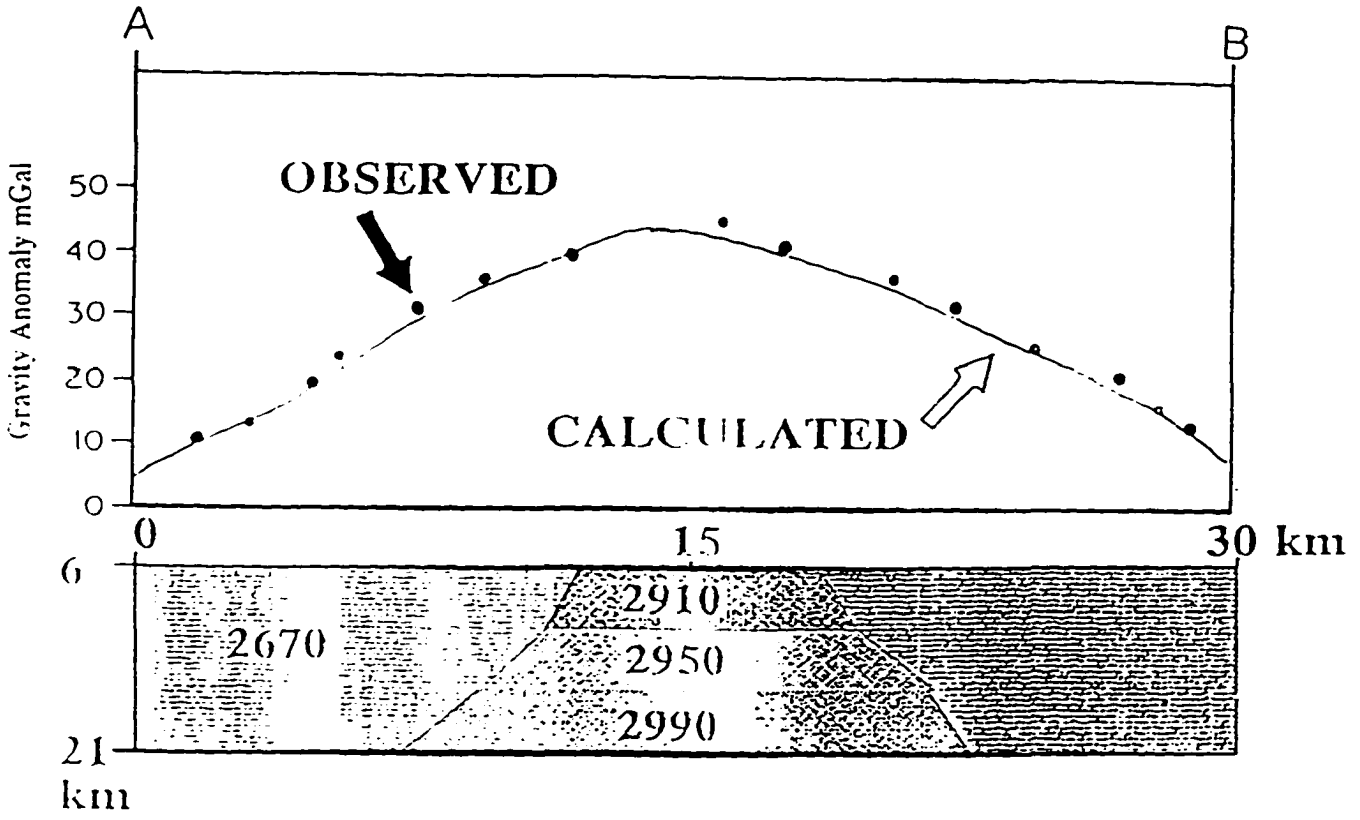

FIGURE 4.3: Observed and calculated gravity anomalies along Rajula area. The crustal structure beneath Rajula is considered to be similar along Navibander -Amreli profile (Figure 4.2). Calculated and observed gravity anomalies match well

gridding interpolation. Figure 4.4 shows an orthographic view from the southeast direction with a 30^{0} rotation around the vertical axis. The orthographic projection is formed by projecting the three dimensional space coordinates of the mafic body onto a plane oriented perpendicular to the line of sight. Figure 4.4 shows that the mafic body is convexly shaped and slightly elongated in NE-SW direction.

Similar calculations based on the Bouguer gravity data were carried out to calculate two and three dimensional shape of the mafic bodies beneath Palitana and Shihor. Table 4.1 also shows the estimated values of Z_c in NE, NW, SW and SE directions for Palitana and Shihor. Average depths of the center of the mafic bodies(equations 4.3 and 4.4) at Palitana and Shihor are 11.8 ± 1.2 km and 10.9 ± 1.1 km respectively. Figures 4.5 and 4.6 show the observed and calculated (Talwani, 1959) Bouguer anomalies along X-Y and P-Q at Palitana and Shihor. The best fit between the observed and calculated anomalies are when the shape of the mafic bodies at both locations are taken as convex upward and emplaced at a depth of $6\pm.6$ km. At Palitana the best fit is when the convex body is considered with an average density of 2950 kg/m^3. From these dimensions we have deduced the three dimensional shape of the mafic bodies beneath Palitana and Shihor. Figures 4.7 and 4.8 show three dimensional convexly upward shape of these mafic bodies at a depth of 6 ± 0.6 km, along Palitana and Shihor. The estimated densities of these mafic bodies beneath Palitana and Shihor are 2950 kg/m^3 and 2990 kg/m^3, respectively. Figures 4.7 and 4.8 indicate that the mafic bodies beneath Palitana and Shihor are also elongated in NE-SW direction. Estimated dimensions are listed in Table 4.2 (depth from the surface, length, width, thickness, and

FIGURE 4.4: Three dimensional gravity modelling over Rajula area. The three dimensional shape of mafic body indicates an upward curvature with undulations and elongation in NE-SW direction.

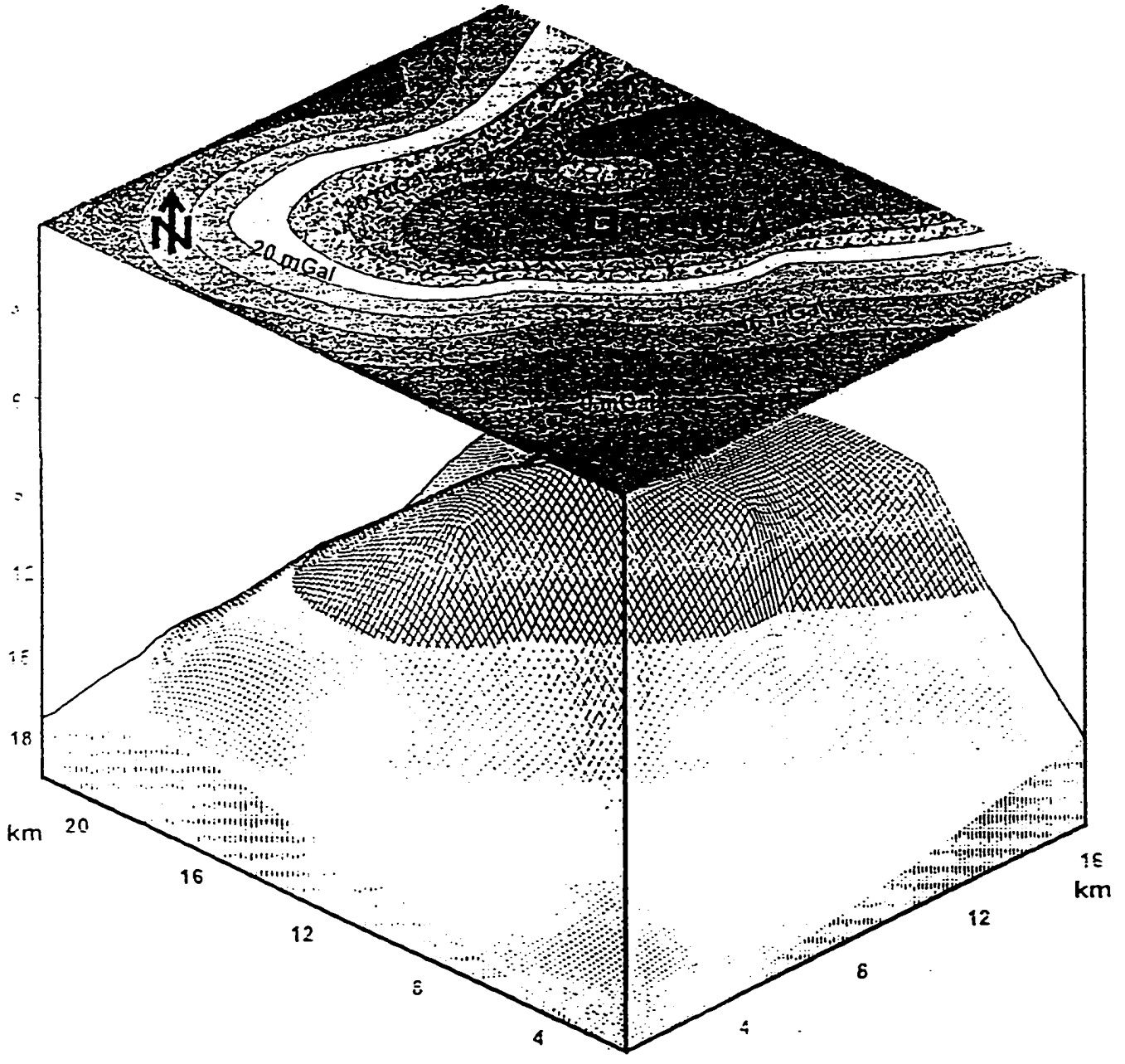

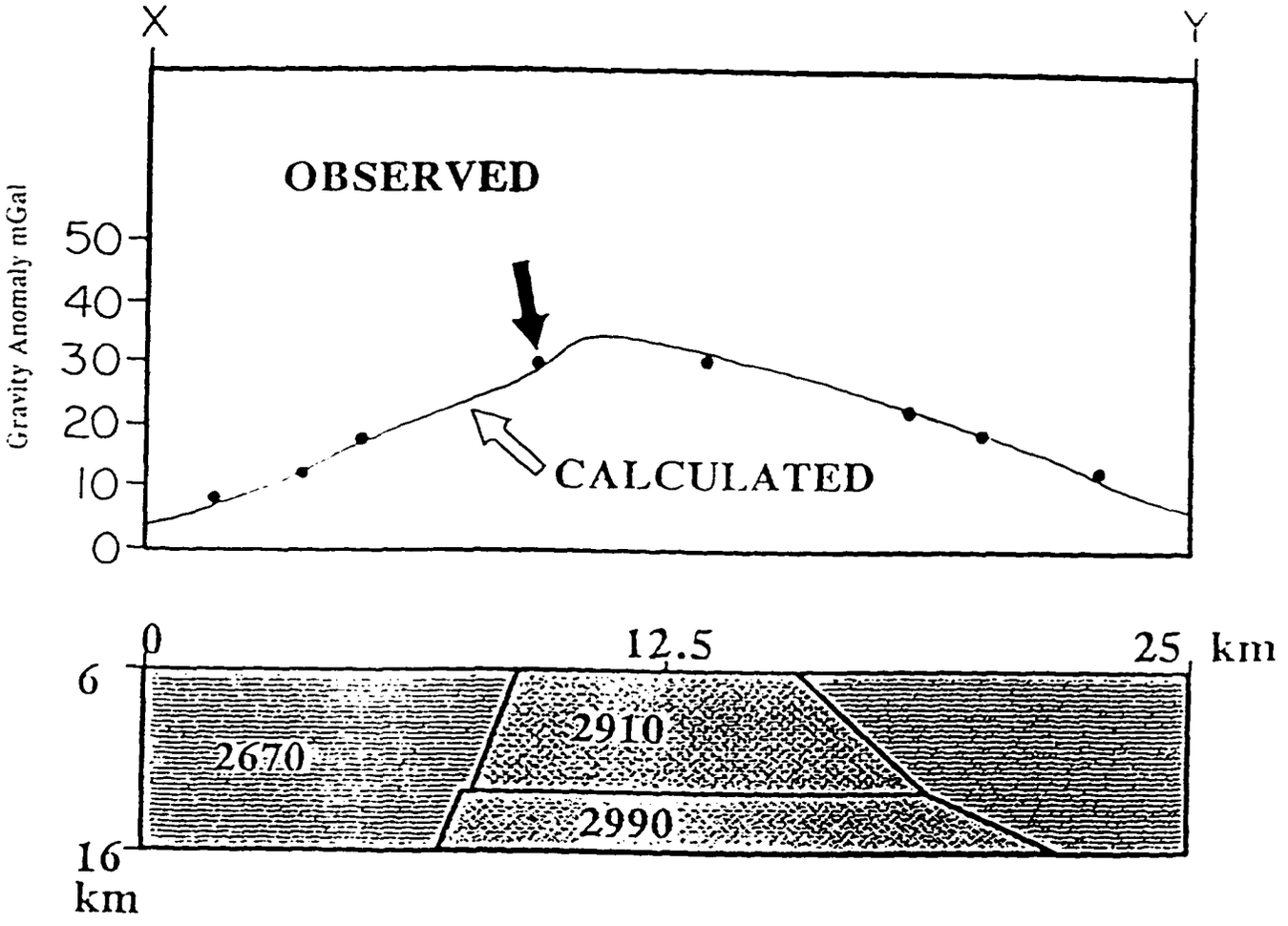

FIGURE 4.5: Two dimensional gravity modelling along X-Y over Palitana. Observed and calculated anomalies matches well when a convexly shaped body with an average density of 2900 kg/m^3 is assumed to have emplaced at a depth of 6±0.6 km.

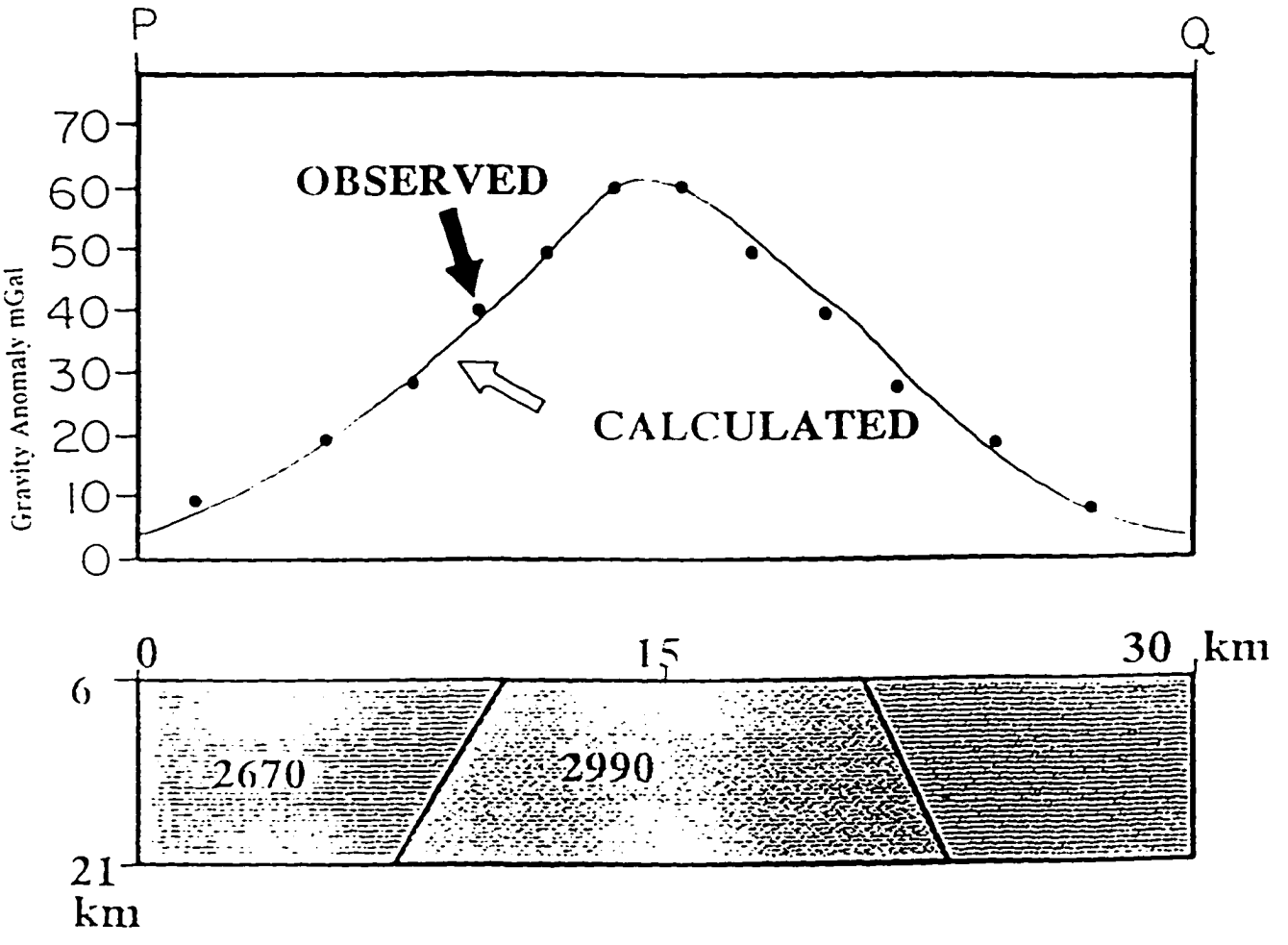

FIGURE 4.6: Two dimensional shape of mafic body along P-Q (Figure 4.1) beneath Shihor. The shape of the mafic body is deciphered on the basis of two dimensional gravity modelling. Observed and calculated anomalies match well when a mafic body with 2900 kg/m^3 density is assumed to have emplaced at a depth of 6±0.6 km.

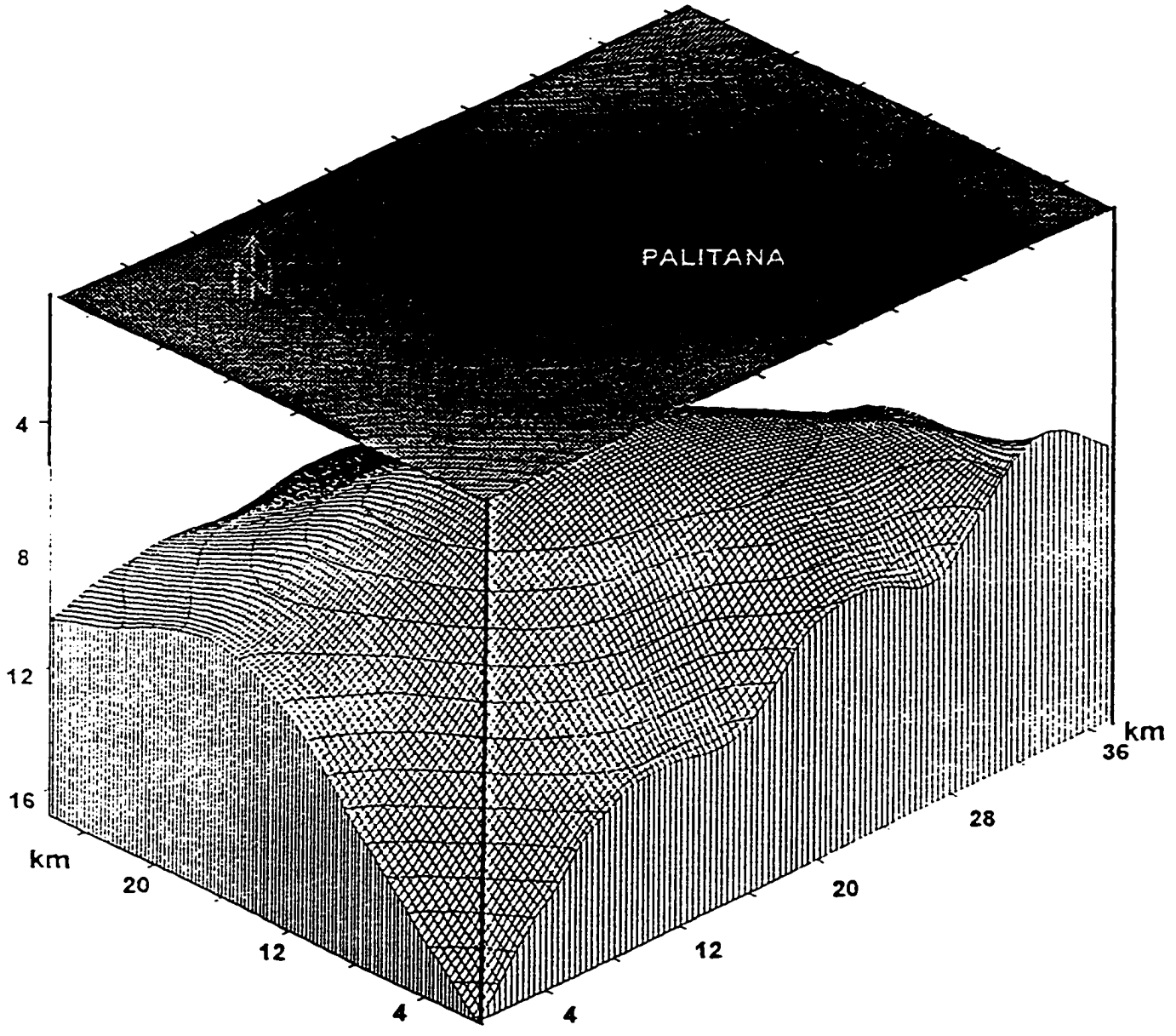

FIGURE 4.7: **Three dimensional shape of the mafic body beneath Palitana. Convexly upward shape of the mafic body shows elongation in NE-SW direction.**

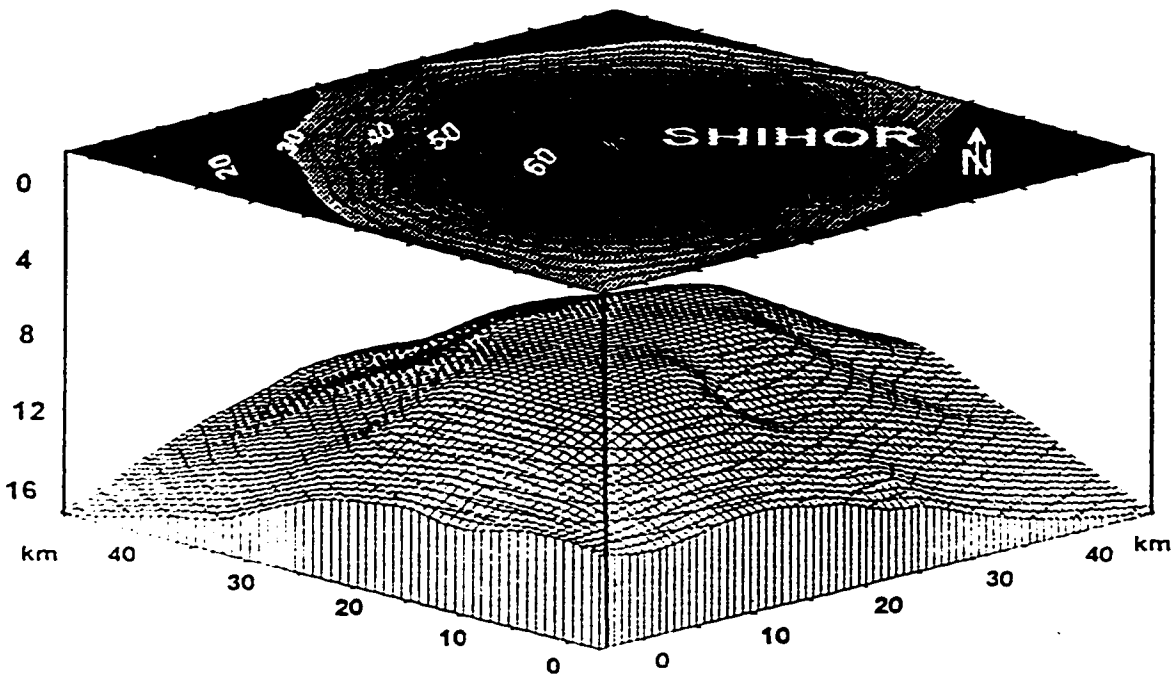

FIGURE 4.8: Three dimensional shape of the mafic body beneath Shihor. The mafic body is convexly upward and elongated in NE-SW direction.

TABLE 4.2: The dimensions (width, length and thickness), depth and estimated densities of mafic bodies beneath Rajula, Palitana and Shihor in Saurashtra. They are determined from two and three dimensional gravity modelling. Note that the mafic body beneath Shihor is larger in dimension and has higher density.

LOCATION	WIDTH TOP (km)	WIDTH BOTTOM (km)	LENGTH TOP (km)	THICKNESS (km)	DEPTH (km)	DENSITY (kg/m^3)	CHARACTERS-TICS
RAJULA	3±0.3	8±0.8	18±1.8	14±1.4	6±0.6	2910±291 2950±295 2990±299	Density Stratified
PALITANA	6.5±0.6	15±1.5	20±2	10±1	6±0.6	2910±291 2990±299	Density Stratified
SHIHOR	11±1	16±1.6	22±2.2	15±1.5	6±0.6	2990±299	Unstratified

densities of mafic bodies beneath Rajula, Palitana and Shihor). Based on these parameters we have constructed a combined three dimensional shape of the mafic bodies along NE-SW direction in Saurashtra (Figure 4.9). Here also all the gravity data points are gridded in the grid of 49x49 in N-S and E-W directions. Figure 4.9 clearly shows that the mafic body beneath Shihor is larger in dimensions (width, length and thickness, Table 4.2) than the mafic bodies beneath Rajula and Palitana, hence giving rise to +60 mGal Bouguer gravity anomaly.

4.4 MECHANISM OF EMPLACEMENT OF MAFIC PLUTONS ALONG RAJULA, PALITANA AND SAURASHTRA:

Two models that can account for the emplacement of these three large pluton like mafic bodies beneath Rajula, Palitana and Shihor are diapiric and dike models. The diapiric model deals with the balloon shaped diapiric ascent of the magmatic bodies through the upper mantle and the crust (Grout, 1932). This model can be elaborate further by considering the rise of a diapir through either the temperature dependent viscous crust and/or mantle (Mahon *et al.*, 1988) or shear strain rate dependent (power law) crust or mantle (Weinberg and Podladchikov, 1994).

The dike model however considers emplacement of the pluton like mafic bodies in the form of extremely large and wide dikes of mafic bodies. These two models are end members in the real world and the emplacement mechanism for the mafic bodies could be a combination of both diapiric and dike models.

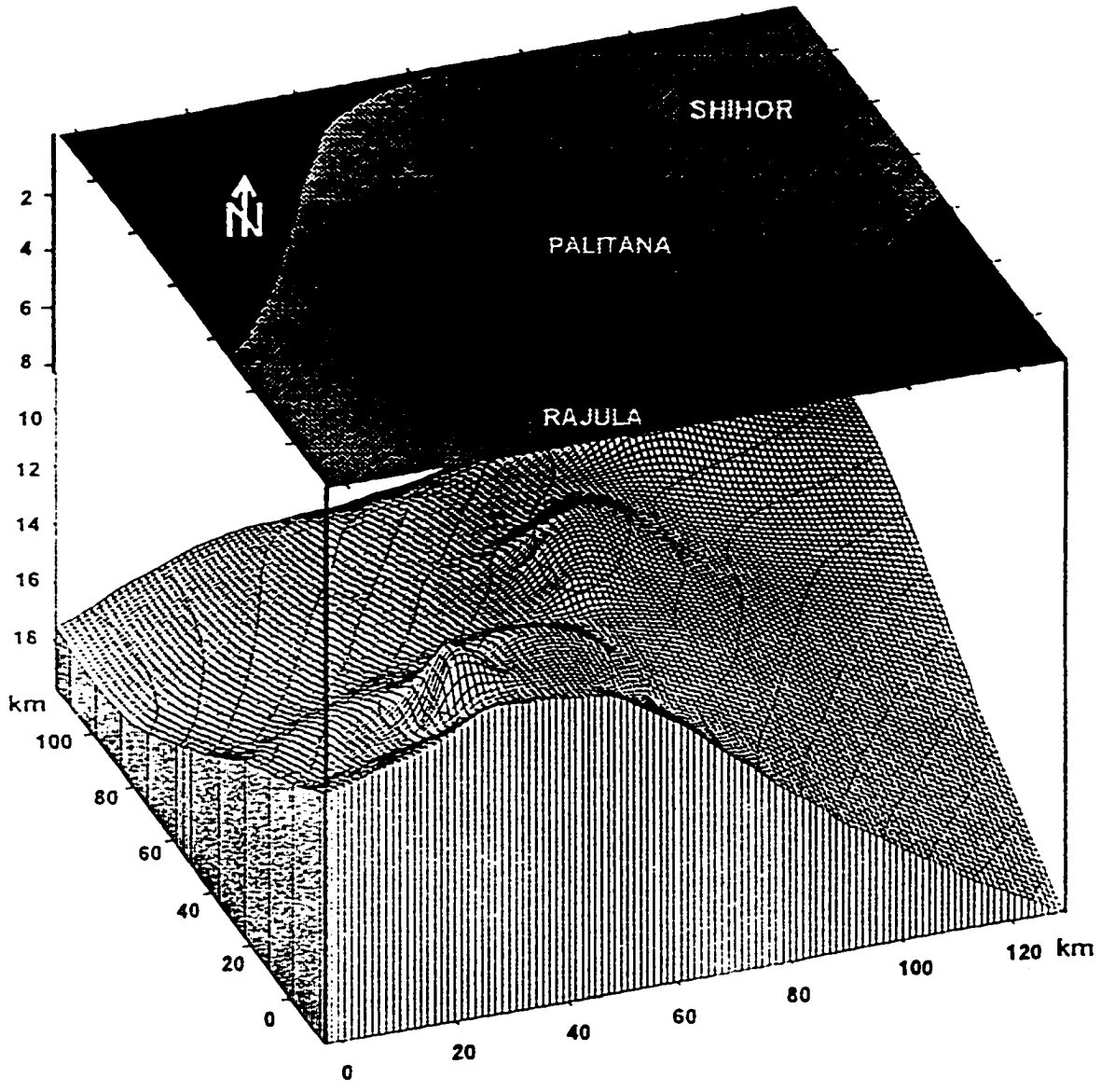

FIGURE 4.9: Combined three dimensional shapes of the mafic bodies beneath Rajula, Palitana and Shihor.

(i) DIAPIRIC MODEL:

The abundance of granitoid bodies in the form of large plutons and their mechanism of emplacement is still uncertain and conjectural. For a pluton to rise through the crust and/or upper mantle in the absence of extensional stresses, it needs an energy conservative mechanism. The initial formation of these large mafic bodies may be explained using Rayleigh Taylor instability theory (Crane, 1985). According to this model instantaneous harmonic upwelling of less dense material takes place when it is overlain by layers of higher density. Figure 4.10(a) shows the initial model that includes two layers: upper layer of thickness h_1 and viscosity η_1 and a lower layer with thickness h_2 and viscosity η_2, where $\eta_2 < \eta_1$. Instabilities develop in the low-viscosity layer (h_2) when it is perturbed due to disequilibrium. This leads to the penetration of the low viscosity layer into the high viscosity layer in the form of diapirs at evenly spaced points with wavelength λ. The spacing of diapirs depends on the viscosity contrast (η_1/η_2) and the thickness ratio of two layers (h_1/h_2) and is given by equation:

$$\lambda = \frac{2\pi}{2.15} h_2 \left\{ \frac{\eta_1}{\eta_2} \right\}^{1/3} \qquad (4.11)$$

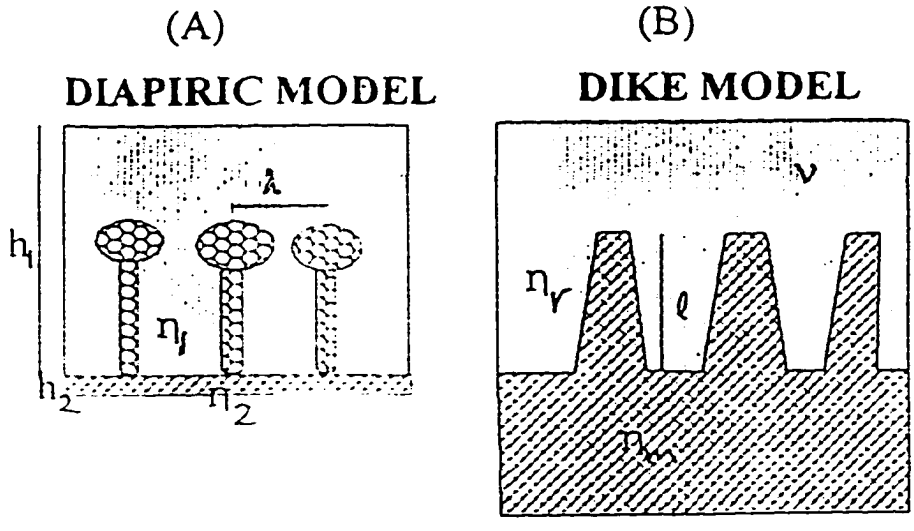

FIGURE 4.10: Schematic diagram showing comparison of diapiric and dike models for the emplacement of mafic bodies beneath Rajula, Palitana and Shihor. The diapiric model contains two layers with thickness h_1 and h_2 with the viscosities of η_1 and η_2 where $\eta_1 > \eta_2$. Instabilities develop in the low viscosity layer (h_2) when it is perturbed due to disequilibrium. The dike model explains the emplacement of three mafic bodies in the form of large dikes, here $\mu/(1-\nu)$ is host rock stiffness, η_m and η_r are the viscosities of dikes and host rock and ℓ is the length of dike.

and the diameter (d) of diapir is governed by the equation:

$$d = h_2(\eta_1/\eta_2)^{1/4} \qquad (4.12).$$

Lingenfelter and Schubert (1974) and Marsh (1975) used the Rayleigh Taylor model to explain the generation and distribution of island arc volcanoes. This model was also used by Crane (1985) to demonstrate that the rift axis highs along spreading centers depend upon the harmonic rise of diapirs. Recently, Rohrman and Beek (1996) analyzed the Cenozoic postrift domal uplift of north Atlantic margin using Rayleigh Taylor instability.

The spacing between the mafic bodies beneath Rajula, Palitana and Shihor is approximately 50 km, which is λ (Figure 4.1). The average thickness of the upper layer h_1 is around 20 km. The viscosity contrast between the wall rock and the mafic bodies with density varying from 2910 ± 291 kg/m^3 to 2990 ± 299 kg/m^3 is approximately 10^6 MPa. Substituting these values into equation 4.11 gives an approximate value of h_2 between 100 and 200 m. This value for h_2 is very low to produce such large mafic bodies beneath Rajula, Palitana and Shihor.

(ii) EXPLANATION FOR THE ELLIPSOIDAL SHAPE OF MAFIC BODIES:

The three mafic bodies beneath Rajula, Palitana and Shihor are distorted convexly upward shaped ellipsoids. For example, the aspect ratios (width/thickness) of the

mafic body beneath Rajula are 1:4.76 and 1:1.75, respectively, in the vertical section. However, in plan view they are 1:5.8 and 1:2.28, respectively. These different values of the aspect ratios for the top and the bottom of mafic body suggest that it has more ellipticity at the top than the bottom. Similar calculations of the aspect ratios for the mafic bodies beneath Palitana and Shihor (Table 4.2) again suggest that these mafic bodies also have higher ellipticity at the top than the bottom.

The deformation of diapirs from spherical to ellipsoidal shape may be due to (i) upward increase in viscosity of the upper lithosphere due to decrease in temperature, (ii) heterogeneities of the wall rock properties, (iii) asymmetrical thermal aureole around diapirs and (iv) interaction with other rising diapirs. The first effect, is an increase in viscosity of the upper lithosphere due to decrease in temperature and causes the diapir to expand laterally and deform from spherical to a flat lying ellipsoidal shape. In the lower lithosphere, the isoviscous lines produced by the geothermal gradient have larger vertical spacing relative to the diameter of a diapir. As a result, in this region the viscosity can be considered constant therefore drag suffered by diapir is similar in the front and the back. Thus in the lower lithosphere the diapirs may retain their spherical shapes. However, in the upper crustal region the isoviscous lines have smaller vertical spacing as compared to the diameter of the diapirs. Hence, in this region the drag on the front of the body may be more than the back of the body. The drag depends on the local shear stress, as well as on the surface area and the shape of the body. This is expressed by the equation:

$$D_s = (4\pi r^2)\,(\eta 3V/2r) \qquad (4.13)$$

where D_s is the drag, r is the radius of the diapir, η is the viscosity of wall rock, and V is the velocity. Equation 4.13 clearly states that as the viscosity of the wall rock increases the drag on the diapir increases (directly proportional to each other) and its ascent velocity decreases. Thus in the upper crust the greater vertical variation in viscosity, the diapir expands laterally and flattens vertically. This can explain greater ellipticity of the shape of mafic bodies beneath Rajula, Palitana and Shihor. For example, the ellipticity of the mafic body beneath Palitana has an ellipticity of 3 for the top and 1.33 for the bottom. Similarly the mafic body beneath Shihor shows ellipticity of 2 and 1.36 at the top and the bottom. These observations clearly indicate that vertical variation in the viscosity of the upper crust was the dominant factor in causing the ellipsoidal shape of the mafic bodies beneath Rajula, Palitana and Shihor. The interaction between the diapirs which may cause the ellipticity can be ruled out as the gravity highs over Rajula, Palitana and Shihor have distinct and regular shapes. The interacting mafic bodies generally show asymmetrical gravity highs which is not the case here. It is possible that the asymmetrical thermal aureole around diapirs may have played an additional role in causing ellipticity at the end of their ascent when they were primarily deformed due to the variation in viscosity (around 10^6 MPa) of the upper crust.

(iii) DIKE MODEL:

The ascent of mafic magma through the upper lithosphere generally occur in the

form of dikes (see eg. Rubin 1993 a; b). The mafic bodies beneath Rajula, Palitana and Shihor have an average density of 2990 kg/m^3 suggesting gabbroic type body. These mafic bodies are extremely large generally in the form of plutons implying that the mafic magma not only ascends in the form of dikes but also in the form of plutons. Figure 4.10(b) shows a schematic diagram of the emplacement of mafic bodies along Saurashtra in the form of large dikes. The propagation of a dike is controlled by three dimensionless parameters. These are (i)

$$B = g\Delta\rho w^4/\eta\kappa\ell \qquad (4.14)$$

where B is the Biot number, g is acceleration due to gravity, $\Delta\rho$ is the density difference, w is the width of dike, η is magma viscosity, κ is thermal diffusivity and ℓ is the length of dike. The other two parameters are the Stefan numbers

$$S_- = L/c(T_w - T_-) \qquad (4.15)$$

and

$$S_m = L/c(T_m - T_w) \qquad (4.16)$$

here L is the latent heat of solidification, c is the specific heat, T_- is the far-field temperature of the crust, T_m is the initial magmatic temperature and T_w is the temperature at which magma near the dike wall is immobile. The critical width to transport magma through the upper lithosphere is:

$$w_c = 1.5(S_m/S_-^2)^{3/4}(\eta\kappa H/g\Delta\rho)^{1/4} \qquad (4.17)$$

We assume that c=730 J kg^{-1} ^{0}C^{-1}, L=8x10^5 J kg^{-1}, κ=10^{-6} m^{2}s^{-1}, T_m=1200 ^{0}C,

$T_w = 1150\,^{o}C$ and $\eta = 100$ Pa s (Huppert and Sparks, 1980). Substituting these values into equation 4.16 the S_m is around 1.3. The value of T_s can vary from 180 ^{o}C to 1150 ^{o}C, if we consider the geothermal gradient of 30 ^{o}C. Substituting these values of T_s into equation 4.15 to calculate S_s which can vary from 1.13 onwards to ∞. Substituting these values into equation 4.17 for the estimation of critical width of dike to transport magma without freezing comes to around 4 m. The width of mafic plutons along Saurashtra varies from 3 ± 0.3 km to 16 ± 1.6 km suggesting that these bodies may have been emplaced as forcible intrusions into the upper lithosphere without freezing. However, how these plutons made room for their emplacement in the upper crust is problematical. Absence of extensional stresses (example: expressed in the form of rift) in the Saurashtra peninsula however suggests that the mafic bodies must have been emplaced in the form of diapirs rather that forceful and rapid intrusions.

4.5 DISCUSSION:

Basaltic bodies commonly occur as planar dikes whereas granitoid bodies exist in equi-dimensional plutons. Contrary to these common modes, large mafic plutons can also occur in the upper lithosphere as confirmed by the three dimensional gravity models of positive anomalies in Saurashtra peninsula over Rajula, Palitana and Shihor. The dominant processes that occur in a mafic diapir during its ascent through the upper lithosphere are heat transfer to the surrounding rocks and the movement of wall rock either in the form of thermal softening or strain rate softening (Mahon *et al.*, 1988; Weinberg and Podladchikov, 1994). The ascent of such diapirs through the upper lithosphere by strain rate softening appear to be

the dominant process as suggested by the absence of extensive migmatites around plutons (Weinberg and Podladchikov, 1994). As the mafic diapir rises, it looses thermal energy to the surrounding rocks and encounters lower ambient upper lithosphere temperature. This upward decrease in temperature causes an increase in viscosity, hence the drag in front of a diapir is generally more than its back. This phenomenon causes the diapir to expand laterally and flatten vertically. As a result the plutonic mafic bodies beneath Rajula, Palitana and Shihor are not only ellipsoidal in shape but also have greater ellipticity at the top than the bottom as shown earlier by gravity analyses. Eventually, the mafic plutons along Rajula, Palitana and Shihor in Saurashtra may have cooled to a point and ceased to ascend when reached depth of $\approx 6 \pm 0.6$ km. It is also possible that stoppage of plutons at a depth of $\approx 6 \pm 0.6$ km could be due to difference in rheology in the upper crust, as the upper crust is made of pre-Cambrian granulitic basement, Mesozoic sediments, and Deccan volcanics which are about 6.5 km in thickness in this region (Kaila, 1988). Here the main parameters that appear to have control the solidification depth of mafic diapirs are: (i) volume of mafic magma, (ii) temperature contrast between the mafic magma and the surrounding rocks and (iii) the viscosity contrast between the magma and the country rock.

CHAPTER 5

VENTING, REPLENISHMENT, ASSIMILATION, AND FRACTIONAL CRYSTALLIZATION MODELLING (VRAFC) OF THE MAGMA CHAMBER AND ITS APPLICATION TO THE DECCAN VOLCANIC PROVINCE, WESTERN INDIA

5.1 INTRODUCTION:

The western margin of the peninsular India is covered by Deccan Traps, one of the largest continental flood basalt provinces of the world. Besides being predominantly tholeiitic in composition, Deccan Traps also include other rock types, such as, sodic-alkalic intrusives, silicic rocks and carbonatites which are reported by Sukheswala and Udas (1963), Sethna (1971) and Yellur (1968) from Chota Udaipur (Ambadongar) area of the intra plate Narmada-Tapti rift. Similarly a range of rock types from gabbro to diorite to nepheline syenite have been reported from Girnar intrusive complex in south western Saurashtra (Bose, 1973; Murli *et al.*, 1976; Paul *et al.*, 1977). The Rajpipla volcanic suite consists of highly porphyritic flows of basalt and trachybasalt. The major rock types are ankaramite, mugearite, picritic basalt and rhyolite (Krishnamurthy and Cox, 1980; Mahoney *et al.*, 1985). The potassic alkalic basalts are underlain by low K-tholeiitic basalts and intruded by alkalic dikes

or plugs. The alkalic and tholeiitic basalts alternate stratigraphically in the Rajpipla area (Figure 5.1) indicating that they erupted contemporaneously (Mahoney *et al.*, 1985). The petrogenesis of rhyolites and trachytes from the west coast of India was studied by Lightfoot *et al.*, (1987) using Sr, Nd, Pb isotopes and trace elements.

The study area Rajula (includes Rajula, Palitana, and Shihor, Figure 5.1 B,C) lies on the southeastern and central parts of the Saurashtra peninsula. The Rajula area is characterized by the presence of differentiated dikes and dike swarms cutting across the Deccan Traps. Mishra (1977) proposed possible westward extension of the Narmada-Son lineament (presently known as Narmada-Tapti rift) towards Murray ridge (Arabian sea) and on the eastern side to the eastern syntaxial bend of Himalayas, thereby making it a part of the world wide rift system. He explained the westward and eastward extensions of the Narmada-Tapti rift on the basis of air borne magnetic anomaly map of the north Arabian sea and Bouguer gravity anomaly map of the Indian ocean which include the study area Rajula as a part of the postulated westward extension of the Narmada-Tapti rift (Figure 5.1). So far very limited geological study has been carried out in Rajula area primarily by Misra (1976 and 1983) and Melluso *et al.*, (1995). Misra (1983) used remote sensing techniques to interpret the Landsat imageries in order to interpret the tectonic setting and aerial extension of Deccan volcanism in the southern part of Saurashtra peninsula. He has shown that various suites of rocks (such as rhyolite, trachyte, dolerite and pitchstone) occurring as dikes and flows are associated with tholeiitic Deccan basalts in the Rajula area. Recently, Melluso *et al.*, (1995) studied the petrology and geochemistry of the basalts of the Saurashtra (except Rajula area)

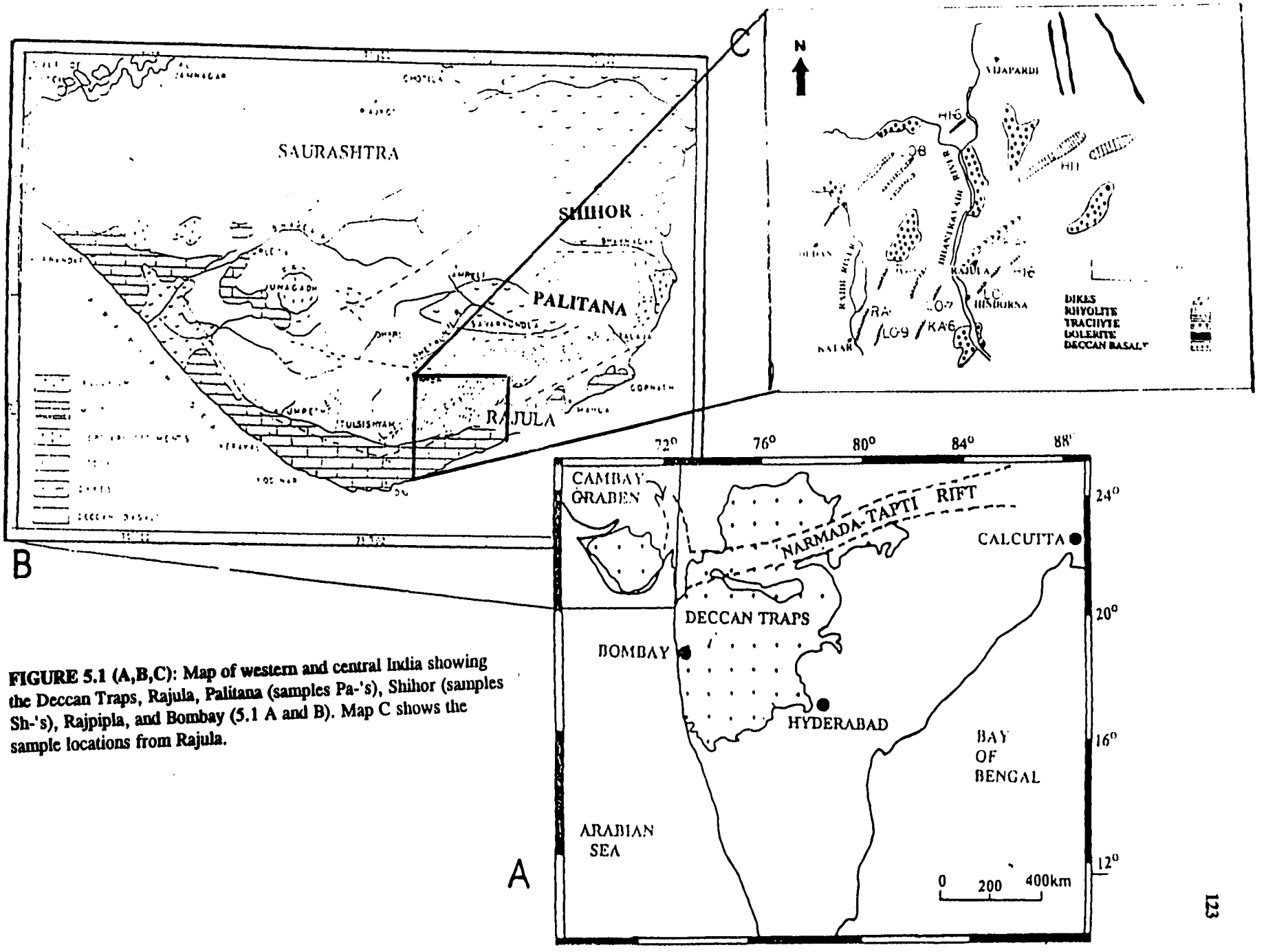

FIGURE 5.1 (A,B,C): Map of western and central India showing the Deccan Traps, Rajula, Palitana (samples Pa-'s), Shihor (samples Sh-'s), Rajpipla, and Bombay (5.1 A and B). Map C shows the sample locations from Rajula.

and tried to establish the mantle source for these basalts. The main aim of the present study is to describe the geochemical characteristics and evolution of the rocks of Rajula area and compare them with the rocks from other parts of western India, (Saurashtra, Narmada-Tapti rift, Deccan tholeiitic basalts from west coast of India) and the Reunion Islands.

5.2 PETROGRAPHICAL AND GEOCHEMICAL CHARACTERISTICS OF THE ROCKS OF RAJULA AREA (Rajula, Palitana and Shihor):INDICATIONS OF THE PROCESSES OF FRACTIONATION AND CONTAMINATION

PETROGRAPHY:

Total 80 thin sections of rhyolite, trachyte, pitchstone, dolerite and basalts from Rajula area were studied to understand the type, shape, and size of phenocrysts. Another emphasis to study thin sections is to understand degree and products of alteration of these phenocrysts. Following are the main characteristics features of the rocks present in Rajula area.

RHYOLITES: The rhyolites of the Rajula area are hypocrystalline in nature and characterized by the presence of anhedral to subhedral phenocrysts of sanidine, quartz and anorthoclase (Figure 5.2). Few phenocrysts of augite and plagioclase are also observed. The groundmass is from glassy to microlitic. Phenocrysts are generally randomly distributed, but at places they show glomeroporphyritic texture. The alteration of the anorthoclase along grain boundaries

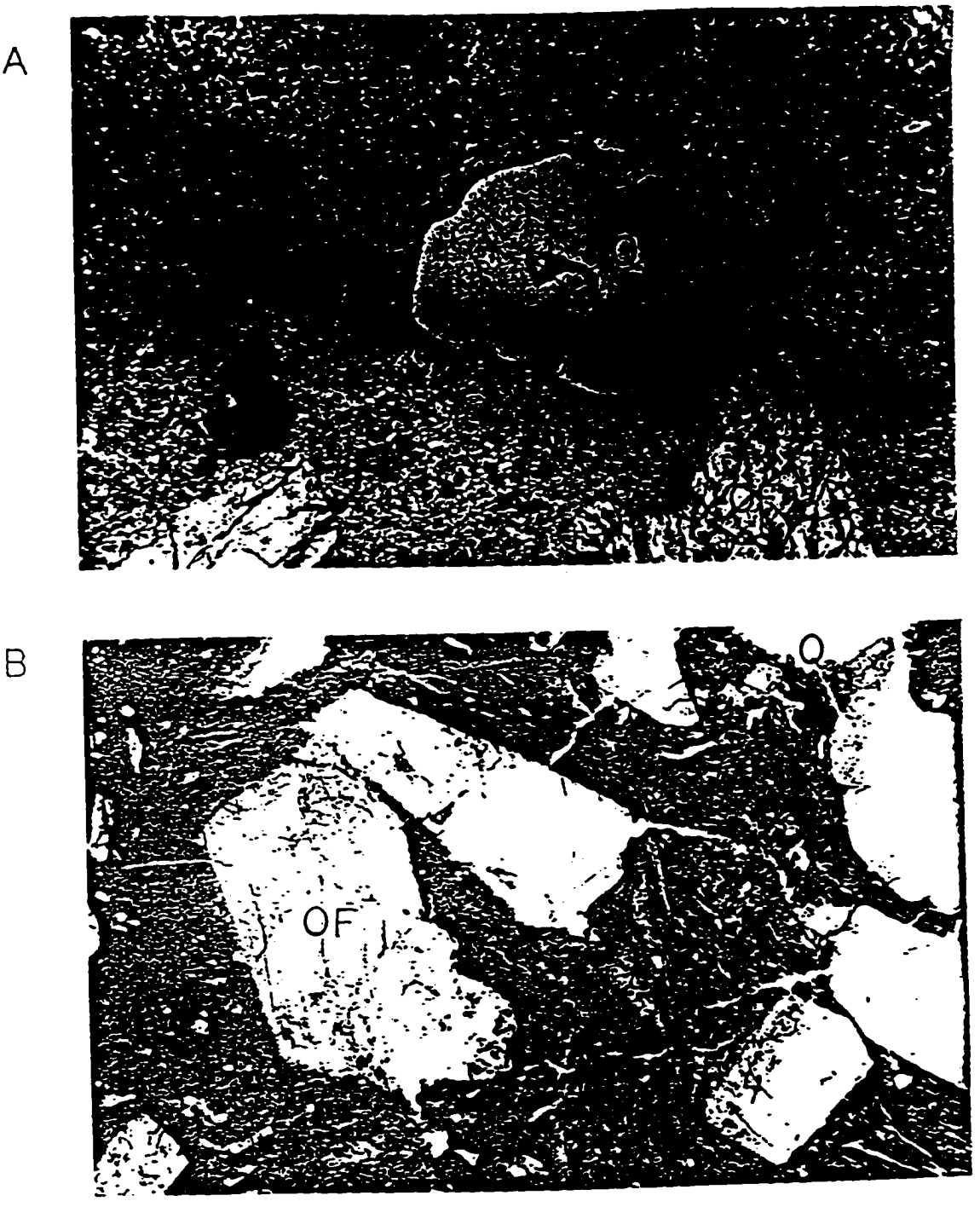

FIGURE 5.2. Microphotographs of rhyolites showing broken fragments of orthoclase feJspars (OF) in both A and . Quartz phenocrysts ar not broken but more rounded. Both photographs are 4 mm in longer dimension.

and fractures is a common feature. Few rhyolites from the Rajula town show primary as well as secondary banding (layering) of quartz and sanidine. These bands are oriented in E-W direction.

TRACHYTES: The trachytes from the study area are hypocrystalline in nature with randomly distributed phenocrysts of anorthoclase, orthoclase and plagioclase in glassy to microlitic groundmass (Figure 5.3). Few crystals of sanidine and quartz are also present. Most of the phenocrysts are partly altered to clay minerals. Microlites in some of the trachytes from Rajula town and Shihor show flow textures in N-S to NNW-SSE directions.

DOLERITES AND BASALTS: Dolerite (dikes) and basalt (flows) from the study area are hypocrystalline with fine to medium grained laths of plagioclase randomly distributed in glassy to microlitic ground mass (Figure 5.4). Aegrine augite is also the dominant mineral present in dolerite and basalt and show ophitic and subophitic texture with plagioclase felspar. Most of the plagioclase felspar are twinned and fractured along which alteration has taken place. Few Aegrine augite crystals show reaction rims along grain boundaries (corona texture). The radiating acicular crystals which form the reaction rim are of hornblende. The dolerite from the Vijapardi area show the presence of anhedral quartz crystals as an amygdoloidal mineral.

PITCHSTONE: An outcrop of pitchstone has been found on the southeastern margin of Rajula town (Figure 2). The pitchstone is glassy and shows flow texture (Figure 5.5). Only seven orthoclase and quartz phenocrysts are observed in an area of 8 cm^2.

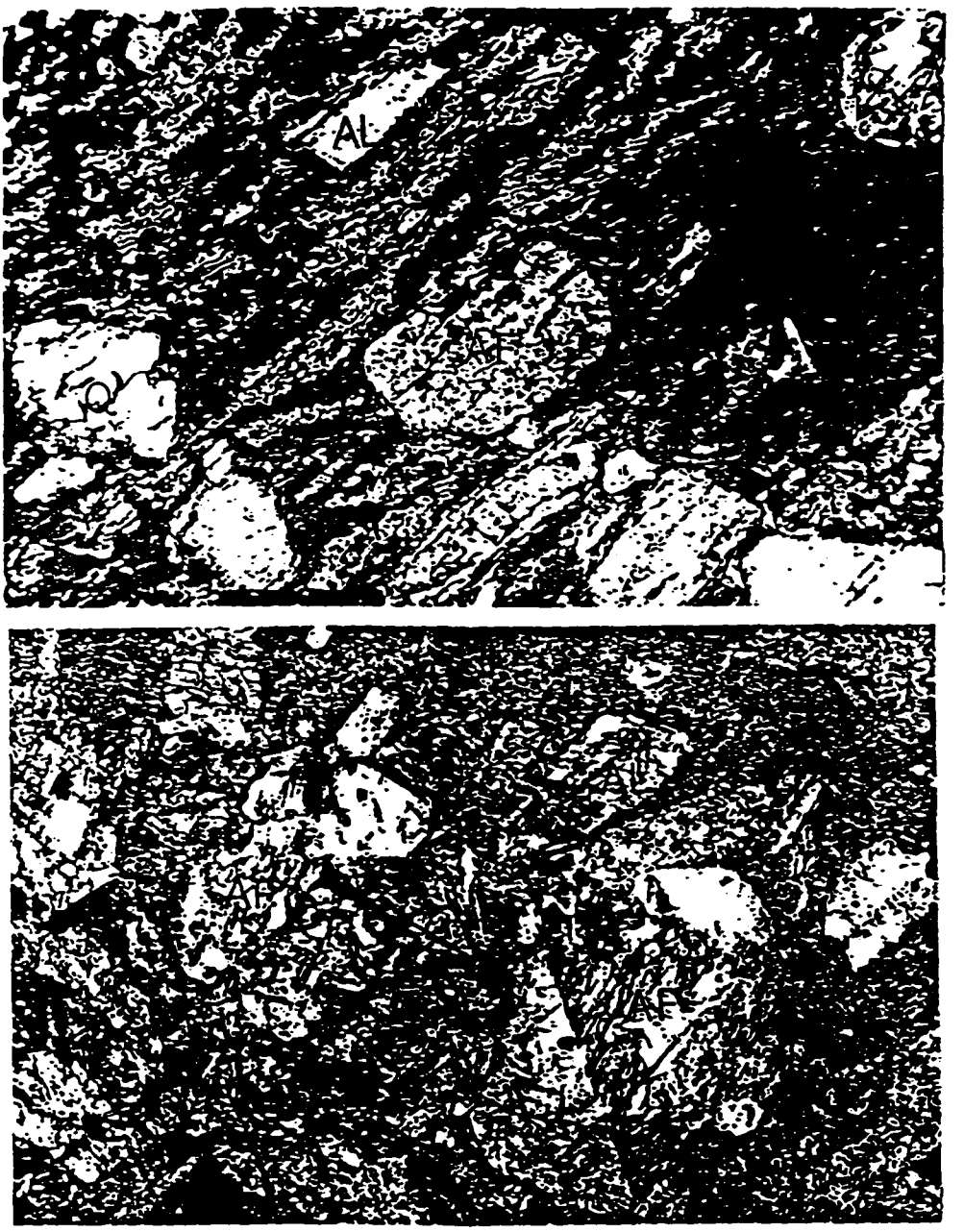

FIGURE 5.3: (A) Plane polarized microphotograph of trachyte showing slightly altered anorthoclase felspar (AF) and albite (AL) phenocrysts in glassy (dark gray) to microlitic matrix (light gray). (B) anorthoclase felspars (AF) and albite (AL) phenocrysts in this X-Nicol photograph show slight alteration to microlitic clay mineral. Both photographs are 4 mm in length.

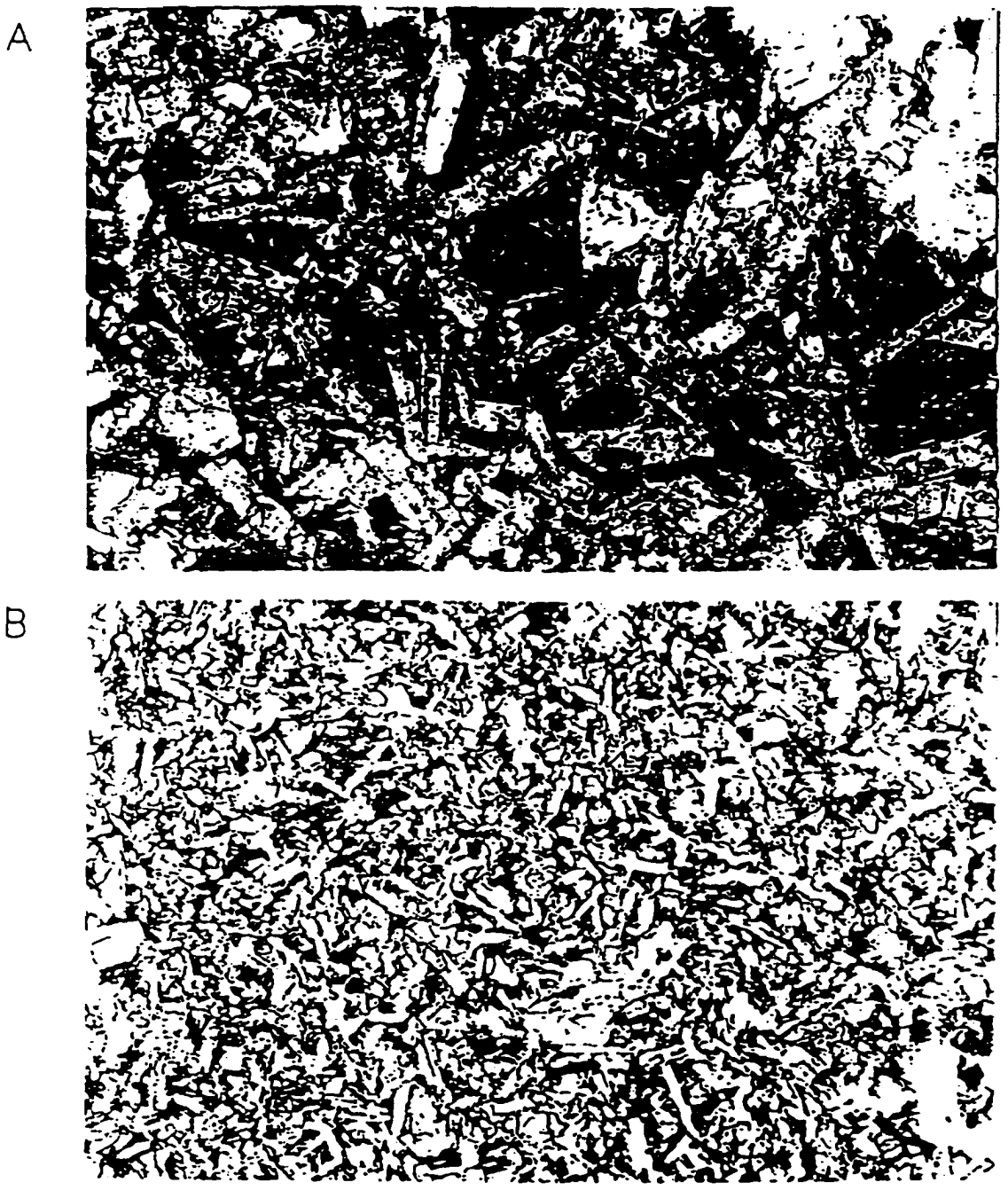

FIGURE 5.4: (A) Randomly distributed lath shaped phenocrysts of plagioclase felspars with slightly green to bluish green colored aegrine augite crystals in dolerite. Length of plane polarized microphotograph is 4 mm. (B) Plane polarized microphotograph of basalt showing randomly oriented lath shaped phenocrysts of plagioclase felspars. The average length of these phenocrysts is 1.7 mm.

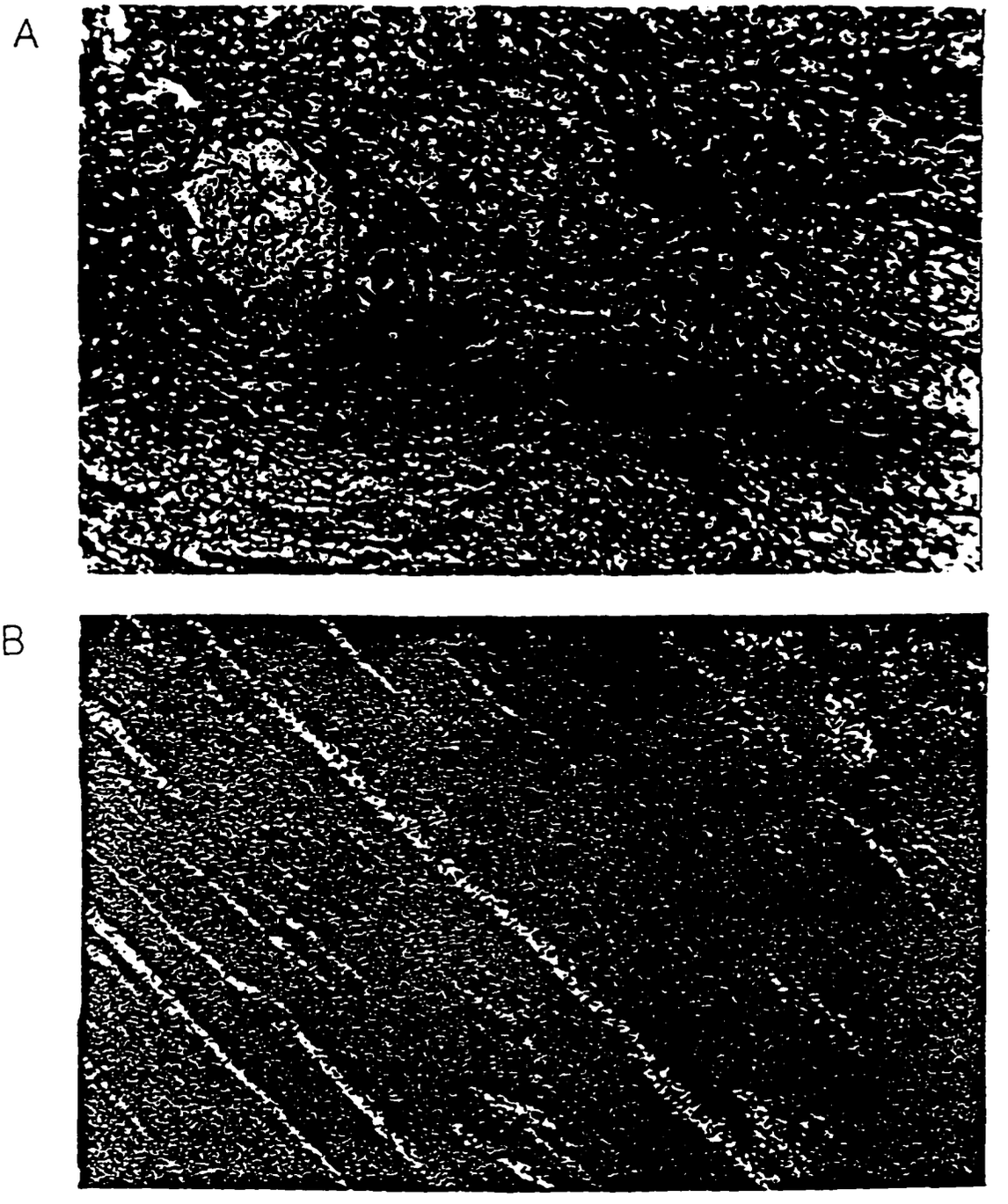

FIGURE 5.5: Few broken phenocrysts of quartz (Q) are present in pitchstone. Note that the glassy to microlitic groundmass shows flow texture in both microphotographs A and B. Both A and B are 4 mm long

GEOCHEMISTRY:

Major, trace and rare earth elements analyses were carried out on seventeen samples of rhyolite, trachyte, dolerite, and pitchstone basalts at National laboratory (CNR), Nancy, France (Table 5.1). Whole rock samples were prepared by fusion with $LiBiO_2$ and HNO_3 dissolution . Major and minor elements, including Sc were analyzed by Inductively Coupled Plasma (ICP)-Emission technique. However, the concentration of trace and rare earth elements in the whole rock were determined by ICP-Mass Spectroscopic technique.

(i) MAJOR ELEMENTS

The tholeiitic nature of the rocks from Rajula can be seen in a plot of alkali index ($A.I.=(Na_2O+K_2O)/(SiO_2-43)x.17$) versus weight % of Al_2O_3 (Figure 5.6 (a), after Middlemost, 1975). The solid circles represent acidic rocks (rhyolite, trachyte and pitchstone) and solid squares are for basic rocks (basalts and dolerite). All the data points of acidic rocks and basic rocks are within the tholeiitic field.

Figure 5.6 (b) is a modified TAS (Total Alkalis vs Silica) diagram (after Middlemost, 1991). The Na_2O+K_2O wt% of acidic rocks range from 5.07 to 8.08 and concentration of SiO_2 varies from 63.37 to 75.93%. All the points of acidic rocks lie in the field I. Basic rocks from study area have 46.45 to 51.68% SiO_2 and 3.67 to 3.85% total alkalis. In the TAS diagram acidic and basic rocks show two clusters I and II. However, all

TABLE 5.1

	Hi-1 Rhyolite	Lo-11 Rhyolite	Lo-9 Rhyolite	Lo-8 Rhyolite	Lo-7 Rhyolite	Hi-6 Rhyolite
SiO_2	75.31	71.92	73.15	74.31	71.9	75.31
Al_2O_3	11.73	11.66	11.44	11.17	11.94	10.8
Fe_2O_3	2.77	4.45	3.84	3.22	4.25	1.41
MnO	.02	.03	0	0	.01	0
MgO	.07	.51	.25	.41	.5	.2
CaO	.25	.68	.83	1.11	.7	.43
Na_2O	2.91	1.67	1.5	2.08	1.67	.28
K_2O	5.25	6.37	7.34	5.72	6.37	8.46
TiO_2	4.82	.46	.44	.45	.5	.16
P_2O_5	.08	.16	.15	.15	.14	.07
Loss on Ignition	1.11	1.83	.78	1.05	1.75	2.02
Total	99.67	99.74	99.72	99.67	99.73	99.76
Q	36.79	34.48	33.38	36.79	34.49	38.45
OR	31	37.62	43.35	33.78	37.62	47.49
AB	24.61	14.13	12.69	17.59	14.13	2.25
AN	.72	2.33	2.8	4.25	2.56	1.59
DI	0	0	.29	.24	0	0
HY	2.62	4.8	3.39	3.2	4.51	1.49
OL	0	0	0	0	0	0
NE	0	0	0	0	0	0
AC	0	0	0	0	0	0
C	1	1.17	0	0	1.36	.54
AP	.19	.37	.35	.35	.33	.16
IL	.32	.88	.84	.86	.76	.29
MT	1.31	2.15	1.86	1.55	2.03	.65

Table 5.1 contd.

	Hi-1 Rhyolite	Lo-11 Rhyolite	Lo-9 Rhyolite	Lo-8 Rhyolite	Lo-7 Rhyolite	Hi-6 Rhyolite
Ba	1026	675	819	1061	723	325
Be	1.79	1.7	2.7	2.7	3.4	1.7
Co	<5	<5	<5	<5	<5	<5
Cr	<5	<5	<5	<5	<5	<5
Cu	25	9	7	8	7	11
Ga	25	24	23	22	24	22
Nb	32	20	19	19	21	32
Ni	5	<5	<5	<5	<5	<5
Rb	201	250	272	240	265	167
Sc	1.5	6.9	6.9	7	7.09	1.5
Sr	30	39	33	53	42	27
Th	26	34	36	38	38	24
V	12	10	13	12	14	<5
Y	44	33	34	34	38	45
Zn	83	67	57	69	38	46
Zr	429	360	349	347	378	494
Ba/La	15.23	8.36	11.85	14.62	8.48	5.14
Ba/Nb	32.06	33.75	43.1	55.84	34.42	10.15
Rb/Nb	6.28	12.5	14.31	12.63	12.61	5.38
Ba/Th	39.46	19.86	22.75	27.92	19	13.54
Zr/Nb	13.4	18	18.3	18.26	18	15.43
Th/Nb	.82	1.7	1.89	2	1.81	.75
Th/La	.37	.42	.59	.52	.44	.38
La/Nb	2.1	4.03	3.09	3.82	4.06	1.98

Table 5.1 cont.

REE	Hi-1 Rhyolite	Lo-11 Rhyolite	Lo-9 Rhyolite	Lo-8 Rhyolite	Lo-7 Rhyolite	Hi-6 Rhyolite
La	204.74	245.44	210	220.61	259.24	192.31
Ce	132.89	170.05	153.78	157.56	179.77	133.33
Pr	104.82	133.5	117.4	121.9	141.4	104.5
Nd	76.75	96.77	80.88	86.25	103.62	75.9
Sm	56	64.33	52.95	55.47	67.78	55.96
Eu	23.12	23.12	21.56	22.2	25.7	21.69
Gd	38.73	41.59	35.65	32.14	42.78	39.93
Tb	35.45	34.8	29.52	28.42	36.43	36.81
Dy	32.39	28.25	23.35	24.81	29.56	32.79
Er	31.6	26.47	22.16	22.91	26.57	32.17
Tm	30	23.4	20.89	21.8	24.89	31.86
Yb	28.86	21.59	19.14	20.9	22.77	31.5

TABLE 5.1 contd

	Ka-6 Trachyte	Ka-1 Trachyte	Ra-1 Trachyte	Ra-1' Trachyte	Vi-2 Dolerite	Hi-8 Pitchstone
SiO_2	63.37	65.3	69.18	68.65	51.78	67.68
Al_2O_3	13.28	13.39	13.01	12.91	14.63	12.63
Fe_2O_3	7.08	6.86	4.44	4.33	10.48	6.41
MnO	.07	.07	.03	.02	.13	.07
MgO	.6	.68	.85	1.04	4.73	.8
CaO	3.95	2.66	1.93	2.04	8.78	1.14
Na_2O	3.37	3.29	2.37	2.22	2.22	3.37
K_2O	1.7	4.48	4.77	4.85	1.45	4.8
TiO_2	.79	.75	.63	.59	1.18	.48
P_2O_5	.22	.2	.19	.17	.16	.11
Loss on Ignition	5.26	2.03	2.33	2.9	3.96	2.19
Total	99.69	99.71	99.73	99.72	99.8	99.7
Q	26.37	21.13	30.87	30.14	7.49	23.77
OR	10.04	26.46	28.17	28.64	8.23	28.47
AB	28.5	27.83	20.05	18.78	18.04	28.51
AN	16.08	8.3	8.33	9.01	24.66	4.94
DI	1.79	2.88	0	0	13.25	0
HY	6.33	5.65	5.25	6.13	12.73	7.61
OL	0	0	0	0	0	0
NE	0	0	0	0	0	0
AC	0	0	0	0	0	0
C	0	0	.89	.71	0	0
AP	.51	.47	.44	.4	.36	.26
IL	1.5	1.5	1.2	1.12	2.16	.91
MT	3.31	3.27	2.15	2.09	4.87	3.2

TABLE 5.1 contd.

	Ka-6 Trachyte	Ka-1 Trachyte	Ra-1 Trachyte	Ra-1' Trachyte	Vi-2 Dolerite	Hi-8 Pitchston
Ba	774	660	669	668	309	858
Be	2	2.5	2.5	2.5	1.1	2.2
Co	6	7	5	5	38	<5
Cr	9	5	11	14	134	<5
Cu	17	17	14	12	89	29
Ga	30	26	28	25	36	30
Nb	22	21	22	20	8	34
Ni	13	5	13	11	82	5
Rb	138	193	221	229	43	173
Sc	10.8	9.6	8.6	8.1	28	6.09
Sr	316	118	70	71	126	81
Th	32	31	34	55	6	22
V	16	13	34	32	250	18
Y	36	40	34	32	21	61
Zn	85	84	59	49	77	117
Zr	342	367	328	308	123	517
Ba/La	12.76	10.99	10.67	10.49	15.5	13.29
Ba/Nb	35.18	31.42	33.45	33.4	38.65	25.23
Rb/Nb	6.27	9.19	10.04	11.45	5.38	5.1
Ba/Th	24.19	21.3	19.67	19	51.5	39
Zr/Nb	15.54	17.47	14.9	15.4	15.37	15.2
Th/Nb	1.46	1.48	1.55	1.75	.75	.65
Th/La	.53	.52	.54	.53	.3	34
La/Nb	2.75	2.86	2.85	3.1	2.49	1.9

Table 5.1 cont.

REE	Ka-6 Trachyte	Ka-1 Trachyte	Ra-1 Trachyte	Ra-1' Trachyte	Vi-2 Dolerite	Hi-8 Pitchstone
La	184.6	182.58	190.55	193.46	60.57	196.26
Ce	156.49	146.26	142.03	141.79	163.99	145.79
Pr	122.3	110.43	107.5	108	99.5	116.85
Nd	79.33	74.62	73.38	73.96	35.49	88.03
Sm	55.22	52.41	49.76	48.62	25.86	70.59
Eu	28.83	26.75	23.38	22.47	20	35.37
Gd	38.59	36.77	32.57	32.97	26.92	52.32
Tb	32.6	31.5	27.94	27.86	20.1	48.24
Dy	28.63	26.26	23.26	23.18	13.7	44.75
Er	26.47	24.7	21.97	22.05	12.9	43.37
Tm	22.86	22.89	20.13	20.18	11.6	42.61
Yb	23	21.36	18.73	18.64	10.5	40.05

TABLE 5.1 contd.

	PA-1 BASALT	PA-2 BASALT	PA-3 BASALT	PA-6 BASALT	PA-8 BASALT	PA-10 BASALT	PA-11 BASALT
SiO_2	48.39	49.41	48.53	51.58	50.7	50.44	48.73
Al_2O_3	16.37	16.17	15.45	14.19	14.4	14.98	13.22
Fe_2O_3	10.6	10.59	11.4	11.2	11.38	10.65	13.51
MnO	.14	.15	.14	.15	.14	.14	.17
MgO	5.35	5.75	4.11	4.83	5.55	5.34	6.35
CaO	10.67	10.71	10.88	9.13	9.41	10.26	9.07
Na_2O	2.29	2.2	1.35	2.76	2.69	2.09	2.69
K_2O	.29	.28	.02	1.09	.71	.68	.63
TiO_2	1.16	1.09	1.98	1.73	1.62	1.09	2.23
P_2O_5	.18	.18	.27	.25	.27	.2	.29
Loss on Ignition	4.37	3.32	5.69	3.12	3.15	4	2.88
Total	99.81	99.85	99.82	99.85	99.92	99.88	99.77
Q	3.34	4.72	11.87	6.03	5.16	6.63	2.74
OR	1.71	1.65	.12	6.44	4.19	4.27	3.92
AB	19.37	18.61	11.42	23.34	22.75	19.93	25.44
AN	33.52	33.41	36.02	23.10	25.11	31.13	23.32
DI	14.93	15.10	13.28	16.81	16.14	17.08	17.67
HY	15.3	15.33	11.51	11.94	14.24	14.79	18.04
OL	0	0	0	0	0	0	0
NE	0	0	0	0	0	0	0
AC	0	0	0	0	0	0	0
C	0	0	0	0	0	0	0
AP	.42	.42	.63	.58	.63	.44	.64
IL	2.21	2.07	3.77	3.29	3.08	1.61	3.27
MT	4.65	5.22	5.52	5.37	5.46	3.94	4.96

TABLE 5.1 (Contd.)

	PA-1	PA-2	PA-3	PA-6	PA-8	PA-10	PA-11
Ba	164	102	17.4	226	175	206	191
Be	0.36	0 61	0.69	0.98	0 66	0.74	0 74
Co	36.9	37 1	33.4	32.8	37 4	37.9	43.4
Cr	167	121	173	118	125	104	283
Cu	104	98 5	41.7	9.88	48 3	85.5	159
Ga	18.8	19 3	28.9	23 9	21 9	20.9	23.3
Nb	3.36	4 18	11.1	6.96	8 11	5.76	12.5
Ni	74.4	75 4	66.4	40.0	51 5	74.6	95.6
Rb	8.68	8 87	8.45	31.8	19 6	20.9	17.2
Sm	2.8	3 11	5.35	4.98	4 8	3.91	5 76
Sr	306	214	337	261	365	248	324
Th	1.0	2 52	4.58	4.43	3 41	3.71	3.66
V	265	244	298	302	283	255	329
Y	21.1	21	26.9	24.3	22 4	25.0	28.1
Zn	80.6	76 3	97.8	93.2	91 4	85.5	112
Zr	72.1	84 6	153	147	140	117	164
Ba/La	21.6	9 29	0.94	12.28	8 69	12.94	9.64
BA/Nb	48.8	24 4	1.57	32.47	21 58	35.76	15.28
Rb/Nb	2.58	2 12	0.76	4.57	2 42	3.63	1.38
Ba/Th	164	40 48	3.8	51.0	51 3	55.5	52 18
Zr/Nb	21.46	2 21	13 78	21.12	17 26	20.13	13 12
Th/Nb	0.3	61	0 41	0.64	0 42	0.64	0.29
Th/La	0.13	0 23	0.25	0.24	0 17	0.23	0.18
La/Nb	2.26	1	1 66	2.64	1 8	2.76	1 59

Table 5.1 cont.

REE	PA-1 BASALT	PA-2 BASALT	PA-3 BASALT	PA-6 BASALT	PA-8 BASALT	PA-10 BASALT	PA-11 BASALT
La	23.02	33.37	55.96	55.9	61.22	48.4	60.24
Ce	19.02	26.96	45.75	46.2	49.94	37.14	49.83
Pr	17.5	24	40	40	42.5	32	45
Nd	16.44	20.91	34.22	33.57	35.76	26.14	39.4
Sm	13.79	15.71	26.35	24.53	23.64	19.26	28.37
Eu	14.93	13.64	22.2	19.74	20.13	15.58	23.51
Gd	11.53	12.1	18.3	17.5	17.7	14.13	20.36
Tb	10.5	11.35	16.5	15.3	14.6	13.2	17.5
Dy	10.12	10.67	14.96	13.18	12.3	12.39	14.87
Er	9.94	9.89	13.02	11.2	10.8	11.25	12.9
Tm	9.78	9.2	11.4	9.4	9.2	10.8	11.3
Yb	9.55	8.95	10.45	8.63	8.36	10.14	10.45

TABLE 5.1 (Contd.)

	SH-1 RHYOLITE	SH-2 RHYOLITE	SH-3 TRACHYTE	SH-4 DOLERITE	SH-11 BASALT	SH-A-1 BASALT
SiO_2	71.2	69.08	66 89	46.83	49 84	50.11
Al_2O_3	11 72	11.9	12.01	14.45	13.85	14.32
Fe_2O_3	5.06	5.18	5.21	10.68	12.54	12.92
MnO	0.13	0.04	0.08	0.16	0.14	0.2
MgO	0 43	1.07	1 11	4.86	5.85	6 43
CaO	0.9	1.46	2 7	11.46	9.91	11.39
Na_2O	2.33	2.21	2.02	0.69	2.03	2.25
K_2O	3.69	3.84	3.89	0.09	0.94	0.34
TiO_2	0.94	0.99	0 97	1.25	1.51	1.17
P_2O_5	0.15	0.18	0 19	0.23	0.25	0 21
Loss on ignition	3 18	3 75	4 64	9 15	2.92	0 47
Total	99 73	99.7	99 71	99.85	99.78	99 81
Q	42 55	38 08	16 15	33 38	10.76	8 84
OR	22 39	23 13	.53	22.98	5.49	1 99
AB	20 25	19.07	5 78	17.09	16.99	18 89
AN	3 58	6 19	35 72	12 15	25.62	27 75
DI	0	0	12 03	0	13.06	18 49
HY	1 1	2 71	6 41	2 76	8.35	7.32
OL	0	0	0	0	0	0
NE	0	0	0	0	0	0
AC	0	0	0	0	0	0
C	05	04	0	0	0	0
AP	36	43	53	44	58	49
IL	29	09	34	17	3	43
MT	5 21	5 3	10 61	5 22	12 44	12 85

TABLE 5.1 (Contd.)

	SH-1 RHYOLITE	SH-3 RHYOLITE	SH-3 TRACHYTE	SH-4 DOLERITE	SH-11 BASALT	SH-A-11 BASALT
Ba	36	685	612	25	121	100
Be	Traces	1.85	2 14	0.74	0.83	0.41
Co	0.21	4.72	5.66	34	40	45.1
Cr	Traces	2.68	2.34	46.6	25.8	120
Cs	0.143	0.748	0.668	1.42	0.531	0.128
Cu	Traces	18.6	17.7	102	129	153
Ga	0.94	16.0	16.1	26.1	19.8	16.5
Nb	1.58	28.13	27 17	10.08	12.02	8.1
Ni	Traces	2.6	2.37	77	55.2	64 9
Rb	9 82	151.0	137 6	3.91	47.96	9 62
Sm	0 585	7.34	9 01	4.31	4.83	3 11
Sr	6 55	143	141	129	274	151
Th	0 89	22.95	23 85	4.87	6.08	1 71
V	Traces	35.1	31 8	269	309	313
Y	2 72	44.8	43 3	26.4	28.6	25 4
Zn	Traces	64.6	59 8	72.1	82.3	80 5
Zr	22 3	342	344	123	147	85 0
Ba/La	10 56	14.29	1 47	12.78	5.92	9 6
Ba/Nb	22.78	24.35	2.48	22.5	10.07	12.35
Rb/Nb	6 22	5.77	0.39	5.06	4.0	1 9
Ba/Th	40 45	29.84	5.13	25.66	19.9	58 48
Zr/Nb	14 11	12.16	12.2	12.66	12.23	10 49
Th/Nb	0 56	0.82	0 48	0.88	0.51	0 21
Th/La	0 26	0.48	0.29	0 5	0.3	0 16
La/Nb	2 16	1.7	1.68	1.76	1.7	1 29

Table 5.1 cont.

REE	SH-1 Rhyolite	SH-2 Rhyolite	SH-3 Trachyte	SH-4 Dolerite	SH-11 Basalt	SH-A-1 Basalt
La	10.36	145.65	145.59	51.61	62.1	31.76
Ce	8.69	93.56	107.93	40.32	48.39	24.73
Pr	6.84	75.51	86.4	31.5	40.2	21.06
Nd	4.9	57.42	68.65	27.62	33.49	17.6
Sm	2.88	36.16	44.38	21.23	23.79	15.32
Eu	0.31	18.44	24.42	15.97	19.22	15.06
Gd	1.49	27.46	28.95	15.25	17.93	14.2
Tb	1.36	23.76	24.15	13.74	16.4	12.64
Dy	0.25	20.16	20.03	12.19	14.43	11.37
Er	1.08	20.24	20.14	11.2	13.4	11.6
Tm	0.96	19.76	19.96	10.4	12.1	12.6
Yb	0.85	19.14	19.86	9.95	11.23	14.4

FIGURE 5.6 (a)

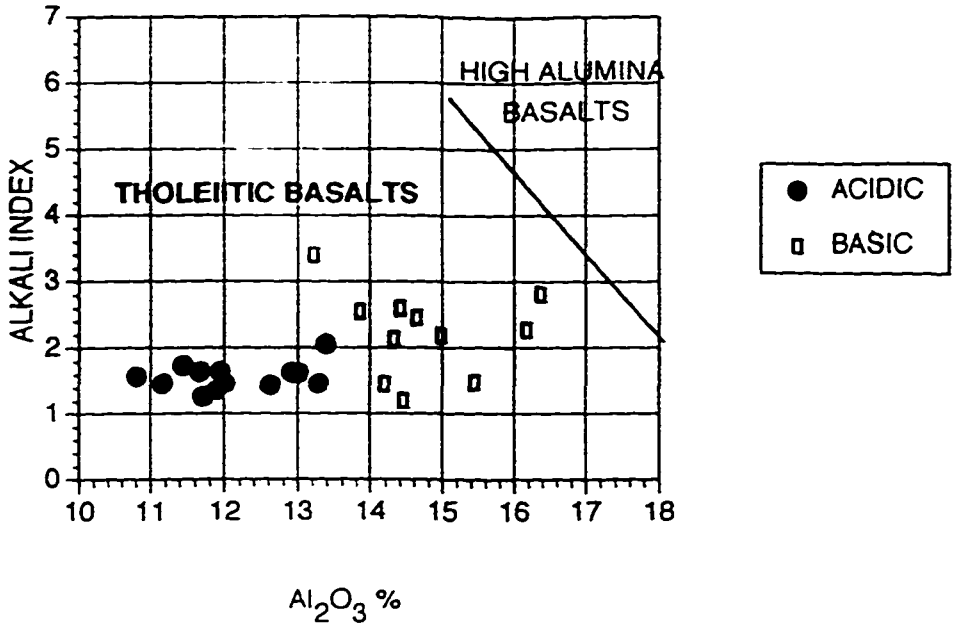

FIGURE 5.6 (b)

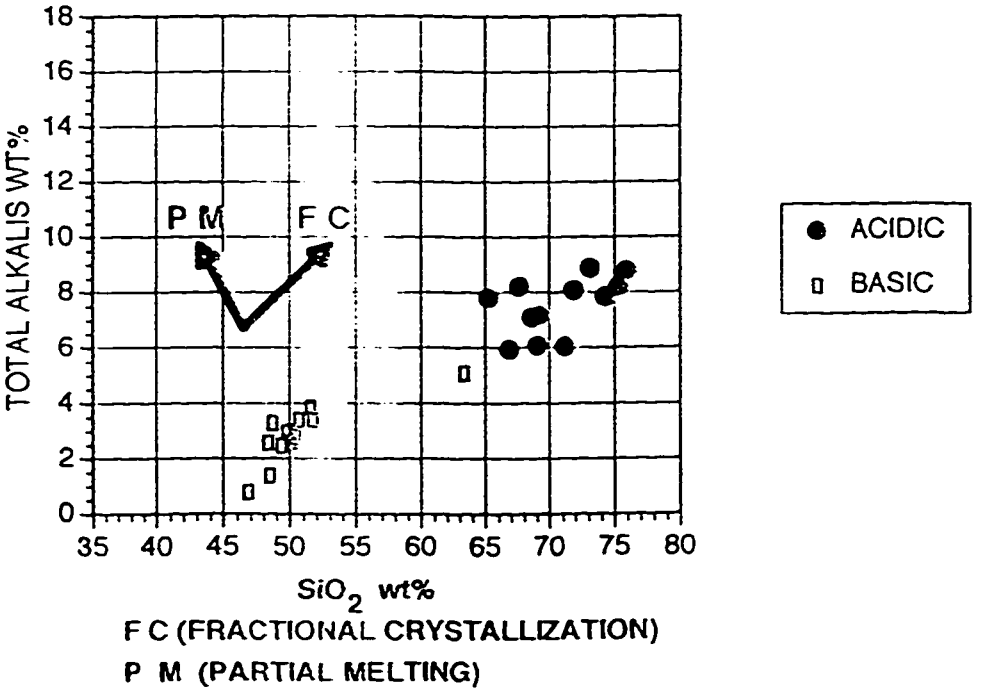

these rocks show a positive correlation between total alkalis and silica. One important characteristic of the rocks of Rajula area is the absence of the rocks of intermediate composition between acidic and basic rocks, contributing to two clusters. In the following section(s) I will investigate whether the acidic rocks of the study area are highly differentiated products of Deccan tholeiitic type magma or both acidic and basic rocks of Rajula originated from two different parental sources.

Figure 5.6 (c) shows variation of K_2O wt% with increasing SiO_2 wt% (after Middlemost (1975). The data points for the acidic rocks cluster in the alkalic field. However, the basic rocks are of sub-alkalic type. Middlemost (1975) proposed the name transitional type for the rocks which are in the alkalic field in one diagram(Figure 5.6(c)) but in subalkalic field (Figure 5.6(b)) of the other.

Figure 5.6 (d) shows K_2O wt% of the rocks against Na_2O wt%. The acidic rocks are of high K and K series, while, the basic rocks are of Na-Series. Normally the members of the high K series tend to be silica poor, however in some cases like shallow magma chambers more basic magma may differentiate to produce more silica rich and high K magma (Wilson, 1990). Based on this the rocks in the study area seem to be differentiated products of Deccan tholeiite type basic magma.

In Table 5.1 are shown the CIPW norms for the rhyolite, trachyte, pitchstone, dolerite and basalts of the study area. The normative quartz in the rhyolite varies from 38.45%

FIGURE 5.6 (c)

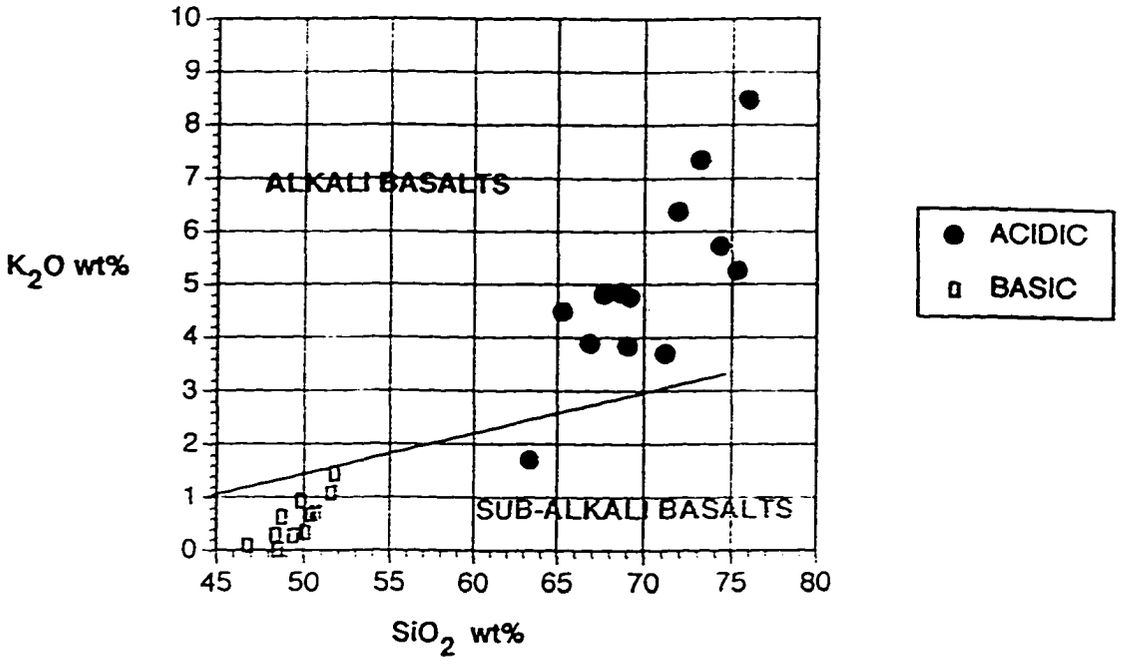

FIGURE 5.6 (d)

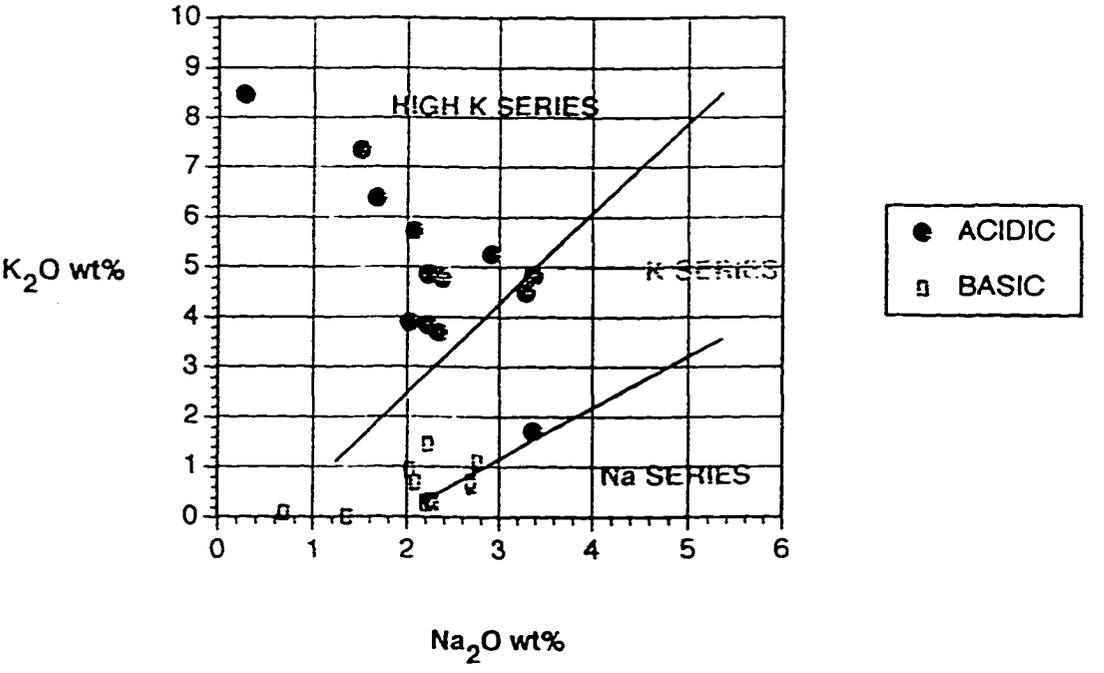

to 33.38% and normative orthoclase from 31% to 47.49%. The normative quartz in trachyte shows marked decrease with respect to rhyolite from 21.13% to 30.87% but a corresponding increase in the concentrations of albite and anorthite. A dolerite sample (Vi-2) shows highest concentration of anorthite 24.66% followed by albite 18.04%, diopside 13.25% and hypersthene 12.73% but no normative olivine. However, olivine phenocrysts are present in several thin sections.

Figure 5.7 shows the data points from the study area plotted on a triangular AFM diagram, where $A=Na_2O+K_2O$ wt%, $F=FeO+Fe_2O_3$ and $M=MgO$ respectively. The solid line in Figure 5.7 depicts the differentiation trend for the tholeiitic type mafic magma and dashed line shows the differentiation trend for calc-alkaline magma. The acidic and basic rocks of the Rajula area follow the tholeiitic differentiation trend suggesting that the more acidic rocks of the study area were evolved from basic magma. This observation also give evidence against the possibility of two types of parental sources for the acidic and basic rocks of Rajula area, as they tend to group themselves in two clusters (Figure 5.6).

(ii) TRACE ELEMENTS

Figure 5.8 shows the chondrite-normalized REE patterns for acidic (5.8 a) and basic rocks (5.8 b) from the study area. The light rare earth elements (LREE) are highly enriched in both acidic and basic rocks as compared to heavy rare earth elements (HREE). Enrichment of LREE and low concentration of HREE suggest a LREE enriched source. The concentration

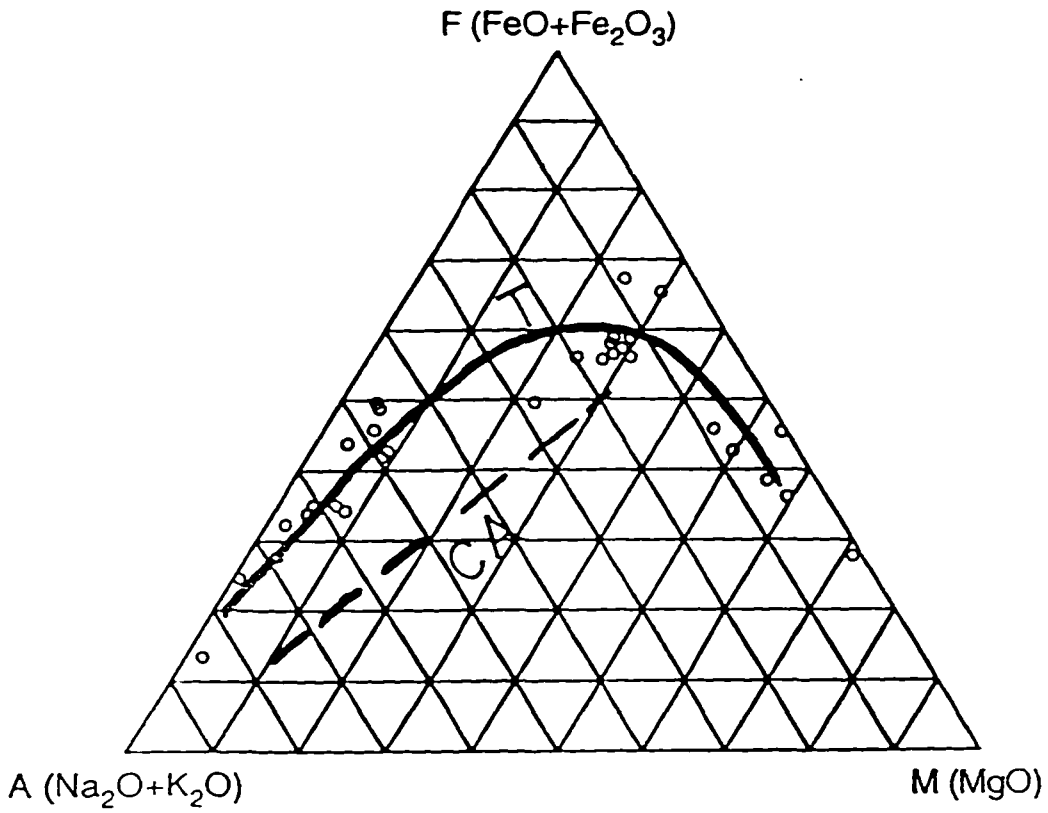

FIGURE 5.7: AFM ($A=Na_2O+K_2O$, $F=Fe_2O_3+FeO$, M=MgO wt%s) triangular diagram showing differentiation trends for tholeiite magma (solid line, T) and calc-alkaline magma (dashed line, CA). The acidic and basic rocks of Rajula area with basalts from Reunion hotspot (Fisk, 1988) follow the tholeiite trend excluding the possibility of two types of parental sources for basic and acidic rocks of Rajula.

FIGURE 5.8 (a)

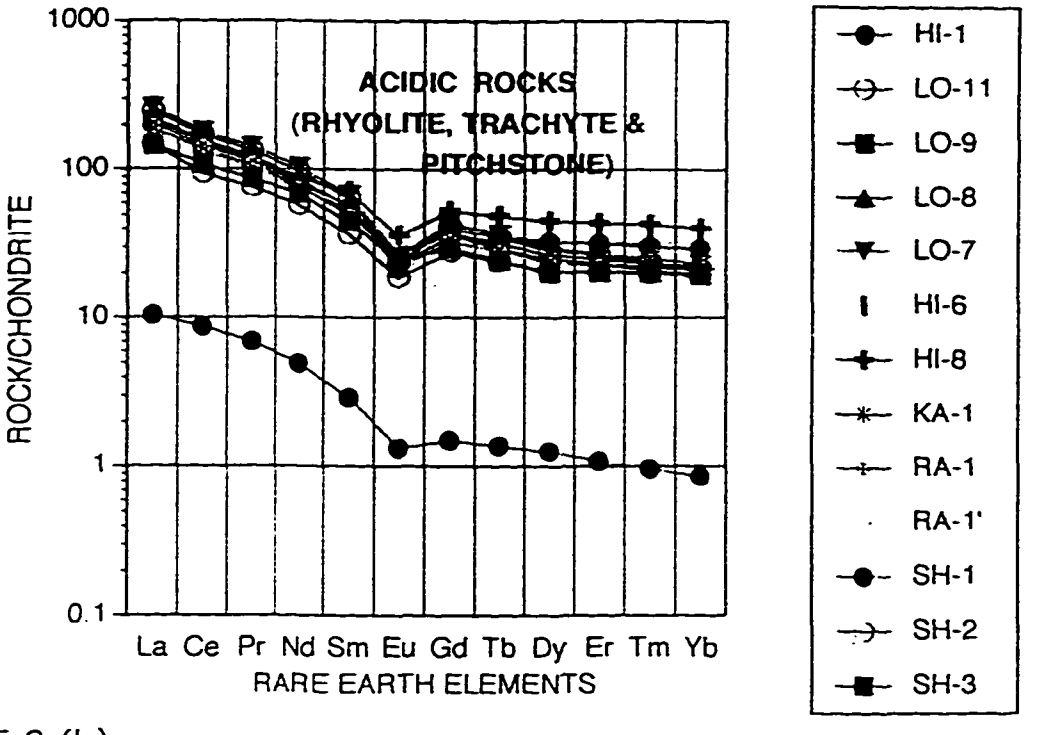

FIGURE 5.8 (b)

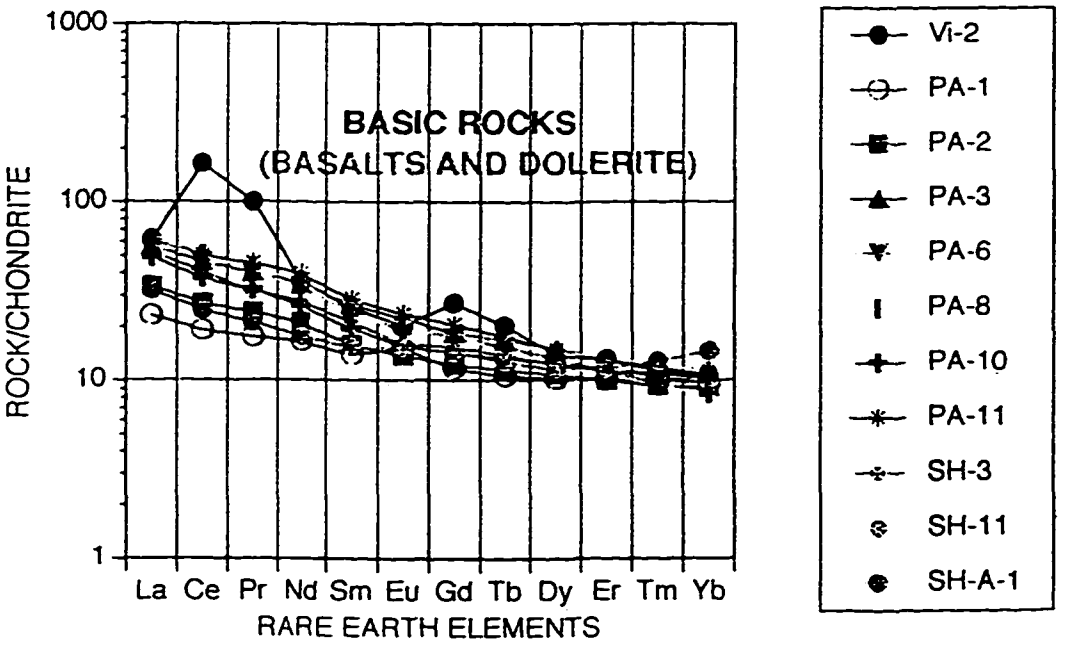

of HREE is more than 10 times of chondritic value indicating that garnet is absent from the source. The REE patterns for acidic rocks show negative Eu anomalies which is suggestive of plagioclase fractionation. Interestingly, the Eu negative anomaly is absent in the REE patterns for basic rocks from the study area (Figure 5.8(b)). Absence of Eu anomaly from basic rocks is due to the presence of plagioclase phenocrysts in these basalts (Figure 5.4). Similar types of REE pattern (without Eu anomaly) for Deccan basalts were reported by Dupuy and Dostal (1984) and Mahoney (1988).

Figure 5.9 shows the ratios of highly incompatible elements (such as Zr/Nb, La/Nb, Ba/Nb, Ba/Th, Rb/Nb, Th/Nb, Th/La and Ba/La) in acidic (5.9 a) and basic rocks (5.9 b) respectively. The constant ratios of these elements in rocks of varying silica content indicate the fractionation controlled origin of more silicic magma from basic magma (Weaver *et al.*, 1972; Lippard, 1973). The ratios of incompatible elements in both acidic and basic rocks show little variation (an average ratio of Zr/Nb ≈ 16.27, La/Nb ≈ 2.96, Ba/Nb ≈ 33.88, Rb/Nb ≈ 9.25, Th/Nb ≈ 1.37, Th/La ≈ 0.46, Ba/La ≈ 11.45, Nb/La ≈ 0.34 and Rb/La ≈ 2.85). The constant ratios of these trace elements in different types of rocks from this area indicate a low pressure fractionation of more silicic magma from more basic magma.

Figure 5.10 shows trace elements spider diagrams normalized with respect to N-MORB (Normal-Mid Oceanic Ridge Basalt, Humphris *et al.*, 1984) for acidic (Figure 5.10 a) and basic rocks (Figure 5.10 b). All trace elements except Sr in Figure 5.10 (a and b) are enriched with respect to N-MORB. The N-MORB normalized diagrams for both acidic and

FIGURE 5.9 (a)

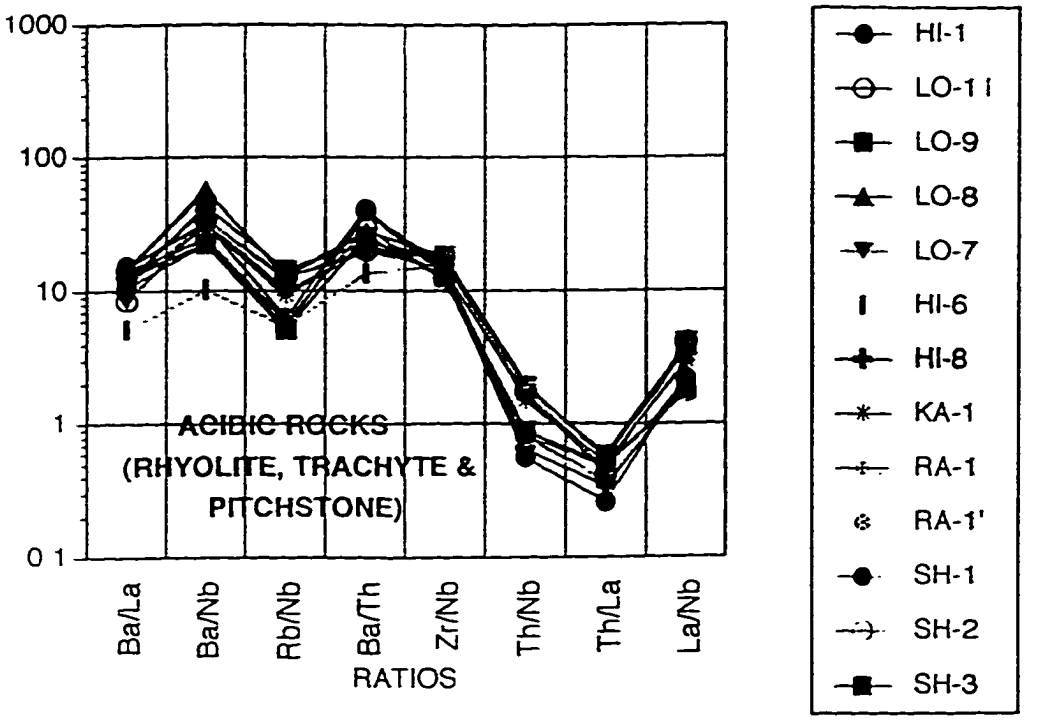

FIGURE 5.9 (b)

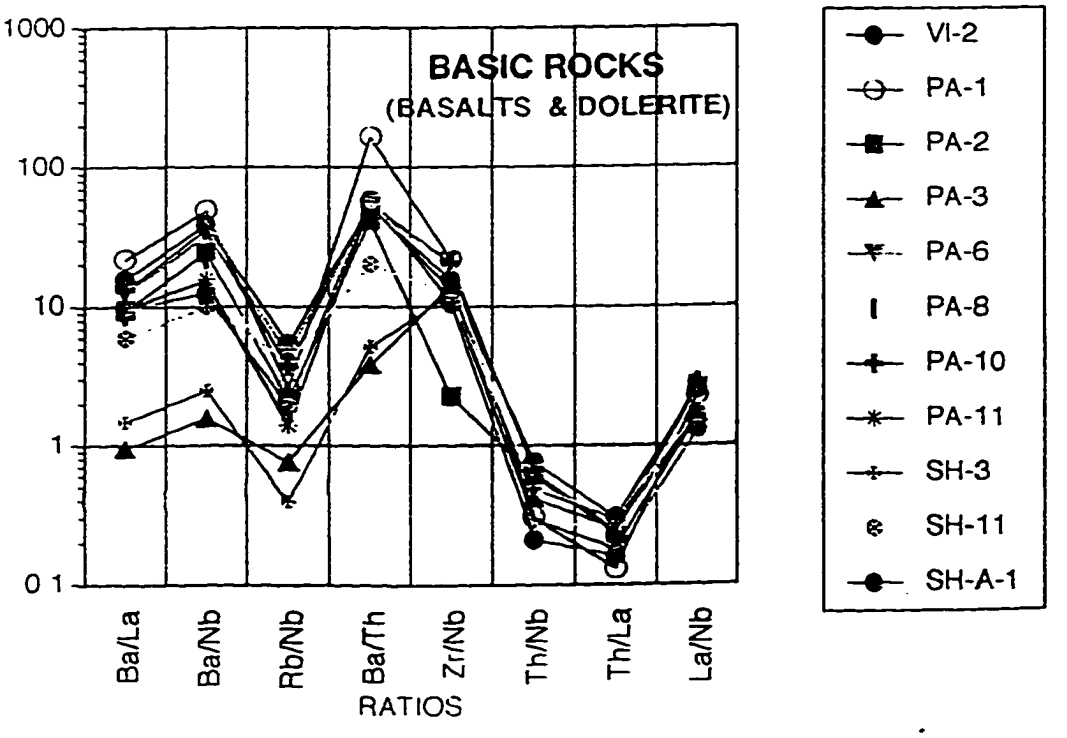

FIGURE 5.10 (a)

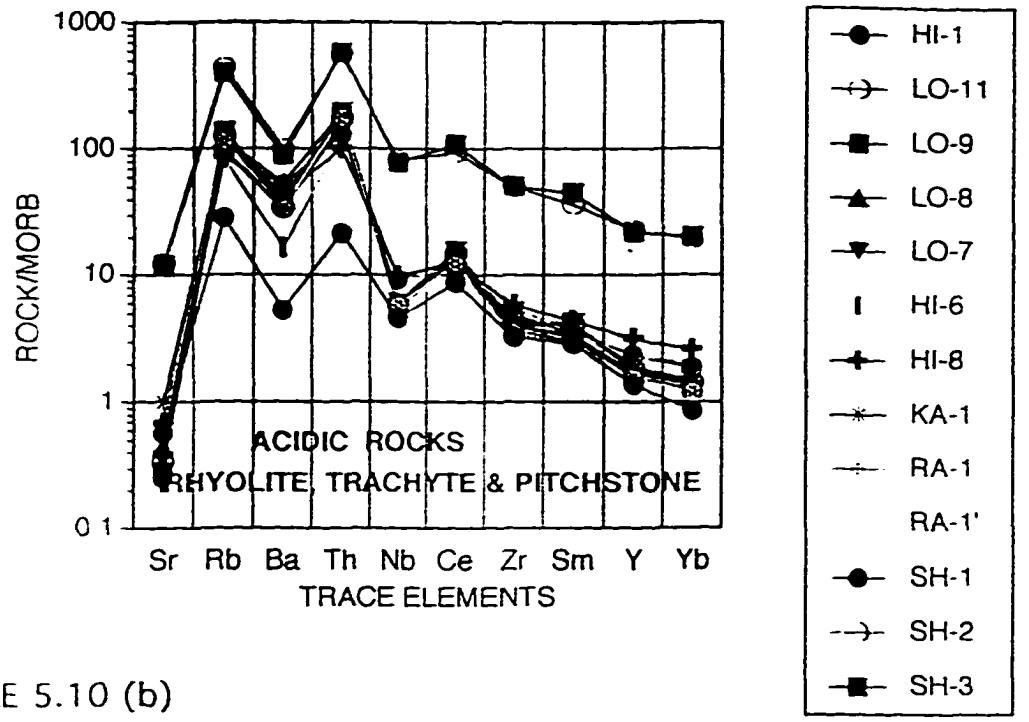

FIGURE 5.10 (b)

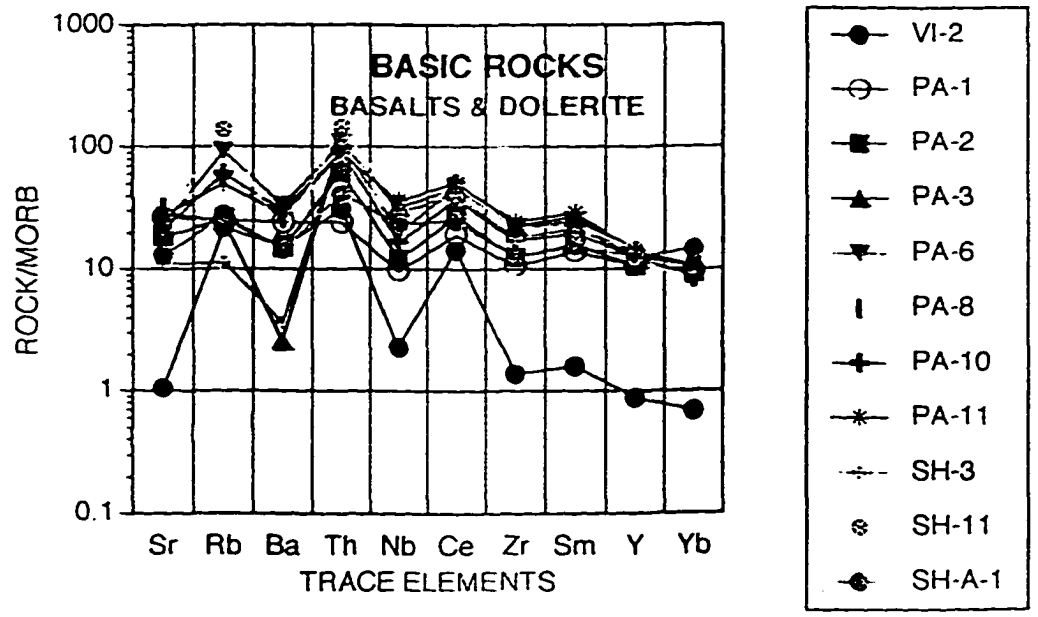

basic rocks show similar spiked patterns, for example presence of positive spikes for Rb and Th and negative anomalies for Sr, Ba and Nb. The negative anomaly shown by Sr is an indicator of fractionation and separation of plagioclase feldspar. However, the negative anomalies at Nb and Ba suggest either the contamination of acidic rocks and the basic rocks by the upper crustal rocks or the presence of residual phases Nb and Ta in the parent magma (Cox and Hawkesworth, 1980; Wilson, 1989). However, very low amount of Nb and Ta in the upper crustal rocks strongly suggest the possibility of contamination of acidic and basic rocks by upper crustal rocks.

Figure 5.11 shows OIT (Oceanic Island Tholeiites) normalized spider diagrams for acidic (Fig. 5.11 a) and basic rocks (Fig. 5.11 b). The normalizing constants are taken from Thompson *et al.*, (1984). The OIT normalized trace element patterns for both acidic and basic rocks are similar to that of N-MORB normalized patterns (Figure 5.11, a and b). All the trace elements are enriched with respect to OIT. The presence of positive spikes at Th and Rb indicate presence of contamination by crustal rocks. Similarly, the negative anomaly of Nb has been interpreted as a result of contamination by upper crustal rocks (Cox and Hawkesworth ,1980). Both Figures 5.10 and 5.11 indicate that acidic and basic rocks are contaminated by crustal rocks. Again, the negative anomaly shown by Sr is an indicator of low pressure fractionation of plagioclase feldspar.

FIGURE 5.11 (a)

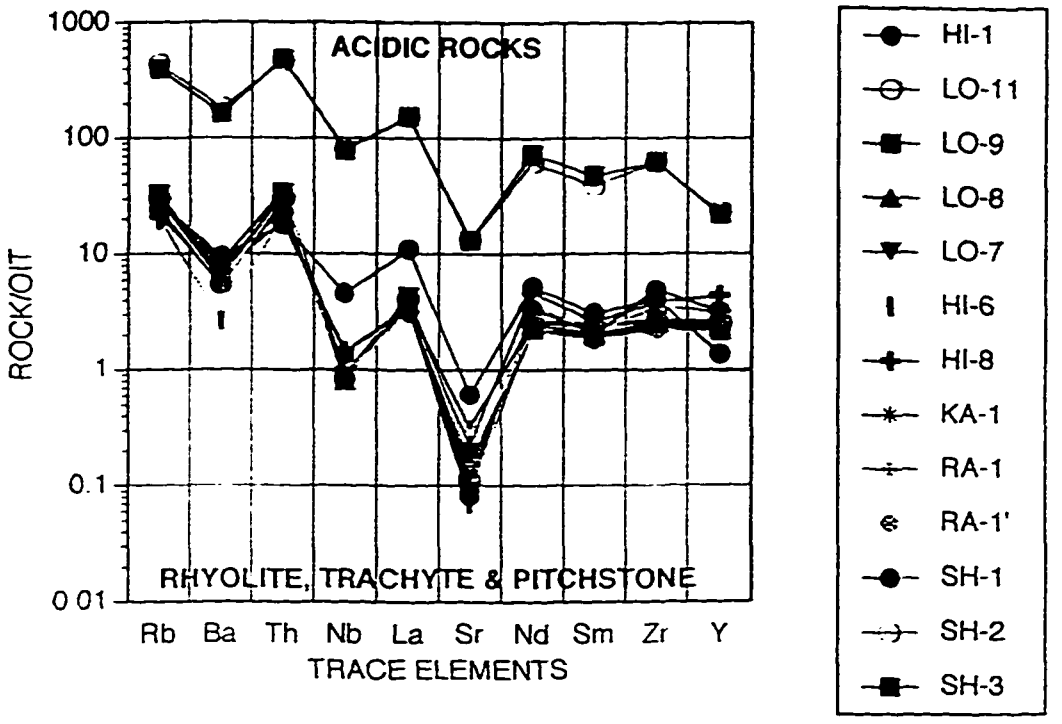

FIGURE 5.11 (b)

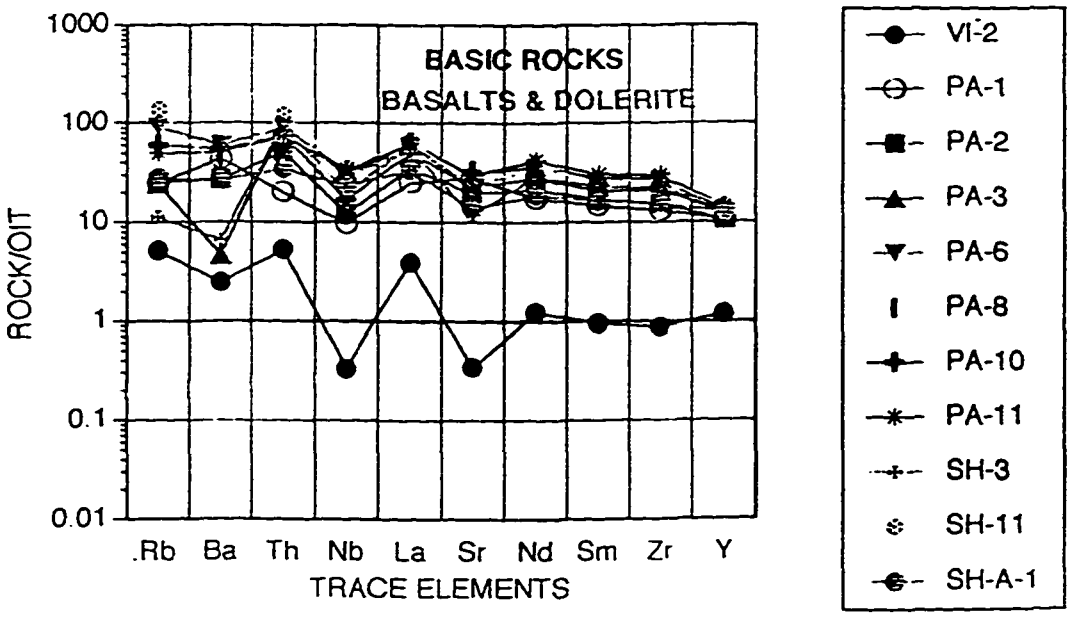

5.3 GEOCHEMICAL EVOLUTION OF THE ACIDIC ROCKS AND DECCAN VOLCANICS IN RAJULA, SAURASHTRA AND COMPARISON WITH NARMADA TAPTI RIFT , OTHER DECCAN VOLCANIC PROVINCES, AND REUNION HOTSPOT BASALTS:

On the basis of geophysical evidence Mishra (1977) extended the western margin of Narmada-Tapti rift beyond the Cambay bay into the southeastern part of Saurashtra peninsula, including the Rajula area (Figure 5.1). If this were the case, the acidic and the basic rocks of Rajula area should show some geochemical affinity with the rocks from adjacent Narmada-Tapti rift basalts and their differentiates. The major oxides from Rajula area, Rajpipla in the Narmada-Tapti rift, (Melluso *et al.*, 1995, Krishnamurthy and Cox, 1980), other Deccan volcanic provinces of Saurashtra (Melluso *et al.*, 1995), Deccan basalts from adjacent west coast, (Cox and Hawkesworth, 1985; Lightfoot *et al.*, 1987; Peng *et al.*, 1994) and the Reunion Islands (Fisk *et al.*, 1988) are plotted in Figure 5.12 with SiO_2 % as fractionation index.

The negative slopes in variation diagrams of SiO_2 wt% vs MgO and Fe_2O_3 wt% (Figure 5.12) are attributed to the fractionation and removal of olivine, as shown by the Reunion data, followed by the fractionation of olivine± clinopyroxene± plagioclase feldspar±Fe-Oxides and the fractionation of K and Na feldspars at the end, as shown by the acidic rocks from Rajula area. However, the variation diagrams of SiO_2 wt% versus CaO wt% and Al_2O_3 wt% show a positive correlation from 40 to 50% SiO_2 and a negative correlation

FIGURE 5.12

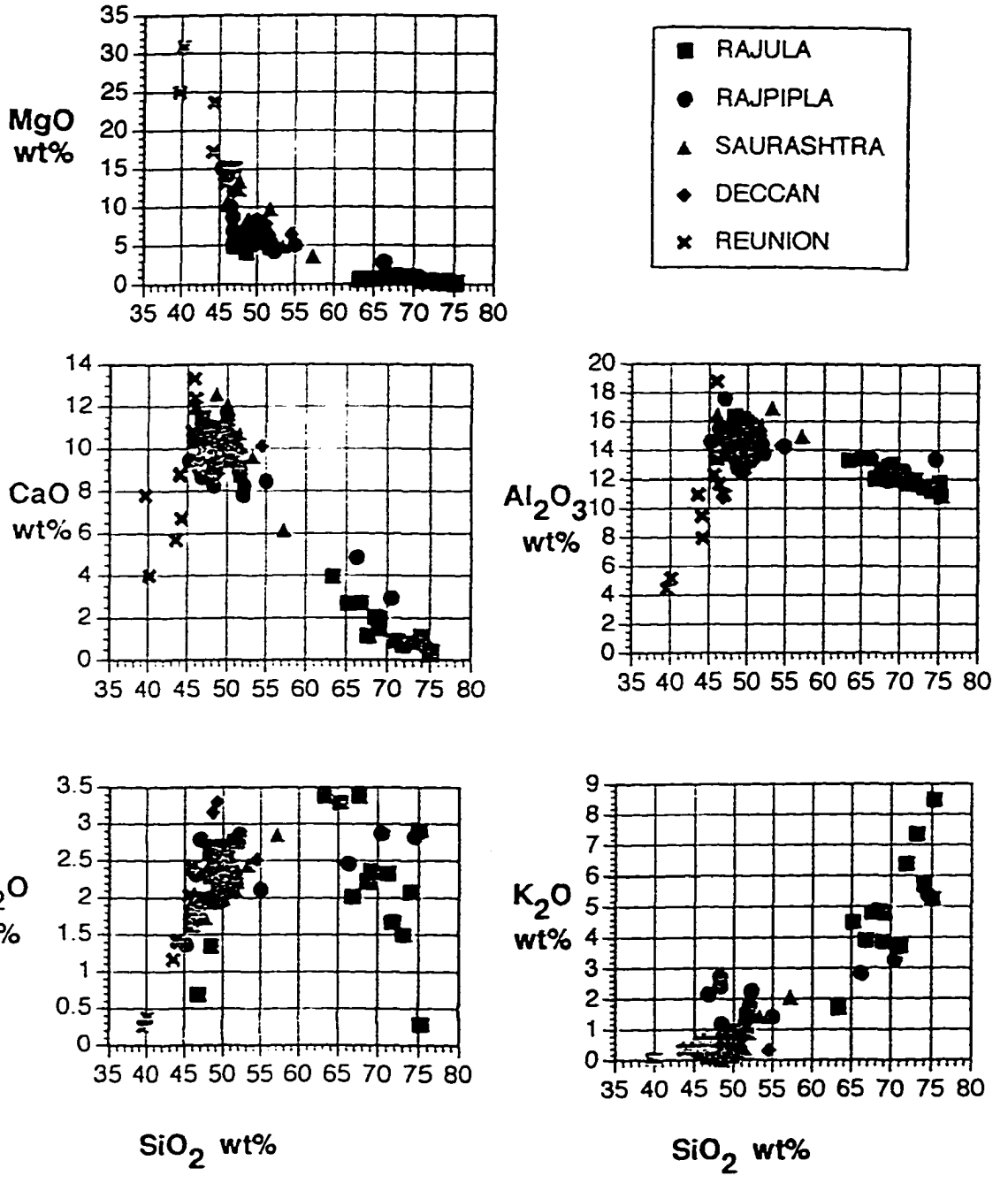

FIGURE 5.12

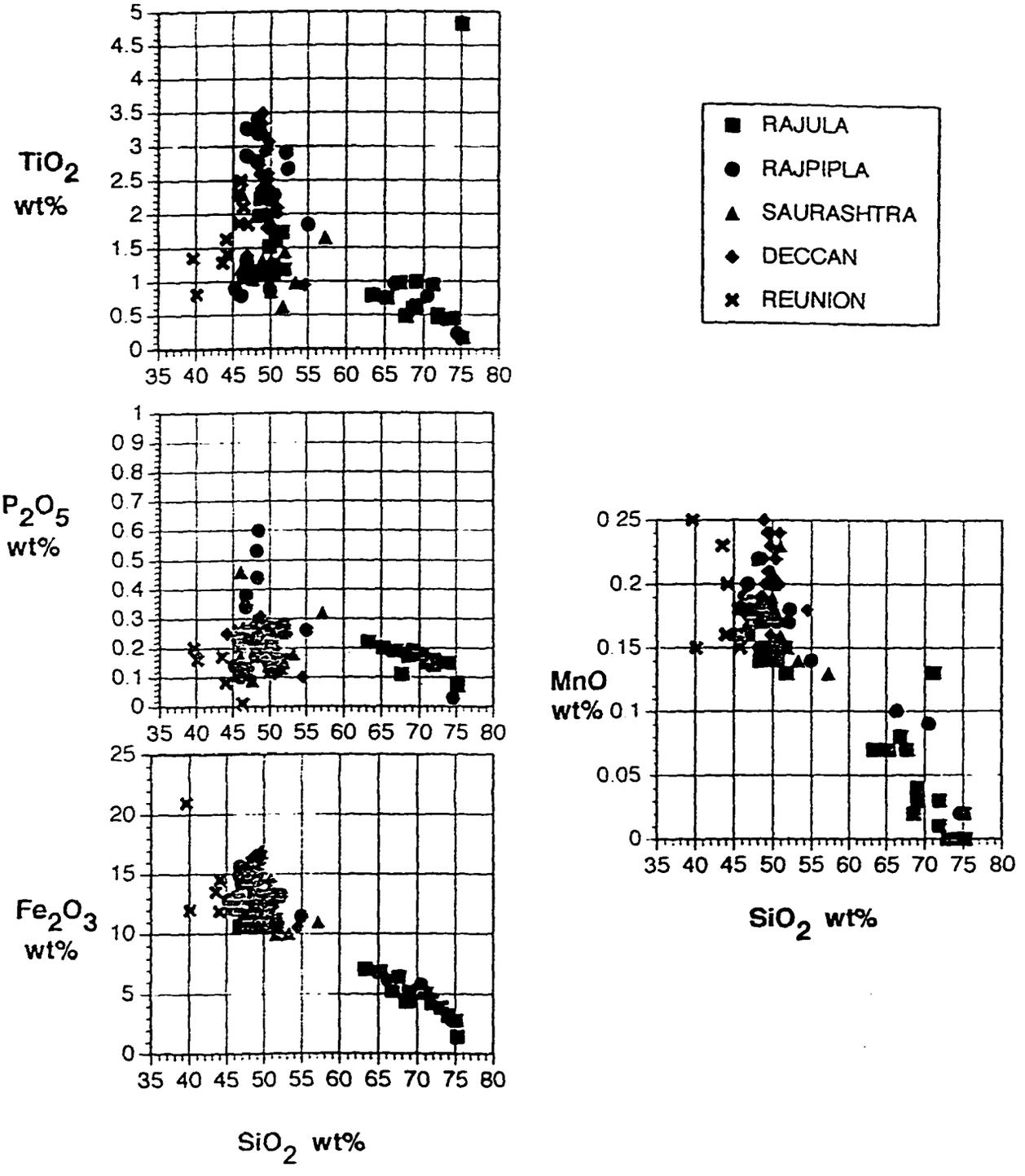

from 64 to 75% SiO_2. One of the characteristic of Figure 5.12 is the existence of a distinct and striking compositional gap from 53 to 64 wt% SiO_2. Similar type of compositional gaps between rhyolites, trachytes and Deccan volcanics were reported by Lightfoot *et al.*, (1987) from west coast of India. Another important aspect of Figure 5.12 is the large scattering of data points at ≈50% of SiO_2. This large scattering of data points is an indication of the crustal contamination which has been shown by the trace and rare earth elements.

Similar type of compositional gap and widely scattered data points are observed in variation diagrams between SiO_2% and incompatible elements Rb, Ba, Zr, Th, La, Nb, Y, Sr, V, and Ni (Figure 5.13). The plots for Zr, Th and La show slightly positive correlation with SiO_2%. However, the data points for the Ba and Rb from Rajpipla, Saurashtra and Deccan from west coast are widely scattered, even though Ba and Rb are also incompatible elements.

Combined geochemical study of the rocks of Rajula, Rajpipla, Saurashtra, Deccan and Reunion shows the existence of compositional gap from 53 to 64% SiO_2. Similar type of compositional gaps between rhyolites, trachytes and Deccan volcanics were reported by Lightfoot *et al.*, (1987) from west coast of India. They attributed this compositional gap to the combined effects of fractional crystallization and partial melting of mafic rocks in the crust. In this study I try to explore processes responsible for the generation of compositional gap not only in Rajula area but also in other parts of Deccan volcanic provinces. This bimodal distribution of rocks invoke the origin of acidic rocks by crustal melting rather than a

FIGURE 5.13

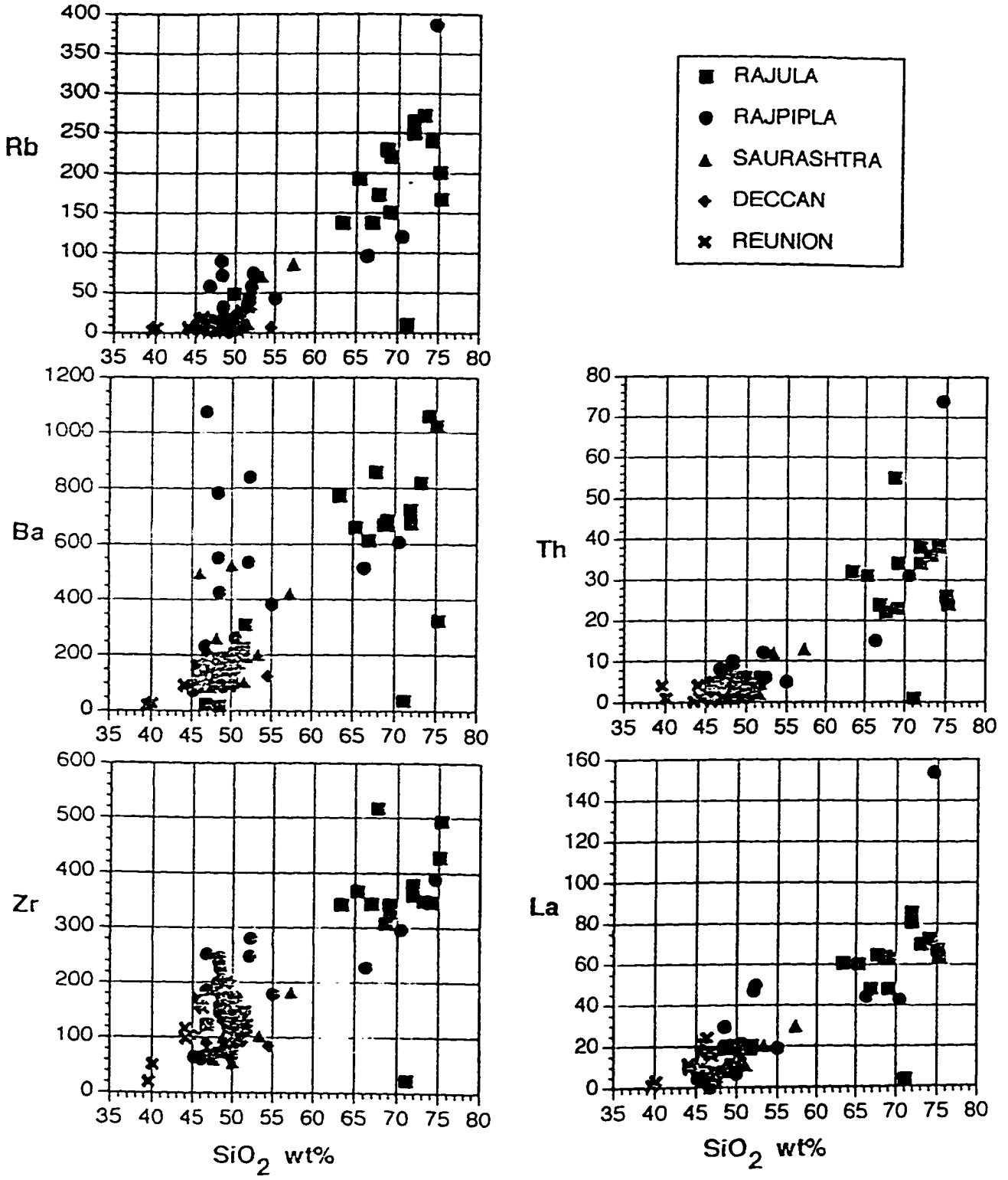

FIGURE 5.13

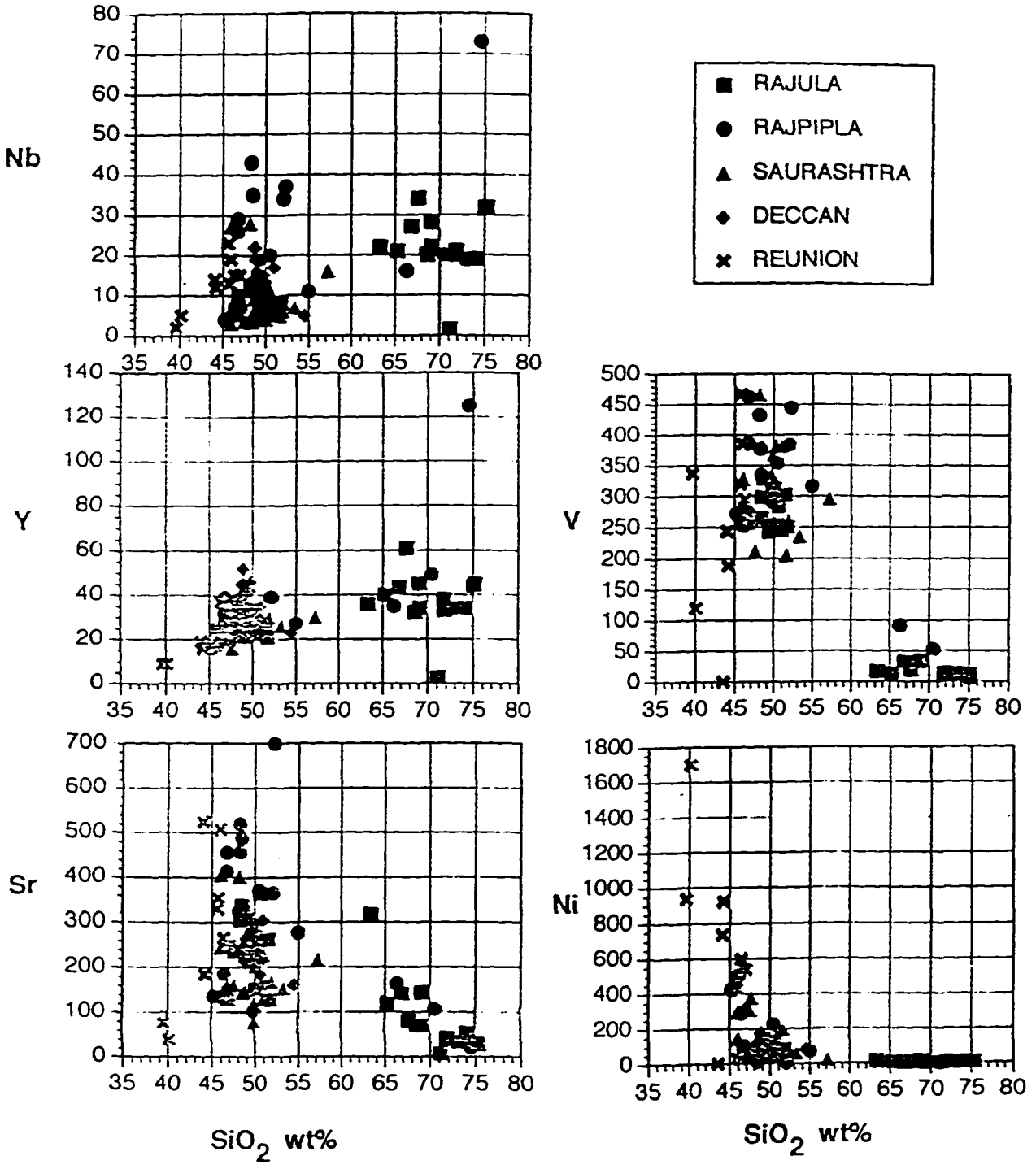

fractionation link to the associated Deccan tholeiite type basalts.

The Rb/Sr ratio for the acidic rocks from Rajula area (Table 5.1) varies from 0.98 to 8.2. Only one sample of trachyte (Ka-6) shows a value of 0.44. The reported Rb/Sr ratios for the Archean gneisses and charnockites from the peninsular India are extremely low varying from 0.22 to 0.86 (Rogers *et al.*, 1986; Stahle *et al.*, 1987). These low values of Rb/Sr eliminate the possibility of **direct** generation of acidic rocks in Deccan volcanics by the crustal melting of Archean basement.

Generation of acidic rocks by crustal melting or fractional crystallization can further be examined by their Al_2O_3 wt%. Al_2O_3 wt% in acidic rocks varies from 10.08 to 13.39 (Table 5.1). However, Al_2O_3 wt% in Archean gneisses and charnockites varies from 12.6 to 15.1 (see Rogers *et al.*, 1986; Stahle *et al.*, 1987), with most of the values > 13.7. Patino and Johnston (1991) carried out melting experiments on metasediments and established that Al_2O_3 wt% is always > 13.5 in the generated melt. Similarly, melting of metapelites by Vielzeuf and Holloway (1988) show Al_2O_3 wt% > 16. Very low Al_2O_3 wt% in acidic rocks in comparison with high Al_2O_3 wt% in Archean gneisses and charnockites again exclude the possibility of generation of these rocks by **direct** crustal melting.

The reported eruption temperatures for acidic and basic rocks from Saurashtra peninsula vary from 1000 °C to 1240 °C (Melluso *et al.*, 1995). The depth of origin of acidic rocks and Deccan basalts may be ascertain by plotting them on normative quartz, albite and

orthoclase triangular diagram. This is a semi-quantitative estimation of most recent pressure of equilibration for the acidic and basic rocks (Deccan volcanics). Figure 5.14 shows that the estimated depth of equilibration for acidic rocks (< 5 kbar) is upper crust and for Deccan volcanics (4 to 15 kbar) it varies from middle to upper crust. Thermally, melting of upper crust is also considered unlikely due to higher temperature of eruption of rhyolites and trachytes (> 1000 °C) as discussed by Melluso *et al.*, (1995) from low to moderate pressures (< 5 kbar). Thus Rb/Sr ratios, Al2O3%, temperature of eruption and estimated depth of equilibration suggests that the fractionation of minerals (such as olivine± clinopyroxene± plagioclase feldspar±K-feldspar and/or Na-feldspars) and crustal contamination were important factors in the geochemical evolution of acidic and basic rocks from Rajula, Rajpipla, Saurashtra, other Deccan provinces and Reunion.

5.4 GEOCHEMICAL MODELLING OF A MAGMA CHAMBER:

Fractional crystallization, crustal contamination and venting played an important role in the geochemical evolution of the rocks of Deccan volcanics of western margin of India and Reunion basalts.

5.4(a) FRACTIONAL CRYSTALLIZATION MODEL (FC) OF A MAGMA CHAMBER:

This is the simplest process to control the evolution of the abundance of trace elements and isotopic ratios in a magma chamber. In Rayleigh fractional crystallization model

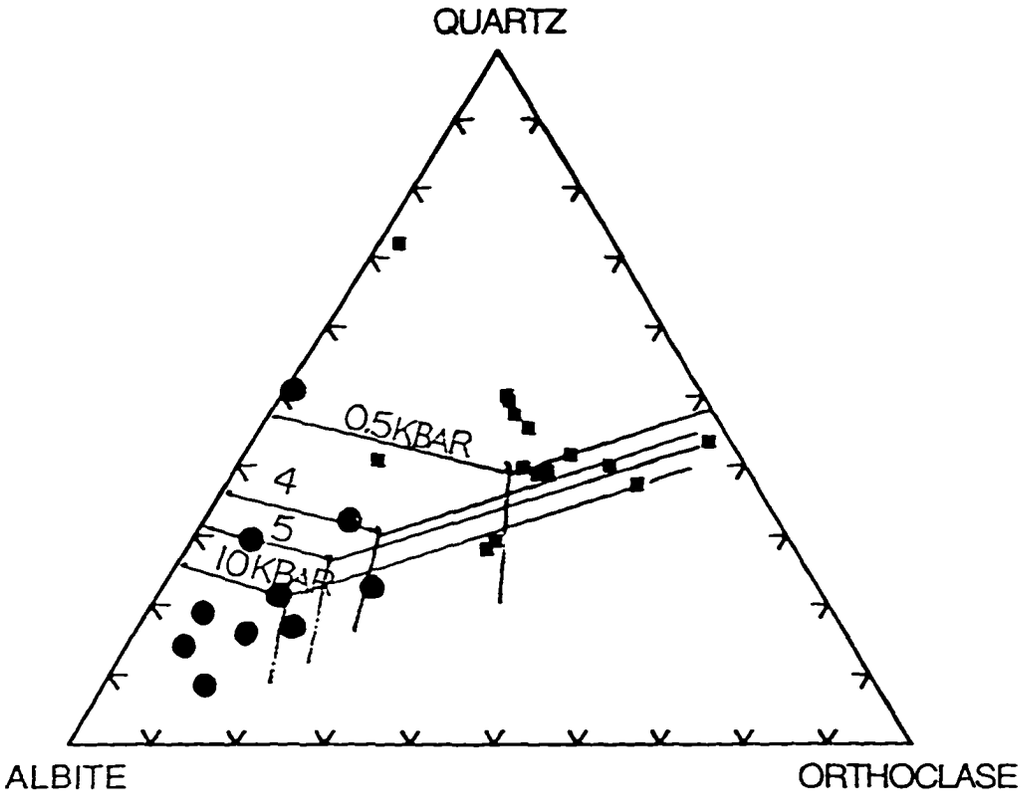

FIGURE 5.14: Semi-quantitative estimation of recent pressures of equilibration on normative quartz, albite, orthoclase triangular diagram. Estimated depth of equilibration for acidic rocks (squares) is upper crust. However, for basic rocks (solid circles) depth varies from middle to upper crust.

the abundance of a given element in the magma C_m, relative to the abundance in the original magma C^0_m as a function of mass of magma remaining F is given by (for example Neumann *et al.*, 1954):

$$C_m/C^0_m = F^{(D-1)} \qquad (5.1)$$

where D is the partition coefficient (the ratio between concentration of an element in mineral to its concentration in liquid). The extent of fractional crystallization is (1- F). As D approaches 0, in the case of incompatible element, equation is $C_m/C^0_m = 1/F$. Figure 5.15 shows the plot between the C_m/C^0_m and F, for the elements with different partition coefficients (D). Figure 5.15 clearly states the rapid removal of highly compatible elements (when D=2, 10) for degree of crystallization and extreme enrichment of incompatible elements (when D=0, 0.1, 0.5) for higher degree of fractional crystallization.

5.4 (b) ASSIMILATION- FRACTIONAL CRYSTALLIZATION (AFC) AND REPLENISHMENT- ASSIMILATION- FRACTIONAL CRYSTALLIZATION (RAFC) MODELS OF A MAGMA CHAMBER:

DePaolo (1981) presented equations describing trace elements concentrations and isotopic ratios evolution in a magma chamber affected simultaneously by fractional crystallization and wall rock assimilation (AFC, modelling of magma chamber). The

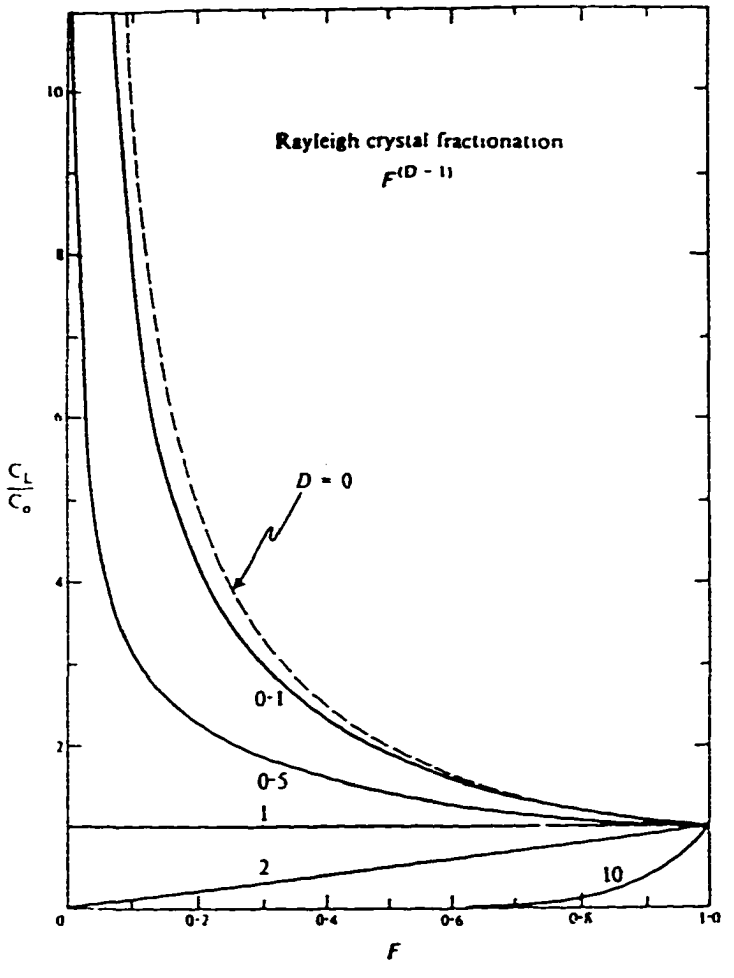

FIGURE 5.15: Theoretical variation of trace element concentrations in the melt during Rayleigh fractional crystallization. F is fraction of mass of magma remaining, value marked on each curve is distribution coefficient, C_L (C_m) and C_0 are the concentrations in magma and original magma respectively.

governing equation for the trace elements concentrations evolution is:

$$\frac{C_a}{C^o_a} = F^{-z} \frac{a}{(a-1)} \frac{C_a}{zC^o_a}(1-F^{z}) \qquad (5.2)$$

where C_a is the concentration of an element in the assimilated host rock, a is the ratio between the rates of change of masses in the assimilated rocks and fractionated material and $z=(a+D-1)/(a-1)$, again D is the partition coefficient. Figure 5.16 shows the relationships between the relative concentration of an element in a magma and relative mass of magma remaining (F) in a magma chamber undergoing assimilation and fractional crystallization. The short dashed lines are for simple fractional crystallization.

DePaolo (1985) further extended the AFC model to include the process of replenishment of a magma chamber (RAFC model). For this model the expression is:

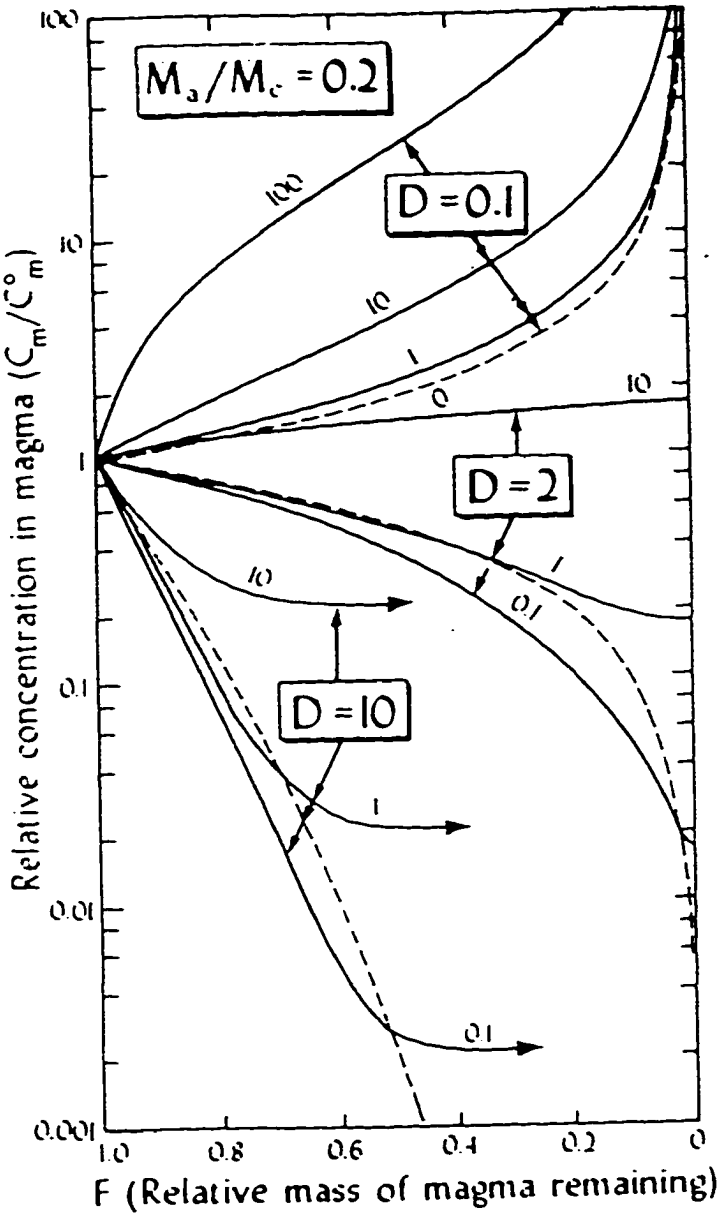

FIGURE 5.16: Relationship between the relative concentration of an element in a magma experiencing assimilation-fractional crystallization (AFC) and F- fraction of mass of magma remaining. The short dashed lines are for Rayleigh fractional crystallization. The numbers on the curves give the values of C_a/C^o_m (after DePaolo, 1981).

$$\frac{d\,C_m}{d\,\ln F} = (a+r-1)^{-1}\{a(C_a - C_m)+r(C_r - C_m)-(D-1)C_m \qquad (5.3)$$

where C_r is the concentration of an element in replenished magma and r is the ratio between the rates of changes of masses of replenished and fractionated magmas. Figure 5.17 depicts the type of trace elements ratios variations that might be expected in the cumulate rocks in a situation where replenishment occurs in pulses while assimilation is continuous. The Figure 5.17 shows that the magma evolution in the periods between replenishment pulses is described by the above equation with r=0, and the replenishment is a simple mixing of two magmas.

5.4(c) VENTING, REPLENISHMENT, ASSIMILATION AND FRACTIONAL CRYSTALLIZATION (VRAFC) MODEL FOR A MAGMA CHAMBER:

In the present study I have incorporated the RAFC magma chamber model to include the effects of rate of change of mass of magma due to venting (eruption) on the trace and isotope elements evolution (VRAFC model of the magma chamber). O'Hara and Mathews (1981) have shown that the geochemical evolution of the magma chamber in the upper lithosphere is not only controlled by the fractionation, assimilation and replenishment but also by venting of magma.

Figure 5.18 illustrates the essential parameters of the VRAFC model where M_m, is mass of the magma in chamber. M_a, M_r, M_c and M_v are the rate of change of mass of

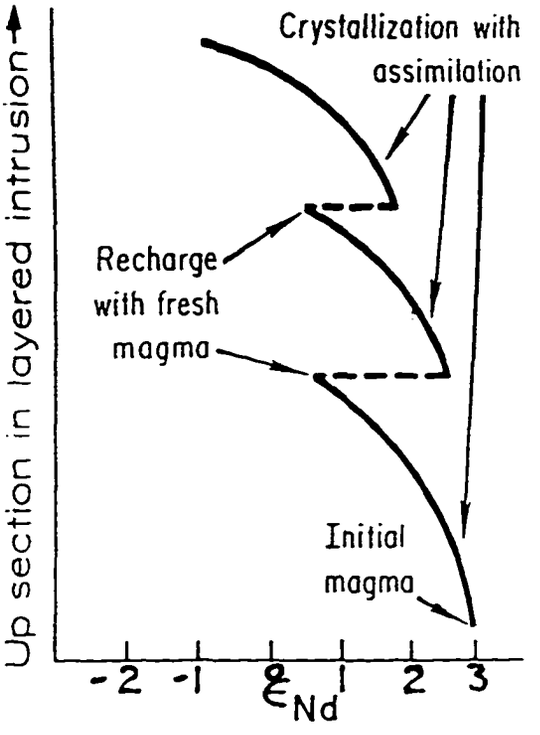

FIGURE 5.17: Schematic isotope stratigraphy in cumulate rocks forming from magma undergoing continuous fractional crystallization accompanied by assimilation with periodic instantaneous injections of uncontaminated magma (after DePaolo, 1985).

FIGURE 5.18

VENTING, REPLENISHMENT, ASSIMILATION AND FRACTIONAL CRYSTALLIZATION (VRAFC) MODEL OF A MAGMA CHAMBER

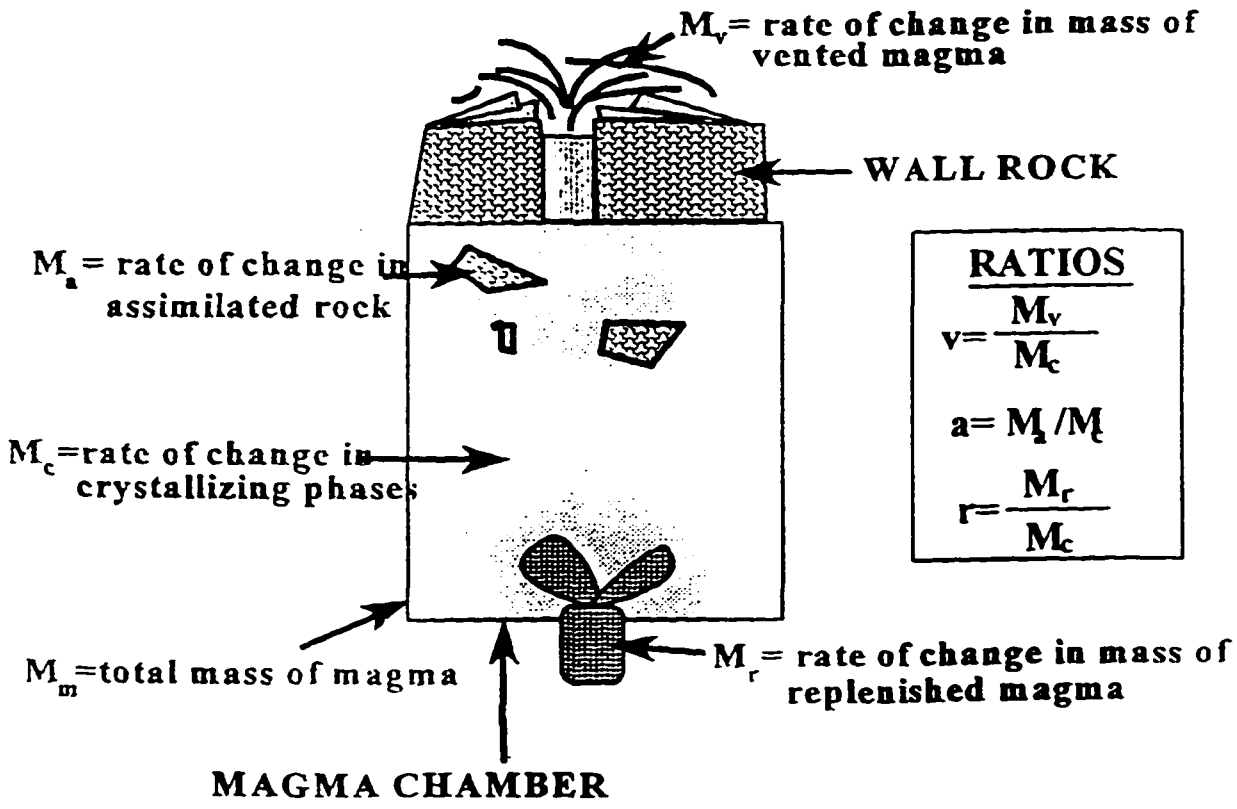

magma due to assimilation, replenishment, crystallization and venting respectively. C_m, C_a, C_r, C_c, and C_v are the concentration of an element in the magma, assimilated material, replenishing magma, crystallizing minerals and venting magma from the magma chamber. e_m, e_a, e_r, e_c, and e_v are the isotopic ratios in the magma, assimilated material, replenishing magma, fractionating mineral assemblage and in the venting magma respectively.

Generally two type of venting can be assumed from a magma chamber. (i) In first type of venting the eruption of magma takes place continuously from the magma chamber through time. In such a case, the concentration of trace element in the venting magma depends directly on the concentration in the batch of previously vented magma. (ii) For the second type venting occurs when the magma from the magma chamber comes out in pulses. In such a case there is a residence time for the magma in the magma chamber in between each pulse, during which C_m/C^0_m ratio for the magma reach a steady state ratio (constant value). However, in both cases the concentration of an element in the venting magma depends not only on the concentration in the crystallizing phases but also its concentration in the residual magma in the magma chamber. Here we consider that magma consists of silicate liquid and the mineral phases are unable to separate from the magma. The rate of change of an element in the magma (e) is a function of concentration of an element in fractionating phase (C_m). It is given by:

$$\frac{de}{dt} = -M_v C_v - M_c D C_m = C_m \frac{dM_m}{dt} + M_m \frac{dC_m}{dt} \qquad (5.4)$$

where D is the partition coefficient of an element between the mineral phase and the remaining magma. The change in the mass of magma through time , dM_m/dt, is the sum of masses of vented magma and fractionated mineral phases= $-(M_v + M_c)$. Here we have taken the negative value for the sum because of depletion in the mass of magma due to venting and crystallization. Substituting of $-(M_v + M_c)$ for the dM_m/dt in equation (5.4) gives:

$$M_v (C_m - C_v) - M_c (D C_m - C_m) = M_m \frac{dC_m}{dt} \qquad (5.5)$$

The equation (5.5) can also be written as

$$\frac{dC_m}{dt} = \frac{M_v}{M_m}(C_m - C_v) - \frac{M_c}{M_m}(D - 1)C_m \qquad (5.6)$$

Equation (5.6) governs the concentration of an element in the magma chamber affected simultaneously by venting and the fractional crystallization. In order to solve the equation (5.6) I have consider the ratio $v = M_v / M_c$, as it is difficult to estimate the rate of change of mass of magma due to venting and the fractionating mineral phases. The expansion of the equation (5.6) in terms of fraction (relative mass) of magma in magma chamber F leads to:

$$M_m \frac{dC_m}{dt} = -M_v C_v - (M_v D - M_c - M_v) C_m \qquad (5.7)$$

The inclusion of ratio v into the equation (5.7) gives

$$\frac{dC_m}{d\ln F} = \frac{v}{(v+1)} C_v - pC_m \qquad (5.8)$$

$$\text{where } p = \frac{D - v - 1}{-v - 1}$$

$$F = \frac{M_m}{M_m^0}$$

and M^0_m is the initial mass of magma. The explanation for using the dlnF in equation (5.8) can be found in DePaolo (1981; equation 5). DePaolo (1981) has taken $F=M_m/M^0_m$ = relative mass of magma remaining in the magma chamber. However, for VFC model we have taken F_v $=-F$ which is withdrawal of relative mass of magma from the magma chamber. Integration of equation (5.8) from C^0_m to C_m gives:

$$\frac{C_m}{C_m^0} = F^{-p} \left\{\frac{v}{v+1}\right\} \frac{C_v}{p C_m^0} F^{-p} + \frac{(v)C_v}{(v+1)C_m^0} \qquad (5.9)$$

rearrangement of equation (5.9) gives:

$$\frac{C_m}{C_m^0} = F^{-p}\left[1 - \left\{\frac{v}{v+1}\right\}\frac{C_v}{p\,C_m^0}\right] + \frac{(v)C_v}{(v+1)C_m^0} \qquad (5.10)$$

Equation 5.10 is the solution for an equation describing the effects of processes of venting and fractional crystallization in a magma chamber on the trace element's concentration. In case of large ion lithophile elements, where $D << 1$ (incompatible elements) than $p=1$ and the equation (5.10) reduces to

$$\frac{C_m}{C_m^0} = F^{-1}\left[1 - \left\{\frac{v}{v+1}\right\}\frac{C_v}{C_m^0}\right] \qquad (5.11)$$

when there is no venting of magma taking place from the magma chamber then equation (5.11) reduces to $C_m/C^0_m = F^{-1}$, which is the Rayleigh's equation for the fractional crystallization.

Equation 5.11 for VFC model of a magma chamber can be combined with the RAFC model of DePaolo (1985) to obtain the final expression for the VRAFC model of a magma chamber. For evolution of trace elements concentrations and isotopic ratios the equations are:

$$\frac{dC_m}{dM_c} = -\frac{1}{M_m}\left[a(C_a - C_m) + r(C_r - C_m) - v(C_v - C_m) - (D - 1)C_m\right] \quad (5.12)$$

$$a = \frac{M_a}{M_c}$$

and

$$r = \frac{M_r}{M_c}$$

$$d\epsilon_m/dM_c = 1/M\{(aC_a/C_m)(\epsilon_a - \epsilon_m) + (rC_r/C_m)(\epsilon_r - \epsilon_m) + (vC_v/C_m)(\epsilon_v - \epsilon_m) \quad (5.13)$$

equations 5.12 and 5.13 in terms of F (mass of magma remaining)

$$\frac{dC_m}{dlnF} = (a+r+v-1)^{-1}\{a(C_s - C_m) + r(C_r - C_m) - v(C_v - C_m) - (D-1)C_m \quad (5.14)$$

and for the isotopic ratios the equation is

$$\frac{d\epsilon}{dlnF} = (a+r-v-1)^{-1}\left\{a\frac{C_s}{C_m}(\epsilon_s - \epsilon_m) + r\frac{C_r}{C_m}(\epsilon_r - \epsilon_m) - v\frac{C_v}{C_m}(\epsilon_v - \epsilon_m)\right. \quad (5.15)$$

Equations 5.14 and 5.15 give complete expression for the trace elements and isotope ratios in a magma chamber under going venting, replenishment, assimilation and fractional crystallization.

5.5 THE AFC MODELLING OF THE ROCKS OF RAJULA, RAJPIPLA, SAURASHTRA, OTHER DECCAN VOLCANIC PROVINCES AND THE REUNION:

The geochemical characteristics of the rocks from the Rajula area and other parts of Deccan Traps show that both crustal contamination by rocks of granitic composition and fractional crystallization were important factors in their geochemical evolution. This section deals with the estimation of the ratio a (Ma/Mc, using equation 5.2) between the rate of change of mass of assimilated rocks and mass of crystallizing magma for the rocks of Rajula, Rajpipla, Saurashtra, other Deccan volcanic provinces and Reunion. For these rocks a parental magma having the composition of Deccan Basalts with the lowest LILE contents (i.e. least contaminated) is considered. The rocks of our study areas show contamination only by

upper crustal rocks of granitic composition (Cox and Clifford, 1982; Stahle *et al.*, 1987).

Ba, Y and Rb are highly incompatible elements ($D << 1$), and their concentrations are used to calculate the values of a and F. For the calculation of F for each value of Ba, Y and Rb we have used equation 5.13. Ba, Y and Rb concentrations in the parental magma (C^{o}_{m}) are taken as 20 ppm, 2 ppm and 2 ppm, respectively, (McKenzie and Onion's; 1995). Ba, Rb and Y in the assimilated rocks are taken as 704 ppm, 72 ppm and 9 ppm respectively (an average of following their concentrations reported in the Archean gneisses and charnockites of peninsular India by Rogers *et al.*, (1987) and Stahle *et al.*, (1987). Values of F are calculated for different values of a (0.05, 0.1, 0.15) in order to estimate the correct ratio a which could generate the geochemical characteristics of the rocks of Rajula, Rajpipla, Saurashtra, other Deccan volcanic provinces and the Reunion.

The volumetric proportions of different compositional types of Deccan basalts i.e. picritic basalt, tholeiitic basalt, alkalic basalt and acidic rocks are poorly known. However, on the basis of known distribution of the Deccan basalts it is estimated that volumetrically the tholeiitic Deccan basalts (TDB) are the dominant types of all the Deccan basalts. High MgO and Mg^{*} lavas (picritic Deccan basalts) are present in the lower basaltic formations of the western coast and in parts of Cambay graben. The differentiated flows and dikes of alkalic and acidic types are exposed locally within Rajula, Narmada-Tapti rift and along the west coast, south of Bombay.

Figure 5.19 shows the plot between the C_m/C^o_m and the calculated F for Ba, Rb and Y for different values of Ma/Mc. First, consider a magma chamber with 100% magma (i.e. absence of fractionation of mineral phases or assimilation of rocks). In this case $M_m = M^o_m$ and $C_m = C^o_m$ hence the ratios $F(M_m/M^o_m)$ and C_m/C^o_m have the value 1, which is the maximum value F can reach. As assimilation and fractionation of the minerals occur in the magma chamber, one should expect appearance of olivine in **picritic** type magma of Reunion followed by olivine± clinopyroxene± plagioclase feldspar in **tholeiitic** type magma (TDB) of Rajpipla, Saurashtra and Deccan basalts from west coast and last K and/or Na feldspars± quartz in acidic rocks from Rajula.

Figure 5.19 shows that when Ma/Mc is taken as 0.05, then the first and last batches of TDB occurred when the value of F decreased from 0.4 to 0.15 indicating the production of 25% of the TDB and 15% of acidic magma. The picritic magma of Reunion dominated (60%) when the value of a is considered 0.05. As mentioned earlier tholeiitic basalts are the most abundant and the picritic and acidic rocks are least abundant types of rocks in Deccan volcanic province. Hence, one can discard the value of Ma/Mc as 5% relative contamination for the rocks of Rajula, Rajpipla, Saurashtra, Deccan basalts from west coast and Reunion.

Figure 5.19 also shows that when Ma/Mc is considered 0.1 then relative fraction of picritic, tholeiitic and acidic magmas produced from the AFC model are 0.2 (20%), 0.65 (65%) and 0.15 (15%), respectively. In such case the abundance of different types of

FIGURE 5.19

M_a=Mass of assimilated rock

M_c=Mass of Fractionated Magma

C_m=Concentration of Trace Element in Magma

C^0_m=Concentration in Original Magma

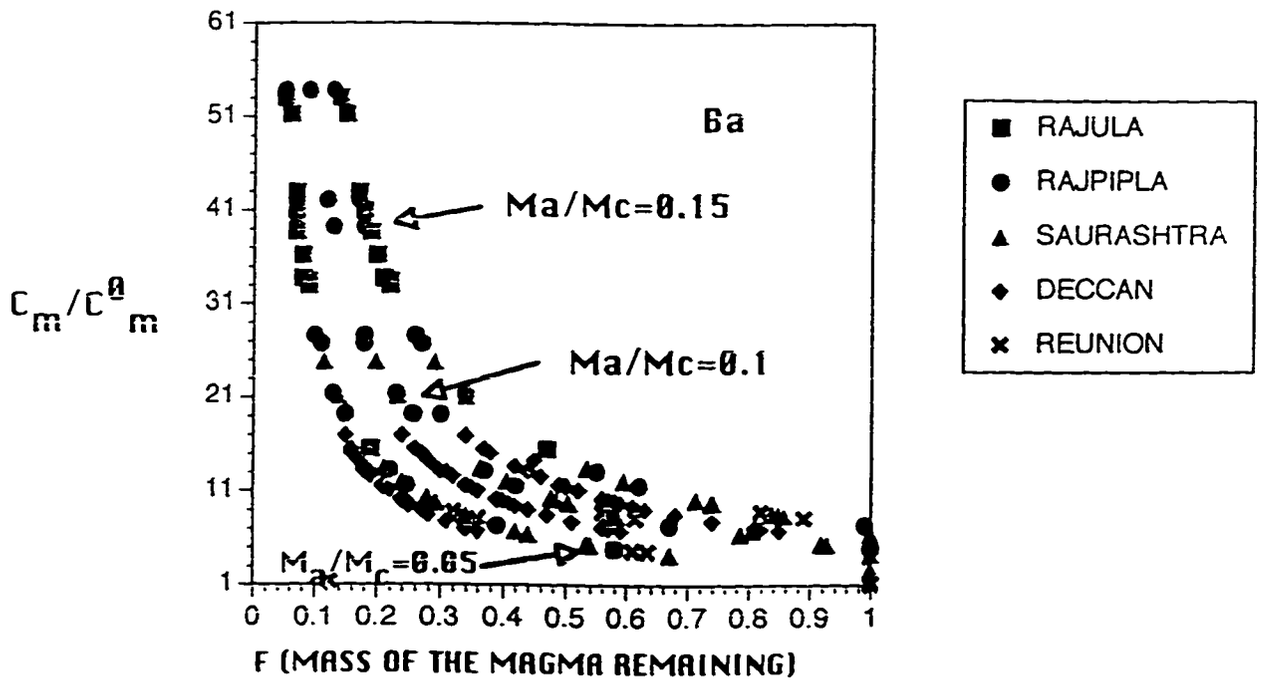

FIGURE 5.19

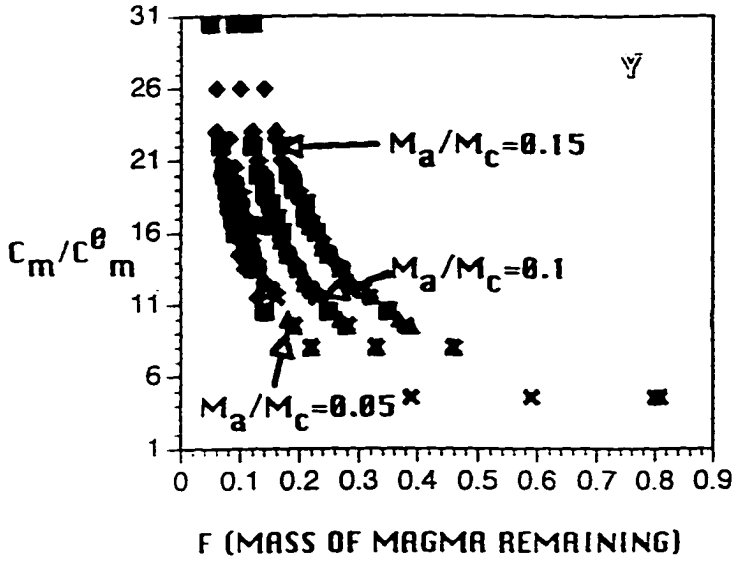

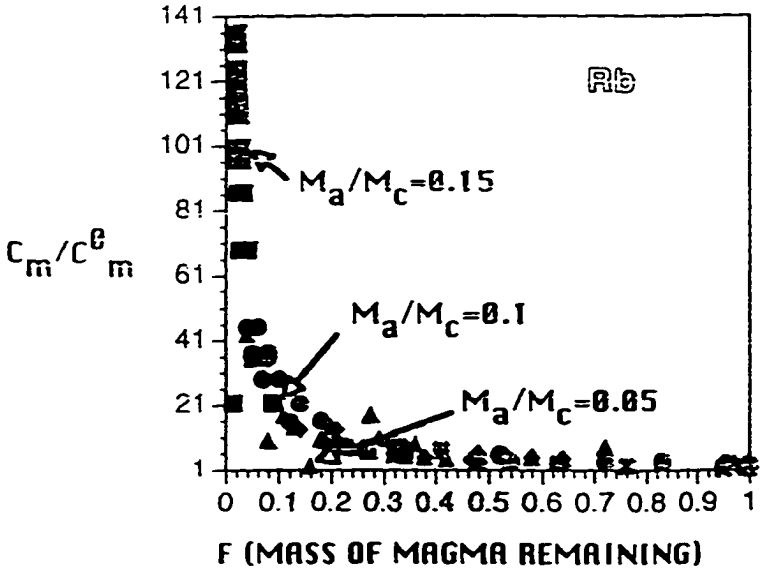

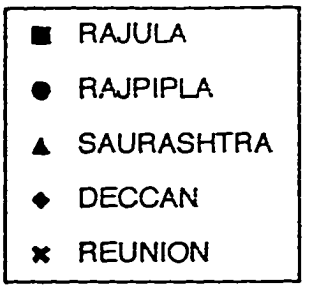

generated magma is similar to the observed abundance of different rock types of Deccan Traps. When the value of Ma/Mc is increased to 0.15 , then the three values of C_m/C^o_m for Ba, Rb and Y reached the value of F either one or more than one. As explained earlier F equals one only when there is no fractionation of minerals or assimilation of rocks. These calculations show that the 10% to 15% relative contamination of the N-MORB type magma by the granitic type crustal rocks can generate the geochemical characteristics observed in the Deccan traps rocks of Rajula, Rajpipla, Saurashtra, other Deccan volcanic provinces and the Reunion basalts.

5.6 THE VFC MODELLING OF THE ROCKS OF RAJULA, RAJPIPLA, SAURASHTRA, OTHER DECCAN VOLCANIC PROVINCES AND THE REUNION:

Here we show the estimated values of v, the ratio between the vented magma and the fractionated magma. Equation 5.10 controls the evolution of trace elements concentrations in VFC model of magma chamber. However, for this study we have used the equation 5.11 for the incompatible elements (i.e. p=1). Figure 5.20 shows the plot between the C_v/C^o_m versus F_v (relative mass of magma withdrawal from the magma chamber) for Ba. All these data points of the calculated F_v for 0.2, 0.3 and 0.4 values of v are randomly scattered when we considered continuous venting for the formations of Deccan Traps through time. Figure 5.13 suggests that the eruption of the Deccan Traps were not continuous through time.

FIGURE 5.20

CONTINOUS VENTING OF MAGMA

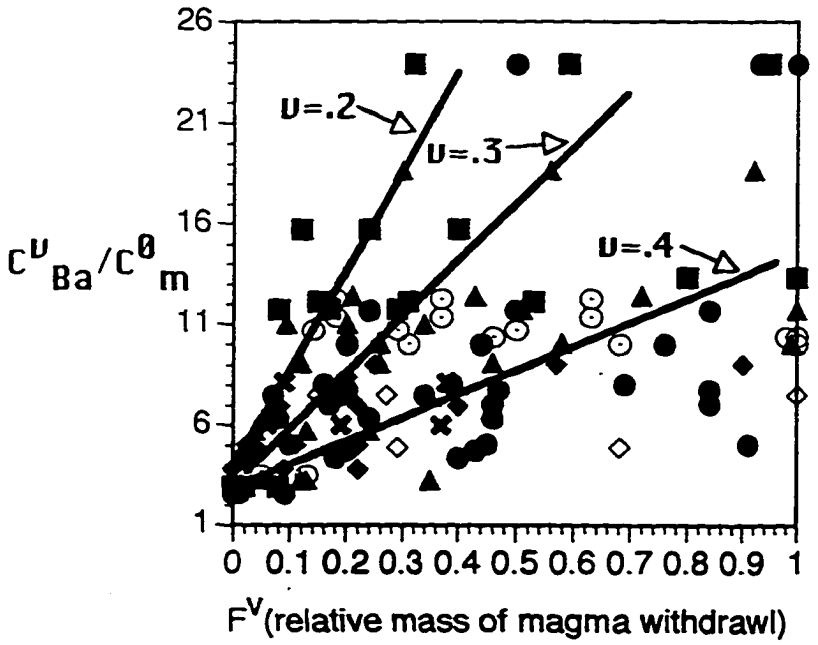

In equation 5.11 we have considered a constant value of C_m/C^o_m for Ba, Rb and Y. Figure 5.21 shows plot of C_v/C^o_m for Ba, Rb and Y versus the F_v, when the venting of the magma occurred in pulses. The maximum value the F_v can reach is 1, when all the magma generated is vented out from the magma chamber. Figure 5.21 for Ba, Rb and Y shows that when the value of v is considered as 0.2 then all the calculated values of F_v lie within 1. However, the estimated values of F_v become more than 1 when v is taken as 0.6. These calculations indicate that 40% to 60% of relative mass of magma vented out from the magma chamber forming Deccan traps rocks of Rajula, Rajpipla, Saurashtra, other Deccan volcanic provinces and the Reunion.

5.7 DISCUSSION:

The inclusion of the process of venting into the RAFC model has greatly enhanced our understanding on how the eruption of magma effects evolution of trace elements and isotopic ratios in a magma chamber. The significance of the role of assimilation on the rocks of Deccan Volcanics has been described by (for example) Cox and Hawkesworth (1985) and Dupuy and Dostal (1986). Most of these workers including Mahoney *et al.*, (1985) suggested that around 35% of the granitic type upper crustal rocks assimilated into the magma chamber from which the eruption of Deccan Volcanics took place. However, when we included the venting into the RAFC model and then applied the developed VRAFC model to trace elements of Deccan Volcanics we discovered that only 10 to 15% upper crustal contamination of magma chamber can explain the geochemical characteristics for the rocks of

FIGURE 5.21

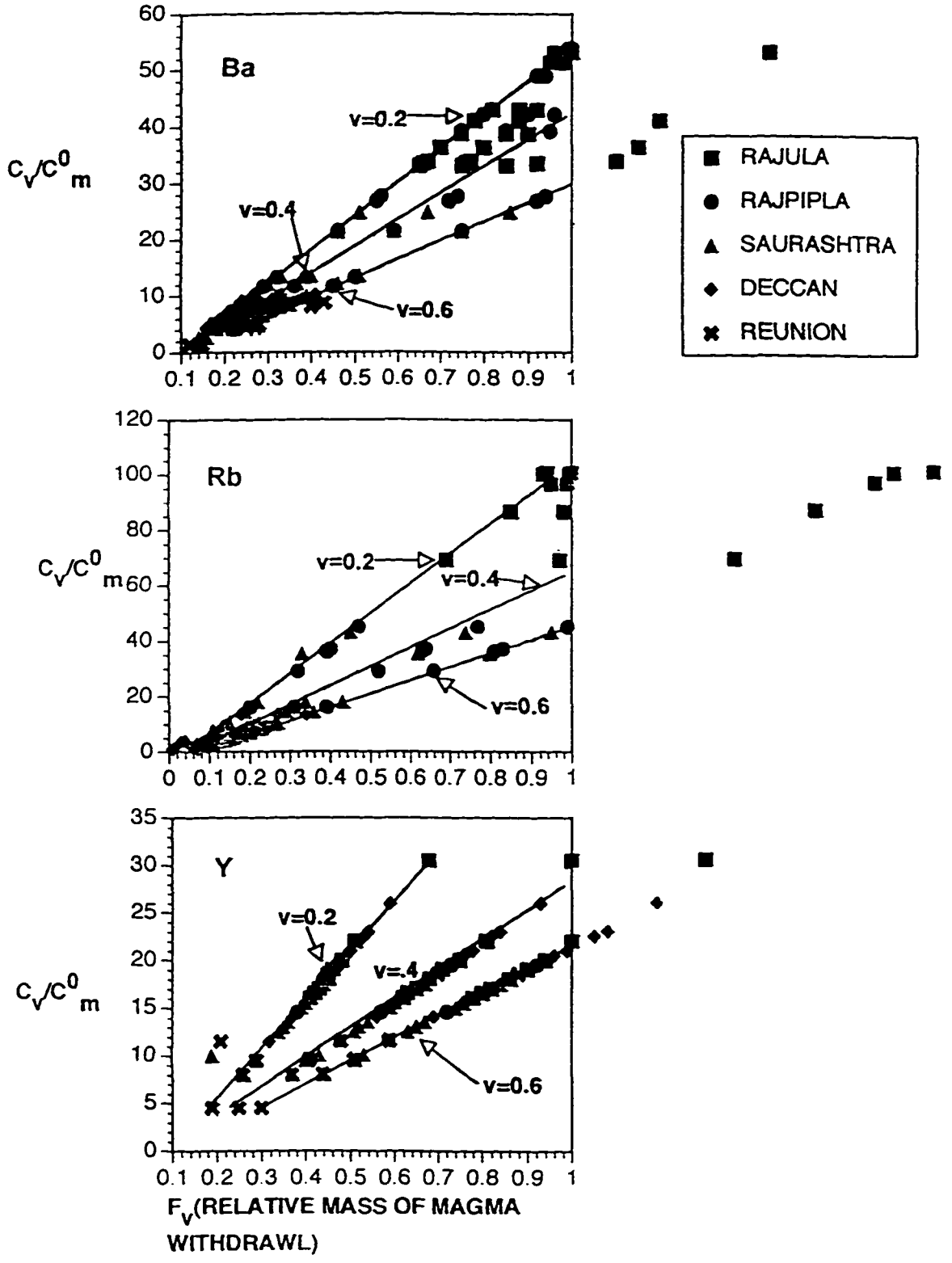

Deccan volcanics. Eruption of magma is a physical process that can be observed directly in volcanic provinces. However, this study extended the way in which the amount and type of venting controls the evolution of concentration of trace elements and isotopic ratios in the magma chamber which has been largely unknown and conjectural. When the VRAFC model is applied to the rocks of Deccan Volcanics it shows that 40 to 60% of the magma vented out from a magma chamber which gave rise to the Deccan Traps. The occurrence of residual 60% to 40% magma is explained by Sharma and Bhattacharji earlier (1996 a, b; and Chapters 3 and 4) on the basis of three dimensional gravity modelling along the western margin and the Narmada-Tapti rifts. Modelling of gravity highs along Narmada-Tapti rift has shown the presence of at least eight small isolated high density mafic bodies. These mafic bodies are convexly upward shape and appear to have emplaced at a depth of 6.7 ± 0.6 km with an average density of 2910 ± 291 kg/m^3, suggesting gabbroic type bodies. Estimations show that these mafic bodies have an average width of 16 ± 1.6 km, 25 ± 2.5 km length and an average thickness of 10 ± 1.0 km. Three dimensional gravity modelling of Bouguer gravity highs along the western margin rift also indicates two sub-surface high density mafic bodies. These bodies are ellipsoidal in shape occurring at a depth varying from 6 ± 0.6 km to 18 ± 1.8 km with a density of 2940 ± 294 kg/m^3 They have a horizontal dimensions of 300 ± 30 km and 50 ± 5.0 km. These mafic bodies in the upper lithosphere were interpreted by Sharma and Bhattacharji (1996b) earlier as a major source for Deccan volcanics.

CHAPTER 6

CONCLUSIONS

In this study we have developed geophysical and geochemical models of a magma chamber which are then applied to the emplacement and evolution of Deccan volcanics. The models developed in this study can be applied to other volcanic provinces. The following conclusions are made based on the geophysical and geochemical studies of various differentiated dikes and associated Deccan Volcanics in western India.

6.1 (i) The rhyolite, trachyte and dolerite dikes of NE-SW dike swarm in Deccan volcanic province of western India were emplaced with their own hydraulic fracturing. (ii) The dikes were emplaced from a convexly shaped magma chamber. (iii) The projections of dikes on the surface of a magma chamber indicate that the upper part was filled by rhyolitic magma which was underlain by trachytic and basaltic magmas, thus indicating zoning of the magma chamber. (iv) Convective fractionation was the major factor for the zoning of the magma chamber. (v) It is concluded that the dikes emplaced from a convex shaped magma chamber will show lower magma driving pressures at the central part of the dike swarm and higher magma driving pressure at the outer margin.

6.2 (i) Three dimensional gravity modeling of Bouguer gravity highs along the continental western margin suggested two large elongated ellipsoidal shape gabbroic mafic bodies. (ii)

These mafic bodies occur at a depth from 6±0.6 km to 13±1.3 km. Estimated length and width of these bodies vary from 18±1.8 km to 300±30 km and 8±0.8 km to 50±5 km. (iii) At least eight convexly shaped gabbroic mafic bodies are present along the Narmada-Tapti rift. The widths of these mafic bodies vary from 9±0.9 km to 38±3.8 km and have an average density of 2.91±.29 gm/cm^3. The length of these bodies varies from 18±1.8 km to 28±2.8 km. (iv) Three dimensional gravity modelling suggest concentration of large gabbroic mafic bodies along western margin and smaller dimensions mafic bodies along intraplate Narmada-Tapti rifts.

6.3 Four large gabbroic type plutonic mafic bodies are present in Saurashtra peninsula, western India. From the analyses of three such bodies it is inferred that the ellipsoidal shape of these mafic bodies is caused by upward increase in viscosity of the upper crust and may also be related to asymmetrical thermal aureole as well as emplacement of mafic plutons as diapirs in the upper crust as a result of differential drag due to strain softening of upper lithosphere.

6.4 (i) The model developed for the combined effects of venting, replenishment, assimilation and fractional crystallization (VRAFC) on the geochemical evolution of trace elements in a magma chamber can be used to estimate the ratios between the rate of change of masses of vented (v) and replenished magmas, assimilated rocks (a) and crystallizing phases. (ii) Major, trace and rare earth elements for the rocks of Rajula, and other areas of Saurashtra, Rajpipla, other Deccan volcanic provinces and the Reunion suggest upper crustal contamination and fractionation. (iii) The application of AFC model on the rocks of Deccan volcanics from

various provinces implies that 10 to 15% assimilation of upper crustal rocks. (iv) The application of VRAFC model on the trace elements for the rocks of Deccan volcanics suggests 40% to 60% of venting of magma from the magma chamber. (v) The residual 60% to 40% of magma in the lithosphere is explained based on three dimensional gravity modeling of Bouguer gravity highs along the continental western margin and the Narmada-Tapti rifts. The modelling indicates the presence of ellipsoidal shape gabbroic bodies in the upper lithosphere and these mafic bodies in the upper crust were the major source for the Deccan Volcanics.

REFERENCES

Aitchenson, S.J. and Forrest, A.H. (1994). Quantification of crustal contamination in open magmatic systems. *Jour. of Petrol.* 35, 461-488.

Anderson, E.M. (1936). The dynamics of the formation of cone-sheets, ring dikes and caldron subsidence. *Proc. R. Soc. Edinburgh.* 56, 128-163.

Atkinson, B.K., (1984). Subcritical crack growth in geological materials. *Jour. Geophy. Res.*, 89, 4077-4114.

Bailey, R.A., Dalrymple, G.B. and Lanphere, M.A., (1976). Volcanism, structure and geochronology of Long Valley Caldera, Mono county, California. *Jour. Geophys. Res.*, 81, 725-744.

Bhattacharji S., Chatterjee, N., Wampler, J.M., Nayak, P.N. and Deshmukh, S.S.(1996). Indian Intraplate and Continental Margin Rifting, Lithospheric Extension, and Mantle Upwelling in Deccan Flood Basalt Volcanism near the K.T Boundary: Evidence from Mafic Dike Swarms. *Jour. of Geol.*, 104, 379-398.

Bose,M.K. (1973). Petrology and geochemistry of igneous complex of Mount Girnar, Gujrat, India. *Contrib. Mineral. Petrol.* 39,247-266.

Bottinga, Y. and Weill, D.F.,(1972). The viscosity of magmatic silicate liquids: A model for calculation. *Am. Jour. Sci.*, 272, 438-475.

Braille, L.W., Keller, G.R., and Peeples, W.J.(1974). Inversion of gravity data for two dimensional gravity distributions. *Jour. Geophys. Res.*, 79, 2017-2021.

Briggs, I. C., (1974). Machine contouring using Minimum Curvature. *Geophysics*, 39, 39-47.

Campbell, I., and Griffith, R.W. (1990). Implications of mantle plume structure for the evolution of flood basalts. *Earth Planet. Sci. Lett.* 99, 79-93.

Carslaw, H.S. and Jaeger, J.C.(1959). Conduction of heat in solids. Oxford Univ. Press. London, pp 342.

Chen, C.F. and Turner, J.S. (1980). Crystallization in a double diffusive system. *Jour. Geophys. Res.*, 85, 2537-2539.

Clemens, J.D. and Mawer, C.K. (1992). Granitic magma transport by fracture propagation. *Tectonophysics*, 204, 339-360.

Cox, K.G. and Hawkesworth, C.J. (1985). Geochemical stratigraphy of the Deccan Traps at Mahabaleswar, Western Ghats, India, with implications for open system magmatic processes. *Jour. Petrol.* 26, 355-377.

Cox, K.G. and Clifford, P., (1982). Correlation coefficient patterns and their interpretation in three basaltic suites. *Contri. Mineral. Petrol.*, 79, 268-278.

Crane, K. (1985). The spacing of rift axis highs: dependence upon diapiric processes in the underlying asthenosphere? *Earth and Planet. Sci. Lett.*, 72, 405-414.

Currie, K.L. and Ferguson, J. (1970). The mechanism of intrusion of lamphrophyre dikes indicated by offsetting of dikes. *Tectonophysics*, 9, 525-535.

Daly, R.A. (1933). Igneous rocks and depth in the earth. McGraw Hill, New York, 598 pp.

Das, B. and Patel, N.P. (1984). Nature of the Narmada-Son lineament. *Jour. Geol. Soc. Ind.*, 25(5), 267-276.

Davis, J. C., (1986). Statistics and Data analysis in Geology. John Wiley & Sons, New York, pp 389.

Delaney, P.T., Pollard, D.D., Ziony, J.I. and McKee, E.H. (1986). Field relations between dikes and joints: Emplacement processes and paleostress analysis. *Jour. Geophys. Res.*, 91, 4920-4938.

DePaolo, D.J., (1981). Trace element and isotopic effects of combined wallrock assimilation and fractional crystallization. *Earth and Planet. Sci. Lett.*,53, 189-202.

DePaolo, D.J., (1985). Isotopic studies of processes in mafic magma chambers: I The Kiglapait intrusion, Labrador. *Jour. of Petrol.*, 26, 925-951.

Deshmukh, S.S. and Sehgal, M.N. (1988). Mafic dyke swarms in Deccan Volcanic Province of Madhya Pradesh and Maharashtra. in Deccan Flood Basalts, ed. Subbarao, K.V., *Geol. Soc. of India*, Mem. 10, 323-339

Duncan, R.A. (1990). The volcanic record of Reunion hotspot. *Proceedings of Ocean Drill. Proj.*, 115, 3-10.

Duncan, R.A., and Richards, M.A. (1991). Hotspots, mantle plumes, flood basalts, and true polar wander. *Reviews of Geophy.* 29, 31-50.

Dupuy, C. and Dostal, J. (1984). Trace element geochemistry of some continental tholeiites. *Earth Planet. Sci. Lett.*, 67, 61-69.

Fisher, N.J. and Howard, L.E. (1980). Gravity interpretation with the aid of the quadratic programming. *Geophysics*, 45, 403-419.

Fisk, M.R., Upton, B.G.J., Ford, C.E., and White, W.M. (1988). Geochemical and experimental study of the genesis of magmas of Reunion Island, Indian Ocean. *Jour. of Geophy. Res.*, 93, 4933-4950.

Fiske, R.S. and Jackson, E.D. (1972). Orientation and growth of Hawaiian volcanic rifts: the effect of regional structure and gravitational stress. *Proc. Royal Soc. London*, 329, 303- 312.

Garcia-Abdeslem, J. (1995). Inversion of the power spectrum from gravity anomalies of prismatic bodies. *Geophysics*, 60, 1698-1703.

Griggs, D.T., Turner, F.J., and Heard, H.C., (1960). Deformation of rocks at 500°C to 800 °C. in Rock deformation. *Geol. Soc. Am. Mem.*, 79, 39-104.

Grout, F. F. (1932). Petrography and Petrology. McGraw Hill, New York, 522 pp.

Hamilton, W.B. (1988). Plate tectonics and island arcs. *Geol. Soc. Am. Bull.*, 100, 1503-1527.

Hanson, R.B. and Glazner, A.F. (1995). Thermal requirements for extensional emplacement of granitoids. *Geology*, 23, 213-216.

Haris, P.G. (1957). Zone refining and the origin of potassic basalts. *Geochim. Cosmochim Acta*. 12, 195-208.

Hess, P.C. (1989). Origins of igneous rocks. Harvard Univ. Press, 336pp.

Hildreth, W. (1981). Gradients in silicic magma chambers: implications for lithospheric magmatism. *Jour. Geophys. Res.*, 86, 10153-10192.

Hirs, G.G. (1973). A bulk flow theory for turbulence in lubricant films. *J. Lubric. Tech.*, 95, 137, 146.

Hooper, P.R.(1990). The timing of crustal extension and the eruption of continental flood basalts. *Nature*, 345, 246-249.

Humphris, S.E., Thompson, G., Schilling, J.G., and Kingsley, R.A. (1984). Petrological and geochemical variations along the Mid Atlantic ridge between 46 S and 32 S: influence of the

Tristan da Cunha mantle plume. *Geochim. Cosmochim. Acta*, 49, 1445-64.

Huppert H.E. and Sparks R.S.J.(1980). The fluid dynamics of a basaltic magma chamber replenished by influx of hot dense ultrabasic magma. *Contrib. Mineral. Petrol.*, 75, 279-289.

Huppert H.E., Sparks R.S.J., Wilson J.R. and Hallworth M.A. (1986). Cooling and crystallization at an inclined plane. *Earth Planet. Sci. Lett.*, 79, 319-328.

Ihinger, P.D. (1955). Mantle flow beneath the Pacific plate: Evidence from seamount segments in the Hawaiian-Emperor chain. *Ame. Jour. of Sci.*, 295, 1035-1057.

Irvine T.N., Keith D.W. and Todd S.G. (1983). The J-M platinum palladium reef of the stillwater complex, Montana II : origin by double diffusive convecting magma mixing and implications for the Bushveld Complex. *Econ. Geol.*, 78, 1287-1334.

Jones, T. A., (1986). Contouring Geological Surfaces with the Computer, Van Nostrand Rheinhold Comp., New York, pp 398.

Kaila, K.L., Roy Chaudhury, K., Reddy, P., Krishna, V.G., Narain, H., Subbotin, S.I., Sollogub, V.B., Chekunov, A.V., Kharetchko, G.E., Lazarenko, M.A. and Itchenko, T.V., (1979). Crustal structure along Kavali-Udipi profile in the Indian peninsular shield from deep seismic sounding. Geol Soc. of India, 20, 307-333.

Kaila, K.L., Murty, P.R.K., Mall, D.M., Dixit, M.M. and Sarkar, D. (1987). Deep seismic soundings along Hirapur-Mandala profile, central India. *Geophysics*, 89, 339-404.

Kaila, K.L., Rao, J.B.P., Koteshwara Rao, P., Madhawa Rao, N., Krishna V.G., and Sridhar, A.R. (1988). DSS studies over Deccan Traps along the Thuadara-Sindhwa-Sindad profile across Narmada-Son lineament, India. *AGU Mono. Geody. Ser.*, vol. 7.

Kaila, K.L.; Krishna, V.G. and Mall, D.M. (1981). Crustal structure along Mehmabad-Billmora profile in the Cambay basin, India from deep seismic soundings. *Tectonophysics,* 76, 99-130.

Kaila, K.L. (1988). Mapping the thickness of Deccan Trap flows in India from DSS studies and inferences about a hidden Mesozoic basin in Narmada-Tapti region. in *Deccan Flood Basalts*, Mem. 10, *Geol. Soc. India*, 91-116.

Kaila, K.L., and Koteswara R. (1985). Crustal structure along Khajuriakalan-Rahatgaon-Betul-Multai-Pulgaon profile across the Narmada lineament from deep seismic soundings. In : Deep seismic soundings and crustal tectonics., by K.L. Kaila and R.C. Tewari (eds.), AEG Publ., 43-57.

Kaila K.L., Tewari H.C. and Sarma P.L.N.(1980). Crustal structure from Deep Seismic Sounding studies along Navibander-Amreli profile in Saurashtra. *Mem. Geol. Soc. India*, 3, 218-232.

Kailasam, L.N., Murthy, B.G.K. and Chayanulu, A.Y.S.R. (1972). Regional gravity studies of Deccan trap areas of Peninsular India. *Curr.Sci.*, 41, 40-47.

Karanth, M. and Sant, P. (1995). Mafic dike swarms of peninsular India. editors S.S. Deshmukh, Nair, K.K.K., Yedekar, D.B., Mohabey, D.M. and Chatterjee, A.K. *Geological Society of India* special publication 267-281.

Knapp, R.B. and Norton, D. (1981). Preliminary numerical analyses of processes related to magma crystallization and stress evolution in cooling pluton environments. *Am. Jour. Sci.*, 281, 35-68.

Kolstad, C.D. and McGetchin, T.R. (1978). Thermal evolution models for the valles caldera with reference to a hot dry rock geothermal experiment. *Jour. Volcanol. Geotherm. Res.*, 3, 297-318.

Krishna, K.S., Murty, G.P.S., and Gopala Rao, D. (1994). Identification and origin of a subsurface ridge on the continental margin of western India. Marine Geology, 118, 283-290.

Krishnamurthy, P. and Cox, K.G. (1977). Picritic basalts and related lavas from the Deccan traps of western India. *Contrib. Miner. Petrol.*, 62, 53-75.

Krishnamurthy,P. and Cox,K.G. (1980). A potassium rich alkalic suite from the Deccan Traps, Rajpipla, India. *Contrib. Mineral. Petrol.* 73,179-189.

Lange, R.L. and Carmichael, I.S.E. (1990). Thermodynamic properties of silicate liquids with emphasis on density, thermal expansion and compressibility. *Reviews in Mineralogy*, 25, 25-63.

Ligenfelter, R.E. and Schubert, G. (1974). Hot spots and trench volcano separations. *Nature*, 249, 820.

Lightfoot, P.C., Hawkesworth, C.J., and Sethna, S.F., (1987). Petrogenesis of rhyolites and trachytes from Deccan Trap: Sr, Nd, and Pb isotope and trace element evidence. *Contrib. Mineral. Petrol.*, 95, 44-54.

Lippard, S.J. (1973). The petrology of the phonolites from the Kenya rift. *Lithos*, 6, 217-234.

Lister, J.R. (1990). Buoyancy driven fluid fracture: the effects of material toughness and of low viscosity precursors. *Jour. Fluid Mech.*, 210, 263-280.

Mahon, K.I., Harrison, T.M., Drew, D.A. (1988). Ascent of a granitoid diapir in a temperature varying medium. *Jour. Geophys. Res.* 93, 1174-1188.

Mahoney, J.J. (1988). Deccan Traps. In *Continental Flood Basalts*, ed. Macdougall, J.D. Kluwer Academic Publishers, 151-194.

Mahoney, J.J.; Macdougall, J.D.; Lugmair, G.W.; Murali, A.V.; Shankar Das, M. and Gopalan, K. (1985). Origin of contemporaneous tholeiitic and K-rich alkalic lavas: a case study from the northern Deccan plateau, India. *Earth and Planet. Sci Lett.*, 73, 39-53.

Marsh, B.D. (1981). On the crystallanity, probability of occurrence and rheology of lava and magma. *Contri. Mineral. Petrol.*, 78, 85-98.

Marsh, B.D. (1975). Plume spacing and source. *Nature*, 256, 240.

Martin D., Griffiths R.W. and Campbell I.H. (1987). Compositional and thermal convection in magma chambers. *Contri. Mineral. Petrol.*, 96, 465-475.

McBirney, A.R. and Murase, T. (1984). Rheological properties of magmas. *Ann. Rev. Earth Planet. Sci.*, 12, 337-357.

McCarthy, S.M., Powell, C.A., and Rogers, J.J.W., (1983). A relative residual study of the southern peninsula of India using the Gauribidanur seismic array. in Precambrian of South India, eds. Naqvi, S.M. and Rogers, J.J.W., *Geol. Soc. India*, Mem 4, 525-552.

Melluso, L., Lbeccaluva, L., Broizu, P., Gregnanin, A., Gupta, A.K., Morbidelli, L., and Traversa, G., (1995). Constraints on the Mantle Sources of the Deccan Traps from the Petrology and Geochemistry of the Basalts of Gujarat State (Western India). *Jour. Petrol.*, 36, 1393-1432.

Middlemost, E.A.K. (1975).The basalt clan. *Earth Science Rev.*, 11:337-364.

Middlemost, E.A.K. (1991). Towards a comprehensive classification of igneous rocks and magmas. *Earth Science Rev.*, 31:73-87.

Mishra , D.C. (1977). Possible extension of the Narmada-Son lineament towards Murray ridge (Arabian sea) and the eastern syn-taxial bend of the Himalayas. *Earth and Planet. Sci. Lett.*, 36, 301-308.

Mishra, D.C. (1977). Possible extensions of the Narmada-Son lineament towards Murray ridge (Arabian sea) and the eastern syn-taxial bend of the Himalayas. *Earth and Planet. Sci. Lett.* 36, 301-308.

Misra,K.S. (1983). The tectonic setting of Deccan volcanics in southern Saurashtra and Northern Gujarat. *Geol. Soc. Ind. Mem.*,3. 81-86.

Misra, K.S. (1976). A preliminary note on the Deccan Trap basaltic flows in the vicinity of Rajula in Saurashtra. Abstract, symp. on Deccan Traps and bauxite. *Geol. Survey of India*, 18-19.

Moore, D.R. (1975). Numerical models for convection. *Adva. in Chemi. Phy.*, 32, 65-76.

Morgan, J.P., Morgan, W.J., and Price, E. (1995). Hotspot melting generates both hotspot volcanism and a hotspot swell. *Jour. Geophy. Res.* 100, 8045-8062.

Morgan, W.J. (1971). Convection plumes in the lower mantle. *Nature*, 230, 42-43.

Murli, A.V., Sanker Das, M., and Aswathanarayana, U. (1976). Mount Girnar complex, Western India as a continental analog of Iceland. *25th Int. Geol. Cong.*, Sydney Sect.10, 423.

Murty, T.N.G.R.K. and Misra, S.K. (1981). The Narmada-Son lineament and the structure of Narmada rift system. *Jour. of Geol. Soc. of India*, 22, 112-121.

Naini, B.R., and Talwani, M. (1983). Structural framework and the evolution history of the continental margin of western India. In Studies in continental margin geology, Watkins J.S. and Drake C.L. (eds.), *Am. Asso. Petrol. Geol. Mem.* 34, 167-191.

Narain, H., (1973). Crustal structure of the India subcontinent. *Tectonophysics*, 20, 249-260.

Narain, H., and Subrahmanyam, C., (1986). Precambrian tectonics of the south Indian shield inferred from geophysical data. *Jour. of Geology*, 94, 187-198.

Negi, J.G., Aggrawal, P.K., Singh, A.P., and Pandey, O.P. (1992). Bombay gravity high and eruption of Deccan flood basalts (India) from a shallow secondary plume. *Tectonophysics*, 206, 341-350.

O'Hara, M.J. and Mathews, R.E., (1981). Geochemical evolution in an advancing, periodically replenished, periodically tapped, continuously fractionated magma chamber. *Jour. Geol. Soc. London*, 138, 237-277.

Patino,-Douce, A.E. and Johnston, A.D., (1991). Phase equilibria and melt productivity in the pelitic system: implications for the origin of peraluminous granitoids and aluminous granulites. *Contri. Mineral Petrol.*, 107, 202-218.

Paul, D.K., Potts, R.J., Rex, D.C., and Beckinsale, R.D. (1977). Geochemical and the petrological study of the Girnar igneous complex, Deccan volcanic province India. *Bull. Geol.*

Soc. Amer. 88, 227-234.

Peng, Z.X., Mahoney, J.J., Hooper, P.R., Harris, C., and Beane, J.A. (1994). A role for continental crust in flood basalt genesis? Isotopic and incompatible element study of the lower six formations of the Western Deccan Traps. *Geochim. et Cosmo. Acta.* 58, 267-288.

Petford, N., Kerr, R.C., Lister, J.R. (1993). Dike transport of granitoid magmas. *Geology*, 21, 845-848.

Pitcher, W.S. (1979). The nature, ascent and emplacement of granitic magmas. *Jour. Geol. Soc. London.* 136, 627-662.

Pollard, D.D.(1987). Elementary fracture mechanics applied to the structural interpretation of dikes, in Mafic Dike Swarms, eds. H.C. Halls and W.H. Fahrig, *Geol. Soc. Canada*, 34, 5-24.

Qureshi, M.N. (1981), Gravity anomalies, isostasy and crust mantle relations in the Deccan Traps and the contiguous regions India. *Mem. Geol. Soc. of India*, 3, 184-197, 1981.

Ramaswamy, G., and Rao, K.L.N. (1980). Geology of the continental shelf of the west coast of India. In: Facts and principles of world petroleum occurrences. *Can. Soc. Petrol. Geo. Mem.*, 6, 801-821.

Rao, T.C.S. (1970). Seismic and magnetic surveys over the continental shelf of Konkan coast. In: *Geophys. Res. Board Nat. Geophy. Res. Ins.*, Hyderabad, India, 59-71.

Read, H.H. (1948). Granites and granites. *Mem. Geol. Soc. America.* 28, 1-19.

Richards, M.A., Hager, B.H., and Sleep, N.H. (1988). Dynamically supported geoid highs over Hotspots: Observation and theory. *Jour. Geophy. Res.*, 93, 7690-7708.

Richardson, R.M. and MacInnes, S.C. (1989). The inversion of gravity data into three dimensional polyhedral models. *Jour. Geophys. Res.*, 94, 7555-7562.

Ritchey, J.L. (1980). Divergent magma at Crater lake, Oregon: products of fractional crystallization and vertical zoning in a shallow water under saturated chamber. *Jour. Volcanol. Geotherm. Res.*, 7, 373-386.

Rogers, J.J.W., (1986). The Dharwar craton and the assembly of peninsular India. *Jour. of Geology*, 94, 129-143.

Rogers, J.J.W., Callahan, E.J., Dennen, K.O., Fullgar, P.D., Stroh, P.T., and Wood, L.F., (1986). Chemical evolution of peninsular gneiss in the western Dharwar craton, southern

India. *Jour. of Geology*. 94, 233-246.

Rohrman, M. and Beek, P.V.D. (1996). Cenozoic postrift domal uplift of north Atlantic margins: an asthenospheric diapirism model. *Geology*, 24, 901-904.

Rubin A.M. (1993b). Tensile fracture of rock at high confining pressure: implications for dike propagation. *Jour. Geophy. Res.*, 98, 15919-15935.

Rubin, A.M. and Pollard, D.D. (1987). Origins of blade like dikes in volcanic rift zones. *USGS professional paper*, 1350, 1449-1470.

Rubin A.M. (1993a). Dikes vs. diapirs in viscoelastic rock. *Earth and Planet. Sci. Lett.*, 117, 653-670.

Sethna, S.F. and Battiwala, H.K. (1980). Major element geochemistry of the intermediate and acidic rocks associated with the Deccan Trap basalts. *Proc. 3rd. Ind. Geol. Cong.*, Poona, 281-294.

Sethna, S.F. (1971). A note on the trace element content of carbonatites of Ambadongar and surrounding areas. Chota Udaipur. *Jour. Geol. Soc. Ind.*, 12, 411-417.

Sharma, P.V. (1986). Geophysical methods in geology. Elsevier Science Publ., 442pp.

Sharma, R. and Bhattacharji, S. (1996a). Three dimensional gravity modelling along Narmada-Tapti and western margin rifts, India. *EOS Transactions*, 77, 74.

Sharma, R. and Bhattacharji, S. (1996b). VFC (venting and fractional crystallization) modelling of the magma chamber and it's application on Deccan volcanic province, western India. *Geol. Soc. of America*. Annual Meet., A483.

Sharma, R. and Bhattacharji, S. (1994). Geochemical and petrographical variations in lava flows at Palitana, Deccan Volcanic Province, Western India: Results of continuous gradients in a magma chamber. *EOS Transactions*, v.75, 16, 354.

Sharma, R. and Bhattacharji, S. (1993). Geochemical evolution of differentiated dikes in Deccan Volcanics. Western India: indicator of zoned magma chambers. *Geol. Soc. of America*, Annual meeting, Abstract with programs, 25, no. 6, 97.

Shaw, H.R. (1980). The fracture mechanism of magma transport from the mantle to the surface. in Physics of magmatic processes, ed. Hargraves, R.B., Princeton Univ. Press, Princeton, New Jersey, 201-264.

Shaw, H.R. (1972). Viscosities of magmatic silicate liquids: An empirical method of

prediction. *Am. Jour. Sci.*, 272, 870-893.

Sigudsson, H. and Sparks, S.R.J. (1978). Lateral magma flow within rifted Icelandic crust. *Nature*, 274, 126-130.

Sleep, N.H. (1990). Hotspots and mantle plumes: Some phenomology. *Jour. Geophy. Res.*, 95, 6715-6736.

Sleep, N.H. (1992). Hotspot volcanism and mantle plumes. *Annu. Rev. Earth Planet. Sci.*, 20, 19-43.

Smith, R.A. (1960). Some formulae for interpreting local gravity anomalies. Geophys. Prospect., 8, 607-613.

Smith, R.A. (1959). Some depth formulae for local magnetic and gravity anomalies. Geophys. Prospect., 7, 55-63.

Spera, F.J., Yuen, D.A. and Kirchvink, S.J. (1982). Thermal boundary layer convection in Silicic magma chambers: Effects of temperature dependent rheology and implications for thermogravitational chemical fractionation. *Jour. Geophy. Res.*, 87, 8755-8767.

Spera, F.J. (1980). Thermal evolution of plutons: A parametrized approach. *Science*, 207, 299-301.

Stahle, H.J., Raith, M., Hoernes, S. and Delfs, A., (1987). Element mobility during incipient granulite formation at Kabbaldurga, southern India. *Jour. Petrol.*, 28,803-834.

Subramanyam, V., Gopala Rao, D., Ramprasad, T., Kamesh Raju, K.A., and Gandhara Rao, M.(1991). Gravity anomalies and crustal structure of the western continental margin off Goa and Mulki, India. *Marine Geology*, 99, 247-256.

Sukheswala, R.N. and Udas, G.R. (1963). Note on carbonatite of Ambadongar and its economic potentialities. *Sci.Cult.*, 26, 563-568.

Takin, M. (1966). An interpretation of the positive gravity anomaly over Bombay on the west coast of India. Geophy. *Jour. Royal Astro. Soc.*, 11, 527-537.

Talwani, M., Worzel, J.L. and Landisman, M. (1959). Rapid gravity computations for two dimensional bodies with application to the Mendocine submarine fracture zone. *Jour. Geophy. Res.*, 64, 49-59.

Thakur, N.K., Nagarajan, N., and Joshi, M.S. (1993). Estimation of the Bouguer gravity field over the peninsula using two dimensional filtering. *Tectonophysics*, 225, 543-550.

Thompson, R.N., Morrison, M.A., Hendry, G.L., and Parry, S.J. (1984). An assessment of the relative roles of a crust and mantle in a magma genesis : an elemental approach. *Phil. Trans. R. Soc. Lond.* A310, 549-590.

Thompson, R.N., Morrison, M.A., Dickin, A.P., and Hendry, G.L. (1983). Continental Flood basalts... arachnids rule O.K.? In *Continental basalts and Mantle xenoliths*, C.J. Hawkeworth and M.J. Norry (eds). 158-85, Nantwitch: Shiva.

Tsunakawa, H. (1983). Simple two dimensional model of propagation of magma filled cracks. *Jour. Volcanol. Geotherm. Res.*, 16, 335-342.

Turcotte D. and Schubert G. (1982). *Geodynamics*, John Wiley, New York, 450p.

Turner, J.S. (1980). A fluid dynamical modal of differentiation and layering in magma chambers. *Nature*, 285, 213-215.

Turner, J.S. and Campbell, I.H. (1986). Convection and mixing in magma chambers. *Earth Science Reviews*, 23, 255- 352.

Verma, R.K., and Banerjee, P. (1992). Nature of continental crust along the Narmada-Son lineament inferred from gravity and deep seismic sounding data. *Tectonophysics*, 202, 375-397.

Verma, R.K. and Subrahmanayam, C., (1984). Gravity anomalies and the Indian lithosphere: review and analysis of existing gravity data. *Tectonophysics*, 105, 141-161.

Vielzeuf, D., and Holloway, J.R., (1988). Experimental determination of fluid absent melting relations in the pelitic system. Consequences for crustal differentiation. *Contri. Mineral. Petrol.*, 98, 257-276.

Wada, Y. (1994). On the relationship between dike width and magma viscosity. *Jour. Geophy. Res.*, 99, 17743-17,755.

Weaver, B.L., (1991). The origin of ocean island basalt end- member compositions: trace elements and isotopic constraints. *Earth and Planet. Sci. Lett.*, 104, 381-397.

Weaver, S.D., Sceal, J.S.C., and Gibson, I.L. (1972). Trace element data relevant to the origin of trachyte and pantelleritic lavas in the East African rift system. *Contrib. Mineral. Petrol.*, 36, 181-194.

Weertman, J. (1971). Theory of water filled crevasses in glaciers applied to vertical magma transport beneath oceanic ridges. *Jour. Geophys. Res.*, 76, 1171-1183.

Weinberg, R.F. and Podladchikov, Y. (1994). Diapiric ascent of magmas through power law crust and mantle. *Jour. Geophys. Res.* 99, 9543-9559.

Wickham S.M. (1987). The segregation and emplacement of granitic magmas. *Jour. Geol. Soc. London*, 144, 281-297.

Williams, H. and McBirney, A.R. (1979). *Volcanology*, San- Francisco, Freeman Cooper and Co., 397 pp.

Wilson, G. (1970) Wrench movements in the Aristarchus region of the moon. *Proc. Geol. Assoc.*, 81. 595-608.

Wilson, M. (1990). Igneous Petrogenesis. Unwin Hyman, London, 466 pp.

Winkler, H.C.F., (1979). Petrogenesis of Metamorphic rocks. 5 th edn., Springer-Verlag, pp 348.

Yellur, D.D. (1968). Carbonatite complexes as related to the structure of Narmada valley. *Jour. Geol. Soc. Ind.* 9, 118-123.